Modelling Bioremediation of Uranium Contaminated Aquifers

by
Ben E. G. Rotter

A thesis submitted to the College of Science and Engineering
in conformity with the requirements
for the degree of Doctor of Philosophy

The University of Edinburgh
Edinburgh, United Kingdom
2007

Declaration

I hereby declare that this thesis has been composed by myself, that all the material presented within it is original unless stated otherwise, and that no part of this work has been submitted for any other degree or professional qualification.

Ben E. Rotter Date

Abstract

Radionuclide extraction, processing and storage have resulted in a legacy of radionuclide-contaminated groundwater aquifers worldwide. An emerging remediation technology for such sites is the in situ immobilisation of radionuclides via biostimulation of dissimilatory metal reducing bacteria. While this approach has been successfully demonstrated in experimental studies, advances in understanding and optimization of the technique are needed. Mass transfer processes in heterogeneous and structured porous media may significantly affect the geochemical and microbial processes taking place in contaminated sites, impacting remediation efficiency significantly. The objective of this work was to understand better how heterogeneous porous media may affect immobilisation efficiency through interactions with the dominant geochemical, microbial and transport processes. A biogeochemical reactive transport model was developed for uranium immobilisation by DMRB. Physical heterogeneity is conceptually represented by a two-region model. Simulations investigate the parameter sensitivities of the system over wide ranging geochemical, microbial and groundwater transport conditions. The simulations highlight the conditions under which optimal remediation occurs. The relative significance of regional microbial residence patterns, U(VI)-surface complexation, geochemical conditions such as mineralogy, and porous media characteristics such as porosity and regional mass transfer are identified. Additionally, low level radioactive waste disposal sites typically contain significant quantities of cellulose, whose hydrolysis can have a significant impact on the geochemical conditions in these sites. Those geochemical conditions, in turn, can affect radionuclide mobility and bioimmobilisation. To investigate the potentially critical role of cellulose, process-based predictive model was developed, which includes a novel approach to biomass transfer between a cellulose-bound biofilm and biomass in the bulk liquid. A sensitivity analysis of the system parameters revealed the significance of bacterial colonisation of cellulose particles by attachment through contact in solution. The thesis concludes that the processes involved in uranium bioimmobilisation are sensitive to regional residence characteristics, media porosity, surface complexation, microbial efficiency, and mass transfer under varying conditions. Careful characterisation of potential sites and use of a model that includes

these processes in sufficient detail is therefore deemed necessary before the remediation effectiveness can be reliably predicted.

Acknowledgements

Financial support for this research was provided by an Engineering and Physical Sciences Research Council (EPSRC) CASE studentship with additional funding by the Nuclear Decommissioning Authority (NDA).

The author would like to thank Prof. Andrew D. Barry and Dr. Jason I. Gerhard for their generous time and support.

The assistance of David L. Parkhurst for PHREEQC coding advice, and Joe S. Small for advice regarding geochemistry is gratefully acknowledged.

The provision of data by Prof. Mark O. Barnett (uranium adsorption data in Chapter 3), Prof. Peter R. Jaffé (model comparison data in Chapter 4), and Dr. Jiamin Wan (experimental data used for model evaluation in Chapter 4) is much appreciated.

The author is grateful to Prof. Ulrich Mayer, Prof. Roger Beckie and Prof. Leslie Smith for their generous hospitality while visiting the University of British Columbia.

The support of former Nexia Solutions Ltd (BNFL) staff members Alan Paulley, Ian Beadle and Benabdellah Tahar is appreciated, as well as University of Edinburgh staff members Prof. Mike Forde, Dr. Xiaomin Mao, Dr. Bryne Ngwenya, and Dr Robin Wardlaw.

The support of family and friends has been invaluable.

Table of Contents

List of Tables

List of Figures

Notation

a	dispersivity [L]
A	average distance between one biomass cell and another [L]
A_m	mineral specific surface area [L^2L^{-3}]
A_i	chemical formula of the i^{th} primary species
B	average distance between one cellulose particle and another [L]
B_{EA}	biomass population carrying out the terminal electron accepting process involving the respective electron acceptor [ML^{-3}]
C	concentration (subscripts *m* and *i* indicate the mobile and immobile region, respectively; other subscripts indicate chemical species) [ML^{-3}]
C_{DOC}	concentration of electron donor [ML^{-3}]
C_{EA}	concentration of electron acceptor [ML^{-3}]
C_i	initial cellulose concentration [ML^{-3}]
C_j	concentration of the j^{th} primary species [ML^{-3}]
d	diffusion capability of a cellulose particle (subscript "2") or biomass cell (subscript "1") [L^2T^{-1}]
D	hydrodynamic dispersion coefficient [L^2T^{-1}]
Da	Damköhler number
D_b	bound biomass death rate [T^{-1}]
D_e	effective diffusion coefficient [L^2T^{-1}]
D_f	free biomass death rate [T^{-1}]
Dk	dimensionless parameter group associated with microbial activity
F	cumulative spatial uraninite metric [ML^{-2}]
G	goodness of fit metric [-]
G_{arg}	argument for the shape factor W
GFW_b	gram formula weight of biofilm [$M^{-1}M$]
h	biofilm thickness [L]
h_h	hydraulic head [L]
H	Heaviside step function
J	stoichiometric coefficient for products such as acetic acid, hydrogen and carbon dioxide
k	microbial rate [T^{-1}]
k_B	Boltzmann constant [$L^2MT^{-2}K^{-1}$]
K_b	half saturation constant for cellulose hydrolysis [ML^{-3}]
K_{OC}	half saturation constant for OC species [ML^{-3}]
K_{EA}	half saturation constant for specific EA species [ML^{-3}]
K	hydraulic conductivity [LT^{-1}]
K_e	equilibrium constant
K_i	solubility product for mineral
L	length scale [L]
L_c	cellulose cylinder length [L]
m_0	initial number of moles of mineral for mineral kinetic dissolution [M]
M	remediation efficiency metric
n	arbitrary positive integer
N_c	number of cellulose particles
N_b	number of free-floating biomass cells
N_m	number of mineral phases

N_p	number of primary species
N_s	number of secondary species
O	arbitrary model output
P	probability of contact between characteristic free biomass cells and cellulose particles
Pe	Péclet number
q	source/sink term for chemical reactions (specifically for biomass in cellulose hydrolysis chapter) [ML^{-3}]
R	concentration of reaction product [ML^{-3}]
s	characteristic distance between the centres of cellulose particles and biomass cells [L]
S	function shape factor
S_{min}	minimum value which can be taken by the shape factor S
S_{max}	maximum value which can be taken by the shape factor S
t	time [T]
t_r	timescale representative of the geochemical reactions [T]
t_t	timescale representative of all transport processes [T]
T	dimensionless time
T_{c90}	time taken for cellulose to degrade to 90% of its initial concentration [T]
T_K	temperature [K]
$T_{advection}$	timescale associated with advection [T]
T_{flux}	timescale associated with volumetric flux [T]
T_j	total concentration
$T_{microbial}$	timescale associated with microbial OC fermentation [T]
$T_{transfer}$	timescale associated with mobile-immobile regional mass transfer [T]
v	pore water velocity [LT^{-1}]
v_{ij}	stoichiometric coefficient for species
V_b	maximum substrate utilization rate [T^{-1}]
W	step function
x	distance [L]
X	dimensionless distance
X_{diff}	indicator for the switch between functional states for step function W
X_b	bound biomass population [ML^{-3}]
X_{bi}	initial bound biomass population [ML^{-3}]
X_f	free biomass population [ML^{-3}]
X_{fi}	initial free biomass population [ML^{-3}]
X_i	concentration of the i^{th} secondary species [ML^{-3}]
X_{max}	maximum number of moles of biomass on the collective group of spherical cellulose particles [ML^{-3}]
y	y-coordinate
Y_b	microbial yield coefficient
Y_d	fraction of dead biomass cells recycled
z	coerror function calculation parameter
α	sticking efficiency of biomass cells
β_n	arbitrary parameter
χ_{EA}	limiting concentration of (subscripted) electron acceptor for TEAP switching, [ML^{-3}]
δ	arbitrary parameter value

ϕ	characteristic diameter of cellulose particles or biomass cells [L]
ϕ_i	initial cellulose particle diameter [L]
γ	mobile-immobile mass transfer coefficient [T^{-1}]
γ_i	activity coefficient of the i^{th} primary species
γ_j	activity coefficient of the j^{th} secondary species
μ	liquid viscosity [$ML^{-2}T$]
μ_{EA}	maximum OC fermentation (subscripted) electron acceptor [$ML^{-3}T^{-1}$]
θ_m	mobile region porosity [L^3L^{-3}]
θ_i	immobile region porosity [L^3L^{-3}]
θ_p	dimensionless parameter group associated with media porosities
θ_T	total media porosity (equal to $\theta_m + \theta_i$) [L^3L^{-3}]
θ_z	arbitrary porosity, equal to either θ_m or θ_i, depending on the region in which microbial activity takes place [L^3L^{-3}]
ρ_b	density of biofilm layer [ML^{-3}]
$\rho_{cellulose}$	density of cellulose [ML^{-3}]
ς_n	sensitivity of the model output
σ_n	dimensionless sensitivity of the model output
ω	dimensionless parameter group associated with mobile-immobile mass transfer

List of abbreviations

BNFL	British Nuclear Fuels Ltd.
DMRB	Dissimilatory Metal Reducing Bacteria
OC	Dissolved Organic Carbon
DOE	U.S. Department Of Energy
DPG	Dimensionless Parameter Group
EA	Electron Acceptor
ED	Electron Donor
FRC	Field Research Center
LLW	Low Level Radioactive Waste
MSW	Municipal Solid Waste
NABIR	Natural and Accelerated Bioremediation
SCM	Surface Complexation Model
TEA	Terminal Electron Acceptor
TEAP	Terminal Electron Accepting Process
U	Uranium

1. Introduction

Radionuclide extraction, processing and storage have resulted in a legacy of radionuclide-contaminated groundwater aquifers worldwide. Contaminant release from mining, ore extraction, nuclear fuel reprocessing or ammunitions manufacture is of serious concern in large numbers of countries (e.g., DOE, 1991; Riley et al., 1992; Folger, 1994; Landa and Gray, 1995; National Research Council, 2000; BNFL, 2002; Landa, 2004; DOE, 2007a). The scale of this problem is massive, with 4200 Department of Energy (DOE) sites contaminated with radionuclides in the USA alone (DOE, 2007b), and numerous others in Europe and the former USSR (Lloyd and Renshaw, 2005). Radionuclides may migrate through subsurface groundwater and into the wider environment, posing further risk to human health and the environment. Such sites clearly require cleanup or containment of their contaminants. Indeed, in 1978 US Federal law charged the US DOE with the responsibility for remediating former uranium (U) ore and mill tailings sites (UMTRCA, 1978).

Invasive engineered cleanup and containment strategies can negatively impact biodiversity and increase the spreading of radionuclides (Whicker et al., 2004). Further, such strategies can cost billions of US dollars (Pasternak and Carey, 1992; Hebert, 2003) and cause further environmental damage (Nelson, 2001). Passive in situ remediation strategies that utilize natural biogeochemical cycles therefore represent highly desirable containment options. An emerging remediation technology capable of this is the in-situ immobilisation of radionuclides via biostimulation of dissimilatory metal reducing

bacteria (DMRB). For this reason, the study of naturally ubiquitous DMRB has recently received increased interest (Lloyd and Renshaw, 2005). DMRB are capable of modifying the chemical form of radionuclides, thereby potentially rendering them less soluble and thus less mobile (Hazen and Tabak, 2005).

While radionuclide bioimmobilisation has been successfully demonstrated in small scale experimental studies and at the field scale, advances in understanding and optimization of the technique are needed. The success of this remediation technology is further complicated by the heterogeneous nature of subsurface porous media systems, and the uncertainties associated with them. Mass transfer processes in heterogeneous and structured porous media may significantly affect the geochemical and microbial processes taking place in contaminated sites, impacting the success of remediation.

The goal of this study is to improve the understanding of how heterogeneous porous media may affect radionuclide immobilisation efficiency through interactions with the dominant geochemical, microbial and transport processes. In order to meet this goal, a biogeochemical reactive transport model is developed for DMRB induced immobilisation of U, one of the most significant radionuclides. The model is used to explore the impact which spatial heterogeneity has on remediation efficiency. Spatial heterogeneity is conceptually represented by a dual-region model. The impacts of porous media characteristics such as porosity and regional mass transfer, as well as biological and geochemical conditions, are investigated. The relevance of different microbial media-residency preferences is surveyed, as well as the influence of surface

complexation of U to sediments. A non-dimensional sensitivity analysis is conducted to determine the optimum and adverse conditions under which bioremediation may or may not occur.

Additionally, low level radioactive waste disposal sites typically contain significant quantities of cellulose, whose hydrolysis can have a significant impact on the geochemical conditions in radionuclide contaminated sites. A process-based predictive model relevant to landfill and anaerobic digesters is developed, which includes a novel approach to biomass transfer between a cellulose-bound biofilm and biomass in the bulk liquid. Simulations explore the sensitivities of the system and reveal the significance of bacterial colonisation of cellulose particles by attachment through contact in solution.

The thesis concludes that the processes involved in these remediation strategies are sensitive to regional residence characteristics, media porosity, surface complexation, microbial efficiency, and mass transfer under varying conditions. Careful characterisation of potential sites is therefore deemed necessary before the remediation effectiveness can be reliably predicted.

This research contributes to the field of contaminant hydrogeology, particularly in the area of reactive transport modelling.

This thesis has been written in manuscript format. Chapter 2 provides a review of the relevant literature. Chapter 3 presents the development of the numerical model used in

subsequent chapters, and Chapter 4 provides model evaluation and discussion associated with evaluation related issues. Chapters 5 through 8 consist of manuscripts that have been submitted to refereed journals (see Chapter 13 for a list of submitted manuscripts). They have been modified from their submitted form to meet the needs of a thesis structure to minimise repetition and to provide a complete integrated study. Chapters 5-7 investigate various aspects of U bioimmobilisation remediation strategies and Chapter 8 focuses on cellulose hydrolysis. Chapter 9 provides a summary of the general conclusions of the research and Chapter 10 discusses future research needs in the light of this work and its conclusions.

2. Literature review

This chapter summarises the scientific literature relating to the bioremediation of radionuclides. Particular focus is given to U, which is a radionuclide of primary concern. The scientific background to remediation techniques is first given. This is followed by a discussion of existing modelling techniques and existing models used to better understand remediation technologies. Cellulose as it pertains to low level radioactive waste (LLW) landfill is also discussed. This chapter does not discuss the contribution to knowledge made by this work; this is discussed in the following chapters.

2.1. Radionuclide contamination

Radionuclides are significant groundwater contaminants worldwide, generating obvious health risks and environmental damage. Radionuclide extraction, processing and storage have resulted in a legacy of contaminated groundwater aquifers. Leaching from storage facilities and mill tailings is of serious environmental concern (Riley et al., 1992; Landa and Gray, 1995).

Uranium is one of the most significant contributors to radiological dose in the primary UK LLW waste disposal site Drigg, Cumbria (BNFL, 2002). Uranium is also the contaminant of prime concern at former U mining and milling sites (Landa, 2004). The United States Department of Energy (DOE) notes over 4200 separate subsurface sites contaminated with radionuclides across the US (DOE, 2007b) and classifies U as a high mobility contaminant in a number of these sites (DOE, 1991). Furthermore, the present

US uranium mill tailings inventory is around 220 tonnes (Landa, 2004). This is particularly significant due to the fact that the risk from U mill-associated contamination is likely to exceed that posed by high level nuclear waste after the decay of short-lived (<600 years) isotopes (Landa and Gray, 1995). Consequently, significant interest exists in the development of U containment strategies (National Research Council, 2000). Furthermore, the redox properties of U are similar to other actinides such as plutonium (Pu) and neptunium (Np) (Macaskie, 1991; Suzuki and Banfield, 1999; Lloyd and Macaskie, 2000). U is therefore an exemplar for actinide behaviour more generally.

In natural waters, U in its oxidized U(VI) state commonly forms stable aqueous complexes (e.g., carbonate, hydroxide) of high solubility and mobility (Langmuir, 1978), and is potentially toxic over long periods of time (^{238}U half-life is 4.5×10^9 yr).

2.2. Remediation of radionuclide contamination

Radionuclide and heavy metal contamination of soil is challenging due to the adsorption of radionuclides and heavy metals to subsurface media. Remediation by excavation is often expensive, impractical (due to the large volumes of material), and potentially hazardous. Capture & control strategies, using a pump-and-treat approach, do not solve the source of the problem, can be expensive in the long term, and inefficient. Further, the slow desorption of adsorbed metals mean that the addition of chemical agents is often required (e.g., acids, chelates, reductants) to improve efficiency, thereby further introducing potentially toxic chemicals into the environment (Boyle, 1993). The

traditional methods of immobilising radionuclides by the addition of cement or chemical fixatives, by capping the site, or by in situ vitrification are also expensive and render the soil unfit for future use (Cunningham et al., 1995). Alternatively, use of pump-and-treat technologies reduces excavation costs, but remains expensive and potentially inefficient.

The accumulation of toxic metals by plants, termed phytoremediation, is an alternative remediation option (Tabak et al., 2005). Phytoextraction, the removal of toxic metals by plants, and phytostabilisation, eradication of toxic metal bioavailability, are two techniques used for soil contamination (e.g. Chaney, 1997; Van der Leilie, et al., 2001; Schwitzguebel et al., 2002; Pulford and Watson, 2003; Dutton and Humphreys, 2005). Raskin et al. (1997) and Salt et al. (1998) offer comprehensive reviews of the phytoremediation.

In situ bioremediation technology presents an attractive alternative. This approach makes use of microorganisms in order to reduce, remove, or contain contaminants in water, air, soils and/or sediments. It is particularly useful for dispersed contaminant plumes over large areas and/or at great depth, present in dilute concentrations, or inaccessible due to ground cover. Additionally, it is more cost effective (Macaskie et al., 1997; Quinton et al. 1997; Lovley and Philips, 1992b).

Radionuclide and heavy metal contaminated soils, sediments and groundwater are bioremediated via microbially mediated changes in the redox or valence state of the metal or radionuclide. Such changes can modify the solubility and mobility of

radionuclides. For certain radionuclides, solubility and mobility are increased allowing for it to be flushed from the environment. In other cases, the modified metal will precipitate out of solution and be immobilised. The three primary processes by which microbes may influence the solubility and mobility of metals and radionuclides are biosorption, bioaccumulation, and biotransformation.

Biosorption describes the sorption of heavy metals and radionuclides to living or dead biomass that is independent of microbial metabolism (see McHale and McHale, 1994; Tobin et al., 1994; Volesky and Holan, 1995; Beveridge et al., 1997a,b; Lloyd and Macaskie, 2000). It includes adsorption and absorption (Gadd and White, 1989). The success of this technique depends on the stability of metal-ligand complexes in solution (Macaskie, 1991). Some work in molecular biology has focused on this technique, but to date it has not been developed as a remediation technology to any significant degree (Tabak et al., 2005).

Bioaccumulation is the metabolic-dependent process of metal ion uptake into the microbial cell. Some heavy metals and radionuclides are used by microbes in this way as chemical substitutes in transport processes. The technique has not been used commercially for bioremediation (Tabak et al., 2005), however, due to the difficulty in characterizing the uptake of radionuclides (Lloyd and Macaskie, 2000, 2002).

Bioaugmentation involves the addition of organisms to the contaminated subsurface environment. As yet, no radionuclide-contaminated sites have been proposed for

bioaugmentation and the technique has not proven any more successful in field trials than stimulation of indigenous bacterial communities (Hazen and Tabak, 2005).

Biotransformation involves the microbially mediated reduction of heavy metals and radionuclides. The biological process has been reviewed extensively by Lloyd (2003). Subsurface organisms act as catalysts of oxidation and reduction (redox) reactions by mediating the electrons transferred in the reactions (Baedecker and Back, 1979; Chapelle, 1993; Jakobsen and Postma, 1994; Kent et al., 1994; Vroblesky and Chapelle, 1994; Cozzarelli et al., 1995; Heron and Christensen, 1995). Subsurface microbial metabolism generally consists of a two-step process involving inorganic redox chemistry and organic carbon oxidation (e.g., Lovley and Phillips, 1988; McMahon and Chapelle, 1991; Chapelle and Lovley, 1992; Murphy et al., 1992; Robertson et al., 1996). In doing so they obtain a source of energy required for their maintenance and growth. Electron transfers involving oxidation and reduction are both required to complete the redox reaction. By conceptualizing the electrons (e^-) as a chemical entity, the oxidation and reduction reactions may be separated into half reactions. Each complete redox reaction is then comprised of two steps: an oxidation half reaction and a reduction half reaction. Table 2.1 shows an example oxidation half reaction (O1) and six examples of different reduction half reactions (R1-6). Combinations of these reactions (O1+R1, O1+R2, …) yield the net redox reactions that occur in the subsurface (e.g., aerobic fermentation, denitrification, Mn reduction, Fe reduction, sulfate reduction, and methanogenesis, respectively). The microbially mediated redox reactions occur in a sequence determined by their Gibbs free energy yield (e.g., Berner, 1981a; Stumm and Morgan, 1996), with

the widely accepted sequence itself based on the work of Baedecker and Back (1979a,b), Champ et al. (1979) and Nicholson et al. (1983). The resulting spatial and temporal segregation of the different terminal electron-accepting processes (TEAPs) during degradation of organic matter in sediments, referred to as redox zonation, tends to follow the accepted TEAP sequence. However, the accepted sequence is a simplified and idealized representation of redox zonation. In reality, redox zonation may be affected by a variety of hydrological and geochemical phenomena resulting in the overlap of different redox zones, allowing multiple TEAPs to occur simultaneously, although one particular redox process may dominate. This overlap of simultaneous redox reactions is observed at field sites (e.g., Berner, 1981b; Lovley and Goodwin, 1988; Kuivila *et al.*, 1989; Parkes *et al.*, 1990; Canfield *et al.*, 1993; Wersin *et al.*, 1993; Postma and Jakobsen, 1996; Jakobsen and Postma, 1999).

Table 2.1. Microbially mediated half reactions (Stumm and Morgan, 1996, p474).

Reaction Number	Reaction
O1	$CH_2O + H_2O \rightarrow CO_{2(g)} + 4H^+ + 4e^-$
R1	$0.5O_2 + 2H^+ \rightarrow H_2O$
R2	$NO_3^- + 6H^+ + 5e^- \rightarrow 0.5N_2 + 3H_2O$
R3	$MnO_2 + 4H^+ + 2e^- \rightarrow Mn^{2+} + 2H_2O$
R4	$Fe(OH)_3 + 3H^+ + e^- \rightarrow Fe^{2+} + 3H_2O$
R5	$SO_4^{2-} + 10H^+ + 8e^- \rightarrow H_2S + 4H_2O$
R6	$HCO_3^- + 9H^+ + 8e^- \rightarrow CH_4 + 3H_2O$

Subsurface microorganisms obtain energy from mediating redox reactions. The example in Table 2.1 shows the oxidation of a generic electron donor (CH_2O). Electron donors such as glucose, acetate, ethanol or H_2 may instead take the place of CH_2O. Microbes

respire the electron acceptors such as those listed in reaction R1-5 (O_2, NO_3^-, Fe(III), Mn(IV), SO_4^{2-}).

Dissimilatory metal reducing bacteria (DMRB) are microorganisms that possess the ability to use heavy metals and radionuclides as electron acceptors. Figure 2.1 shows this process diagrammatically. DMRB have been found capable of using uranium (Suzuki et al., 2003; Neal et al., 2004), selenium (Herbel et al., 2003), chromium (Roux et al., 2001; Cheung and Gu, 2003), mercury (Hobman et al., 2000), and technetium. The state and the fate of metals in the subsurface are largely determined by the redox state of the environment, which controls whether the metal will reduce or oxidize. Biotransformation represents the most promising bioremediation technique (Tabak et al., 2005). The present work therefore focuses on the process of biotransformation.

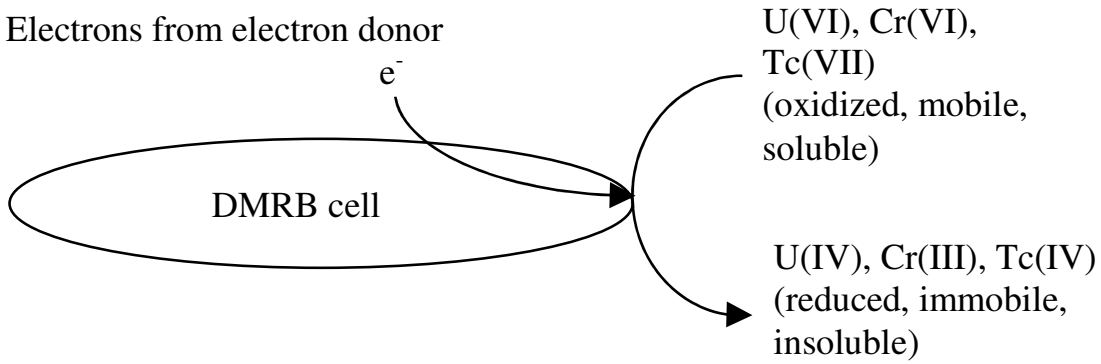

Figure 2.1. Enzymatic reduction of soluble heavy metals or radionuclides by DMRB.

Due to the significance of U (noted in Section 2.1), the specific focus of the present work is on DMRB capable of U(VI) reduction. Biotransformation causes reduction of U(VI) to the reduced U(IV) state, in which U is present as immobile uraninite (UO_2), a mineral of low solubility (Langmuir, 1978; Lovley et al., 1991). The remediation approach thereby reduces U migration in subsurface environments by precipitating and immobilising it (Abdelouas et al., 1998a, 2000; Senko et al., 2002; Anderson et al., 2003). Figure 2.2 displays bioreduced uraninite particles surrounding a bacterium.

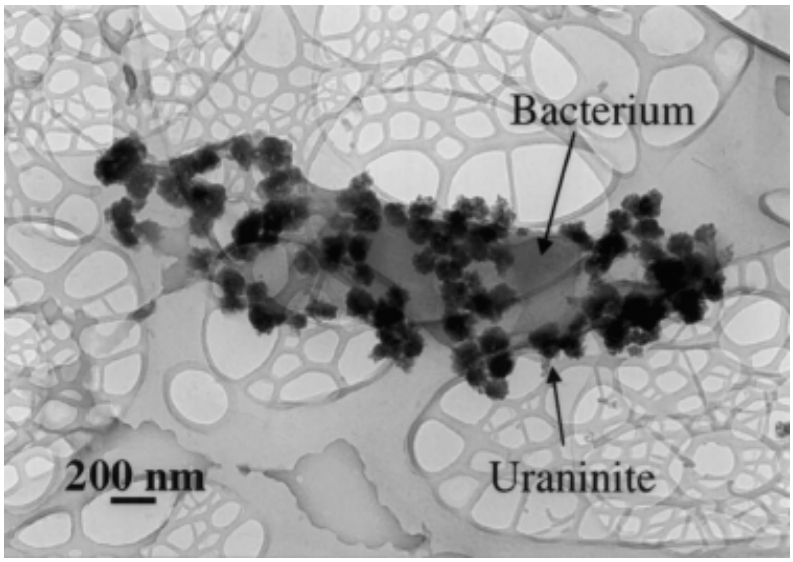

Figure 2.2. Bacterium with bioreduced uraninite mineral (from Abdelouas et al., 1998a).

The study of DMRB has recently received increased interest (e.g., Gorby and Lovley, 1992; Lovley and Phillips, 1992a; Lovley et al., 1991; Ahmann et al., 1994; Oremland et al., 1994; Lovley, 1995) due to the bacteria's ability to carry out this bioreductive process (Lovley and Philips 1992a,b). DMRB use naturally present Fe(III) and Mn(IV)

oxides in aquifers as terminal electron acceptors (TEAs) for the growth and maintenance of their populations (Wilson et al., 1993). The ability for Fe(III)- and sulfate-reducing organisms to enzymatically reduce U(VI) in laboratory cultures has been studied relatively intensively (e.g., Lovley et al., 1991; Lovley and Phillips 1992a, b; Gorby and Lovley, 1992; Lovley, 1993; Caccavo et al., 1994; Lloyd and Macaskie, 1996; Gorby et al., 1998; Tebo and Obraztsova, 1998; Lloyd et al., 2000; Chang, 2005). A further benefit of dissimilatory Fe(III) reduction within U-contaminated sediments is the potential for the Fe(II) product to potentially abiotically reduce other contaminant metals often found in concert with U in radionuclide-contaminated environments (Fendorf et al., 2000; Lloyd et al., 2000; Ortiz-Bernad et al., 2004a).

Stimulation of U(VI) reducing bacteria by addition of an electron donor (ED) - energy source - has proved successful in the laboratory. Truex et al. (1997) studied the kinetics of U(VI) reduction by a *Shewanella* strain, Liu et al. (2002a) studied the kinetics of U(VI) reduction by 4 different DMRB strains using three different EDs, and Gu and Chen (2003) studied U(VI) reduction rates and kinetic mechanisms by different natural organic matter fractions. Suzuki et al. (2005) found U(VI) to have been naturally reduced by organic matter in U-contaminated mine sediment. Suzuki et al. (2003) found *Desulfosporosinus* and *Clostridium* to be major contributors to U(VI)- and sulfate reduction in the same site, respectively. Tebo and Obraztsova (1998) found that a *Desulfotomaculum reducens* strain isolated from heavy metal contaminated sediments grew with Mn(IV), Fe(III), and U(VI) as electron acceptors (EAs). Beyenal et al. (2004) also grew sulfate-reducing bacterium as a biofilm in a flow cell through which U(VI)

was passed. U(VI) was reduced to uraninite both enzymatically and abiotically (by reacting with microbially produced H_2S).

The role of Fe and Mn oxides in U(VI) reduction has also been investigated by numerous authors (Weilinga et al., 2000; Fredrickson et al., 2000 and 2002; Childers et al., 2002; Jeon et al., 2004; Sani et al., 2005; Senko et al., 2005). DMRB are capable of aqueous U(VI) reduction in the presence of these oxides, though their efficiency may be reduced.

The reduction of U(VI) in numerous sediments has been successful in a number of studies. Abdelouas et al. (2000) investigated U(VI) reduction in groundwater from five different sites, including mill-tailing sites and those not contaminated with U. Stimulation of the sediments with ethanol resulted in oxygen, nitrate, Mn(IV) and Fe(III) reduction, with U(VI) reduction accomplished by sulfate-reducing bacteria. U(VI) reduction took place in all sediments, suggesting that DMRB were ubiquitous in both the U-contaminated and the previously uncontaminated natural environment. The work of others supports the ubiquity of DMRB (Snoeyenbos-West et al., 2000; Anderson et al., 2003; Petrie et al., 2003; North et al., 2004; Shelobolina et al., 2004).

Numerous field studies have demonstrated immobilisation of U by DMRB successfully (Finneran et al., 2002; Holmes et al., 2002; Senko et al., 2002; Anderson et al., 2003; Ortiz-Bernard et al., 2004b). U(VI) loss appears to be coincident with Fe(III) reduction (Finneran et al., 2002; Anderson et al., 2003) and occurs prior to sulfate reduction

(Holmes et al., 2002). U(VI) reduction may halt when Fe(III) is depleted and sulfate reduction becomes the dominant process (Ortiz-Bernard et al., 2004b; Anderson et al., 2003). DNA-based analyses reveal enriched Fe(III)- and U(VI) reducing bacteria species, such as *Geobacteraceae*, in the treatment zone of sites that undergo U(VI) immobilisation (Holmes et al., 2002; Anderson et al., 2003). Sorbed U(VI) appears not to be bioavailable for enzymatic reduction, however (Ortiz-Bernard et al., 2004b).

In sites where conditions are less favourable for biostimulation, groundwater adjustments may be made. For example, Wu et al. (2006b) installed a groundwater recirculation system at Area 3 of the US Department of Energy Natural and Accelerated Bioremediation Research (NABIR) Field Research Center (FRC) in Oak Ridge, Tennessee. U-contaminated groundwater was first adjusted for 2-months in order to prepare the site for biostimulation by pumping to remove aluminium, calcium and nitrate and adjust pH. Ethanol was then added to the site over a 13-month period and U(VI) significantly reduced, with a corresponding increase in solid-phase U(IV) in the sediment. Microbial analysis revealed the presence of nitrate, sulfate and iron reducing bacteria in the sediments.

Of course, for biostimulation remediation schemes to be successful it is necessary for the DMRB to be present within the site. Fortunately, DMRB appear to be ubiquitous in, and indigenous to, the subsurface (Abdelouas et al., 2000; Snoeyenbos-West et al., 2000; Röling et al., 2001; Finneran et al. 2002; Holmes et al. 2002; Anderson et al., 2003; Cummings et al., 2003; Petrie et al., 2003; North et al., 2004).

The long-term stability of U(IV) following the biostimulation of contaminated sites is of concern. It is possible for U(IV) to reoxidise after biostimulation ceases in environments where oxic groundwater enters the reduced zone (Zhou and Gu, 2005). Reoxidation of U(IV) is also possible under anaerobic conditions. For example, while nitrate is not capable of oxidizing Fe(II) (Weber et al., 2001) or U(IV) (Senko et al., 2002), nitrate-reducing bacteria produce nitrite, nitrous oxide and nitric oxide during nitrate reduction (Elias et al., 2003; Istok et al., 2004). These intermediates may abiotically oxidize Fe(II) and U(IV) (Senko et al., 2002). Complete reduction of Fe(III) may also be required to prevent Fe(III) oxidation of U(IV) (Sani et al., 2004 and 2005). Evidence of uraninite reoxidation by MnO_2 suggests that Mn(IV) may act similarly (Fredrickson et al., 2002; Liu et al., 2002b). Experimental work further suggests that carbonate-U(VI) complexes may cause reoxidation of U(IV) (Wan et al., 2005). The risk of U(IV) reoxidation is further exacerbated by the small uraninite particle size (1-3 nm) (Suzuki et al. 2002; Fredrickson et al., 2000), which may allow more rapid reoxidation. The release of reoxidised U from bioimmobilised sites may cause significantly high U concentrations downgradient of the remediated zone.

Sites in which U has been immobilised may experience a degree of U(IV) reoxidation and yet remain relatively safe, when the rate of reoxidation is slow enough to maintain U(VI) migration at acceptable levels. Indeed, evidence suggests that the presence of reduced species may contribute significantly to the long-term stability of U(IV). Abdelouas et al. (1999) found that iron-sulfide minerals protected bioreduced U(IV)

from reoxidation by oxygen and Senko et al. (2005) established that nitrate-dependent U(IV) reoxidation did not occur in the presence of reducing compounds including H_2S, Fe(II), or iron-sulfide minerals. The geochemical complexities of these systems are, however, not yet fully understood (Suzuki and Senko, 2006).

2.3. Complications due to subsurface structured porous media

While bioremediation of U has been successfully demonstrated in simple laboratory systems and in a general sense at the field scale, the processes involved in such systems may be further complicated by the interactions between geochemical, biological, and physical processes in heterogeneous and structured porous media. Natural aquifers exhibit heterogeneous and structured porous media through the existence of regions of contrasting hydraulic conductivity, such as fractured clays and rocks or sandy aquifers with frequent low permeability interbeds. Contrasting zones of low- and high- hydraulic conductivity (K), continuous fractures or disjointed sub-domains (for example, lenses) can act as preferential flow paths (see Figure 2.3), leading to interconnected networks of characteristically both high- and low-permeability material.

In such media, sorption and diffusion effects associated with the low flow regions can have significant effects on contaminant behaviour and remediation effectiveness (e.g., Sudicky et al., 198; Chapman and Parker, 2005). Porous media properties such as hydraulic conductivity can be the most limiting environmental factor in the success of remediation (Hazen and Tabak, 2005). The transfer of contaminants and injected fluids

(e.g. electron donor) between aquifer sub-domains may be controlled by diffusion processes, thereby affecting bioremediation efficiency by limiting DMRB accessibility to either the electron donor or contaminant (Luo et al., 2005; Roden and Scheibe, 2005; North et al., 2004). Bioremediation efficiency may also be reduced by induced microbial or mineralogical heterogeneity (Murphy et al., 1997; Vrionis et al., 2005; Nyman et al., 2006). The physical characteristics of sites are therefore potentially likely to significantly impact the success of this remediation technology. Wider application of radionuclide bioremediation would benefit from knowledge of how its effectiveness is influenced by heterogeneous and structured porous media systems.

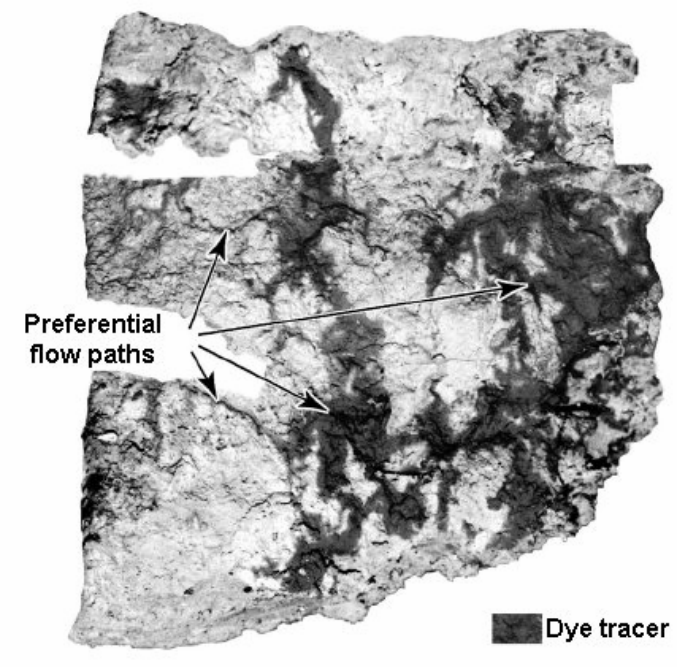

Figure 2.3. Preferential flow paths as revealed by a dye tracer (from Jørgensen et al., 2004).

2.4. Review of existing models and modelling approaches

Subsurface system modelling offers a low-cost, non-intrusive technique for gaining valuable insight into the sensitivities of, and interdependent processes in, remediation systems. Geochemical and hydrodynamic processes have traditionally been modelled autonomously, due to the fact that (i) this allows a mathematical simplification of the system and, (ii) they are traditionally categorized as separate scientific fields. Of course, these processes are interdependent in natural systems in a way that requires their coupling. This has led to the development of multicomponent biogeochemical reactive transport models. This modelling field encompasses numerous engineering and scientific disciplines such as biology, geochemistry, physics, engineering and mathematical modelling.

2.4.1. Reactive transport processes

Biogeochemical reactive transport models that deal with U(VI) immobilisation have generally developed out of the literature-rich field of subsurface biodegradation and redox modelling. This section first outlines the fundamental principles of biogeochemical reactive transport models generally, including a review of literature supporting the modelling concepts used in such models. A review of the literature focused on modelling work relevant to the present work then ensues.

Contemporary multicomponent reactive transport models may incorporate processes such as aqueous speciation, redox reactions including those that are microbially

mediated, mineral precipitation and dissolution, surface complexation, ion exchange, aqueous and gas phase transport, and colloidal transport and interactions.

2.4.2. Biogeochemical processes, modelling approaches and principles

2.4.2.1. Time and spatial scales

Most geochemical models make the reasonable assumption of local thermodynamic equilibrium. This assumes that, at the modelled scale, the dominant chemical reactions of natural waters occur at fast timescales (e.g. Westall, 1986). However, certain redox reactions and some precipitation-dissolution reactions occur at relatively slow timescales and require a kinetic modelling approach.

Whether a reaction should be modelled by equilibrium or kinetics is dependent on the relative timescales of transport processes and geochemical reactions within the system of interest. Use of a Damköhler number (Damköhler, 1936) provides a useful estimate of which modelling approach should be used for individual reactions. A general Damköhler number may be used to compare representative timescales and may be defined as:

$$Da = \frac{t_t}{t_r} \tag{2.1}$$

where t_r is the timescale representative of the geochemical reaction of interest and t_t is the timescale representative of all transport processes. Thus, if $Da >> 1$ the geochemical reaction of interest approaches equilibrium before the reacting species is transported

over the characteristic length scale (e.g. spatial discretisation length), and the geochemical reaction may therefore be modelled using an equilibrium approach (local equilibrium assumption applies). Conversely, when $Da \ll 1$, the geochemical reaction should be modelled using a kinetic approach.

The use of Damköhler numbers has its limitations. The approach requires a constant flow field and a first-order rate constant for accurate estimation, yet these may themselves vary in time. For example, the rate of mineral dissolution may vary depending on whether the mineral is near or far from equilibrium. Nevertheless, as a first estimate this approach is valuable for assessing the appropriateness of different modelling approaches. Further, the use of an equilibrium approach may be compared with use of a kinetic approach to determine whether such a choice is reasonable.

2.4.2.2. Equilibrium reactions

Speciation models are used to determine the composition of solution species at equilibrium. Speciation, complexation, acid-base, ion-exchange, and precipitation-dissolution reactions may all be modelled using this technique.

Equilibrium reaction chemistry is described extensively in the works of Stumm and Morgan (1996) and Langmuir (1997). A brief description is covered here.

Multi-component models typically use the ion-association theory of chemical equilibrium (Yeh and Tripathi, 1989). Two different approaches may be used based on the theory: the Gibbs free-energy approach (Felmy, 1990) and the equilibrium-constant approach (Wolery, 1979; Parkhurst et al., 1980; Felmy et al., 1984; Parkhurst, 1995). The Gibbs free-energy approach bases reaction activity on changes in the Gibbs free energy, a measure of the maximum available work that can be derived from any system. The equilibrium-constant approach is perhaps the most common, and formulates a set of simultaneous nonlinear algebraic equations based on the principles of mole balance and mass action (Stumm and Morgan, 1981).

Multicomponent modelling involves conceptualising complex equilibrium systems in terms of components (Aris, 1965; Westall et al., 1976; Kirkner and Reeves, 1988). Components represent independent species, such that they cannot be represented by a combination of other components. Each chemical species then comprises a combination of individual components (or master species). Chemical species may be in a dissolved, precipitated or complexed form. In a system with N_p primary species and N_s secondary species, the equilibrium chemical reactions between primary and secondary species are defined by

$$A_i \leftrightarrow \sum_{j=1}^{N_p} v_{ij} A_j \quad i = 1...N_s \tag{2.2}$$

where A_i and A_j are the chemical formulas of the primary and secondary species, respectively, and v_{ij} are the stoichiometric coefficients for the species.

The algebraic relationship between primary and secondary species may be determined by the law of mass action. This states that, at a given temperature, the equilibrium of a chemical reaction of the form

$$aA + bB \leftrightarrow cC + dD \tag{2.3}$$

may be described by

$$K_e = \frac{[C]^c[D]^d}{[A]^a[B]^b} \tag{2.4}$$

where K_e is the equilibrium constant for the reaction. The equilibrium constant may alternatively be defined

Applying this to equation 2.2 yields

$$X_i \leftrightarrow K_{e,i}^{-1}\gamma^{-1}\prod_{j=1}^{N_p}(\gamma_j C_j)^{v_{ij}} \quad i = 1\ldots N_s \tag{2.5}$$

where C_j and X_i are the concentrations of the primary and secondary species, respectively; and γ_i and γ_j are the activity coefficients of the primary and secondary species, respectively.

A total concentration, T_j, is used in the governing differential equations and is defined:

$$T_j = C_j + \sum_{i=1}^{N_s} v_{ij} X_i \tag{2.6}$$

For equilibrium dissolution–precipitation reactions, the equilibrium for a pure phase mineral is given by

$$K_i \geq \prod_{j=1}^{N_m} (\gamma_j C_j)^{v_{ij}} \quad i = 1 \ldots N_m \tag{2.7}$$

where K_i is the solubility product for the mineral and N_m is the number of mineral phases. The rate of mineral production is then non-zero only if the mineral phase is saturated in solution.

Numerical codes that calculate equilibrium reactions utilize thermodynamic databases comprised of reaction definitions, components, species, minerals and their equilibrium constants. Equilibrium reaction databases may differ and their data may itself contain uncertainties. Such differences and uncertainties may cause predictive differences in

reactive transport modelling of radionuclides (e.g., Nitzsche et al., 2000). Evaluation using independent databases may therefore be of value (Chandratillake et al., 1998).

2.4.2.3. Kinetic reactions

Most abiotic aqueous reactions occur relatively fast enough to justify an equilibrium approach. However, microbially mediated redox reactions and, under certain conditions, mineral precipitation-dissolution reactions (see Appelo and Postma, 1993; Sposito, 1994) typically occur at time scales that may be longer than transport. In such cases, these processes require a kinetic approach.

Dissolution and precipitation reactions are important as they impact chemical conditions significantly, especially pH and redox potential, significantly. Kinetic mineral dissolution-precipitation reaction rates are typically dependent on a rate constant, a reaction equilibrium constant, and the concentrations of mineral and dissolved species. Further, the reaction rate may be formulated such that it is dependent on reactive mineral surface area. Mayer et al. (2002) provide an in-depth description of kinetic dissolution and precipitation modelling approaches.

Microbially mediated redox reaction kinetics typically employ zero- or first-order rate formulations, or Monod/Michaelis-Menten models. It is the modelling approach to substrate utilization rate and biomass representation that tends to distinguish different modelling approaches. Biomass tends not to be considered in cases where the substrate

utilization rate is modelled as either a zero-order rate or first-order rate with respect to the substrate (e.g., van Breukelen et al., 1998; Jakobsen and Postma, 1999; Basberg and Engesgaard, 1999). Zero- or first-order approaches may further be appropriate when OC concentrations remain low relative to EAs. However, biomass populations experiencing inhibition effects due to toxic compounds or limited nutrient availability may render such an approach inappropriate. Such a formulation would take the form:

$$\frac{\partial C_{substrate}}{\partial t} = -kC_{substrate} \tag{2.8}$$

where k is the first-order degradation rate (T^{-1}) and $C_{substrate}$ is the concentration of substrate in solution (ML^{-3}). The substrate may be the electron donor or electron acceptor involved in the reaction.

In other cases, the rate is dependent on both the concentration of the dissolved organic carbon (OC) electron donor and the electron acceptor (e.g., Hunter et al., 1998; Brun and Engesgaard, 2002). Microbial groups are then implicitly considered, since the consumption of each specific EA is linked to a specific biomass group. (Such models typically consider consumption of the different EAs to progress according to standard TEAP sequencing.) The rate is then defined by the Michaelis-Menten kinetic formulation:

$$\theta_z \frac{\partial C_{\mathrm{DOC}}}{\partial t} = -W(C_{\mathrm{EA}}, \chi_{\mathrm{EA}})\mu_{\mathrm{EA}}\left(\frac{C_{\mathrm{DOC}}}{K_{\mathrm{DOC}} + C_{\mathrm{DOC}}}\right)\left(\frac{C_{\mathrm{EA}}}{K_{\mathrm{EA}} + C_{\mathrm{EA}}}\right) \tag{2.9}$$

where μ_{EA} is the maximum substrate utilization rate that is dependent on the EA being consumed (T^{-1}); C_{EA} is the concentration for the EA being consumed (ML^{-3}), and K_{OC} and K_{EA} are the half saturation constants for the OC and the EA being consumed (ML^{-3}), respectively. W is a basic step function which is equal to one when the concentration of the respective EA is above χ_{EA}, and equal to zero when it is below χ_{EA}. θ_z is the media porosity. When using a dual porosity approach (see Sections 2.4.4 and 3.4), θ_z may be equal to either the porosity of the mobile region, θ_m, or the porosity of the immobile region, θ_i, depending on the region in which microbial activity takes place. The number of $C/(K+C)$ terms in equation 2.9 may be extended to include other chemical species. This approach may therefore be used to account for microbial inhibition effects.

In certain cases non-growth conditions may actually better represent biodegradation at the field-scale due to substrate competition between different bacterial populations (Truex et al., 1997). Further, it may be expected that during OC injection, the degrading biomass populations attain a maximum biomass concentration (Jaffé and Rabitz, 1988). Additionally, methods of measurement for microbial rates at the field-scale such as push-pull tests (e.g., Schroth et al., 1998; North et al., 2004) generate bulk reaction rates that implicitly take account of biomass. Therefore, systems may be better represented in models that do not explicitly model biomass growth. In its favour, this approach reduces the risk of under-constraining model systems that are already difficult to characterize accurately. However, such an approach may fail to capture the lag-time behaviour sometimes associated with biomass growth. In such cases, modelling approaches that

consider the OC fermentation/utilisation rate to be dependent on biomass concentration may be more suitable.

Certain model formulations may reduce to other formulations depending on the conditions. Figure 2.4 displays the OC fermentation rate when modelled as a Monod function with a single species concentration, *C*, which may represent OC or an EA (see equation 2.9). When *C* is small relative to *K*, such a model reduces to a first-order approach (equation 2.8), and when *C* is large relative to *K*, the approach reduces to a zero-order approach.

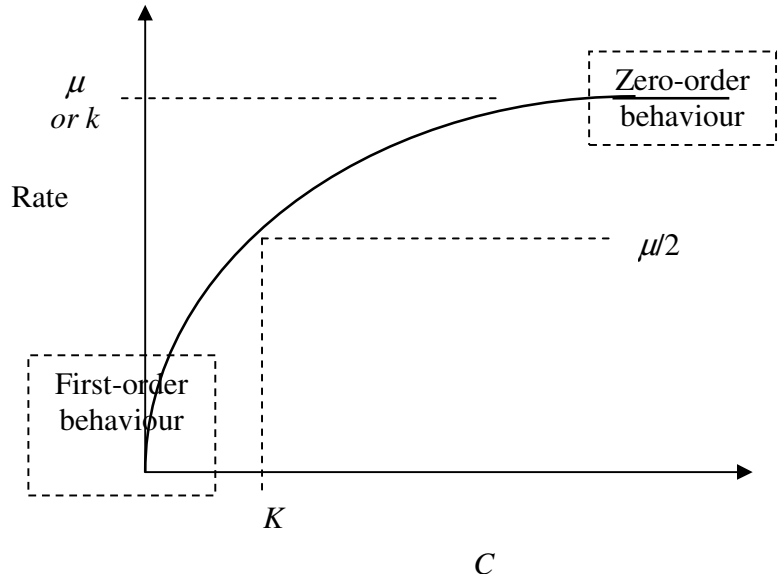

Figure 2.4. OC fermentation rate functions may reduce to different formulations depending on *C* and *K* values.

In systems in which microbial populations change, biomass may also be explicitly defined. In such cases, biomass may be modelled as a single chemical species without reference to its composition, or it may be modelled as a chemical species composed of carbon, oxygen, nitrogen, etc which reacts with other species accordingly (Barry et al., 2002). The TEAPs are considered to be on the biomass concentration (e.g. Prommer et al., 1999a,b). The rate is then defined:

$$\theta z \frac{\partial C_{\mathrm{DOC}}}{\partial t} = -W(\chi_{\mathrm{EA}})\mu_{\mathrm{EA}}\left(\frac{C_{\mathrm{DOC}}}{K_{\mathrm{DOC}} + C_{\mathrm{DOC}}}\right)\left(\frac{C_{\mathrm{EA}}}{K_{\mathrm{EA}} + C_{\mathrm{EA}}}\right)B_{\mathrm{EA}} \qquad (2.10)$$

where B_{EA} is the biomass population [ML^{-3}] carrying out the TEAP involving the respective EA. The biomass population may itself grow or decay subject to OC and EA availability. The growth and decay of biomass populations is typically formulated as dependent on the substrate utilization rate itself, and is therefore formulated as a function of the above equations. Given this approach, some authors have argued that at quasi-steady state, explicit representation of biomass is not necessary, since microbial populations are in fact dependent variables linked to substrate concentrations (Wang and Papenguth, 2001). The constant biomass (B_{EA}) is then automatically factored into the rate. Furthermore, incorporating biomass into the kinetic expressions as in equation 2.10 may yield contaminant profiles very similar to those without such incorporation (e.g. Wang et al., 2003).

2.4.2.4. Microbial representation

Microbes are typically thought to exist in one of two forms within aquifer sediments: as biofilms or as discontinuous colonies. In the biofilm form they cover the sediment surface in a continuous uniform biofilm (Rittman and McCarty, 1980; Bouwer and McCarty, 1984; Bouwer and Cobb, 1987; Taylor and Jaffé, 1990; Taylor et al., 1990). However, numerous authors have raised doubt over the biofilm concept (Baveye and Valocchi, 1989; Widdowson, 1991; Baveye and Valocchi, 1991). Such authors suggest that biofilms occur in the second form, in which they are assumed to be attached to sediment in discontinuous aggregated colonies (termed microcolonies) (Baveye et al., 1992; Chen et al., 1992). Interpretations of experimental data leading to differing conclusions concerning biofilm form are a topic of some debate (e.g. Baveye et al., 1992). Baveye and Valocchi (1989) present an evaluation, classification and comparison of existing biofilm modelling approaches. However, their work is criticized by Widdowson (1991), which was in turn responded to in Baveye and Valocchi (1991). Clearly there remains some uncertainty as to the likely spatial form of bacteria in natural aquifer sediments.

Both forms of biomass subsurface colonisation have been represented in numerical models. For example, Molz et al. (1986) and Widdowson et al. (1988) considered uniform microcolonies with constant dimensions to grow by an increase in microcolony number per unit volume of aquifer. In contrast, Kinzelbach et al. (1991) and Schäfer (1992) considered biomass as constant sized point-colonies. Chen and Li (2002) coupled transport and growth-related equations using a biofilm concept. Chen-Charpentier

(1999) considered microscopic to macroscopic upscaling for biofilm growth in a pore network model.

Thullner et al. (2004) conducted a bioclogging experiment (bioclogging entails the growth of biomass which causes a physical build-up within media pores causing decreased media). The author's experiment was conducted in a glass bead-packed flow cell and modelled the bioclogging using colony and biofilm modelling approaches. The experimental data was matched with a 3-dimensional groundwater flow and transport model (with dual region approach in which the biomass was represented by the second region). They used three different relations between hydraulic conductivity and porosity changes: a macroscopic approach (Clement et al., 1996a,b), a pore network approach (Thullner et al., 2002) for colony growth, and a pore network approach for biofilm growth. The most accurate reproduction of experimental data was achieved with a pore network approach with the colony growth approach.

Cunningham and Mendoza-Sanchez (2006) compared an "idealized biofilm model" (one-dimensional, first-order or Monod biodegradation) to a ''biofilm'' model that accounted for contaminant diffusion and reactions with the biofilm. Their analyses indicated that the two models were precisely equivalent at the macroscopic scale under steady state conditions.

Other authors do not consider diffusion between the bulk solute and the active biomass situated within the biofilm to be significant, and therefore do not represent any such

process within their models (e.g., Borden and Bedient, 1986a,b; Kindred and Celia, 1989; MacQuarrie et al., 1990; Essaid et al., 1995). Odencrantz (1992) modelled biodegradation under typical groundwater conditions using a biofilm modelling approach. Using dimensionless parameters, the author concluded that the mass transfer resistance inherent in the biofilm system was insignificant, and that a (macroscopic) Monod modelling approach could instead be used when biomass attained steady-state conditions as a result of continuous rate-limiting substrate injection.

Nevertheless, under certain conditions, such assumptions may not be made. For example, when bioclogging is significant (e.g., Vandevivre and Baveye, 1992a,b; Taylor and Jaffé, 1990; Schäfer, 1992; Clement et al., 1996a,b; Holm, 1999; Thullner et al., 2004). Furthermore, microbes may be transported in subsurface flow (e.g., Clement et al. 1997; Dorn et al., 2005) and this may assist radionuclide transport (Gillow et al., 1999). In cases where active biomass is transported this process should be accounted for and modelling of only stationary biomass populations may not be sufficient to capture system behaviour.

2.4.2.5. Microbial representation of DMRB

The microbial groups responsible for TEAPs are typically classified by the TEA pathway they take. The principal TEAPs in the subsurface are aerobic respiration, denitrification, manganese reduction, iron reduction, sulfate reduction and methanogenesis (Stumm and Morgan, 1996).

DMRB capable of U(VI) reduction encompass a range of bacterial species, including *Geobacter* (Lovley et al., 1991; Holmes et al., 2002; Finneran et al., 2002a; Anderson et al., 2003; North et al., 2004; Suzuki et al., 2005), fermentative anaerobic *Clostridium* (Francis et al., 1994), *Shewanella* (Tebo and Obraztsova, 1998; Lovley et al., 1991; Wielinga et al., 2000; Fredrickson et al., 2002), *Desulfotomaculum* (Ganesh et al., 1999) and *Desulfovibrio* (Lovley and Philips, 1992b; Sani et al., 2004; Spear et al., 2000; Suzuki et al., 2005). In addition to U(VI) reduction, DMRB have been shown to be capable of reducing nitrate (Finneran et al., 2002a), Fe(III) (Holmes et al., 2002), Mn(IV) (Tebo and Obraztsova, 1998) and sulfate (Lovley and Philips, 1992; Lovley et al., 1993; Ganesh et al., 1999; Spear et al., 2000; Sani et al., 2004; Suzuki et al., 2005).

Most groundwater sediments are host to a variety of microbial species which are, collectively, capable of carrying out the full range of TEAPs (in DMRB-related studies see, for e.g., Anderson et al., 2003; North et al., 2004; Suzuki et al., 2005). The dominant microbial consortium is likely to change as the electron acceptors (EAs) utilized by each bacterial group are progressively depleted (Anderson et al., 2003).

2.4.2.6. Partial equilibrium approach

Of the two redox steps discussed in Section 2, the first involves the fermentation of dissolved organic carbon (OC) which yields products such as acetate, formate and H_2. The fermentation products are consumed as electron acceptors (EAs) by different TEAPs. Since the energy yield from the fermentation step is relatively small, the differences in energy yield largely result from the second TEA step (Postma and Jakobsen, 1996). It is generally accepted that the net reaction is limited by the fermentation step (e.g., Berner, 1980; Westrich and Berner, 1984; Middelburg, 1989; Boudreau and Ruddick, 1991). This is supported by the brief presence and low concentrations of the intermediate fermentation products, suggesting that the TEA step is much faster than the fermenting step. Of the two steps in each net reaction, fermentation is therefore rate-limiting, and the net reaction kinetics cannot be determined by the net energy yield. Rather, the first fermentation step is defined kinetically, and the path of the second TEA step is determined by chemical equilibrium (the energy yield of the TEA step) (Postma and Jakobsen, 1996).

The individual TEAPs are considered to occur in a sequence determined by their Gibbs free energy yield (e.g., Berner, 1981a; Stumm and Morgan, 1981), with the widely accepted TEAP sequence itself based on the work of Baedecker and Back (1979a,b), Champ et al. (1979) and Nicholson et al. (1983). The resulting spatial and temporal segregation of the different TEAPs during degradation of organic matter in sediments, referred to as redox zonation, tends to follow this accepted TEAP sequence. However, the accepted sequence is a simplified and idealized representation of redox zonation. In

reality, redox zonation may be affected by a variety of hydrological and geochemical phenomena resulting in the overlap of different redox zones, allowing multiple TEAPs to occur simultaneously, although one particular redox process may dominate. This overlap of simultaneous redox reactions is observed at field sites (e.g., Berner, 1981b; Lovley and Goodwin, 1988; Kuivila et al., 1989; Parkes et al., 1990; Canfield et al., 1993; Wersin et al., 1993; Postma and Jakobsen, 1996; Jakobsen and Postma, 1999).

To account for the fact that TEAPs are driven by a kinetic first-step and a chemical equilibrium second step, Postma and Jakobsen (1996) recommended use of a partial redox disequilibrium approach modelling approach or Partial Equilibrium Approach (PEA). The PEA was proposed by McNab and Narasimhan (1994) and was further used by, amongst others, McNab and Narasimhan (1995), van Breukelen et al. (1998), Keating and Bahr (1998), Jakobsen and Postma (1999), Prommer et al. (1999a,b) and Brun et al. (2002). The oxidation of organic matter (fermentation) is assumed to be the rate-controlling step and is represented by a kinetically controlled release of zero-valent carbon into solution. The second (equilibrium) step, controlling the TEAP's sequence, occurs instantaneously. This approach allows for simultaneous redox reactions, without violation of thermodynamic laws, and for the straightforward modelling of abiotic processes.

2.4.2.7. Surface complexation

Most surface-chemical processes involve adsorption, which entails the accumulation of substances at the solid-water interface. Adsorption influences the aqueous distribution of

species, the reactivity of surfaces, and the electrostatic properties of suspended particles such as colloids. Surface complexation reactions are primarily responsible for U sorption. This discussion will therefore focus on surface complexation with relevance to U. At typical groundwater pH, U(VI) transport is affected by adsorption to mineral surfaces in soils and sediments (Waite et al., 1994; Kohler et al., 1996; Turner et al., 1996; Pabalan et al., 1998; Chisholm-Brause et al., 2001; Prikryl et al., 2001; Barnett et al., 2002; Davis et al., 2002). Clay-rich sediments may bind U(VI) by ion exchange, but this is limited by specific aqueous conditions such as low ionic strength, low pH and low Ca concentrations (Turner et al., 1996). Mineral surface complex formation exerts the most significant control over U sorption (Pabalan et al., 1998).

The most common reactive transport modelling approach for surface complexation is the use of constant distribution coefficients (constant-K_d) (USEPA, 1999; Bethke and Brady, 2000). However, U(VI) adsorption is significantly influenced by pH and carbonate concentration, as well as changes in aqueous speciation (Dzombak and Morel, 1990; Waite et al., 1994). Constant-K_d modelling approaches are relevant to specific chemical conditions and cannot account for these effects. Consequently, use a constant-K_d modelling approach for U may lead to significant uncertainly in the predicted retardation due to changes in pore water chemistry (Read et al., 1998; Bethke and Brady, 2000; Glynn, 2003).

Surface complexation models (SCM), however, account for pH changes, the effect of variations in solution chemistry, and the complexing properties of sorbing surface sites

(Waite et al., 1994; Langmuir, 1997; Pabalan et al., 1998; Kohler et al., 1999; Koretsky, 2000; Davis, 2001; Davis et al., 2002). This is achieved by describing the equilibria between aqueous species and mineral surfaces species through mass action equations (Bargar et al., 2000; Sylwester et al., 2000; Alcacio et al., 2001; Becker et al., 2001; Brown and Parks, 2001; Sverjensky, 2001). SCM models assume adsorption occurs on specific surface sites, allowing for a number of specific sites to be utilized by the sorbent. Such an approach allows SCMs to be easily incorporated into existing reactive transport models (Kohler et al., 1996; Stollenwerk, 1998; Papini et al., 1999; Kent et al., 2000; Parkhurst et al., 2003; Curtis et al., 2004). Detailed discussion of various surface complexation modelling approaches may be found in Stumm and Morgan (1996) and Langmuir (1997).

Natural organic matter may also play a role in U(VI) sorption (Wood, 1996; Lenhart and Honeyman, 1999). However, OC-complexed U is not included in this work. OC-complexed U is considered insignificant in facilitating U transport where OC concentrations are high (Farquhar and Sykes, 1982; Kjeldsen and Christensen, 1984; Kjeldsen, 1986; Ranville et al., 2006). Since OC concentrations are typically high in biostimulation schemes, such as in this work, OC-complexed U is considered negligible.

2.4.3. Modelling mass transport

Macroscopic conservation of mass for the transport of a dissolved species in one-dimensional space is given by:

$$\frac{\partial C}{\partial t} = -v\frac{\partial C}{\partial x} + D\frac{\partial^2 C}{\partial x^2} + \frac{\partial q}{\partial t} \tag{2.11}$$

where C is the concentration of a chemical species in solution (ML^{-3}), v is the average pore-water velocity in the mobile region (LT^{-1}), D is the hydrodynamic dispersion coefficient (L^2T^{-1}), $\partial q/\partial t$ is a source/sink term that accounts for chemical reactions ($ML^{-3}T^{-1}$), x is the distance along the spatial domain (L), and t is time (T). The chemical species C may experience advective and dispersive transport within the fluid. The advection term describes the transport of the species by the groundwater velocity, as driven by a pressure gradient. The dispersion term describes the process of the spreading and dilution of the species as it is transported. This term itself consists of both mechanical and molecular diffusion, and is thus defined:

$$D = D_e + av_m \tag{2.12}$$

where D_e is the effective diffusion coefficient (L^2T^{-1}) and a is the dispersivity (L). Mechanical dispersion is the result of small changes in flow direction away from the mean flow direction for portions of the flow. Molecular diffusion is caused by the process of Brownian motion which causes molecules to respond to a concentration gradient. The relative importance of dispersion to diffusion is typically governed by hydraulic conductivity, with the former dominating in high-K materials (e.g., sands) and the latter dominating in low-K media (e.g., clays). The macroscopic pore water velocity, v, is defined by Darcy's law:

$$v = \frac{K \partial h_h}{\theta \ \partial x} \tag{2.13}$$

where K is the hydraulic conductivity (LT^{-1}) and h_h is the hydraulic head (L). This model assumes that the porous media and flowing solution may be represented as a continuum. The continuum must apply for averaged processes within a representative elementary volume (Bear, 1972; Hassanizadeh and Gray, 1979a,b; Lichtner, 1996a).

2.4.4. Modelling porous media spatial heterogeneity

Spatial heterogeneity has been represented in models using various approaches. Small-scale heterogeneities associated with media structure are perhaps most commonly modelled using a continuum approach. Models can explicitly account for spatial variability in physical porous media by spatially varying properties such as hydraulic conductivity (Steefel and Yabusaki, 1996; Meile et al., 2003). The basic continuum approach has been extended to multi-region and multi-continuum approaches. For example, a two-region (also termed dual-region or dual-porosity) model may be used to represent heterogeneity (van Genuchten and Wierenga, 1976). This is a well-established technique (c.f., Gardner and Brooks, 1957; Barenblatt et al., 1960; Deans, 1963; Coats and Smith, 1964) that represents heterogeneities by the introduction of mass transfer processes. Typically, one region represents media regions of advective-dominated flow within the media while the other region represents media regions of diffusion-dominated (stagnant or immobile) flow. The technique has been applied to the modelling transport

in structured soils or fractured porous media (Skopp and Warrick, 1974; van Genuchten et al., 1974; Selim et al., 1977; van Genuchten and Wierenga, 1977; Rao et al., 1979, 1980; Grisak and Pickens, 1980; Grisak et al., 1980; Huyakorn et al., 1983; Nkedi-Kizaa et al., 1983; Goltz and Roberts, 1986; Herr et al., 1989; Haselow and Greenkorn, 1991; Gerke and van Genuchten, 1993; Zimmerman et al., 1993; Brusseau et al., 1994; Li et al., 1994; Haggerty and Gorelick, 1995, 1998; Hamm and Bidaux, 1996; Hu and Brusseau, 1996; Bajracharya and Barry, 1997; Hantush and Marino, 1998; Zhang and Brusseau, 1999; Feehley et al., 2000; Harvey and Gorelick, 2000; Stagnitti et al., 2001; Sánchez-Vila and Carrera, 2003; Haws et al., 2004, 2005). Griffioen et al. (1998) provide a review of data requirements for this modelling approach. Modelling systems with heterogeneous hydraulic conductivity employing two-region mass transfer approaches has more successfully reproduced observed solute transport behaviour than classical Fickian advection-dispersion formulations (e.g. Feehley et al., 2000).

The multi-region modelling approach has also been modified to consider convection and dispersion mechanisms in all regions within the model (Skopp et al., 1981; Dykhuizen, 1990; Gerke and Van Genuchten, 1996; Ahmadi et al, 1998; Gwo et al., 1998; Vogel et al., 2000; Zinn and Harvey, 2003; Zinn et al., 2004; Van Genuchten et al., 2001). These are often multi-continuum approaches (e.g., Gwo et al., 1995, 1996), in which each region possesses unique boundary conditions and hydraulic conductivity (Dykhuizen, 1987; Liu and Chen, 1990; Jarvis et al., 1991; Gerke and van Genuchten, 1993; Gwo et al., 1994 and 1995). The dual-permeability approach may also be extended to a 2D system, thereby including spatial variability of hydraulic properties and preferential flow

phenomena (Vogel et al., 2000). The approach has been further expanded to capture more complex systems by including multiple mass transfer rates (i.e., a distribution of rate coefficients) (Haggerty and Gorelick, 1995; Haggerty et al., 2000; Dentz and Berkowitz, 2003). The parameters used in these models are typically extracted from experimental data using curve-fitting methods (Gaudet et al., 1977; Grisak and Pickens, 1980; Goltz and Roberts, 1988; Maraga, 2001; Johnson et al., 2003). Further, Ahmadi et al. (1998) and Cherblanc et al. (2003) present an approach that allows connection between different scales and the acquisition of macroscopic properties associated with heterogeneous dual-porosity systems.

Discrete fracture network models have also been used to represent spatial heterogeneity in the subsurface (e.g., Sudicky and McLaren, 1992; Therrien and Sudicky, 1996; Berkowitz, 2002). Governing equations are provided for both the porous matrix and the fracture network, with the factures idealized as two-dimensional parallel plates.

Stochastic approaches (for example, by using autocorrelated random fields) are a further alternative modelling approach (e.g., Sposito and Barry, 1987; Kabala and Sposito, 1991; Srivastava and Brusseau, 1996). Stochastic approaches typically model hydraulic conductivity as random (log normally distributed), and the governing model flow equation becomes a stochastic differential equation. However, the computation speeds required for uncertainty analysis in stochastic approaches may limit their applicability (e.g., Spycher et al., 2003).

Yet other approaches include particle tracking, in which the pore water velocity flow field determines the motion of the solute (e.g., Tompson et al., 1988), or the use of fractal theory (Wheatcraft and Tyler, 1988).

2.4.5. Coupling method

One of two methods is typically used to couple the solving of physical transport and geochemical reactions in reactive transport models. The first is the global implicit formulation, and the second is the operator splitting formulation (Engesgaard and Christensen, 1988; Yeh and Tripathi, 1989; Saaltink et al., 2001). The global implicit method solves physical transport and geochemical reactions simultaneously while the operator splitting technique solves the two sequentially (the latter may or may not involve iteration between the two steps) (Steefel and Lasaga, 1994; Walter et al., 1994). The former is more accurate (typically second order in time) but is more computationally expensive, while the latter is more efficient but with first-order accuracy (Barry et al., 2002).

2.4.6. Existing reactive transport models

Reactive transport models covering redox processes and the biodegradation of organic matter have been a focus of research for decades. Many models couple the simulation of transport with equilibrium geochemistry (e.g., Miller and Benson, 1983; Cederberg et al., 1985; Hostetler and Erickson, 1989; Narasimhan et al., 1986; Liu and Narasimhan, 1989a,b; Griffioen, 1993; Yeh and Tripathi, 1991; Cheng, 1995; Parkhurst, 1995;

Parkhurst and Appelo, 1999). Early models may have been limited to a single redox process (e.g., Kinzelbach et al., 1991), or have ignored microbial complexities or secondary redox reactions (reactions in which reduced species may be reoxidised). Further development yielded models that accounted for secondary redox reactions (e.g., Schäfer, 1992) as well as multiple microbial groups and EA consumption (e.g., Lensing et al., 1994). Models have been developed to couple transport with numerous kinetic geochemical reactions such as adsorption (e.g., Theis et al., 1982; Szecsody et al., 1998), redox processes (Lensing et al., 1994; Wang and Van Cappellen, 1996; Hunter et al., 1998; Smith and Jaffé, 1998; Saiers et al., 2000), biodegradation processes (MacQuarrie et al., 1990; Chen et al., 1992; Chang et al., 1993; Cheng and Yeh, 1994; Wood et al., 1994) or precipitation-dissolution (e.g., Lichtner, 1996; Steefel and Yabusaki, 1996; Suarez and Šimůnek, 1996). Essaid et al. (1995) presented an extensive summary of such pre-1995 models. Since the mid-1990s, models that couple transport with equilibrium and kinetic reactions have been developed (e.g., Steefel and Lasaga, 1994; McNab and Narasimhan, 1994, 1995; Chilakapati, 1995; Salvage et al., 1996; Yeh et al., 1996; Abrams et al., 1998; Chilakapati et al., 1998; Saaltink et al., 1998; Tebes-Stevens et al., 1998; Salvage and Yeh, 1998; Chilakapati et al., 2000; Robinson et al., 2000; Yeh et al., 2001a and b; Brun and Engesgaard, 2002; Molins et al., 2004; Kräutle and Knabner, 2005). More recent techniques implement “reaction-network” based modelling (Fang et al., 2003; Zhang et al., 2007). This approach uses matrix methods to derive governing equations that model mixed equilibrium and kinetic reactions by transforming reactive transport equations into a set of thermodynamic equilibrium equations (for equilibrium reactions) and a set of reactive transport equations for kinetic variables.

Partial differential equations for kinetic-variables are then solved rather than individual chemical species.

Reactive biogeochemical transport models have tended to either add geochemical reactions to biodegradation transport models or add simple biodegradation reactions to geochemical transport models (Brun and Engesgaard, 2002).

McNab and Narasimhan (1994), Brun et al. (1994) and Lensing et al. (1994) used a partial redox disequilibrium (or partial equilibrium approach (PEA)) in which the OC fermentation step was kinetically controlled and the TEA step was equilibrium controlled. Such an approach would, for example, model the oxidation half reaction O1 in Table 2.1 kinetically and the reduction half reactions R1-6 (Table 2.1) based on equilibrium thermodynamics. Such an approach considers the "two steps" of reduction and oxidation involved in redox reactions separately. This enables the simultaneous modelling of complex geochemical reactions and kinetic biodegradation reactions, as well as allowing use of existing equilibrium databases, and is also faster to solve than a fully kinetic approach. Further, robust and consistent equilibrium databases exist, whereas kinetic databases remain comparatively incomprehensive and are highly dependent on geochemical conditions. These factors have doubtless led to the widespread popularity of this technique (van Breukelen et al., 1998; Keating and Bahr, 1998; Jakobsen and Postma, 1998; Basberg and Engesgaard, 1999; Prommer et al., 1999a,b). Fully kinetic approaches model net redox reactions kinetically. The net reaction resulting from a combination of, for example, reactions O1 and R1 in Table 2.1

would be represented as a single reaction. Such an approach might be termed “one step”, since only single net reactions exist. Other authors have retained a kinetic approach but allowed the OC fermentation step to be explicitly decoupled from the TEA step (Hunter et al., 1998).

A number of relatively comprehensive numerical codes now exist capable of carrying out a host of geochemical processes coupled to transport. These include, but are not limited to, the codes MT3D (Zheng, 1990), RT3D (Clement, 1997), MT3DMS code (Zheng and Wang, 1999), PHREEQC (Parkhurst and Appelo, 1999), MIN3P (Mayer, 1999), HydroBioGeoChem 123D (ORNL, 1999), PHT3D (Prommer, 2000), PHAST (Parkhurst et al., 2004), and PHWAT (Mao et al., 2006).

In radionuclide-contaminated environments, the interest is in the geochemical environment and its impact on radionuclide solubility and mobility. Such a focus may therefore also lead to the development of models that focus on the geochemical environmental changes due to biodegradation processes (e.g., Manton et al., 1995; Humphreys et al., 1997).

As discussed in Section 2.3, porous media spatial structure and heterogeneity may significantly affect the success of bioremediation techniques. Unfortunately, while many models can account for spatial variability by means of variable hydraulic conductivity and other parameters, few multicomponent reactive transport models actively account for spatial heterogeneity (van der Lee and De Windt, 2001). Further, Meile et al. (2003)

included an explicit representation of physical heterogeneity in their reactive transport model, while Malmstrom et al. (2004) coupled a stochastic advective-reactive model with random heterogeneity to a multicomponent geochemical code. Huang and Hu (2001) used a stochastic reactive transport model which accounted for physical and chemical heterogeneity with interregional mass diffusion and nonequilibrium sorption processes.

2.4.7. Existing reactive transport models incorporating radionuclide redox chemistry

Contemporary reactive transport models that account for microbially mediated redox reactions are generally built as extensions of existing reactive transport models. Nevertheless, numerous reactive transport models that do not account for microbially mediated redox reactions, at least in their applications, have been used to explore radionuclide migration in subsurface environments without a specific focus on microbial mediation. For example, the multicomponent reactive transport code TOUGHREACT (Xu et al., 2000) has been used to explore radionuclide migration and issues related to radioactive waste disposal for the Yucca Mountain Project (e.g., Xu et al., 2003; Spycher et al., 2003). De Windt et al. (2003) compared three different reactive transport codes for UO_2 dissolution by rainwater infiltration and spent fuel degradation in an oxidising waste disposal. Chen and Yiacoumi (2002) modelled the sorption and transport of depleted U. De Windt et al. (2004) included cement/claystone interactions in their modelling of radionuclide migration in an intermediate-level radioactive waste

repository. Bain et al. (2001) used a model to evaluate the potential groundwater contamination effects of flooding in a decommissioned U mine.

Other work has focused on the modelling of natural analogue sites in order to better understand the likely geochemical and transport processes which might occur within U contaminated (waste disposal) sites over the long term (e.g., Salas and Ayora, 2004; Steefel and Lichtner, 1998; Gurban et al., 2003). However, such models tend not to consider microbially mediated redox reactions. Besides, other authors (Read and Hooker, 1992) caution that such exercises should be limited to the observation of net geochemical effects. It is further argued that the quantitative evaluation of models using natural analogue data is unrealistic due to the complexity of the system, the difficulty in limiting boundary conditions (Amter, 1989), and the fact that no single natural analogue may be convincingly compared to engineered waste repositories (Read and Hooker, 1992).

The inclusion of microbially mediated redox reactions are particularly important for the modelling of radionuclide migration, since microorganisms are both directly involved in redox reactions (see Section 2.2) and more generally control the chemical conditions in groundwater such as pH, Eh, CO_2 and secondary mineral precipitation/dissolution phenomena (Van Cappellen and Wang, 1996; Hunter et al., 1998) which in turn effect radionuclide speciation.

Several studies have coupled radionuclide redox chemistry and microbially mediated redox reactions to existing reactive transport models. Applications using such models may be particularly appropriate for improving understanding of U(VI) bioremediation strategies. Wang and Papenguth (2001) extended the kinetic biogeochemical transport model of Hunter et al. (1998) to include radionuclide redox chemistry and modelled the injection of a generic electron donor into an anoxic aquifer through which U(VI) was passing. The authors reported on the geochemical changes to the aquifer after 15 years of biostimulation. Wang et al. (2003) developed a biogeochemical transport model using the PEA and kinetic mineral precipitation/dissolution, with kinetically modelled U redox reactions. The authors modelled an aquifer contaminated by U(VI) influent and conducted a global uncertainty assessment on the system in order to identify parameter sensitivities (for primary and secondary redox reaction rates).

Very few reactive transport models incorporating radionuclide redox chemistry have accounted for the spatial heterogeneity of porous media. Luo et al. (2007) used a kinetic one-dimensional dual-porosity model to reproduce geochemical data in a well from the field-scale U(VI) bioremediation experiment conducted by Wu et al. (2006b). However, their model used the "immobile" region in the model to account for mass transfer processes associated with surface complexation rather than spatial heterogeneity. Further, the work of Huang and Hu (2001) has highlighted the importance of separating interregional mass transfer (diffusion) and chemical sorption processes into separate mass transfer processes. Roden and Scheibe (2005) used a one-dimensional tri-porosity (i.e. three-region) model to explore the feasibility of biomineralisation of U(VI) in

structured porous media (fractured rock). However, they used a one-step fully kinetic model rather than a multicomponent reactive transport model, thereby excluding potentially important geochemical processes (including, but not limited to, redox reactions).

A list of biogeochemical reactive transport models is given in Table 2.2. The presence (or lack) of several key modelling features is noted for each model listed.

Table 2.2. List of biogeochemical reactive transport models and their features.

Reference	CM[a]	MK[b]	EB[c]	SD[d]
Kinzelbach et al. (1991)	1	M	Y	2
Lensing et al. (1994)	1	M	Y	1
McNab and Narasimhan (1994, 1995)	2 PEA	1	N	2
Essaid et al. (1995)	1	M	Y	2
Griffioen et al. (1995)	2 PEA	1	N	2
Schäfer and Therrien (1995)	1	M	Y	3
Steefel and Yabusaki (1996)	N/I	N/I	N	3
Wang and Van Cappellen (1996)	1	1	N	1
Schäfer et al. (1998a,b)	1	M	Y	3
Abrams et al. (1998)	1	M	N	2
Tebes et al. (1998)	1	M	Y	1
Salvage and Yeh (1998)	1	M	Y	1
Smith and Jaffé (1998)	2 PEA	M	N	1
Chilakapati et al. (1998)	1	M	Y	1
Amirbaham et al. (1998)	1	0	N	1
Hunter et al. (1998)	2 K	1	N	1
van Breukelen et al. (1998)	2 PEA	1	N	1
Keating and Bahr (1998)	2 PEA	0	N	2
Jakobsen and Postma (1998)	2 PEA	0	N	1
Basberg and Engesgaard (1999)	2 PEA	0	N	1/2/3
Prommer et al. (1999a,b)	2 PEA	M	Y	1/2
Abrams and Loague (2000a,b)	1	M	N	2
Brun et al. (2002)	2 PEA	M	Y	2
Wang and Papenguth (2001)	2 K	M	N	1
Wang et al. (2003)	2 PEA	M	N	1
Roden and Scheibe (2005)	1 K	M	Y	1
Thullner et al. (2005)	1	M	Y	1
Luo et al. (2007)	1 K	M	Y	1
this work	2 PEA	1 & M	N	1

[a]CM = Coupling Method; 1 or 2 step (see this Section), K – Kinetic (see Section 2.4.2.3), PEA – Partial Equilibrium Approach (see Section 2.4.2.6), N/I – Not Included in model.

[b]MK = Microbial Kinetics approach; 0 or first-order (0/1) or Monod (M) kinetic approach (see Section 2.4.2.3).

[c]EB = Explicit Biomass modelled; Y – Yes, N – No (see Section 2.4.2.3).

[d]SD = number of Spatial Dimensions.

2.5. Cellulose in low level radionuclide contamination

Cellulose is a sizeable component of the material deposited into municipal solid waste (MSW) and low-level radioactive waste (LLW) disposal sites (BNFL, 2002; Bookter and Ham, 1982). It is present in the form of paper, cardboard, wood and fabrics and undergoes enzymatic hydrolysis in situ by microbes in such anaerobic environments, the products of which become substrates for subsequent microbial groups such as methanogens, acetogens and acidogens (El Fadel et al., 1997). These processes may cause geochemical changes in the disposal site. In LLW sites, such changes can affect the solubility of radionuclides that, once mobilized, may then migrate in the groundwater (Humphreys et al., 1997; Askarieh, 2000). Enhanced cellulose hydrolysis leads to more rapid stabilization of the landfill site and a decrease in the leaching of organic acids. The rate of cellulose hydrolysis, and that of the subsequent microbial processes, is therefore important in determining the stability of landfill sites and their potential impact on the environment (Eleazer et al., 1997).

Additionally, the anaerobic digestion of the organic fraction of MSW is now a common ex situ treatment for landfill waste/leachate (de Baere, 2000; Mata-Alvarez et al., 2000; O'Keefe and Chynoweth, 2000). Cellulose hydrolysis is also more generally relevant to sequential leach bed anaerobic processing, which has also been applied to treat putrescible fractions of MSW (Chynnoweth et al., 1992; Chugh et al., 1999), and

wastewater treatment systems (e.g., Batstone et al., 2000). The key processes occurring at the microscale in such anaerobic digesters are identical to those occurring in landfill.

The presence of cellulose-bound cellulolytic bacteria in landfill sites is significant. For example, Lockhart (2004) found numerous cellulolytic clostridia strains in an LLW site and noted that conditions in the site were suitable for a wide diversity of clostridia. The clostridia are well known for their extracellular multi-enzyme complex called cellulosome (Schwarz, 2001) which binds the cells to crystalline cellulose particles (Bayer et al., 1983; Lamed et al., 1987; Mayer et al., 1987). Figure 2.5 displays a portion of a cellulose fibre coated and then stripped of cellulose hydrolyzing bacteria.

The most common approach to modelling cellulose hydrolyzing bacteria involves approximating the hydrolysis as a zero- or first-order, biomass-independent reaction (e.g., Gusakov and Sinitsyn, 1985; Humphreys et al., 1997; Bezerra and Dias, 2004). Other models have explored methods for incorporating the effects of biomass-substrate binding in the cellulose hydrolysis process. Nopharatana et al. (2003) developed a model that recognized the association between biomass and hydrolysis rate. Lai et al. (2005) presented a model in which biomass grew until it approached a limiting value at which substrate coverage was reached. Vavilin et al. (1996) developed a model that incorporated colonisation of cellulose particles by a pre-existing cellulose-bound bacterial population, with the associated progressive reduction in particle size as the cellulose hydrolyzed. Other models have investigated the hydrolysis process on an

enzymatic level (e.g., Movagarnejad et al., 2000; Gan et al., 2003; Movagarnejad et al., 2003), considering the binding mechanisms of enzymes to the cellulose substrate.

The simplifying assumptions of existing models, issues related to cellulose hydrolysis, and importance of parameters and processes in the modelling of cellulose degradation is dealt with in Chapter 8.

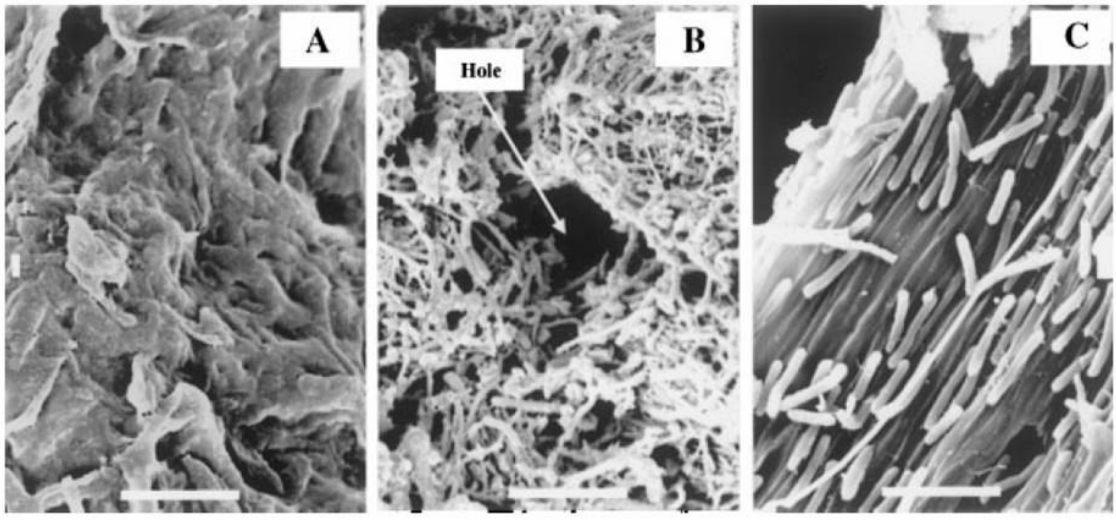

Figure 2.5. Cellulose fibre covered with biofilm (A), a hole in the biofilm (B) and the fibre stripped of most bacteria (C) (from Song et al., 2005).

3. A one-dimensional biogeochemical reactive transport model for bioimmobilisation of U(VI) in heterogeneous and structured porous media

3.1. Introduction

The impact of media heterogeneity is explored in the present work via a biogeochemical reactive transport model that accounts for the key physical and biogeochemical processes involved. This chapter discusses the development of a one-dimensional biogeochemical reactive transport model built for the purpose of modelling the bioimmobilisation of U(VI) in single and dual porosity media. The chapter first discusses the biogeochemical aspects of the model, followed by the transport features and surface complexation model. Model discretisation and model assumptions are then detailed.

3.2. Theoretical background and model development

A conceptual model for biomineralisation of U(VI) by DMRB is developed here in order to explore the efficiency of U(VI) remediation by DMRB in porous media exhibiting both single and dual porosity behaviour. The model is built in the widely used and fully verified USGS code PHREEQC (Parkhurst and Appelo, 1999), and couples 1D advective-dispersive solute transport with a comprehensive set of aqueous speciation, precipitation/dissolution and primary and secondary redox reactions included in the MINTEQA2 4.00 chemical database (Allison et al., 1991). The transport equation is solved with an explicit finite difference scheme. The coupling approach is split-operator,

except that unlike most reactive transport models (Yeh and Tripathi, 1989), the kinetic and equilibrium reactions are calculated after both the advection and the dispersion step. This is performed to reduce numerical dispersion.

A flow path (one-dimensional) system is considered as an appropriate first step towards simulating and understanding such complex systems. Due to its free availability and the U.S. Geological Survey's development and application of the PHREEQC code, the code has been tested in numerous applications and used in modelling work reported in numerous publications. It is a verified and reliable code that can be used with confidence in model development.

3.3. Biogeochemical model

3.3.1. Microbial representation

The model employs the PEA (see Section 2.4.2.3). The model assumes the presence of a host of microbial species which are collectively capable of carrying out the full range of TEAPs (in DMRB-related studies see, for e.g., Anderson et al., 2003; North et al., 2004; Suzuki et al., 2005). This approach is considered to capture system behaviour adequately in the majority of sites.

The explicit modelling of microbial processes requires microbial yield factors and rate constant for growth and decay to be specified. However, the values of these parameters are poorly constrained by field or laboratory experiments (Gasol and Duarte, 2000). For these reasons the model presented here models only the substrate utilisation processes carried out by the biomass, and does not explicitly model the biomass itself (i.e., biomass concentration is not considered). As this modelling approach reduces the number of parameters required, the risk of under- or over-constraining the model system is reduced.

It should be noted that modelling microbial processes without explicitly considering biomass concentration implicitly assumes that biomass growth is insignificant. The model therefore implicitly assumes that the biomass is in a quasi-steady-state condition. This may be inappropriate when representing systems in which biomass growth is significant. However, models that do not consider biomass concentrations should be considered appropriate for the following reasons:

(i) It may reasonably be expected that during OC injection, the degrading biomass populations attain a maximum biomass concentration (Jaffé and Rabitz, 1988). Once the biomass has reached this maximum concentration the system is inherentally at quasi-steady-state (with respect to biomass), and the model is therefore appropriate.

(ii) Methods of measurement for microbial rates at the field-scale such as push-pull tests (e.g., Schroth et al., 1998; North et al., 2004) generate bulk reaction rates that implicitly take account of biomass. Therefore exclusion of biomass concentration from the model allows a more accurate parameterisation of the system microbial rates.

(iii) The majority of experimental studies investigating U(VI) reduction rates are conducted under non-growth conditions, making it difficult to parameterise accurately for growth conditions.

(iv) Since the modelling interest here is on global biogeochemical processes rather than microbial populations, explicit representation of biomass is not necessary in systems at quasi-steady state, since microbial populations are in fact dependent variables linked to substrate concentrations (Wang and

Papenguth, 2001). The results of Thullner et al. (2005), in which the authors compared different microbial modelling approaches to biodegradation of lactate in a sand column, further support this.

(v) In certain cases non-growth conditions may actually better represent biomineralisation at the field-scale due to substrate competition between different bacterial populations (Truex et al., 1997).

Since the first step (oxidation half reaction) of each TEAP is the rate-limiting step (see Section 2.4.2.6), the model developed in the present work models this step kinetically. (The second step is modelled according to thermodynamic equilibrium.) The model represents the injected OC compound as CH_2O. OC degradation occurs via microbially mediated oxidation (the first step in the TEAP) and results in the release of zero-valent carbon into solution.

The model employs both first-order and Michaelis-Menten/Monod kinetics approaches to modelling OC oxidation rate (TEAP first-step). The chosen method is subsequently stated where relevant. The first, a first-order formulation, is defined:

$$\theta_z \frac{\partial C_{DOC}}{\partial t} = -kC_{DOC} \tag{3.1}$$

where k is the first-order degradation rate [T^{-1}] and C_{OC} is the concentration of OC in solution [ML^{-3}]. θ_z is equal to either θ_m or θ_i, depending on the region in which microbial activity takes place.

The second approach, where the OC oxidation rate is dependent on the concentration of both the OC and the relevant EA (e.g., Hunter et al., 1998; Brun and Engesgaard, 2002), implicitly considers microbial groups, since OC oxidation is explicitly dependent on the EA being consumed. The OC degradation rate is defined by the Michaelis-Menten kinetic formulation:

$$\theta_z \frac{\partial C_{DOC}}{\partial t} = -W(C_{EA}, \chi_{EA})\mu_{EA}\left(\frac{C_{DOC}}{K_{DOC} + C_{DOC}}\right)\left(\frac{C_{EA}}{K_{EA} + C_{EA}}\right) \qquad (3.2)$$

where μ_{EA} is the maximum OC oxidation rate which is dependent on the EA being consumed [T^{-1}]; C_{EA} is the concentration for the EA being consumed [ML^{-3}], K_{OC} and K_{EA} are the half saturation constants for OC and the EA being consumed, respectively. W is a step function which is equal to one when the concentration of the respective EA is above χ_{EA}, and equal to zero when it is below χ_{EA}. In the model, OC oxidation utilizing U(VI) as the EA is permitted to occur concurrently with OC oxidation utilizing Fe(III) or sulfate as the EA as has been documented (Finneran et al., 2002a,b; Holmes et al., 2002; Senko et al., 2002; Anderson et al., 2003; North et al., 2004).

The stoichiometry defined in the model, together with the defined reaction network set in the MINTEQA2 4.00 database, states that two moles of U(VI) are reduced and two

moles of UO_2 produced for every mole of CH_2O oxidized (in agreement with Wang and Papenguth, 2001; Roden and Scheibe, 2005).

3.3.2. DMRB and redox sequence

Generally, DMRB activity tends to conform to typical TEAP sequencing (Abdelouas et al., 1998a). For example, nitrate must be reduced prior to Fe(III) or U(VI) reduction (DiChristina, 1992; Lovley and Chapelle, 1995; Finneran et al., 2002a,b; Senko et al., 2002; Istok et al., 2004). This may be due to either DMRB preference for nitrate as an EA or the fact that the presence of nitrate would rapidly reoxidise formerly reduced Fe(II) or U(IV) to Fe(III) and U(VI) (Finneran et al., 2002a). However, extensive and stable U(VI) reduction has also been demonstrated by biostimulation at a field site with high nitrate concentrations in which *Clostridia* and *Clostridia*-like organisms were the dominant bacterial species (Smith *et al.*, 2006). Furthermore, the Fe(III)-, U(VI)- and nitrate-reducing *Geobacter metallireducens* has been found to reduce Fe(III) and U(VI) in the presence of nitrate when it had been grown with Fe(III) as the EA, but not when it had been grown with nitrate as the EA (Finneran et al., 2002a). It is therefore likely that the sequence of TEAPs is sensitive to both bacterial species and the history of the geochemical environment.

Following nitrate reduction, U(VI) and Fe(III) reduction typically occur concurrently (Finneran et al., 2002a,b; Holmes et al., 2002; Anderson et al., 2003; North et al., 2004) and prior to sulfate reduction (Finneran et al., 2002a,b). It is known that numerous

sulfate reducers can reduce U (Tebo and Obraztsova, 1998; Lovley and Philips, 1992; Lovley et al., 1993; Ganesh et al., 1999; Spear et al., 2000; Sani et al., 2004; Suzuki et al., 2005). Ortiz-Bernard et al. (2004b) biostimulated Rifle, Colorado (USA) sediments with acetate and found U(VI) reduction halted when Fe(III) was depleted and sulfate reduction became the dominant process. However, Spear et al. (2000) reported concurrent U(VI) and sulfate reduction by *Desulfovibrio desulfuricans*, with an increase in U(VI) reduction rate in the presence of sulfate. The biostimulation project by Anderson et al. (2003) at the U(VI)-contaminated Rifle field site found an increase in U(VI) when the dominant TEAP switched from Fe(III) to sulfate reduction. Senko et al. (2002) observed concomitant U(VI) and sulfate reduction in sediment incubations in which sulfate did not inhibit U(VI) reduction, however slight inhibition of U(VI) reduction by sulfate was witnessed in associated push-pull tests. Holmes et al. (2002), however, deduced that sulfate-reducing microorganisms were not important for the biostimulated U(VI) reduction in Shiprock, New Mexico (USA) field site sediments, and Lovley and Philips (1992a) noted that the presence of sulfate had no impact on U(VI) reduction by the sulfate-reducing bacterium *Desulfovibrio desulfuricans*.

It appears that the specifics of TEAP sequencing depends on the geochemical environment, the biogeochemical history, and the DMRB stain(s) present, some of which may be capable of sulfate or metal reduction without being capable of U(VI) reduction. The dependence of U(VI) reduction rates on DMRB strain, EA, and electron donor further support this (Liu et al., 2002a). The details of these complex relationships are not yet well understood. Therefore, TEAP sequencing in the model developed here is

controlled by accepted thermodynamic equilibrium. Specifically, the network of equations in the MINTEQA2 4.00 database is employed.

3.3.3. Inhibition

The reduction rate and extent of U(VI) by DMRB may be decreased by solid Fe oxides (Fredrickson et al. 2000; Wielinga et al., 2000) and Mn oxides (Lovley and Chapelle, 1995; Fredrickson et al., 2002**;** Liu et al., 2002b). Nevertheless, DMRB remain capable of aqueous U(VI) reduction in the presence of Fe oxides (Fredrickson et al. 2000; Wielinga et al., 2000; Sani et al., 2004) and Mn oxides (Fredrickson et al., 2002). Additionally, there is evidence that the rate and extent of U(VI) bioreduction is reduced in the presence of calcium. It is thought that this is due to U being a less energetically favourable EA in the presence of Ca-UO_2-CO_3 complexes (Brooks et al., 2003). Whilst biomineralisation activity decreases under these geochemical conditions, U(VI) biomineralisation is not entirely inhibited. The present work implicitly accounts for potentially reduced biomineralisation efficiency by investigating how widely varying biological rates impact U(VI) bioremediation efficiency. Though this approach does not account for dynamic inhibitory effects, it nevertheless covers observed net rates of microbial reduction.

3.3.4. Porous media clogging

Porous media may be subject to clogging via the excessive accumulation of minerals or biomass (e.g., Vandevivre and Baveye, 1992a,b; Taylor and Jaffé, 1990; Schäfer, 1992;

Clement et al., 1996a,b; Holm, 1999; Thullner et al., 2004). However, clogging is neglected in the present work. Abdelouas et al. (1998a) stimulated DMRB at a U mill tailings site near Tuba City, Arizona (USA) and found no evidence of pore clogging due to either biomass accumulation or mineral formation. The hydrological properties of the sandstone media investigated were not changed by increased bacterial activity. In addition, it is noted that at the maximum mineral concentrations encountered in the simulations conducted in the present work, the sum of all mineral volumes accounts for just 0.2% of aquifer pore space. This is considered negligible with regards to aquifer flow plugging. It is acknowledged that bioclogging can be significant in the vicinity of injection/withdrawal wells (e.g., for electron donor). However, the quasi-steady-state biomass assumption employed limits this model's applicability to the treatment (i.e., bioimmobilisation) zone located between wells where this effect is assumed to be minimal.

3.4. Transport model

It is generally accepted that the traditional Fickian advection-dispersion model does not capture the solute transport behaviour exhibited in multi-porosity heterogeneous porous media adequately, particularly at the field scale. This is because factures and other high-hydraulic conductivity (K) flow paths in heterogeneous porous media provide rapid transfer of contaminants into aquifers, while low-K zones act as diffusion-limited reservoirs for contaminants and other aqueous species. Such preferential flow paths have been exposed, for example, through use of dye tracers (Jørgensen et al., 2004).

Groundwater flow systems showing this dual-domain flow phenomenon have been documented in the literature both in column flow experiments (Grisak et al., 1980; Haws et al., 2004, 2005) and at the field scale (Sidle et al., 1998; Ryan et al., 2000; Julian et al., 2001).

Groundwater flow models for heterogeneous porous media which display this dual-domain transport behaviour have been characterized by two separate overlapping flow zone continua. These two zones conceptually combine the effects of local flow variation and inter-region diffusion (Li et al., 1994), such that existing concentration gradients are adequately captured. The first zone, traditionally conceptualized as the "mobile" region, exhibits mass transfer dominated relatively high-velocity range of flows. The second zone, traditionally conceptualized as the "immobile" region, exhibits mass transfer dominated by more localized flow variations with a contrasting low-velocity range of flows. Modelling systems with heterogeneous hydraulic conductivity employing dual-domain mass transfer approaches has more successfully reproduced observed solute transport behaviour than single domain formulations (Feehley et al., 2000).

The set-up of the physical domain is displayed in Figure 3.1. The figure displays individual model cells for both the mobile and immobile regions. Microbial presence may be considered within either or both regions. Advective-diffusive transport occurs within all cells in the mobile region only. Pore water within all cells in the immobile region is stagnant. Each mobile region model cell is associated with a corresponding

immobile region model cell and aqueous chemical species may transfer between the two via diffusive mass transfer.

The partial differential equation describing saturated one-dimensional chemical transport under transient fluid flow conditions in the mobile region is (Coats and Smith, 1964; van Genuchten and Wierenga, 1976)

$$\theta_m \frac{\partial C_m}{\partial t} + \theta_i \frac{\partial C_i}{\partial t} = - \theta_m v_m \frac{\partial C_m}{\partial x} + \theta_m (D_e + a v_m) \frac{\partial^2 C_m}{\partial x^2} - \frac{\partial q}{\partial t} \tag{3.3}$$

where C_m and C_{im} are the concentrations of a chemical species in solution in the mobile and immobile regions, respectively (ML^{-3}), v_m is the average pore-water velocity in the mobile region (LT^{-1}), $\partial q/\partial t$ is a sink term which accounts for chemical reactions [$ML^{-3}T^{-1}$], x is the distance along the spatial domain (L), t is time (T), and θ_m and θ_i are the media porosities in the mobile and immobile regions (L^3L^{-3}), respectively. D_e is the effective diffusion coefficient (L^2T^{-1}) and a is the dispersivity (L). The total porosity of the media is the sum of the mobile and immobile region porosities

$$\theta_T = \theta_m + \theta_i \tag{3.4}$$

and the hydrodynamic dispersion may be defined as

$$D = D_e + a v_m \tag{3.5}$$

In the present work, DP functionality is utilized such that high permeability porous media regions in the aquifer are represented by mobile zones, whilst regions of relatively slow flow are represented by immobile regions. Mass exchange between mobile and immobile groundwater occurs via a first-order mixing process, which is typically assumed to be driven by a concentration gradient and characterized by a mass transfer rate (e.g., Grisak and Pickens, 1980; Tang et al., 1981; Šimůnek et al., 2003; Haws et al., 2004; Gwo et al., 2005). In the PHREEQC model, an immobile cell is associated with each mobile cell. The mass transfer exchange between the mobile and immobile cells is given by (van Genuchten and Wierenga, 1976)

$$\theta_i\left(1 + \frac{\partial q}{\partial C_i}\right)\frac{\partial C_i}{\partial t} = \gamma(C_m - C_i) \tag{3.6}$$

where γ is the first-order exchange coefficient [T^{-1}]. This method is a mobile-immobile model in which convection and dispersion in the immobile region are considered negligible. Modelling heterogeneous porous media in this way is a simplified approach which accounts for non-equilibrium flow effects by using a "lumped" mass transfer term (γ). The method was references in the discussion surrounding it in Chapter 2.

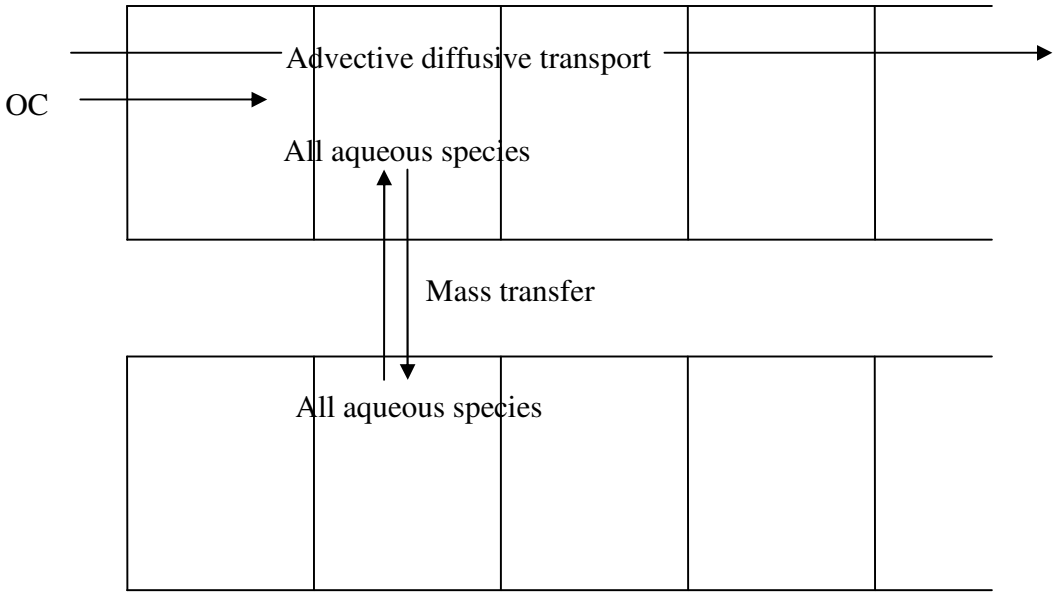

Figure 3.1. Arrangement of dual porosity domain.

3.5. Surface complexation model

Natural systems may exhibit complex sorption behaviour. Specifically, U(VI) adsorption is significantly influenced by pH and carbonate concentration, as well as changes in aqueous speciation (Dzombak and Morel, 1990; Waite et al., 1994). However, numerous reactive transport models ignore this, instead adopting a constant-K_d modelling approach for U(VI) sorption (e.g., Wang and Papenguth, 2001; Wang et al., 2003; Roden and Scheibe, 2005). Surface complexation models (SCM) account for pH changes, the effect of variations in solution chemistry, and the complexing properties of sorbing surface sites (Langmuir, 1997). SCM models assume adsorption occurs on specific surface sites, allowing for a number of specific sites to be utilized by the sorbent.

Waite et al. (1994) developed a model which built on the diffuse double layer (DDL) model (Stumm et al., 1970; Huang and Stumm, 1973; Dzombak and Morel, 1990), applied specifically to ferrihydrite. Barnett et al. (2000) hypothesized that iron oxides control U(VI) sorption and further developed the model by Waite et al. (1994) to successfully simulate the U(VI) sorption behaviour of three heterogeneous subsurface media (from the US Department of Energy Oak Ridge, Savannah River, and Hanford Reservation sites) (Barnett et al., 2002). The Barnett et al. (2002) model successfully predicted the pH-dependent adsorption of the three different media, with only slight differences between observations and predictions in the location of adsorption isotherm pH edges and the maximum amount of U(VI) adsorbed. The SCM model adopted in the present model is therefore believed to adequately represent typical U-contaminated aquifers exhibiting U sorption to iron oxides. The authors also varied U(VI) and carbonate concentration with reasonably favourable model predictions. While the model has been observed to overestimate retardation in the pH region of maximum adsorption on the adsorption isotherm, it remains one of the most accurate models in the literature for U(VI)-iron oxide sorption.

The chemical reaction equations and equilibrium constants related to the surface complexation model are from Barnett et al. (2002), and are given in Table 3.1. (Note that $\equiv Fe_w$ and $\equiv Fe_s$ represent weak and strong sorption sites, respectively.) In addition to these reactions, the aqueous-phase reactions provided by the MINTEQA2 4.00 database (Allison et al., 1991) are adopted. The surface complexation model parameters (number of reactive sites, equilibrium constants, site densities, and specific surface areas) of

Barnett et al. (2002) are adopted in the present work. The parameter values are presented in Table 3.2 under "General iron oxide application". This results in a slightly different model behaviour from that in Barnett et al. (2002). The mass of the binding site solid (i.e., the mass of mineral present in the experiment) was 1×10^{-3} mol (per litre), and the batch solution contained 1 mg/l (4.23×10^{-6} mol/l) U, as were used in the Barnett et al. (2002) experiment. Figure 3.2 provides the pH isotherm output for this formulation of the model, as well as the U(VI) sorption behaviour of the three heterogeneous subsurface media originally published by Barnett et al. (2002). An analysis was conducted to quantify the goodness of fit between the Oak Ridge data (diamond symbols in Figure 3.2) and the model output. The following goodness of fit metric used was

$$G = \frac{1}{n}\sqrt{\sum_{j=1}^{n}\left(\frac{y_{1;j} - y_{2;j}}{y_{1;max}}\right)^2} \qquad (3.7)$$

where y_1 is a y-coordinate value for the data being matched (e.g. experimental data), y_2 is a y-coordinate value for the model data being compared, and $y_{1,max}$ is the maximum value that any y_1 attains in the data sequence. The value of G is therefore a measure of the mean deviation of the model data from the matched (e.g. experimental) data set, expressed as a percentage of the maximum data set value. The value of G for model comparison with the Oak Ridge data was 0.03, suggesting a suitable fit was attained.

The model accurately fits the data provided. Indeed, the model reaction networks used in the present work result in a more accurate approximation of the subsurface media sorption behaviour of the three samples than the model used by Barnett et al. (2002), especially at the near-neutral pH values typical of groundwater in U contaminated sites.

Table 3.1. Surface complexation model reactions and parameters (from Barnett et al., 2002).

U(VI) aqueous complexation reactions	**Log K_e**
$UO_2^{2+} + H_2O \leftrightarrow UO_2OH^+ + H^+$	-5.41
$UO_2^{2+} + 2H_2O \leftrightarrow UO_2(OH)_2 + 2H^+$	-12.23
$UO_2^{2+} + 3H_2O \leftrightarrow UO_2(OH)_3^- + 3H^+$	-20.00
$UO_2^{2+} + 4H_2O \leftrightarrow UO_2(OH)_4^{2-} + 4H^+$	-32.57
$2UO_2^{2+} + H_2O \leftrightarrow (UO_2)_2(OH)^{3+} + H^+$	-2.44
$2UO_2^{2+} + 2H_2O \leftrightarrow (UO_2)_2(OH)_2^{2+} + 2H^+$	-5.79
$3UO_2^{2+} + 4H_2O \leftrightarrow (UO_2)_3(OH)_4^{2+} + 4H^+$	-12.25
$3UO_2^{2+} + 5H_2O \leftrightarrow (UO_2)_3(OH)_5^+ + 5H^+$	-16.22
$3UO_2^{2+} + 7H_2O \leftrightarrow (UO_2)_3(OH)_7^- + 7H^+$	-31.29
$4UO_2^{2+} + 7H_2O \leftrightarrow (UO_2)_4(OH)_7^+ + 7H^+$	-22.62
$UO_2^{+2} + H_2CO_3 \leftrightarrow UO_2CO_3 + 2H^+$	-6.80
$UO_2^{+2} + 2H_2CO_3 \leftrightarrow UO_2(CO_3)_2^{2-} + 4H^+$	-15.90
$UO_2^{+2} + 3H_2CO_3 \leftrightarrow UO_2(CO_3)_3^{4-} + 6H^+$	-26.45
$2UO_2^{+2} + 3H_2O + H_2CO_3 \leftrightarrow (UO_2)_2CO_3(OH)^{3-} + 5H+$	-18.07
Surface complexation reactions	**Log K_e**
$2{\equiv}Fe_sOH + UO_2^{2+} \leftrightarrow ({\equiv}Fe_sO)_2UO_2 + 2H^+$	-2.57
$2{\equiv}Fe_wOH + UO_2^{2+} \leftrightarrow ({\equiv}Fe_wO)_2UO_2 + 2H^+$	-6.28
$2{\equiv}Fe_wOH + UO_2^{2+} + H_2CO_3 \leftrightarrow ({\equiv}Fe_wO)_2UO_2CO_3^{2-} + 4H^+$	-16.43
$2{\equiv}Fe_sOH + UO_2^{2+} + H_2CO_3 \leftrightarrow ({\equiv}Fe_sO)_2UO_2CO_3^{2-} + 4H^+$	-12.34
${\equiv}Fe_{s,w}OH + H^+ \leftrightarrow {\equiv}Fe_{s,w}OH_2^+$	6.51
${\equiv}Fe_{s,w}OH \leftrightarrow {\equiv}Fe_{s,w}O^- + H^+$	-9.13
${\equiv}Fe_{s,w}OH + H_2CO_3 \leftrightarrow {\equiv}Fe_{s,w}CO_3H + H_2O$	2.90
${\equiv}Fe_wOH + H_2CO_3 \leftrightarrow {\equiv}Fe_wCO_3^- + H_2O + H^+$	-5.09
Parameter	**Value**
Strong surface sites (mol sites per mol Fe in Fe oxide)	0.005
Weak surface sites (mol sites per mol Fe in Fe oxide)	0.2
Surface area of Fe oxide (m^2g^{-1})	600

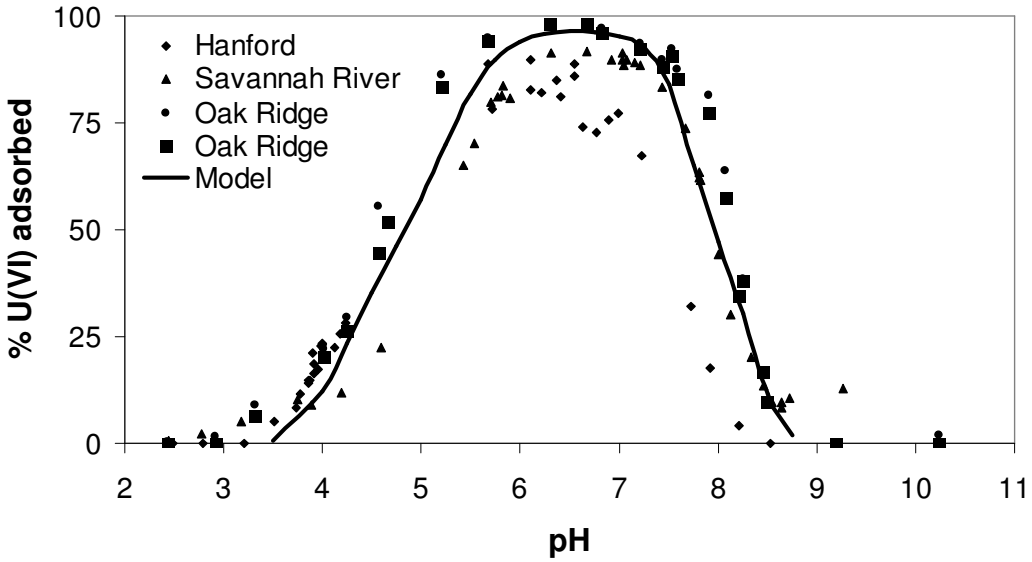

Figure 3.2. Surface complexation model evaluation against Barnett et al. (2002) data.

Since the Waite et al. (1994) model, and therefore implicitly the Barnett et al. (2002) model, assume that ferrihydrite governs U(VI) sorption to sediments, the model formulated here was also compared to the data presented by Missana et al. (2003) for the more crystalline material, magnetite. The model was run with identical reactions and parameters as applied to the Barnett et al. (2002) data (Table 3.1). The mass of the binding site (i.e., the mass of magnetite mineral present in the experiment) was 2 g (per litre of solution used in the experiment), and the batch solution contained 4.4 × 10-7 mol/l U, as were used in the Missana et al. (2003) experiment. Figure 3.3 displays the percentage of U sorbed at various pH values for the model (thick line) over the experimental data and model output presented in Missana et al. (2003). The model qualitatively captures the sorption behaviour. However, at the majority of pH values, U(VI) sorption is overestimated. Naturally, it cannot be expected that a model that

assumes ferrihydrite to be responsible for all U-Fe oxide sorption sites may be applied to magnetite rather than ferrihydrite. In such cases, the number of sorption sites and the surface area of the mineral (in addition to the equilibrium reactions for magnetite and their equilibrium constants) may require adjustment. Adjusting the surface area to that for magnetite (8.5 m^2/g magnetite) reported by Missana et al. (2003) did not change the results significantly (data not shown). However, adjusting the number of sorption sites to, for example, 0.14 mmol strong surface sites per mol Fe in magnetite and 5.6 mmol weak surface sites per mol Fe in magnetite yielded the improved results presented in Figure 3.4. This more appropriate parameterisation captures the sorption behaviour reasonably well at short contact times. However, at pH values over 5.5 the model slightly overestimates the U(VI) sorption for 4 hour and 1 day contact times (all non-star symbols). Nevertheless, values in this pH range correspond with data for sorption with 3 months contact time (star symbols) sufficiently well. This second evaluation to a different kind of sorption site (different metal) demonstrates the versatility of the surface complexation model used within the present work and builds further confidence in the portion of the model that describes surface complexation reactions.

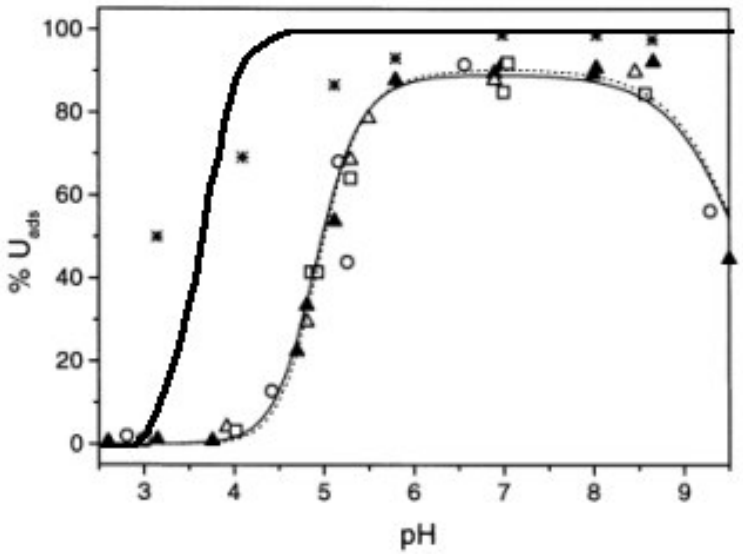

Figure 3.3. Surface complexation model evaluation against Missana et al. (2003) data. Experimental data for 1 day contact time (T), ionic strength (I) = 0.1 mol/L (filled triangles); 4 d T, I = 0.1 (open triangles); 3 months T, I = 0.1 (stars); 4 d T, I = 0.2 (squares); 4 d T, I = 0.001 (circles). Thick line is model presented in this work, other lines are Missana et al. (2003) model.

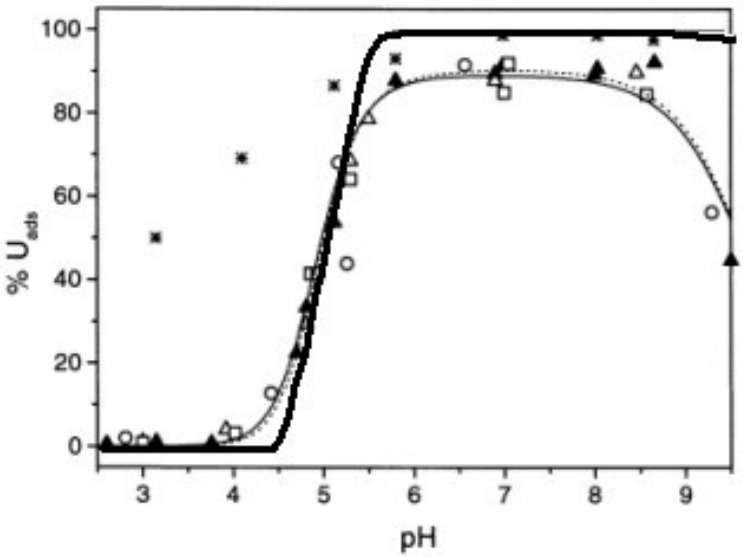

Figure 3.4. Surface complexation model evaluation against Missana et al. (2003) data. Experimental data for 1 day contact time (T), ionic strength (I) = 0.1 mol/L (filled triangles); 4 d T, I = 0.1 (open triangles); 3 months T, I = 0.1 (stars); 4 d T, I = 0.2 (squares); 4 d T, I = 0.001 (circles). Thick line is model presented in this work, other lines are Missana et al. (2003) model.

The surface complexation models presented thus far have been static batch or beaker based models applied to single solutions. In order to account for the dependence of surface complexation on mineral presence, the complexation surface was linked to ferrihydrite mineral presence. As the models assumed ferrihydrite (rather than magnetite) to be the Fe oxide responsible for U(VI) sorption, ferrihydrite is considered the only iron oxide present in subsequent simulations presented in this work. The PHREEQC code allows surfaces to be associated with mineral phases. This modelling option was selected and the parameter values in Table 3.1 were simply modified to reflect a per mole ferrihydrite unitary basis (surface area becomes 33600 m^2mol^{-1}). Figure 3.5 displays the pH isotherm produced by the model that considers sorption surfaces to be directly related to ferrihydrite mineral phase. The figure also shows the experimental data of Barnett et al. (2002) previously presented. Comparison to the experimental data remains reasonable, although the isotherm edges at pH > 8 and pH < 4 underestimate U(VI) surface complexation slightly. Modification of the model in this way allows surface complexation to be realistically affected by ferrihydrite mineral presence.

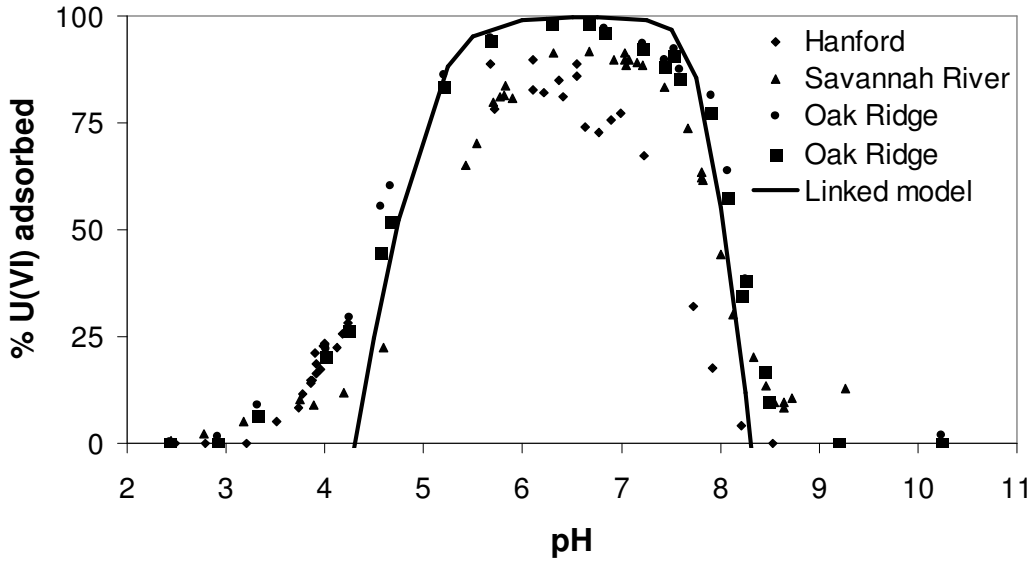

Figure 3.5. Surface complexation model evaluation against Barnett et al. (2002) data for the surface related to the ferrihydrite mineral phase.

Surface complexation is assumed to act throughout the domain. Complexed U(VI) is unavailable to bacteria for bioreduction (Ortiz-Bernard et al., 2004b; Jeon et al., 2004).

3.6. Model discretisation

The PHREEQC code utilises a split-operator approach which adjusts time step to grid size for each individual part of the ARD equation (equation 2.11). Numerical dispersion is reduced by both the iteration technique used (see Section 3.2) and by forcing the Courant condition (equation 3.8) for advective transport and the Von Neumann criterion (equation 3.9) for dispersive transport:

$$(\Delta t)_a = \frac{\Delta x}{v} \tag{3.8}$$

and

$$(\Delta t)_d \leq \frac{(\Delta x)^2}{3D} \tag{3.9}$$

where $(\Delta t)_a$ and $(\Delta t)_d$ are the advection and dispersive/diffusive time steps, respectively, and Δx is the cell length (spatial discretisation length) .

A further two restrictions are imposed on the dispersive/diffusive time step, such that the $(\Delta t)_d$ will be reduced to meet the required conditions. Firstly, when the grid discretisation is small, $(\Delta t)_d$ may become smaller than $(\Delta t)_a$, since $(\Delta t)_d$ has quadratic dependence on grid size. In such cases multiple dispersion time steps are used such that $\Sigma(\Delta t)_d = (\Delta t)_a$, and chemical reactions are calculated after each of the dispersion steps. Secondly, cell mixing may control the dispersive time step based on the condition that

$$\frac{1}{3} \leq \frac{D(\Delta t)_a}{n(\Delta x)^2} \tag{3.10}$$

where n is a positive integer, the value of which is increased to meet the condition. The dispersion time step is then:

$$(\Delta t)_d = \frac{(\Delta t)_a}{n} \tag{3.11}$$

and n cell mixes are performed.

Nevertheless, the algorithm may display numerical dispersion when the model grid is coarse, particularly when surface complexation and dual porosity diffusion occur. Furthermore, all simulations were conducted in effectively infinite spatial domains. The results are affected by the Péclet number, and hence a domain length of the order of magnitude of D/v from the downstream boundary is impacted by the downstream boundary condition. Unless otherwise stated, in this work the impact of the downstream boundary condition was not desired and all data presented was therefore collected at distances (x) no less than D/v orders of magnitude from the downgradient boundary.

In order to ensure that numerical dispersion was minimized in simulations, a number of simulations were conducted for different spatial/temporal discretisations. Both the spatial and temporal U(VI) concentration profiles are compared for 4 different spatial/temporal discretisations. All simulations used the first-order OC rate model (equation 3.1), with the chemical conditions used in Chapter 6 (Table 6.1), a mobile-immobile region exchange rate (γ) of 0.5 yr^{-1}, mobile and immobile porosity (θ_m and θ_i) of 0.5, pore water velocity (v) of 10 myr^{-1}, hydrodynamic dispersion (D) of 0.1 m^2s^{-1}, and a OC fermentation rate (k) of 1 yr^{-1}.

Figure 3.6 presents the temporal U(VI) concentration profile at $x \approx 10$ m for four different spatial/temporal discretisations. The three finest discretisations are those that are used in all subsequent simulations within this work. The curve at the coarsest discretisation ($\Delta x = 5$ m, $\Delta t = 0.5$ yr) is added to show the case for an extremely coarse

discretisation. Additionally, a curve marked with an asterisk shows a spatial/temporal discretisation which does not satisfy the condition noted above regarding the impact of the downgradient boundary condition. The results show that as the discretisations become finer/smaller, the curves converge towards a given result. It should be noted that the changes in slope of the curves at approximately 0.8, 1.9 and 2.5 years are due to expected geochemical changes in the system and not due to numerical instability. Figure 3.7 displays the specific geochemical species which induce these changes. For example, at approximately 0.8 years, the nitrate in the system becomes depleted. Following nitrate depletion, U(VI) reduction may occur and the U(VI) concentration is subsequently observed to begin decreasing. Likewise, the presence of uraninite mineral at $t \approx 1.9$ years changes the geochemical dynamics of U(VI) reduction and the U(VI) concentration slope is again observed to change.

Figure 3.8, presents the spatial U(VI) concentration profile for four different spatial/temporal discretisations. Again, the three finest discretisations are those that are used in all subsequent simulations and an additional curve marked with an asterisk shows a spatial/temporal discretisation allows the downgradient boundary condition to impact the results. For spatial distributions the influence of the downgradient boundary condition is clearly shown to impact the results. Further, as the discretisation becomes finer/smaller results converge on a specific profile.

The different discretisations yield very similar results, demonstrating that the Courant condition and the Von Neumann criterion yield consistently accurate results that avoid numerical dispersion. To a minor extent, results converge as spatial/temporal discretisations become finer. The downgradient boundary condition may impact results when model discretisation is not appropriately selected. All subsequent simulations within this work ensure this does not occur.

The implementation of the Courant condition and the Von Neumann criterion in PHREEQC forces the simulation time step to be inextricably linked to simulation spatial domain step/discretisation. This means that (i) simulations which require small time-steps but not small spatial discretisations (or vice versa) cannot be used, (ii) simulation discretisations cannot change with time throughout a simulation run, preventing the possibility of varying model accuracy within a run and thereby reducing run time. Furthermore, if pore water velocity, v, is changed for different simulation runs, the model discretisation must also change.

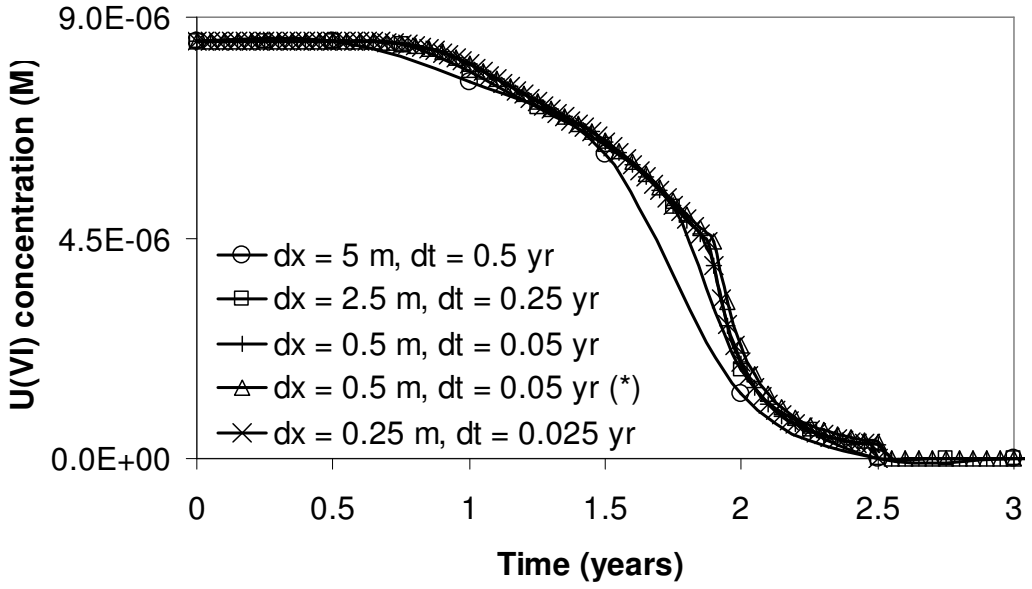

Figure 3.6. Temporal U(VI) concentration profile at different spatial/temporal discretisations.

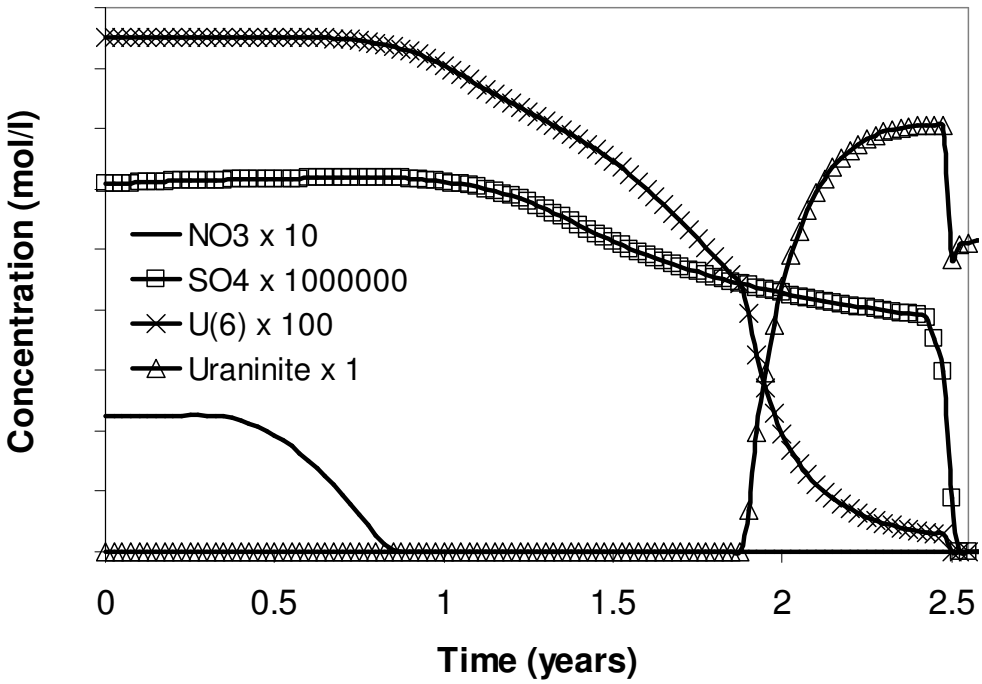

Figure 3.7. Temporal concentration profiles for specific geochemical species at the 0.25m discretisation.

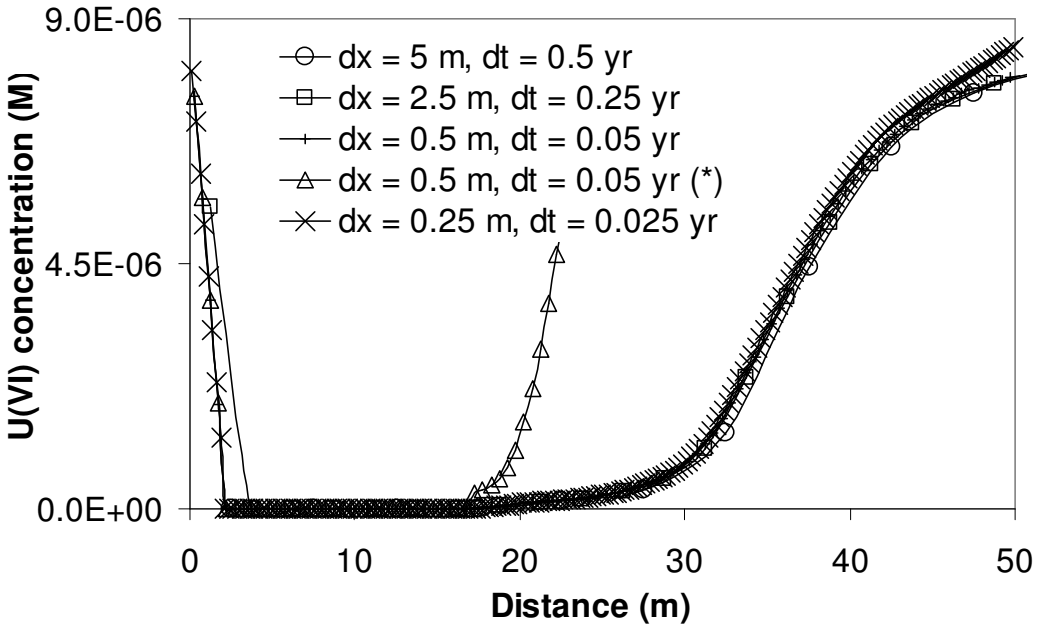

Figure 3.8. Spatial U(VI) concentration profile at different spatial/temporal discretisations.

3.7. Model assumptions

It is important to recognize the modelling assumptions inherent within the developed model in order to understand the limitations and confining conditions under which results are relevant. These include:

- The dual porosity (dual region) modelling approach employed assumes (i) advection and dispersion in the immobile region are negligible, and (ii) ideal physical mixing within each cell. Further, it is likely that the system requires heterogeneity distribution to be random (Bajracharya and Barry, 1997).
- The model developed here assumes that the biomass clogging is insignificant in the systems modelled. Media may become clogged, either via biomass or mineral

precipitation. The volume of aquifer porosity occupied by precipitated minerals does not constitute a significant proportion of total aquifer volume in any of the simulations considered in this work. However, biomass clogging is a process which may impact aquifer permeability significantly (e.g., Vandevivre and Baveye, 1992a,b; Taylor and Jaffé, 1990; Schäfer, 1992; Clement et al., 1996a,b; Holm, 1999; Thullner et al., 2004). Furthermore, the production of gases in saturated porous media may result in the formation of gas bubbles which affect aquifer hydraulic conductivity (Amos and Mayer, 2006). The model developed here assumes that the effects of gas bubble evolution are insignificant.

- The model assumes biomass to be at quasi-steady-state. Because biomass growth and decay do not occur, microbial lag times are effectively zero. The model is therefore valid for steady-state systems in which the introduction of organic carbon does not significantly alter degradation rates. Biomass presence is considered homogeneous throughout a region (which may exhibit advective or diffusive dominant flow) within the media. Biomass transport via pore water flow is assumed to be insignificant.
- The model assumes surface complexation of U(VI) to take place on ferrihydrite mineral and that OC-complexed U is negligible.
- The systems modelled (modelling applications) in this work assume uranium is not dissolved *within* the biostimulated region. The region of focus is assumed to be downgradient of the dissolution source.

- The model assumes OC is represented by a single generic OC species. This is the typical approach taken in most modelling work, though an interesting alternative modelling approach is that multiple OC species exist which degrade at different rates (see Hunter et al., 1998).
- The systems modelled (modelling applications) in this work consider excess OC to be supplied to the advective pore water of the aquifer only. This is considered reasonable for the majority of real world applications.

4. Validating a one-dimensional biogeochemical reactive transport model for bioimmobilisation of U(VI) in dual porosity porous media

4.1. Introduction

Conducting performance assessment studies using reactive transport models is difficult due to the hydrogeochemical complexity of radionuclide-contaminated sites (MacQuarrie and Mayer, 2005). Models are necessarily simplification of real systems. This is particularly true in the earth sciences of hydrology and geochemistry, where numerical models are created to represent complex open systems that exhibit uncertain boundary and initial conditions and simulations may produce results that are non-unique. The primary function of reactive transport numerical modelling is therefore to determine parameter sensitivities, identify dominant processes, test hypotheses (the implications of qualitative or conceptual models), identify discrepancies between models and observed data, further informing understanding of field observations, conduct sensitivity analyses, identify specific areas in which empirical data is needed, and explore potential scenario outcomes (Oreskes et al., 1994). Of course, in order to build confidence in these capabilities, it is necessary to ensure that the model accurately solves the intended governing equations (i.e., model verification) and that its formulation adequately captures the behaviour of the natural system(s) of interest (i.e., model validation).

The concepts of model validation and verification raise numerous issues, some of which have been discussed recently by numerous authors (Konikow and Bredehoeft, 1992; Bredehoeft and Konikow 1993; Oreskes et al., 1994; Narasimhan, 1995). Models remain

simplifications of real systems due to lack of data. Validation requires the selection of data sets that provide enough information to assure that system behaviours are captured. Proper validation of all significant system processes simultaneously (i.e., including their interaction with each other) in biogeochemical transport models requires comprehensive data sets containing biological, geochemical and physical information. Unfortunately, there exist very few such data sets, particularly in the area of U(VI) bioimmobilisation; most provide only a subset of the required information. In the absence of comprehensive data, validation is only possible for those processes that have been documented. It is noted that multiple-parameter fitting to match experimental data is common, which does not represent a rigorous model validation exercise. Moreover, parameterising a system with a host of unknowns may lead to erroneous conclusions, since fundamental processes may be ignored by way of this approach. Nevertheless, when data is lacking, model validation using lacking data sets remains the best that may be achieved. Unfortunately, there exist very few thorough data sets in the area of U(VI) bioimmobilisation. Data sets detailing combined microbial, geochemical and transport processes is particularly lacking. The next section lists a number of potential data sets for evaluation of the model developed in Chapter 3, and discusses the usefulness and relevance of each. The model is then (i) compared against an existing model and (ii) validated against an experimental data set.

4.2. Model testing structure

In order to evaluate the performace of the model a number of tasks were performed, some of which have been discussed in previous chapters. The PHREEQC code has been tested by its authors in numerous applications, as well as used in modelling work reported in numerous publications. It is a verified and reliable code that can be used with confidence in model development. Therefore, the model testing required in this work relates to the specific features of the developed model and their ability to successfully model real behaviour rather than, for example, testing chemical mass balance or verification of the transport equations using analytical solutions.

Figure 4.1 displays the sequence of major model testing exercises conducted. The surface complexation model was tested in Section 3.5 and the model discretisation tested in Section 3.6. This chapter details the evaluation of the model against both an existing model and an experimental data set.

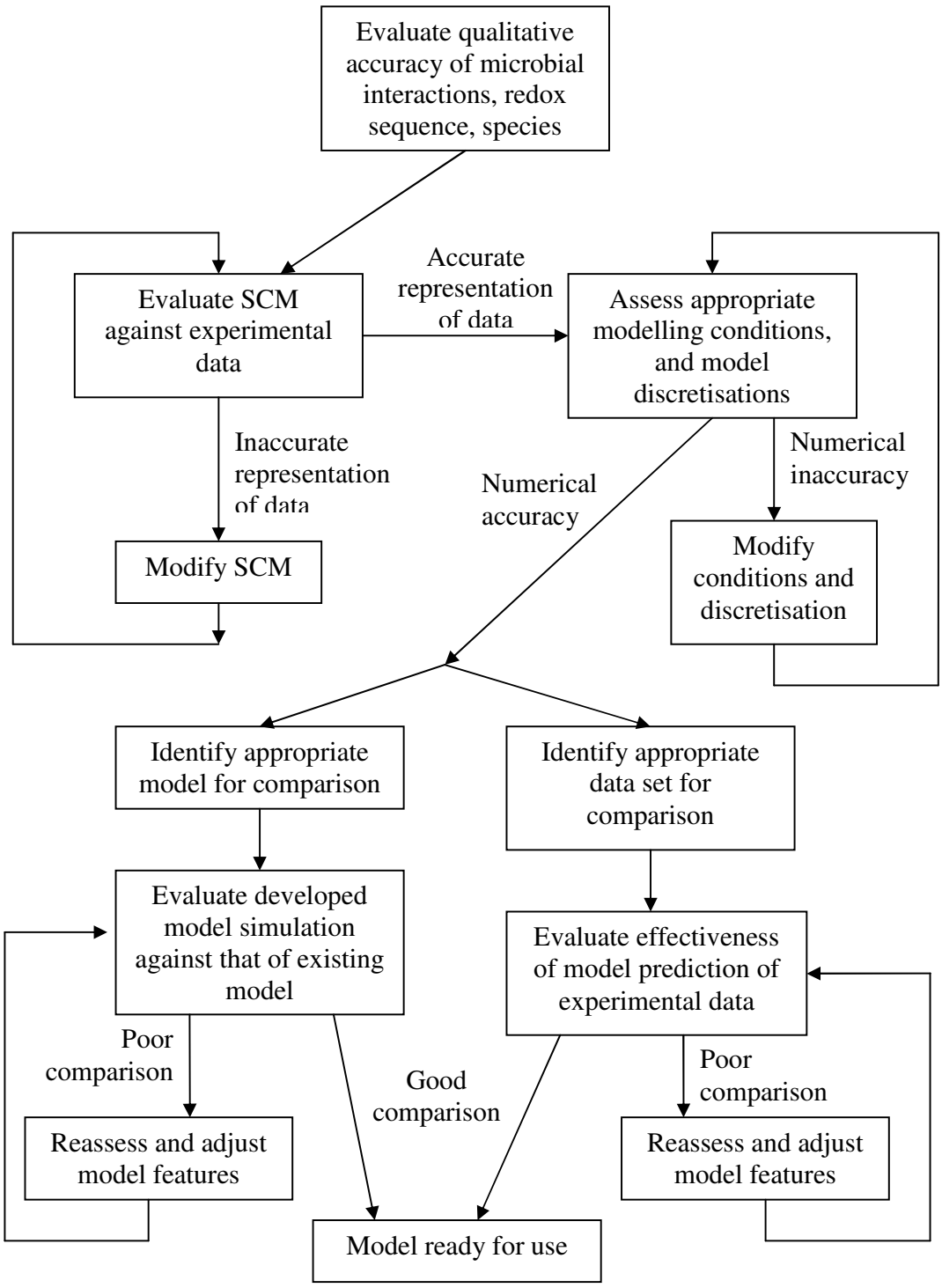

Figure 4.1. Model evaluation process.

4.3. Data available for evaluation of the developed model

Models may be compared to existing models or validated against experimental data. Experimental data in the U(VI) bioremediation research field may be divided into three categories: (i) field site data, (ii) laboratory batch experimental data in which "batch" (or uniformly mixed volume) experiments have been conducted without fluid transport through a porous media, and (iii) laboratory column experimental data in which the experiment has been conducted in a porous media-packed column with one-dimensional fluid transport.

A number of data sets were collated and the appropriateness of each was considered for potential evaluation exercises. The list of potential data sets includes the following:

1. Field scale data
    1.1. Anderson et al. (2003): Twenty-well injection gallery with acetate stimulation (Rifle, CO). Data: well data over time for tracer, U(VI), Fe(II), sulfate, acetate, bacterial communities (qualitative biomass and communities).
    1.2. Vrionis et al. (2005): Post-stimulation static analysis of stimulated field site (Rifle, CO). Borehole data with depth: U(VI), Fe(II):Fe(total), bacterial community types.
    1.3. Wu et al. (2006a,b): Four-well recirculation system, treatment zone flushing and conditioning followed by ethanol stimulation of indigenous bacteria (Oak Ridge, TN). Data: tracers, NO_3^- flushing;

well data over time for pH, NO_3^-, SO_4^{2-}, OD, and U during stimulation.

2. Laboratory column experimental data
    2.1. Abdelouas et al. (1998a): Contaminated crushed sandstone, site groundwater influent. Data over time: NO_3^-, SO_4^{2-}, U.
    2.2. Gu et al. (2005): Closed-loop recirculated contaminated column. Flushing and conditioning followed by ethanol injection. Data with time: ethanol, acetate, sulfate, U(VI), pH.
    2.3. Wan et al. (2005): Contaminated sediments with lactate injection. Data over time: effluent U, OC, bicarbonate.
    2.4. Tokunaga et al. (2005): Vertical diffusion in columns with OC injection. Data at depths for redox potential (mV), U(VI):U(total), DNA.
    2.5. Michalsen et al. (2006): Long term (20-month) stimulation of uncontaminated sediments with influent from contaminated site groundwater. Data: spatially averaged NO_3^-, SO_4^{2-}, and U concentrations over (120 hour) time period.
3. Batch experimental data
    3.1. Holmes et al. (2002): Acetate-amended batch U(VI) reduction with concurrent Fe(III) reduction – prior to sulfate reduction. Data: bacterial communities, U(VI) and Fe(II)
    3.2. Finneran et al. (2002b): Sediment incubation, U(VI) reduction and nitrate presence study. Data: U(VI), NO_3^-, Fe(III), Fe(II)

3.3. Suzuki et al. (2003): Sediment incubation. Data: initial water composition, pH, U, SO_4^{2-}, Mn.

3.4. Beyenal et al. (2004): Biofilms grown in continuous flat-plate reactors. U(VI) reduced in reactor. Data: immobilised U, H_2S.

3.5. Jeon et al. (2004): Batch DMRB U(VI) reduction under Fe(III) sorbed U(VI). Data with time: U(VI), Fe(II).

3.6. Ortiz-Bernad et al. (2004b): Acetate addition. Inability of DMRB to reduce U(VI) adsorbed to sediments. Data with time: acetate, U(total), U(ads), U(VI), sulfate, Fe(II):Fe(total).

4. Existing modelling data

4.1. Wang and Papenguth (2001): Single porosity biogeochemical reactive transport model. Data: numerous TEAP presented at particular point in time.

4.2. Wang et al. (2003): Single porosity biogeochemical reactive transport model. Data: numerous TEAP species presented at particular point in time.

4.3. Roden and Scheibe (2005): Tri-porosity fully kinetic reactive transport model (no chemistry). Data: U(VI) concentrations.

None of the available data sets permits comprehensive evaluation to the simultaneous and interactive biological, geochemical and transport processes of the system under investigation. The batch data sets listed above may be useful to confirm the net biological processes, or very specific mechanisms such as microbial inhibition,

occurring in U(VI) bioimmobilisation schemes. However, the fact that they cannot account for the impacts of other processes as, for example, transport behaviour, which may exert influence on redox or surface complexation processes, renders them of limited value for this purpose.

Furthermore, the availability of data in field scale studies listed above is limited. For example, data is primarily confined to only a few boreholes or and a few chemical species. Furthermore, none of the studies listed above provide sufficient data on the characteristics of the porous media in which the experiments took place to allow suitable modelling. Luo et al. (2007) modelled the field-scale experiment conducted by Wu et al. (2006a). Their work appears to provide the only existing experimental evaluation of a biogeochemical transport model dealing with DMRB mediated U immobilisation. However, the authors avoid the complexity inherent in field-scale porous media systems by fitting the model to well data at a specific spatial location within the stimulated domain. In order to obtain a solution, the multi-dimensional advection-dispersion equation is transformed to a one-dimensional (time) transport equation along a streamline in travel-time coordinates. While the streamlines may be affected by spatial heterogeneity, the model does not explicitly consider the spatial heterogeneity of the system.

The listed laboratory column experiments provide the opportunity to collect more useful data due to the fact that they were conducted in a controlled environment from which extensive select data may be obtained from simplified systems. Furthermore, well

constrained laboratory experiments are also better capable of eliminating non-uniqueness when modelling systems in which transport and biogeochemical interactions occur (e.g., Postma and Appelo, 2000; Saiers et al., 2000; Guha et al., 2001; Amos et al., 2004; Jurjovec et al., 2004). Given that the modelling of an experimental data set is a significant undertaking, only a small number of analyses are possible.

Numerous studies present ambiguity over experimental conditions such as media characteristics (hydraulic conductivity/pore water velocity, media porosity, mineralogy) and results collation (spatial location of data collation) (Abdelouas et al., 1998a), including generic and spatially averaged data over a relatively short time period (Michalsen et al., 2006). Complications in some studies lead to reduced confidence in the relevance of the results to real systems; for e.g., lack of bioactivity due to potential loss biomass via media flushing (Gu et al., 2005). Still others are limited to investigation of only a subset of processes; for e.g., vertical diffusive transport only (Tokunaga et al., 2005).

The experimental data set of Wan et al. (2005) was deemed the most suitable. This experiment considers bioimmobilisation of a U-contaminated sediment in five duplicate columns. The sediment used in the experiment is from Area 2 of the NABIR FRC site at the Oak Ridge National Laboratory, USA. This sediment contains shale saprolites (Jardine et al., 1993) which exhibit multi-porosity flow behaviour (Gwo et al., 1995) and therefore represent a suitable sediment against which to validate the dual porosity model developed in the present work. The bacteria present in the experiment are native to the

sediment, thus providing the appropriate scenario for a naturally attenuated field site. The column is subjected to advective-diffusive transport with defined pore water velocities. The work notes the sediment characteristics such as mineralogy, porosity and density required for modelling the system, and presents effluent concentrations against time for U, OC and carbonate. The geochemical data is specific with regard to both space and time. Duplicate columns provide valuable experimental consistency and the useful inclusion of OC in the reported data allows the two-step modelling of TEAPs to be more accurately defined. For these reasons, this experimental data set was chosen as the most appropriate against which to validate the model developed in the present work.

Few modelling studies on U(VI) bioimmobilisation by DMRB in heterogeneous or structured porous media exist. Three existing models were identified for potential comparison to the model developed within the present work. The multi-porosity model used by Roden and Scheibe (2005) offers a suitable basis against which to compare the physical formulation of the developed model. However, that model uses a fully kinetic approach to biogeochemical processes rather than a biogeochemical reactive transport model, and therefore lacks the appropriate biogeochemical complexities for appropriate comparison. Wang et al. (2003) developed a one-dimensional biogeochemical reactive transport that included U redox geochemistry, but is a single-region model. Nevertheless, it covers the biogeochemical and transport processes relevant to U(VI) immobilisation and therefore represents a suitable model against which to compare those aspects of the model developed in the present work. It is noted that Wang and Papenguth (2001) also developed a single-region model by coupling the biogeochemical model of

Hunter et al. (1998) with U redox geochemistry. That model uses a two-step kinetic approach to primary and secondary redox reactions and therefore uses a different formulation to the model developed within this work. In order to build confidence in the accuracy of a developed model by comparing it with other models, the compared model is required to be similarly formulated. Thus, it was deemed preferable to use the model developed by Wang et al. (2003) for comparison with the model developed in the present work.

4.4. Comparison with an existing model

The developed model was compared to the model of Wang et al. (2003) by simulation of an oxic recharge water rich in OC entering a U-contaminated aquifer. The comparison (1) verifies the developed biochemical redox formulation and, (2) compares results with a simulator that employs a different U(VI) adsorption model.

The presented model was operated in SP mode and was parameterised so as to reproduce the Wang et al (2003) scenario as closely as possible. The simulated geochemical conditions, including concentrations of the electron acceptors, are detailed in Table 4.1. The transport conditions simulated are detailed in Table 4.2, and the parameters relating to the microbial formulation (equation 3.2) are listed in Table 4.3. As the model developed by Wang et al. (2003) is a single porosity model, the dual porosity model developed in this work was used with a mobile-immobile mass transfer (γ) of value zero to provide a single porosity system. All parameter values were taken from Wang et al.

(2003) except the immobile region porosity (DP case), the mobile-immobile mass transfer and the domain discretisation. Note that the domain is discretised to a finer grid in this work (Δx = 0.25 m) than that used by Wang et al. (2003) (Δx = 0.5 m).

Every effort was made to use the same conditions reported in Wang et al. (2003). However, the differences in modelling approach between the two models mean the following differences remain: (i) the U(VI) adsorption model, in which Wang et al. (2003) use an empirical isotherm adsorption model whereas this work uses a SCM, and (ii) the approach to secondary redox reactions, which are modelled kinetically by Wang et al. (2003) whereas the PEA model formulation adopted in the present model considers such reactions to occur strictly based on equilibrium constraints. The implications of these differences are discussed below.

A Dirichlet boundary condition is used at the upstream end of the domain and the domain is physically semi-infinite. Wang et al. (2003) do not explicitly state which minerals are present in their simulations. In this work, Fe(III) and Mn(IV) are present in the form of ferrihydrite and pyrolusite minerals, as these minerals are likely to be present in typical aquifers. Uraninite is not initially present but is capable of forming. Carbonate, while often found in natural groundwaters, is omitted here to provide similarity with Wang et al. (2003). It is acknowledged that the inclusion of carbonate may significantly alter the results, and thus it may not be possible to extrapolate the results presented here to such scenarios. All parameters were obtained independently and the comparison between the two models was made without calibration parameter values.

Table 4.1. Initial and boundary geochemical conditions.

Species	Units	Boundary concentration (x = 0, t)	Initial concentration (x > 0, t = 0)
OC	μmol l^{-1}	3000	0
O_2	μmol l^{-1}	100	100
N(V)	μmol l^{-1}	200	200
S(VI)	μmol l^{-1}	300	300
U(VI)	μmol l^{-1}	0.1	0.1
Ferrihydrite	μmol dm^{-3}	0	50
Pyrolusite	μmol dm^{-3}	0	25
pH	-	6.5	6.5

Table 4.2. Transport conditions used in simulations.

Parameter	Units	Value for Wang et al. (2003) comparison
Groundwater velocity, v	m yr^{-1}	10
Dispersivity, a	m	0.25
Mobile region porosity, θ_m	-	0.35
Immobile region porosity, θ_i	-	N/A
Mobile-immobile mass transfer, γ	yr^{-1}	0
Δx	m	0.25

Table 4.3. Microbial parameter values used in simulations, from Wang et al. (2003).

Parameter	Value	Units
μ_{O_2}	0.1	mol l^{-1} yr^{-1}
μ_{NO_3}	0.004	mol l^{-1} yr^{-1}
μ_{Mn}	0.001	mol l^{-1} yr^{-1}
μ_{Fe}	0.0005	mol l^{-1} yr^{-1}
μ_{U}	0.0002	mol l^{-1} yr^{-1}
$\mu_{SO_4^{2-}}$	0.017	mol l^{-1} yr^{-1}
μ_{CO_2}	0.05	mol l^{-1} yr^{-1}
K_{OC}	54	µmol l^{-1}
K_{O_2}	20	µmol l^{-1}
K_{NO_3}	20	µmol l^{-1}
K_{Mn}	3.7	µmol l^{-1}
K_{Fe}	3.7	µmol l^{-1}
K_{U}	0.1	µmol l^{-1}
$K_{SO_4^{2-}}$	10	µmol l^{-1}
χ_{O_2}	0.5	µmol l^{-1}
χ_{NO_3}	6	µmol l^{-1}
χ_{Mn}	1	µmol l^{-1}
χ_{Fe}	5	µmol l^{-1}
$\chi_{SO_4^{2-}}$	15	µmol l^{-1}

Figures 4.2-4.7 show the simulated spatial concentration distributions of various species and minerals in the domain after one year of biostimulation. Wang et al. (2003) simulated results are also detailed in these figures: if a figure does not include Wang et al. (2003) data, this is because such data was not provided in that work.

Figure 4.2 presents the OC, pH and carbonate concentration along the flow path. Figure 4.3 presents the spatial distribution of EAs compared with those reported by Wang et al. (2003), demonstrating that the model captures the characteristic geochemical behaviour reported in their work. Figure 4.2 reveals that the OC entering the domain is quickly oxidized, and the changes in pH and carbonate qualitatively reflect those that occur in

biostimulated systems (e.g., Wan et al., 2005; Luo et al., 2007). Note, however, that typical porous media may exhibit a smaller pH change than predicted, since a higher buffering capacity is possible than accounted for in this comparison scenario (cf. Abdelouas et al, 2000; Anderson et al., 2003). Additional soil buffering capacity can be easily included in the presented model due to the PHREEQC platform employed.

Figure 4.3 reveals that, as expected, the EAs are reduced sequentially in order of the most energetically favourable and a region forms in the domain that favours reduction (4 m < x < 12 m). The two models exhibit similar concentration profiles, as calculated by a comparison of the spatially integrated concentration over the 30m domain for a given chemical species, for nitrate (present model is within 11% of the result reported by Wang et al. (2003)), Fe(III) (within 12%), Mn(IV) (within 23%) and sulfate (within 12%). Figure 4.2 shows that carbonate concentration and pH increase just downgradient of the reductive region. In addition, Figure 4.4 illustrates that Fe and Mn oxyhydroxides are progressively reduced and dissolved whilst reduced species such as Fe(II), Mn(II) and HS^- accumulate also just downgradient of the reductive region. These geochemical changes are characteristic of U(VI) immobilisation in biostimulated sites and sediments (e.g., Abdelouas et al., 1998a; Finneran et al., 2002b; Holmes et al., 2002).

The abiotic reactions in the presented model proceed similarly to those reported by Wang et al. (2003): Fe(III) and Mn(IV) reduction appears to be less progressed than nitrate (Figure 4.3), but this is due to the occurrence of simultaneous abiotic reactions. The high HS^- concentration in the reduced region may reduce Fe(III) and Mn(IV)

abiotically before bacterial reduction is possible. These processes appear to be enhanced in the presented model, resulting in the reduced species Fe(II) and HS^- exhibiting lower concentrations compared to those predicted by Wang et al. (2003) (Figure 4.4). This difference is likely due to the different models' formulations for secondary redox reactions. While it is difficult to find comprehensive experimental data in which all relevant parameters have been measured, confidence in the model(s) is provided by the qualitative match achieved between the results presented here and the behaviour of similar systems reported in the literature (e.g., Abdelouas et al., 1998a; Finneran et al., 2002b; Holmes et al., 2002; Ortiz-Bernard et al., 2004a).

Figure 4.5 reveals that U(VI) is reduced in the reductive region of the domain once it is energetically favoured as an EA. The spatial position of the U(VI) concentration decrease and increase is slightly different for the two model outputs, reflecting the slightly differing reductive region in the domain noted previously (Figure 4.3). Wang et al. (2003) do not specify if uraninite may form in their model, whereas the presented model allows its formation in order to properly account for known DMRB activity in biostimulated subsurface environments. (The inclusion and exclusion of uraninite in the model was compared and that which included uraninite compares more closely with the results presented by Wang et al. (2003)) Due to this likely difference in approach, the observed U(IV) in solution may not be comparable between the two models. Note that the U(IV) concentration for the presented model is so low as to not be visible in Figure 4.5. The U(IV) and uraninite concentrations are presented in Figure 4.6 for the model developed in this work. The uraninite is present in the reductive region of the domain,

with a low U(IV) concentration present at the downgradient end of this region where the domain becomes more oxidizing.

The present model is within 50% of the result reported for the U(VI) concentration profile reported by Wang et al. (2003). This mismatch is due to the U(VI) concentration spike observed downgradient of the reductive region as shown in Figure 4.5. The maximum concentration of this spike increases as time progresses (data not shown). This phenomenon is not observed in the Wang et al. (2003) model output. This behaviour is a consequence of the more accurate surface complexation model used in this work, and it occurs for multiple reasons. First, the pH in the downgradient U(VI)-spike region has increased due to biological activity (Figure 4.2, 12 m < x < 18 m) resulting in a condition less amenable to adsorption (see Figure 3.5). Second, a snow-plough effect occurs: as the ferrihydrite in the reductive region is reduced, the U(VI) previously complexed to its surface desorbs, causing a net increase in U(VI) in solution downstream of the reductive region. Third, the high carbonate concentrations in this region (Figure 4.2) cause increased adsorption (Figure 4.2). All these factors may increase the propensity for U(VI) to desorb. Figure 4.7 demonstrates that the concentration of all U-sorbed species (i.e., $\equiv Fe_sO)_2UO_2$ + $(\equiv Fe_wO)_2UO_2$ + $(\equiv Fe_sO)_2UO_2CO_3^{2-}$ + $(\equiv Fe_wO)_2UO_2CO_3^{2-}$) reduces in regions where ferrihydrite is less abundant (4 m < x < 12 m). The more ferrihydrite that is reduced, the more desorption occurs and the greater the concentration of the U(VI) spike. Where the ferrihydrite concentration and pH decrease to initial levels (at x > 18 m), the U(VI) concentration also decreases (Figure 4.5). Empirical adsorption models, such as employed by Wang et al. (2003),

appear not to capture this behaviour, likely because they do not account for the variations in pH, bicarbonate or mineral abundance along the flow path. The superior SCM model used in this work is generally likely to provide improved accuracy in modelling systems exhibiting this behaviour.

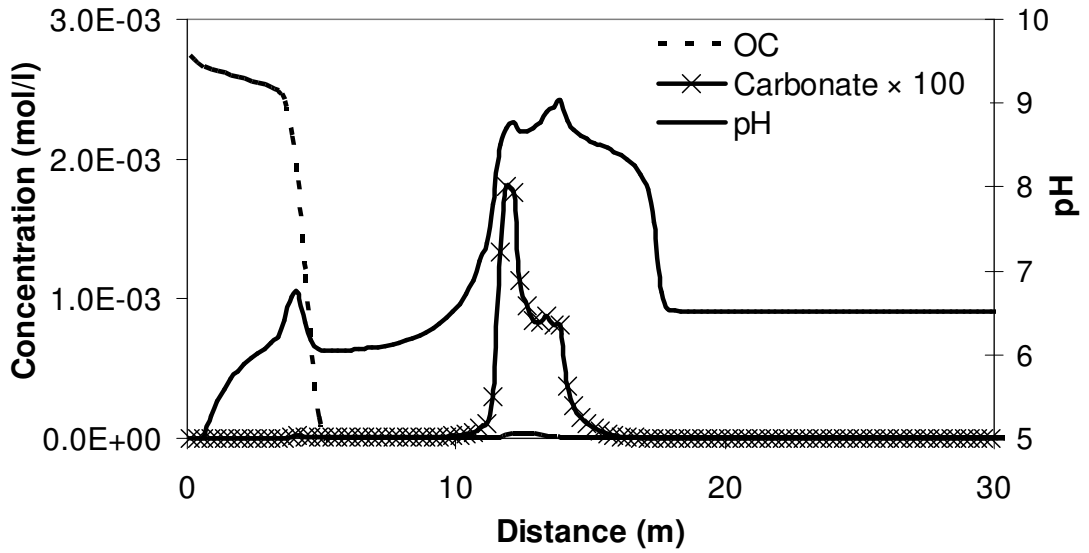

Figure 4.2. OC, carbonate and pH spatial profiles in the model developed in this work after one year of biostimulation.

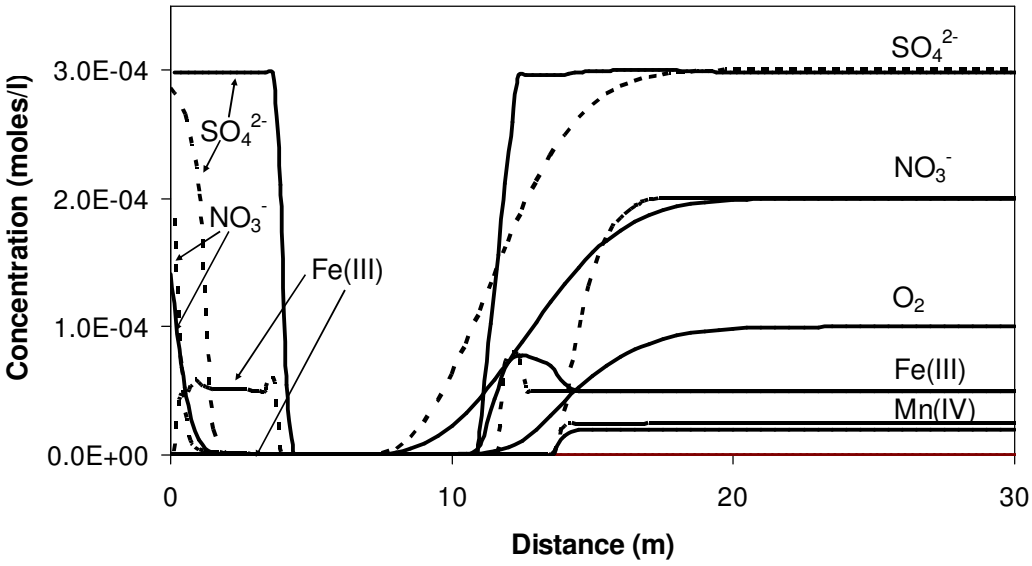

Figure 4.3. Model comparison for electron acceptor species after one year of biostimulation. Dashed lines show this model output, solid lines show Wang et al. (2003) model output.

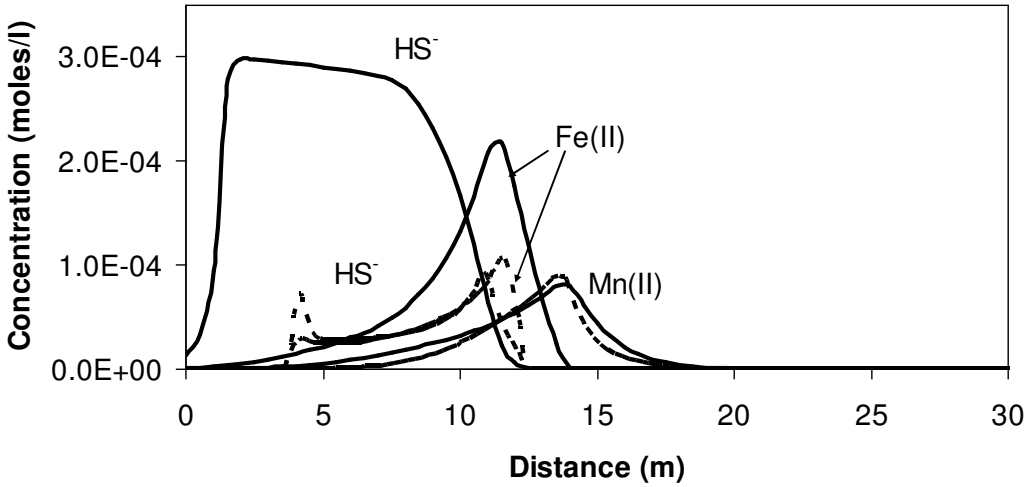

Figure 4.4. Model comparison for reduced geochemical species after one year of biostimulation. Dashed lines show this model output, solid lines show Wang et al. (2003) model output.

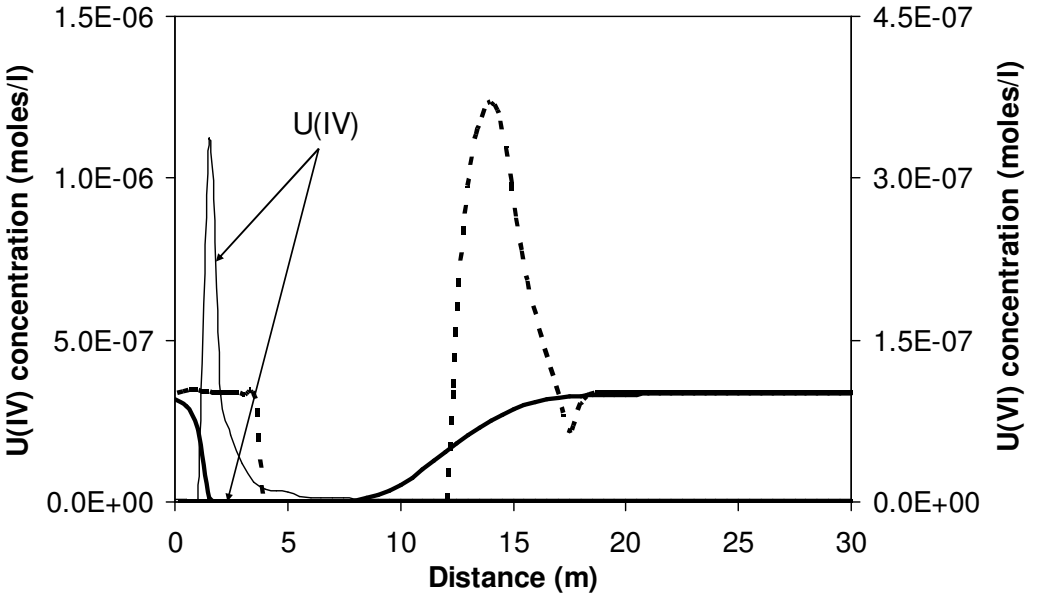

Figure 4.5. Model comparison for U(IV) (thin lines) and U(VI) species (thick lines) after one year of biostimulation. Dashed lines are this work's model output, solid lines are Wang et al. (2003) data.

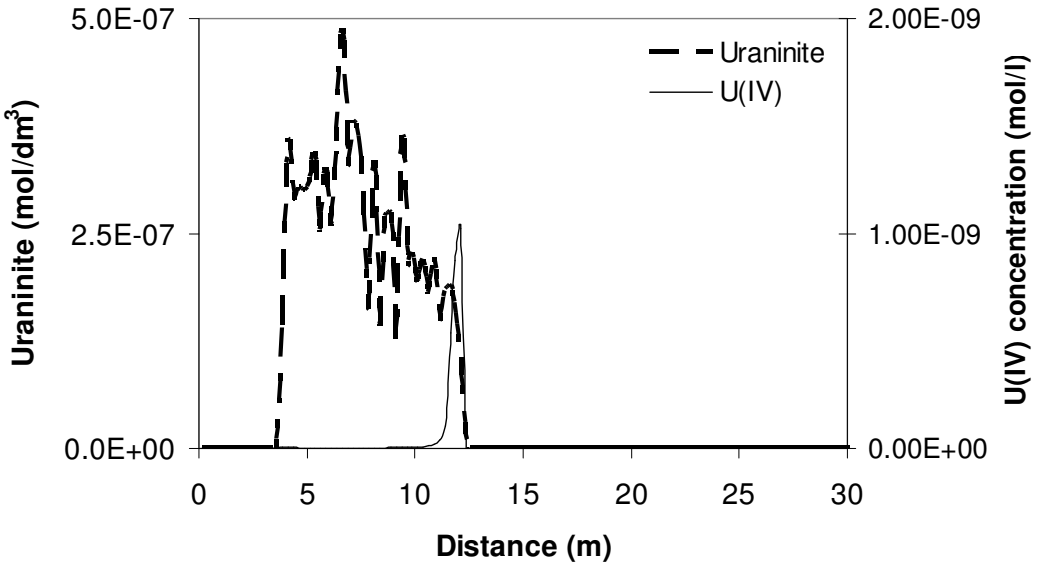

Figure 4.6. Model output for uranium species after one year of biostimulation.

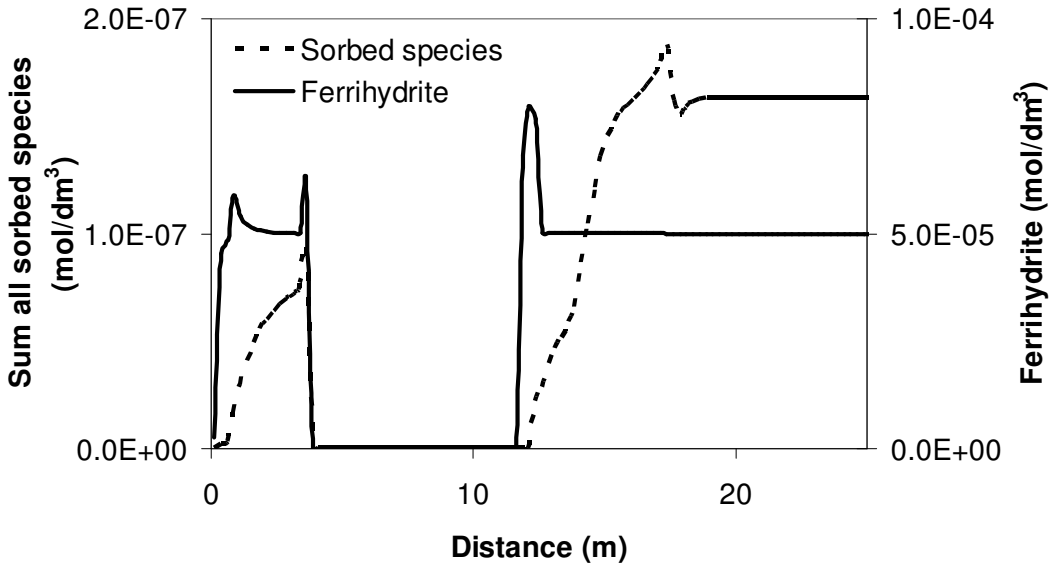

Figure 4.7. Spatial profile of sorbed species and ferrihydrite after one year of biostimulation.

4.5. Evaluation to an experimental data set

Wan et al. (2005) conducted five (duplicated) column experiments using the mixed shale saprolite and gravel sediment from the "Area 2" of the DOE Natural and Accelerated Bioremediation (NABIR) Program's Field Research Center (FRC) in Oak Ridge National Laboratory. The sediment contains shale saprolite that displays multi-porosity behaviour (Roden and Scheibe, 2005; Gwo et al., 1995; Jardine, 1993). A salt and OC solution was continuously injected into the columns. Within 100 days the U(VI) reduced to U(IV) by DMRB indigenous to the sediments. To date, the experiment has not been modelled previously.

Nevertheless, the experiment takes place under conditions that may not be typical of some U-contaminated field sites. The model developed in this chapter is intended for

bioremediation in media downgradient of the contaminant source. Therefore, the influent should contain U(VI), but the modelled domain of interest should not contain a U source. However, the experiment presented by Wan et al. (2005) uses a site sediment (media) which contains U, and the influent solution in the experiment does not contain U. Unfortunately, the proportion of sorbed U initially present within the column in not known (Wan, J., 2007, personal communication).

General column and geochemical conditions used in all evaluation simulations are presented in Table 4.4. Iron and manganese in the sediment are represented by ferrihydrite and pyrolusite, respectively, and are present within both mobile and immobile modelling regions. Simulation transport conditions used are presented in Table 4.5. In order to account for the potential influence of the downstream column boundary condition, the simulated domain length is equal to the length of the column as given in Table 4.5.

As U was not present in the experiment influent solution, any U released from the column must come from the sediment itself. It is evident from the experimental data that this "release" of U is slow relative to other biological and chemical process occurring within the sediment sample. In order to represent the process occurring in this experiment as accurately as possible, two different approaches were used. The first approach considered kinetic dissolution of U as a mechanism within the sediment sample. Thus, the amount of U present in the column at any time is solely based on the amount of U-mineral present. This approach will be discussed first.

Schoepite was assumed to represent the U present within the sediment (in both mobile and immobile regions). The schoepite kinetically dissolves along the entire sediment flow path at the rate (Riba et al., 2005):

$$R = K_r A_m \frac{m}{m_0}\left(1 - \frac{\mathrm{IAP}}{K_{sp}}\right) \tag{4.1}$$

where K_r is the constant rate (mol m^{-2} s^{-1}), A_m is the total surface area of schoepite per litre (m^2 l^{-1}), m is the current number of moles of schoepite (mol), m_0 is the initial number of moles of schoepite (mol), IAP is the ionic activity product, and K_{sp} is the equilibrium constant ($\log K_e = 5.994$) for the reaction

$$UO_2(OH)_2{:}H_2O + 2H^+ = UO_2^{2+} + 3H_2O$$

The surface area (A) was adjusted to represent the amount of schoepite in column, assuming a specific surface area based on the surface area and mass of schoepite used by Riba et al. (2005). Surface complexation was not considered. Kinetic dissolution parameters reported by Riba et al. (2005) were used. These are displayed in Table 4.6. This model failed to yield results that closely matched those of the experiment. Inverse modelling might have been performed in order to fit a set of parameters that would reproduce the results. However, the confidence gained by such a curve-fitting exercise is limited, nor is it appropriate evaluation procedure.

Table 4.4. Column conditions used in evaluation simulations (all data from Wan et al., 2005).

Parameter	Units	Value
Column volume	dm^3	0.16
Sediment density	$Mg\ dm^{-3}$	1.48
U in column sediment	$mg\ kg^{-1}$	206
Influent[a]		
OC	$mmol\ l^{-1}$	32
pH		7.2
Na (represents NaCl)	$mmol\ l^{-1}$	1
Cl (represents NaCl, $CaCl_2$, $MgCl_2$, KCl)	$mmol\ l^{-1}$	6
Ca (represents CaCl)	$mmol\ l^{-1}$	1
Mg (represents $MgCl_2$)	$mmol\ l^{-1}$	1
K (represents KCl)	$mmol\ l^{-1}$	1
Initial conditions in column[a]		
pH		7.4
SO_4^{-2}	$mmol\ l^{-1}$	46.2
Ferrihydrite[b]	$mol\ dm^{-3}$	2.58
Pyrolusite[b]	$mol\ dm^{-3}$	0.12
Calcite[b]	$mol\ dm^{-3}$	0.93

[a]Calculated from % mass of Fe/Mn/Ca in Table 1 of Wan et al. (2005), using column volume and sediment density.

[b]Solutions are charge balanced.

Table 4.5. Transport conditions used in evaluation simulations.

Parameter	Units	Value	Reference
Groundwater velocity, v[a]	$m\ yr^{-1}$	0.013	Wan et al. (2005)
Dispersivity, a[a]	m	0	assumed
Domain length	m	0.2	Wan et al. (2005)
Media mobile region porosity, θ_m	$m^3\ m^{-3}$	0.2	assumed
Media immobile region porosity, θ_i	$m^3\ m^{-3}$	0.35	assumed

Table 4.6. Schoepite dissolution simulations.

Parameter	Units	Value	Reference
Schoepite dissolution rate, K_r	mol m^{-2} s^{-1}	4.1×10^{-10}	Riba et al. (2005)
Surface area of schoepite, A[a]	m^2 l^{-1}	5.64	Riba et al. (2005)
Initial number of moles of schoepite, m_0[b]	mol dm^{-3}	0.003	Wan et al. (2005)
OC fermentation rate, k	d^{-1}	fit to data	
Mobile-immobile mass transfer rate, γ	s^{-1}	5×10^{-5}	Luo et al. (2007)

[a]Adjusted from Riba et al. (2005) for comparative U present in the experiment.

[b]Calculated from column volume, sediment density, and U in column sediment.

The second modelling approach assumed that the kinetic "release" of U was characterised by both a kinetic diffusion of U from the immobile porosity region and (potential) desorption of sorbed U induced by pH changes. A similar approach was used by Luo et al. (2007) and Roden and Scheibe (2005). This better represents the known processes occurring within U contaminated dual porosity media, since it is rather likely that (1) more than 60% of U present in the column was initially present as U(VI) (Wan et al., 2005) and (2) surface complexation is likely to be significant within U-contaminated pore water in which carbonate (from calcite) is present. The model therefore considers surface complexation to occur. Given that equilibration with pore water would allow a distribution of U(VI) throughout both the mobile and immobile regions of the media, U(VI) was considered present within both regions in the model. However, due to diffusive mass transfer limitations within the saprolite media, the relative quantities of U(VI) within the mobile and immobile regions may be different. This has been explored by conducting simulations with various initial U(VI)

concentrations within each region. Table 4.7 presents four cases with varying initial OC concentrations for the mobile (OC_m) and immobile (OC_i) regions.

OC may also be distributed unevenly between regions of different characteristic flow velocities (the mobile and immobile regions), since the collected sediment contained OC from a prior field site remediation experiment (Wan, J., 2007, personal communication). This can be seen in the experimental effluent OC concentrations that are upward of 100 mM, much greater than in the influent OC concentration of 32 mM. This has been explored by conducting simulations that consider initial OC concentrations within each region that appear to fit the experimental data appropriately. Table 4.7 presents four cases with varying initial U(VI) concentrations for the mobile ($U(VI)_m$) and immobile ($U(VI)_i$) regions. The total quantity of U present within the sediment is 2.1×10^{-4} mol (Wan et al., 2005). If this total amount were to dissolve within the column pore water, the result would be a U concentration of 3 mM (see Table 4.7). However, due to the structured nature of the sediment, it is unlikely that all U present within the sediment has the opportunity to dissolve in the pore water. Therefore, pore water U concentrations of less than 3 mM, which fit the experimental data more appropriately, are considered. The OC fermentation rate (k) and mobile-immobile region mass transfer rate (γ) were adjusted to fit the data.

The mass transfer rates (γ) used are within the range reported in the literature (Feehley et al., 2000; Harvey and Gorelick, 2000; Kim and Corapcioglu, 2002; Haws et al., 2004

and 2005; Jørgensen et al., 2004; Luo et al., 2005; Roden and Scheibe, 2005), including those reported for the Area 2 ORNL FRC field site sediment used in the experiment (Luo et al., 2007). Likewise, the OC fermentation rates used are within range of those reported in the literature (cf. Hunter et al., 1998).

Table 4.7. Mass transfer and sorption driven U mechanisms simulations.

Simulation	k	γ	OC_m	OC_i	$U(VI)_m$	$U(VI)_i$
Units	d^{-1}	s^{-1}	mmol l^{-1}	mmol l^{-1}	mmol l^{-1}	mmol l^{-1}
Case A	0.1	5×10^{-8}	500	500	0	0.1
Case B	0.1	1×10^{-5}	900	500	3	0.1
Case C	0.01	5×10^{-8}	700	700	0.02	0.1
Case D	0.05	9×10^{-8}	100	600	0.01	0.15

Case A considers that U(VI) is not initially present in the mobile region. Figure 4.8 shows the effluent log(U(VI)) concentrations for the five columns, as originally presented in Wan et al. (2005), and the model effluent log(U(VI)) concentration for the model. Figure 4.9 presents the same data on an arithmetic U(VI) scale. The arithmetic U(VI) scale is considered more appropriate for this data, since the log(U(VI)) plot gives the impression that the different data sets show similar concentrations, when in fact they do not. In order for a fair comparison to be made between the model predictions and the experimental data, arithmetic plots are deemed more appropriate.

The model matches the data relatively well qualitatively, showing an early rise in U(VI) concentration, followed by a gradual decline as U(VI) is reduced. However, the log plot fails to show that the U(VI) concentration is initially perhaps too low, and that the model does not predict the initial fall in U(VI) concentration accurately. This is reflected in the

modelled OC concentration shown in Figure 4.10, which appears to show the loss of OC as initially too high and later too low. Initially, the OC present in the mobile region is flushed from this region. OC concentrations then drop to level which reflect the combination of the influent OC and the OC diffusing from the immobile region.

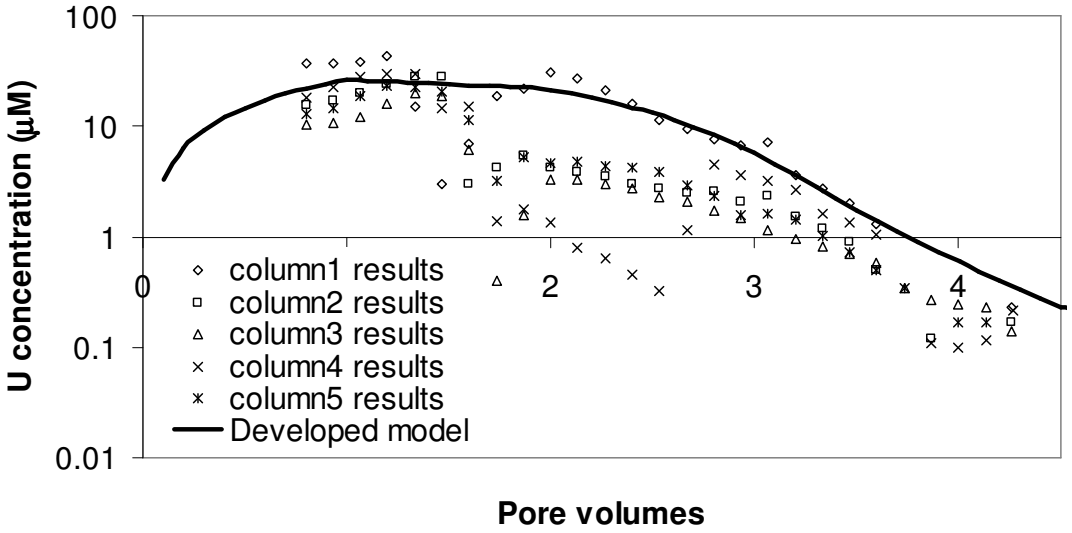

Figure 4.8. Effluent log(U(VI)) concentration for Case A.

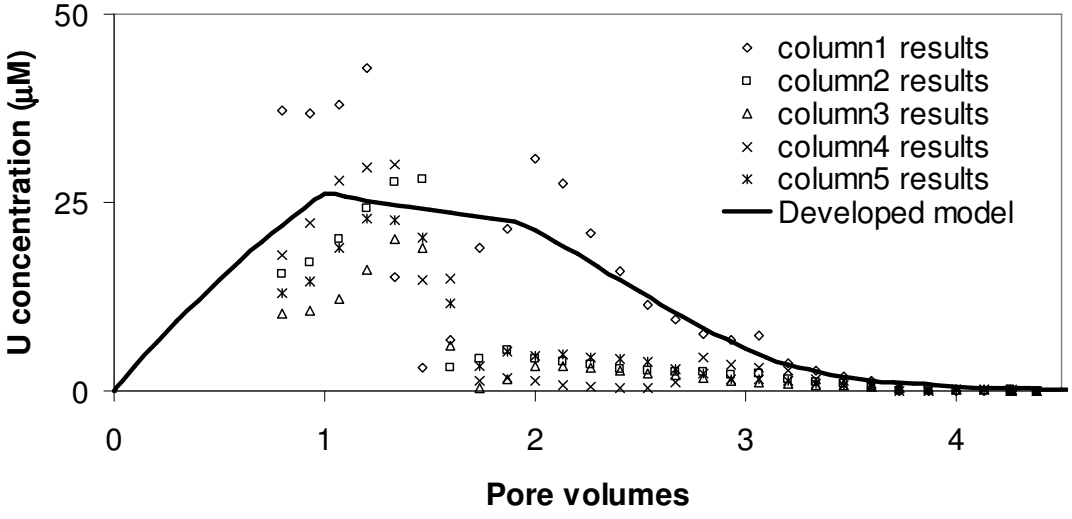

Figure 4.9. Effluent U(VI) concentration for Case A.

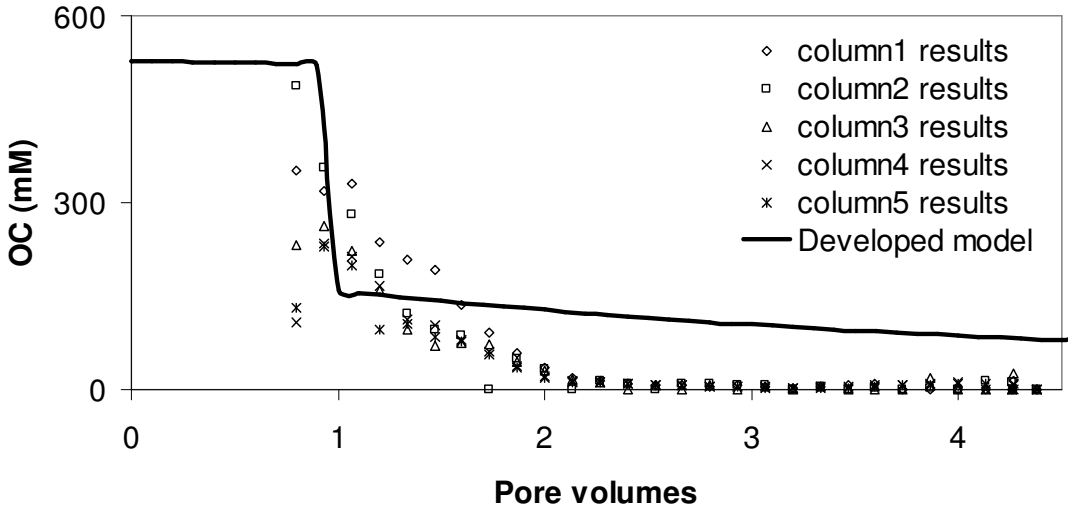

Figure 4.10. Effluent OC concentration for Case A.

Case B assumes greater OC and U(VI) concentrations in the mobile region initially. Regional diffusive mass transfer is also considered to be higher. Figure 4.11 demonstrates that with high initial U(VI) concentration, the presence of U(VI) is overestimated, resulting in a poor match, both quantitatively or qualitatively. Figure 4.12 shows an improved OC concentration profile relative to the data, though it does not capture the early concentration-peaking behaviour observed at around one pore volume.

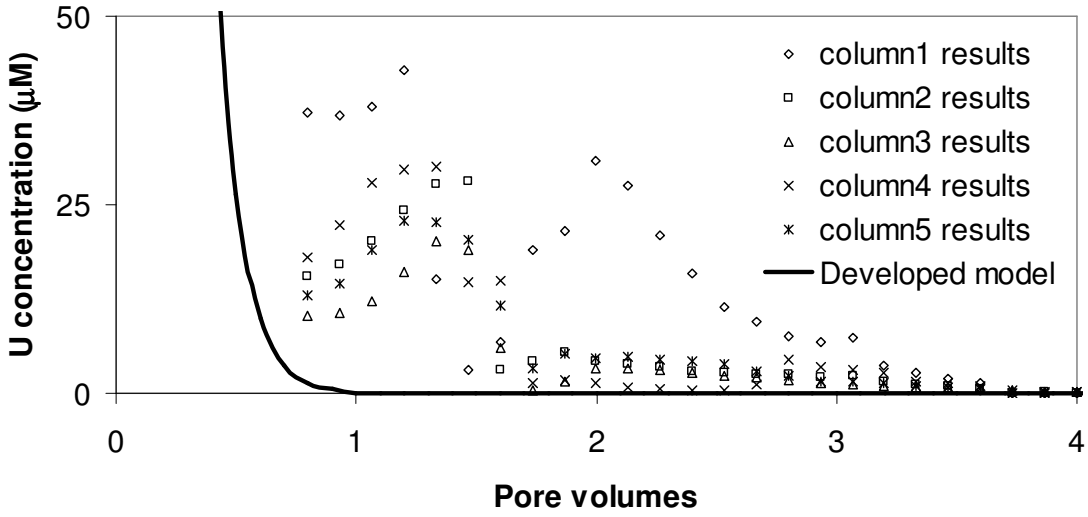

Figure 4.11. Effluent U(VI) concentration for Case B.

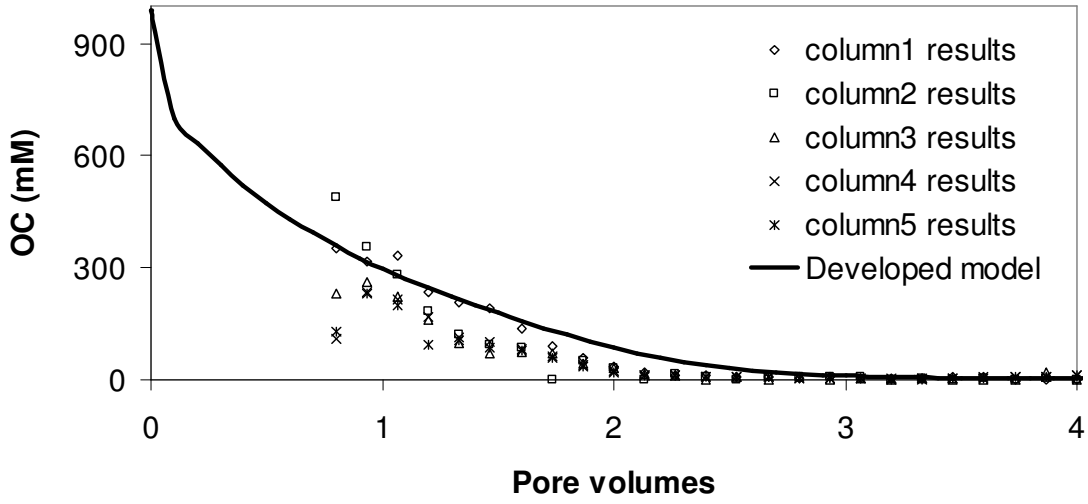

Figure 4.12. Effluent OC concentration for Case B.

Case C assumes a lower OC fermentation rate, and different initial OC and U(VI) concentrations. Although slightly temporally shifted, it successfully captures the U(VI) concentration profile both qualitatively and quantitatively as shown in Figure 4.13. The initial rise in U(VI) concentration to a peak concentration is captured, as is the

subsequent decay. This reflects the experimental data's initial release of U and the ensuing U(VI) decay as U is immobilised. However, while the match of the OC concentration profile is qualitatively sufficient, in a quantitative sense it is less successful (Figure 4.14). The problems associated with matching Case A to the experimental data again apply here for OC.

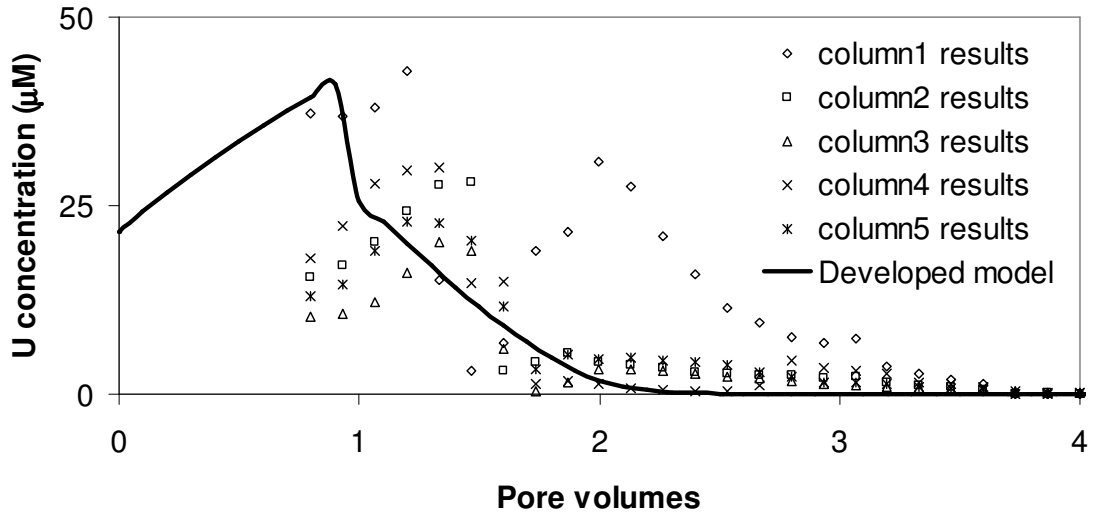

Figure 4.13. Effluent U(VI) concentration for Case C.

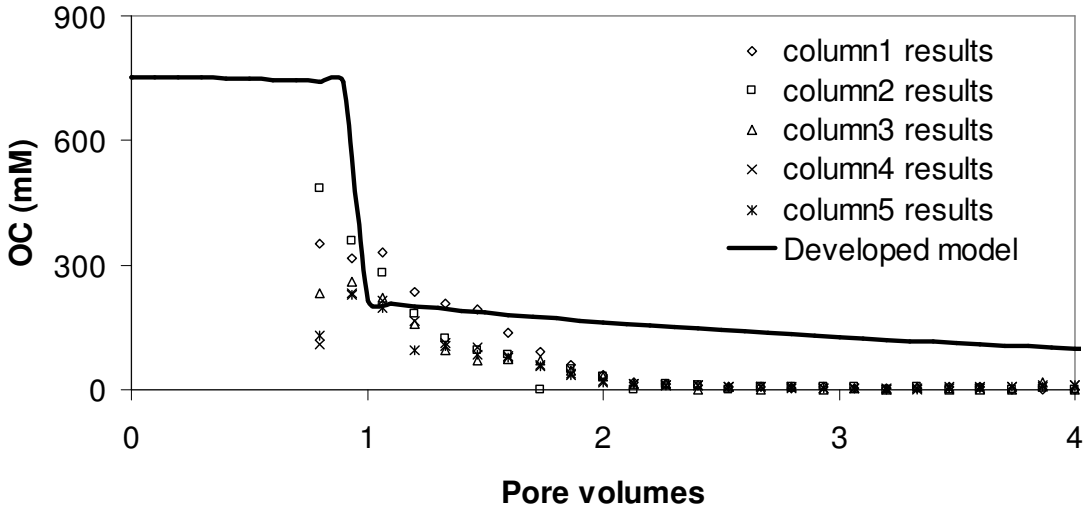

Figure 4.14. Effluent OC concentration for Case C.

The difficulty in quantitatively matching both U(VI) and OC experimental data is partially the result of comparing the modelling results to the data of five different columns. Figure 4.15 therefore presents the OC concentration profile for Case D against the experimental data of column 4 only. The model matches the data favourably, with the same qualitative initial rise and later decay, and similar quantitative concentrations. Figure 4.16 shows the U(VI) concentration profile for Case D. The temporal shift between the model and experimental results is now made clearer. The profiles are similar in both qualitative and quantitative behaviour, except that the model's profile is shifted temporally by approximately one pore volume. This shift may be due to the experimental results showing a delayed equilibration with the pore water or delayed desorption of U(VI) relative to the model. The goodness of fit of the model data to the experimental data was obtained by comparing the temporally integrated concentration profiles for the data presented in Figures 4.15 and 4.16. Using this measure of

comparison yields a 6% difference between the model result and the experimental data for the U(VI) concentration profile presented in Figure 4.16. Naturally, this comparative measure cannot account for the temporal shift witnessed in the results, but nevertheless demonstrates that the model successfully predicts the experimental results quantitatively without consideration of temporal shifts. A similar analysis on the OC data in Figure 4.15 yields a model result at 214% of the experimental data. However, this is due to the significant rise in OC before approximately 0.8 pore volumes has passed through the column. As the concentration of OC in the experimental data is not known before this time (i.e., it is effectively considered to be zero), but the model data assumes a high OC concentration here, it is to be expected that the model results over-estimate the experimental data. If the intial 0.8 pore volumes of the model results are considered to instead display a zero concentration for OC as is assumed for the column then the model data gives a 68% over-estimation of the experimental data. The model is therefore capable of capturing the U(VI) concentration profiles concurrently, though minor temporal shifts may be apparent. The simulations demonstrate that the model can capture the key behaviour of the system with qualitative accuracy and relative quantitative accuracy.

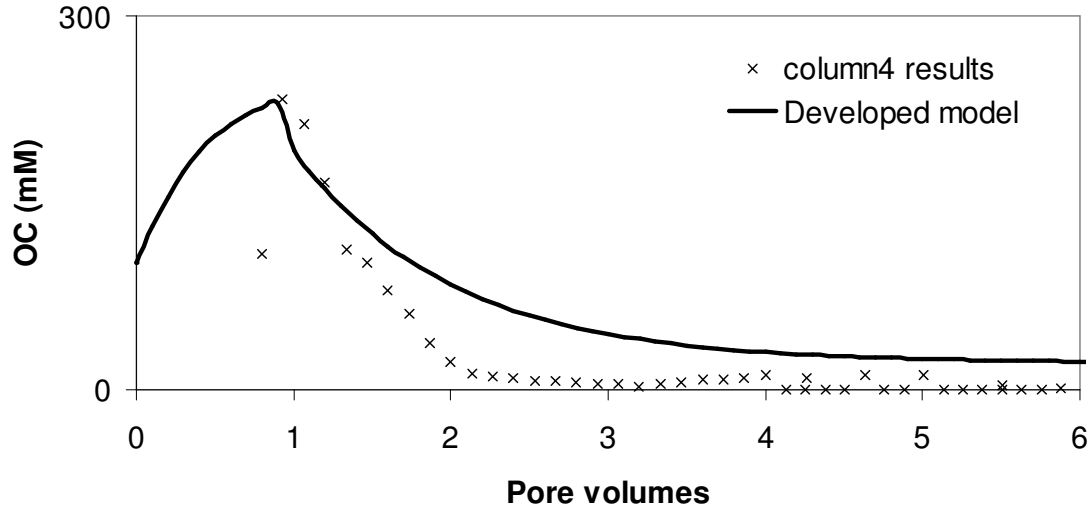

Figure 4.15. Effluent OC concentration for Case D.

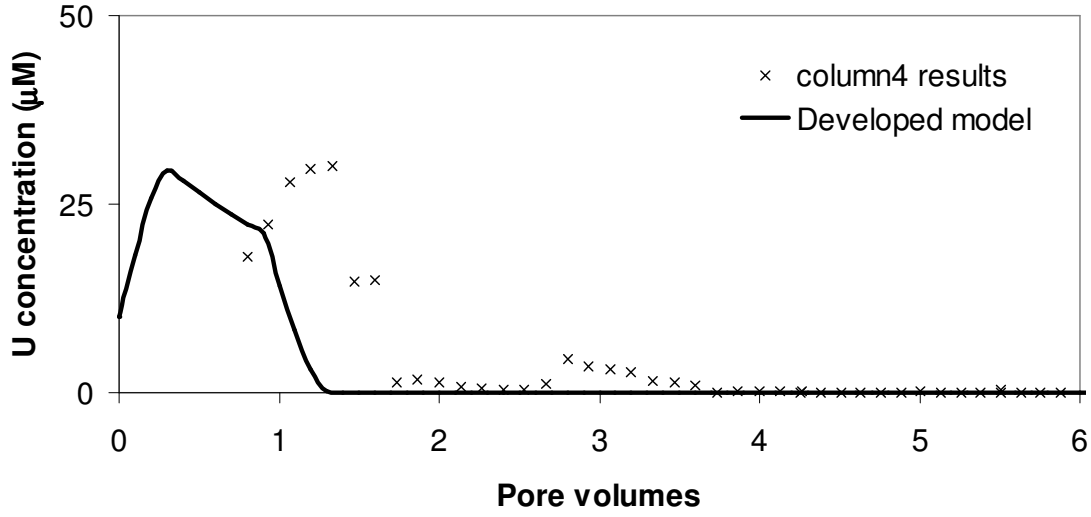

Figure 4.16. Effluent U(VI) concentration for Case D.

The ability to confidently validate biogeochemical transport models is further challenged by the fact that parameter values in natural systems may vary by several orders of magnitude. For example, using 23 references from a variety of environments, Hunter et al. (1998) collected first-order OC oxidation rate values that covered a range of 10 orders of magnitude. When multiple parameters may range over widely varying values,

confidence may not entirely be warranted by fitting a single model to a single data set. This is particularly true when numerous parameters may be "tweaked" to obtain a match to the experimental data. However, evaluation using parameter values which remain within the ranges of values reported in the literature add some degree of confidence in the ability of the model to adequately capture real behaviour.

Relatively minor changes in parameter values can affect results significantly. Case C is reproduced in Figure 4.17 with two additional modelling curves that were obtained using the same conditions as Case C, except that one used a higher value OC fermentation rate value (k = 0.1 d^{-1}) and the other a lower rate value (k = 0.001 d^{-1}). These values remain well within the bounds of the range of possible OC fermentation rates reported (see Hunter et al., 1998). At the higher OC fermentation rate the modelled bacteria operate at a faster rate than those in the experiment and the U(VI) concentration is correspondingly observed to reduce more rapidly. Conversely, at the lower OC fermentation rate the modelled bacteria operate at a slow rate than those in the experiment and the effluent U(VI) concentration is overestimated. Thus, with increased or decreased k values the model fails to accurately capture the behaviour of the system. This simple illustration demonstrates that the model (i) is sensitive to model parameters (in this case, k) and, (ii) the experimental data fits within a specific range of certain parameter values (i.e., those displayed in Table 4.7). The fact that the model can only reproduce the experimental data under such constrained parameter values (at a specific k value in Figure 4.17) highlights the importance of possessing accurately defined parameter values. One of the key difficulties in validating this model to the experimental data is the lack of known

data. For example, the *k* value and the initial concentrations of U(VI) and OC are not known for the experiment. In spite of this, the results presented here demonstrate that a suitable match to experimental data may be attained, and suggest that an improved match might be obtained if only such data were known. This builds confidence in the ability of the model to capture real behaviour.

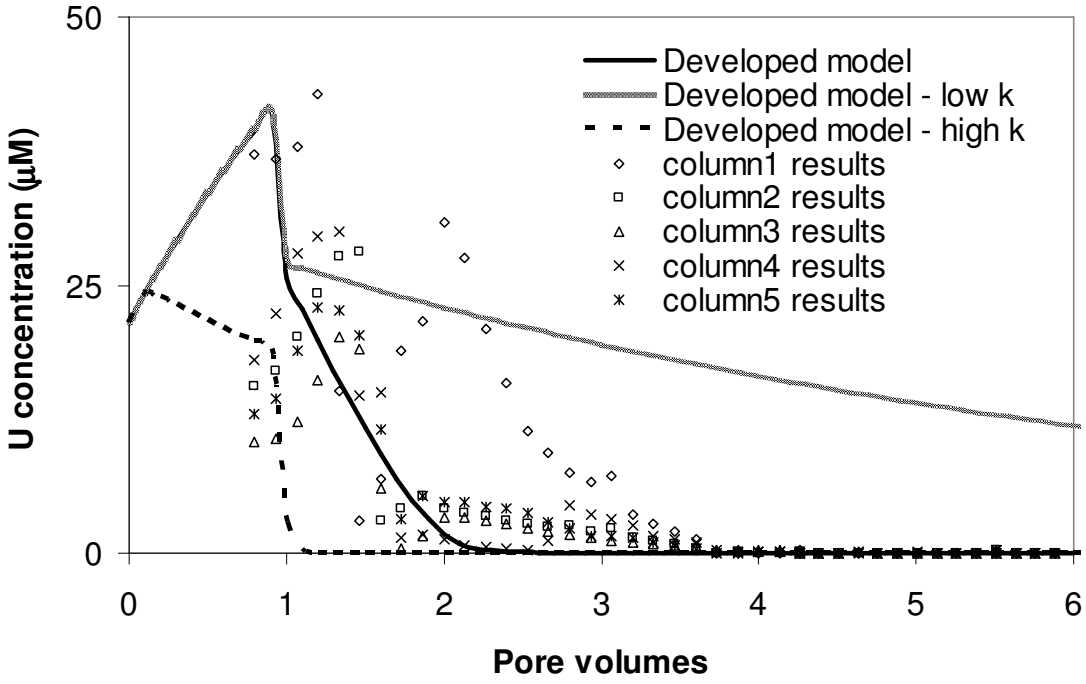

Figure 4.17. Comparison of effluent U concentration for different OC fermentation rates against experimental data.

4.6. Conclusions

In order to build confidence in the capabilities of the model developed in the present work, the model was evaluated against (i) an existing biogeochemical transport model that included redox and U related geochemistry, and (ii) an experimental data of a

column experiment in which DMRB were stimulated to reduce U(VI) reported in the literature. The difficulty in finding appropriate data sets for evaluation highlights the need for more complete data sets in this topical area.

A one-dimensional simulation in a single porosity domain compared favourably to the model developed by Wang et al. (2003) without any model calibration. The geochemical changes predicted were qualitatively characteristic of U(VI) immobilisation in biostimulated sites and sediments. Differences between the concentration profiles of certain species were attributed to the different models' formulations for secondary redox reactions (kinetic versus partial equilibrium approach) and the different surface complexation models utilised (constant K_d versus SCM).

The column experiment of Wan et al. (2005) was modelled in order to provide model evaluation against U(VI) bioimmobilisation in a heterogeneous porous media. The model successfully reproduced the experimental U(VI) and OC concentration profiles independently. However, difficulty arose in reproducing both U(VI) and OC experimental data in parallel.

These evaluation exercises build confidence in the capability of the developed model to capture the relevant processes occurring within U(VI) bioimmobilisation schemes.

5. Impact of dual porosity media on U(VI) bioimmobilisation

5.1. Introduction

The aim of this chapter is to give preliminary insight into the specific effects dual porosity (DP) porous media might have on U(VI) bioremediation efficiency. Comparison is made between the developed model and an existing model for a single porosity (SP) porous medium simulation. Simulations examining model predictions for DP porous media are then considered.

To aid later discussion, it is first worth noting the impact of surface complexation on the system. Figure 5.2 displays the presented model results previously presented in Figure 4.14 in Section 4.5, but shows how the U(VI) concentration varies with time at x = 10 m, with the inclusion and the exclusion of the SCM. When surface complexation is included, the U(VI)-spike is expressed as a "pulse" with respect to time. Following this spike, full reduction of U(VI) is rapid. However, when surface complexation is not included, the U(VI) spike is no longer present. This further confirms that the U(VI)-spiking behaviour is the result of surface complexation behaviour. Thus, the surface complexation behaviour of the system may have a significant impact on downstream contaminant concentrations. Empirical adsorption models, such as employed by Wang et al. (2003), appear not to capture this behaviour, likely because they do not account for the variations in pH, carbonate or mineral abundance along the flow path. This supports similar conclusions made by existing experimental and modelling work (Luo et al.,

2006). However, more detailed research is needed to characterize whether such effects result in U(VI) spikes in lab or field conditions.

5.2. Impact of dual porosity media

Simulations were conducted in order to investigate the potential impact of DP media on the effectiveness of U immobilisation. The SP case presented in Section 4.4, involving a homogeneous sand, is compared here to a similar scenario characterized by a combined low-*K* and high-*K* porous medium (e.g., interspersed sand and clay stringers).

The porosities of the mobile and immobile regions were varied to provide two different "porosity cases". In both cases the total porosity, θ_t, of the media takes the same value (0.35) as the SP system to give equivalent pore space between the SP and DP systems. The first case considers the porosity of the mobile region, θ_m, to be 0.1 and the porosity of the immobile region, θ_i, to be 0.25. The second case considers these porosity values to be reversed, with $\theta_m = 0.25$ and $\theta_i = 0.1$.

Bacterial activity is considered here to take place only in the mobile region, because its presence in both the mobile and immobile regions would result in a net increase in the bacterial activity, creating a biased comparison to the SP system. Figure 5.1 displays the arrangement of the DP model. The figure displays individual model cells for both the mobile region (in which advective-diffusive transport occurs) and the immobile region (in which no transport occurs). Each mobile cell is associated with a corresponding

immobile cell and all aqueous chemical species may transfer between each mobile region cell and its corresponding immobile region cell via diffusive mass transfer. In this chapter, microbially mediated U(VI) reduction occurs only in the mobile region in which the bacteria are present. It should be noted that U(VI) may be sequestered in the immobile region and thereby essentially rendered immobile. U(VI) may therefore be effectively immobilised by both microbially mediated reduction and by sequestration in the immobile region. Clearly, no such sequestration occurs in the SP model and, as such retardation is not considered in the SP model, the DP results may be expected to exaggerate delays in U(VI) immobilisation.

The initial geochemical conditions are maintained the same for all SP and DP simulations (as defined in Table 4.1, initial conditions). This is because differing geochemical conditions of the immobile region may impact the comparison, since the presence of EAs more thermodynamically favourable than U in this region will cause a net delay in immobilisation. The initial geochemical conditions are therefore maintained the same for all SP and DP simulations (as defined in Table 4.1, initial conditions). Geochemical boundary conditions are the same in both cases (Table 4.1). Transport conditions are given in Table 5.1 and the microbial parameter values given in Table 4.3.

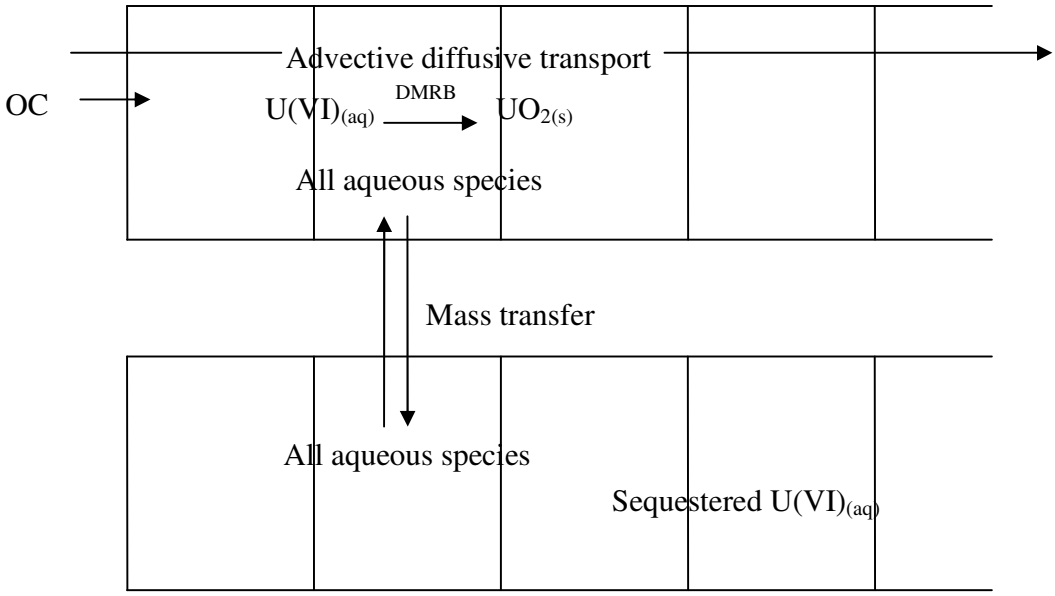

Figure 5.1. Arrangement of dual porosity domain.

Table 5.1. Transport conditions used in simulations

Parameter	Units	Value for SP simulations (from Wang et al. (2003) comparison, Section 4.6)	Value for DP simulations
Groundwater velocity, v[a]	m yr^{-1}	10	10
Dispersivity, a[a]	m	0.25	0.25
Mobile region porosity, θ_m	-	0.35[a]	Varies[b], see text
Immobile region porosity, θ_i	-	0	Varies[b], see text
Mobile-immobile mass transfer, γ[c]	yr^{-1}	0	1900 (high value) 278 (mean value) 1.8 (low value)
Δx	m	0.25	0.25

[a]Wang et al. (2003).

[b]Fetter (1994); Griffioen et al. (1998); Kim and Corapcioglu (2002); Haws et al. (2005); Roden and Scheibe (2005).

[c]Feehley et al. (2000); Harvey and Gorelick (2000); Kim and Corapcioglu (2002); Haws et al. (2004,2005); Jørgensen et al. (2004); Luo et al. (2005); Roden and Scheibe (2005). Note: the porosity values used in this work have been used to calculate mass transfer values from lumped porosity-mass transfer terms reported in the literature.

As the ultimate aim of this bioremediation strategy is significant immobilisation of U(VI), the metric used to compare results is the concentration of U(VI) passing a specific distance (10 m) downgradient of the OC injection point. Figure 5.3 presents the SP and DP results for the first porosity case (i.e., $\theta_m = 0.1$ and $\theta_i = 0.25$). In both SP and DP systems, the U(VI) concentration is observed to increase before immobilisation takes place.

In the DP system, U(VI) immobilisation is significantly delayed relative to the SP system. This is because (i) U(VI) remains sequestered in the immobile region and diffusion limits the rate of its release to the mobile region where reduction occurs (bioactivity is in the mobile region only), and (ii) the bacteria first reduce the other EAs diffusing out of the immobile region before U(VI) becomes energetically preferable for them. As well as the SP simulation, Figure 5.3 displays the U(VI) concentrations for three different mobile-immobile mass transfer rates in the DP media (low, mean and high value rates given in Table 5.1). The DP media at all three transfer rates display relatively similar U(VI) immobilisation behaviour to one another, indicating a relative insensitivity to this parameter in systems in which bioactivity takes place only in the mobile region.

Up to this point, simulations in this work have omitted the presence of carbonate from the groundwater, in order to provide similarity with Wang et al. (2003). In order to compare systems in which carbonate is and is not significant, Figure 5.4 is included as a comparison to Figure 5.3. Figure 5.4 displays the same simulations as were presented in Figure 5.3, except that significant carbonate is present in the groundwater (1 mmol l^{-1} for $x > 0$, $t = 0$ and for $x = 0$, $t > 0$). When carbonate is present, the maximum concentration of the U(VI) spike before immobilisation is predicted to be reduced (note change in vertical axis scale). Note, however, that the time to U(VI) immobilisation remains the same. This suggests that the presence of carbonate may reduce the short-term elevated

U(VI) concentrations exiting the biostimulated zone, yet it appears not to impact the long-term efficiency of remediation significantly.

Figure 5.5 displays the U(VI) concentrations for the second porosity case in which the porosities of the regions are reversed compared to those used in Figure 5.4 (θ_m = 0.25, θ_i = 0.1). (Carbonate is also considered present in this system in order for it to be directly compared with Figure 5.5.) The time taken for U(VI) immobilisation to occur is significantly reduced in this DP scenario relative to the first porosity case (i.e., θ_m = 0.1, θ_i = 0.25). The increased mobile region porosity means the volume over which microbial activity takes place is increased (bacteria are resident in the mobile region) with the result that U(VI) immobilisation is more efficient relative to the first porosity case. This suggests that the time delay for U(VI) immobilisation compared to a SP system may decrease as the porosity of the (microbially active) mobile region approaches that of the total porosity in the SP system. Again, the U(VI) concentrations for the three different mobile-immobile mass transfer rates in the DP media remain similar. As wide-ranging real-site parameterised mobile-immobile mass transfer rate (γ) values have been used for this comparison and the decline in U(VI) concentration is similar in each case (Figure 5.3), the results suggest that the mobile-immobile mass transfer rate (γ) has little impact on remediation efficiency in DP systems in which bioactivity is present in only the mobile region of the medium.

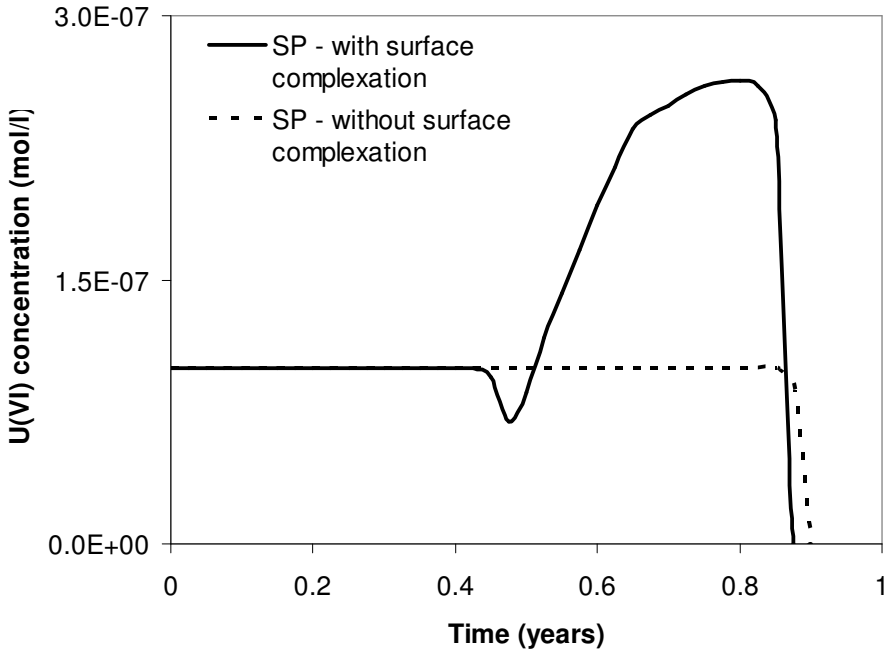

Figure 5.2. U(VI) concentration passing x = 10 m in single porosity (SP) with SCM included and without SCM included.

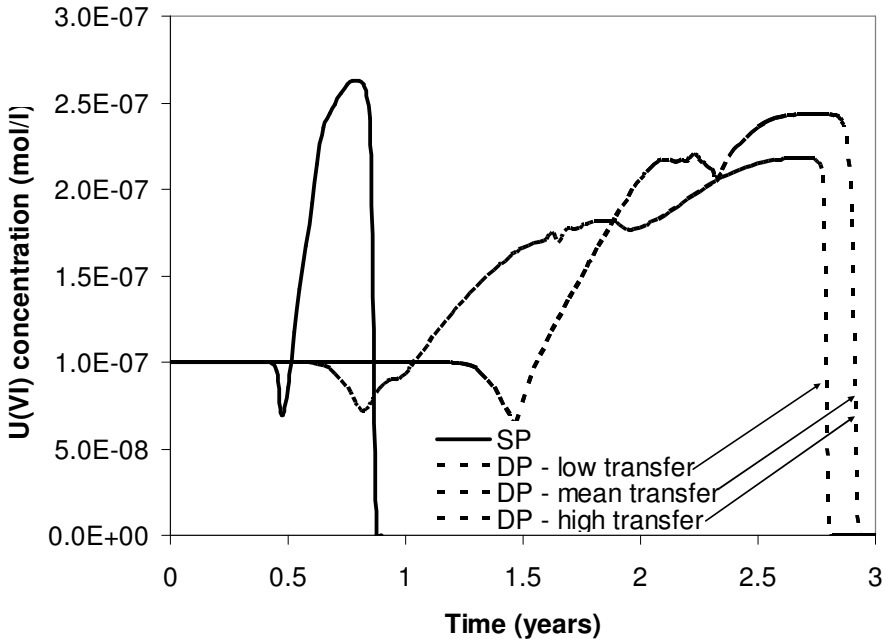

Figure 5.3. U(VI) concentration passing x = 10 m in single porosity (SP) and dual porosity (DP) mobile region. θ_m = 0.1, θ_i = 0.25.

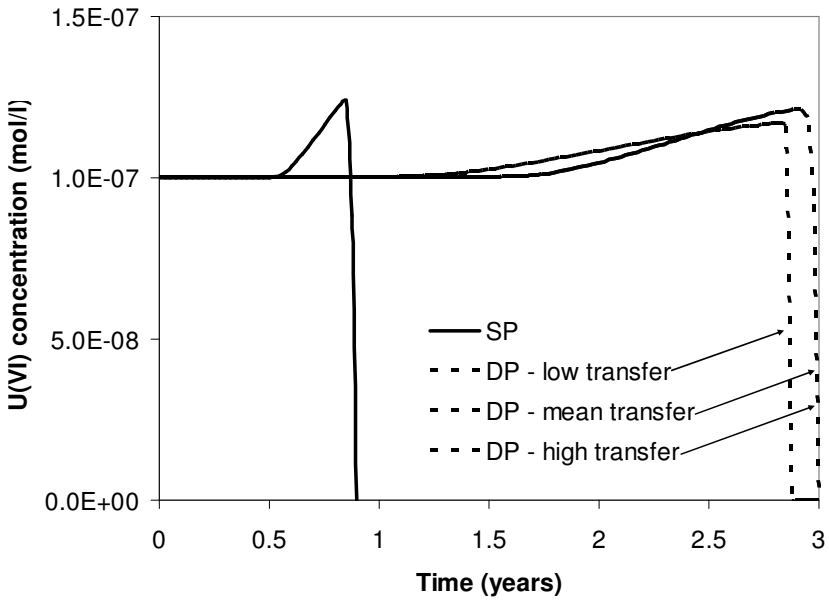

Figure 5.4. U(VI) concentration passing x = 10 m in single porosity (SP)) and dual porosity (DP) mobile region. θ_m = 0.1, θ_i = 0.25. Carbonate present in system.

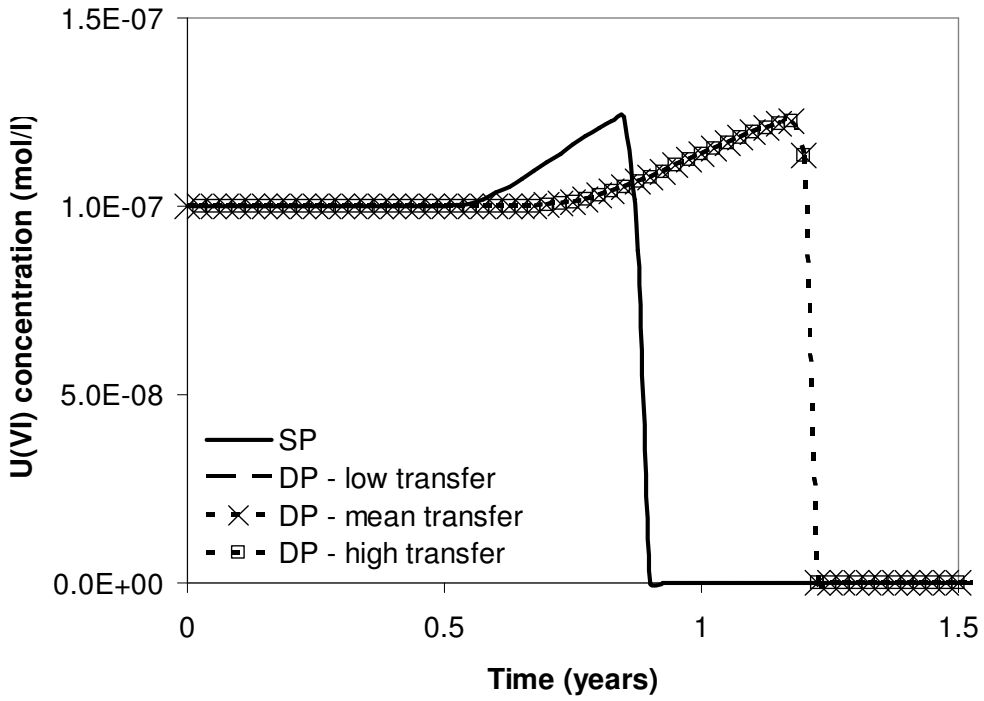

Figure 5.5. U(VI) concentration passing x = 10 m in single porosity (SP) and dual porosity (DP) mobile region. Carbonate present in system. θ_m = 0.25, θ_i = 0.1.

5.3. Comparison of first-order and Michaelis-Menten/Monod microbial kinetics modelling approaches

Two of the most common formulations for modelling microbial kinetics in reactive transport models include modelling microbial activity as (i) a first-order process with respect to the OC substrate (e.g., van Breukelen et al., 1998; Jakobsen and Postma, 1999; Basberg and Engesgaard, 1999) and (ii) a Monod/Michaelis-Menten modelling approach which accounts for OC and EA concentrations (e.g., Hunter et al., 1998; Brun and Engesgaard, 2002). (See Section 2.4.2.3 more on these approaches.)

A first-order approach implies that OC substrates limit microbial enzymatic activity (Van Cappellen and Gaillard, 1996). It may be appropriate when OC concentrations remain low relative to EAs. However, biomass populations experiencing inhibition effects due to toxic compounds or limited nutrient availability would render such an approach inappropriate. The approach further implies that the microbial populations are spontaneously ready to degrade the modelled OC; however this may not be the case when an OC new to the indigenous bacteria is introduced and as they may require time to evolve enzymatic systems to deal with the new OC, resulting in lag times. A Monod/Michaelis Menten approach considers the availability of both OC and EAs in the system, and reduces to a first-order dependency on either OC or EA when the concentration of either becomes very low, or a zero-order dependency when both OC and EA concentrations are high. This approach implicitly accounts for individual microbial populations that carry out separate TEAPs.

These assumptions are obvious when the equations of the formulation are scrutinized (equation 3.1 and 3.2). However, in biostimulated U(VI) immobilisation remediation schemes, numerous other effects such as transport effects and geochemical reactions related to the availability of EAs may complicate the simple assumptions made evident by mathematical analysis. In order to better understand the modelling implications of these two approaches with respect to biostimulated U(VI) immobilisation remediation schemes, the two approaches were compared for the same system. The first-order and Michaelis-Menten/Monod (multi-population) approaches to modelling microbial kinetics outlined in Section 3.3.2 (equations 3.1 and 3.2, respectively) were compared

for the same model and modelling conditions as reported in Section 4.5. As previously explained, the system modelled is fairly typical of biostimulated U(VI) immobilisation schemes: a high OC concentration is injected via U-contaminated oxic influent groundwater into the remediation zone of a U-contaminated aquifer. To parameterise the first-order model in such a way as to be equivalent to the multi-population model, the OC fermentation rate of the first-order model (k) was adjusted such that the spatial U(VI) concentration profile after 1 year of biostimulation for both models was similar. A k value of 3.5 yr^{-1} best provided this match. Figure 5.7 displays the spatial U(VI) concentration profiles of both modelling approaches at five different times. From one year and beyond, the U(VI) concentration profiles are almost identical for both approaches. However, prior to this time, the first-order approach displays increased U(VI) reduction relative to the Michaelis-Menten/Monod approach. This suggests that when modelling typical biostimulated U(VI) immobilisation schemes and observing U(VI) reduction at later times, results may be similar whether a first-order or Michaelis-Menten/Monod approach is used. However, at earlier time, the first-order approach is observed to present a system with more advanced U(VI) reduction than a Michaelis-Menten/Monod approach. As the OC concentration solely controls the microbial activity in the first-order approach and in part controls the microbial activity in the Michaelis-Menten/Monod approach, it might be assumed that changes in the influent OC concentration would negate or highlight the differences in different approaches' U(VI) concentration profiles. Figures 5.7 and 5.8 demonstrate that this is not the case. Figure 5.8 shows the system with the OC influent concentration doubled for the Michaelis-Menten/Monod approach simulation. It might be expected that this would yield slightly

higher rates in the Michaelis-Menten/Monod yielding more rapid U(VI) reduction. However, the change has no significant impact on the modelling outcomes. Figure 5.9 shows the system with the OC influent concentration halved for the first-order approach simulation. It might be expected that this would yield lower rates in the first-order approach, yielding a closer comparison with the Michaelis-Menten/Monod approach at earlier time. However, the results demonstrate that while results are similar at earlier time they remain different at later time. This suggests that the different results produced by the different modelling approaches are not, therefore, strongly dependent on the OC concentrations themselves. Since biostimulated U(VI) immobilisation systems exhibit complex geochemical interactions that are related to, but not entirely dependent on, OC fermentation rates, different approaches to modelling OC fermentation kinetics may result in significantly different modelling outcomes even when parameters are equivalently matched.

Figures 5.9 and 5.10 display the OC concentration profiles at different times for the Michaelis-Menten/Monod approach and the first-order approach, respectively. Clearly, the first-order approach (Figure 5.11) attains steady state with respect to the OC profile much sooner than the Michaelis-Menten/Monod approach. Note that once a steady-state condition is reached with respect to OC profile (after >1 year), both systems exhibit the same U(VI) concentration profiles (cf. Figure 5.7). Once the TEAPs prior to U(VI) reduction are complete and OC profiles have reached steady state, U(VI) concentration profiles are likely to be represented equally well by either modelling approach. However, at times prior to this, a Michaelis-Menten/Monod approach will allow the

modelling of system lag time. Conversely, the first-order-approach may be more appropriate for modelling systems already at steady-state, or with short lag times.

Given that biostimulated U(VI) immobilisation remedial schemes will undoubtedly be monitored, these results demonstrate that the application of different modelling approaches may result in similar modelling outcomes at later time, but give significantly different outcomes at earlier time. This should be recognized when modelling biostimulated U(VI) immobilisation, and care should be taken to ensure that appropriate modelling approaches are used for appropriate temporal periods when modelling experimental data.

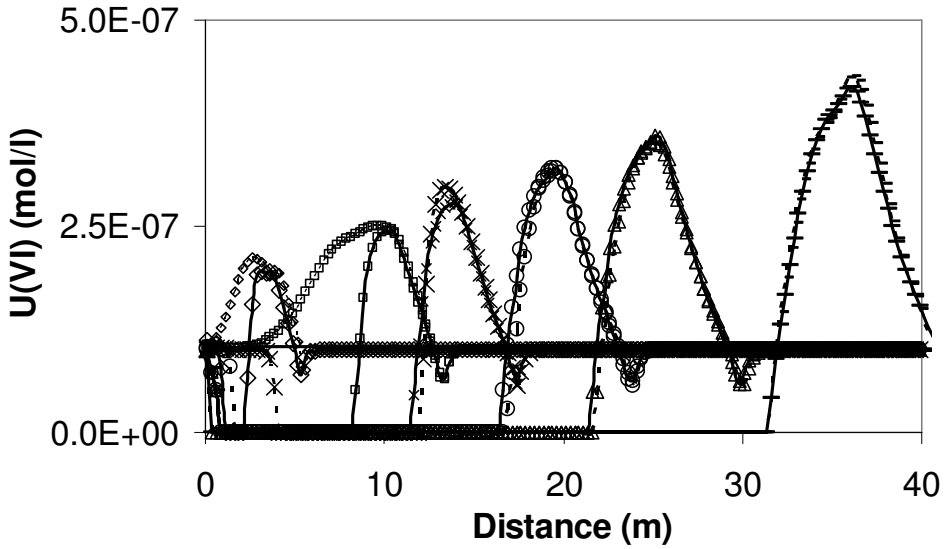

Figure 5.7. Spatial U(VI) concentration profiles for first-order (solid lines) and Michaelis-Menten (dashed lines) after 0.2 (diamonds), 0.7 (squares), 1 (crosses), 1.5 (circles), 2 (triangles) years and 3 (hyphen) years of biostimulation.

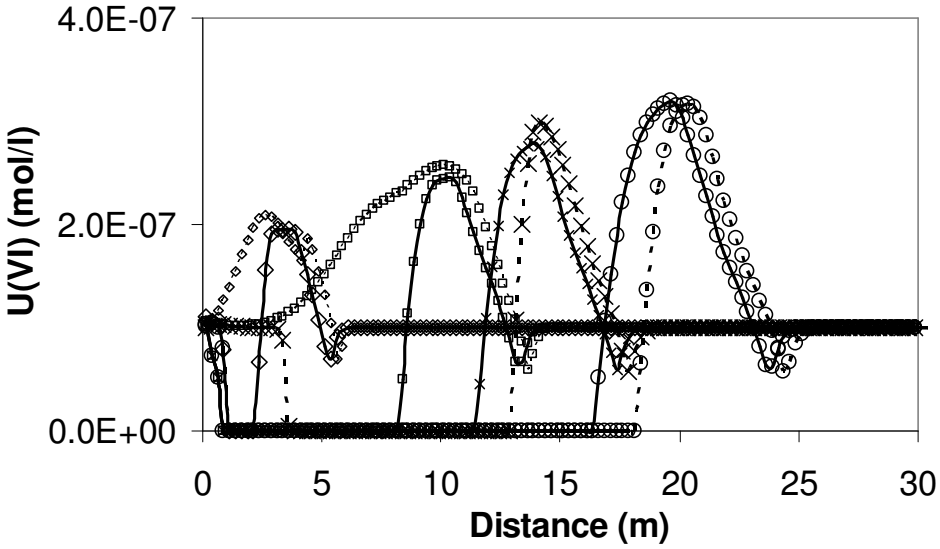

Figure 5.8. Spatial U(VI) concentration profiles for first-order (solid lines) and Michaelis-Menten (dashed lines) after 0.2 (diamonds), 0.7 (squares), 1 (crosses), 1.5 (circles) and 2 (triangles) years of biostimulation. Michaelis-Menten model [OC] = 6 mmol.

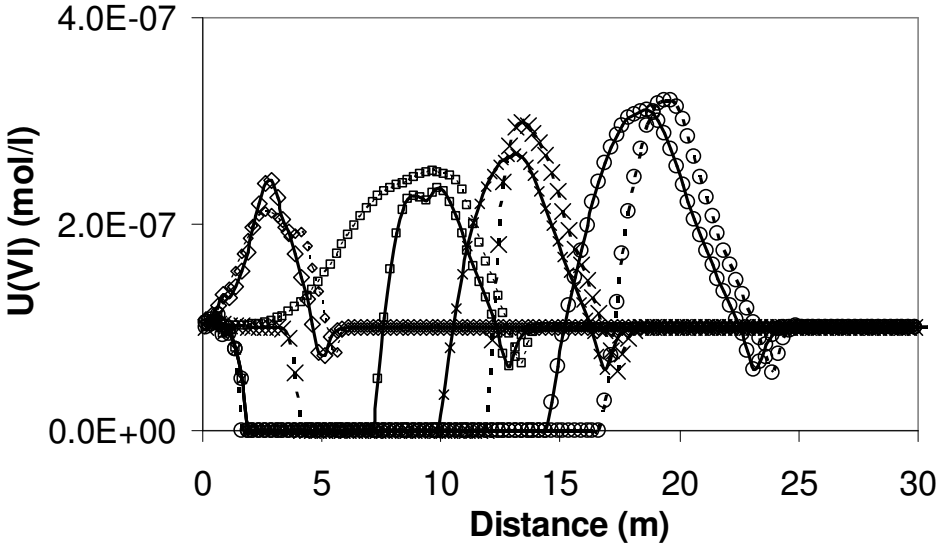

Figure 5.9. Spatial U(VI) concentration profiles for first-order (solid lines) and Michaelis-Menten (dashed lines) after 0.2 (diamonds), 0.7 (squares), 1 (crosses), 1.5 (circles) and 2 (triangles) years of biostimulation. First-order model [OC] = 1.5 mmol.

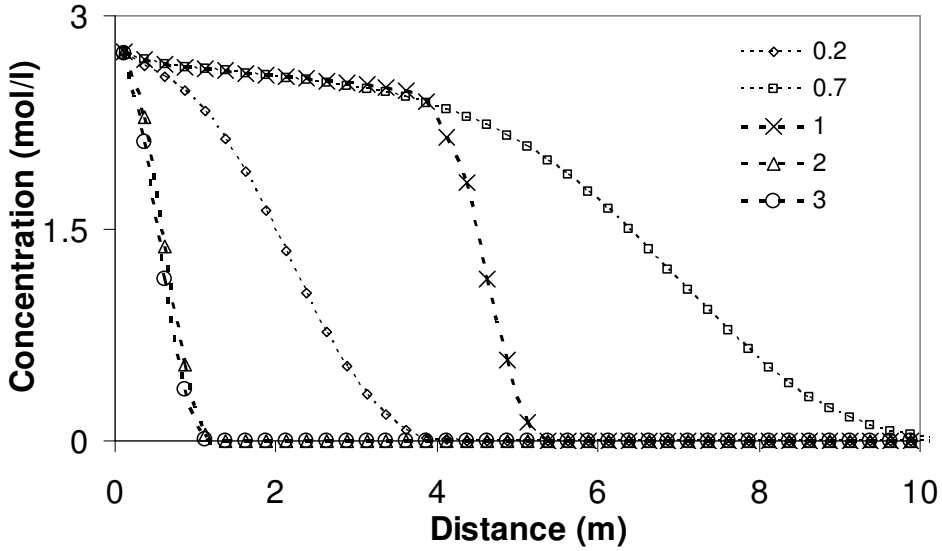

Figure 5.10. Spatial OC concentration profiles for Michaelis-Menten/Monod approach at different times (years) after biostimulation began.

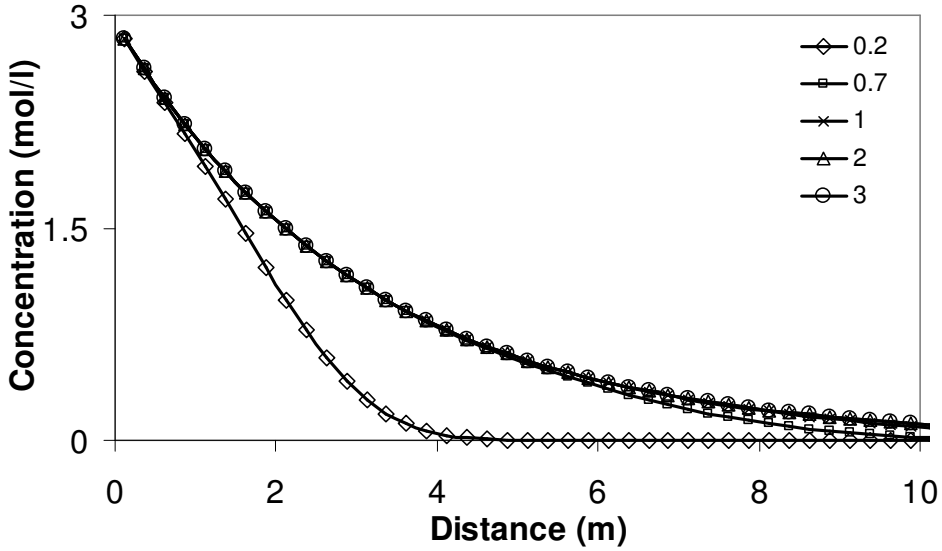

Figure 5.11. Spatial OC concentration profiles for first-order approach at different times (years) after biostimulation began.

5.4. Conclusions

A biogeochemical reactive transport model was developed for U bioimmobilisation in both single and dual porosity media. A one-dimensional simulation in a single porosity domain compared well to the Wang et al. (2003) model without any model calibration. The geochemical changes predicted are qualitatively characteristic of U(VI) immobilisation in biostimulated sites and sediments. Some differences between the models for the predicted quantitative value of certain species are attributed to the different models' formulations for secondary redox reactions (kinetic versus partial equilibrium approach).

A comparison of different microbial kinetics modelling approaches revealed that different modelling approaches may produce very similar outcomes at later time, yet simultaneously produce significantly different outcomes at earlier time. This is due to differences in modelling the influence of OC and EA presence on OC fermentation rate. This should be recognized when modelling biostimulated U(VI) immobilisation remedial schemes, and care should be taken to ensure that appropriate modelling approaches are used for appropriate conditions (OC and EA concentration at steady-state or not?) when modelling experimental data.

The presented model predicts a transient increase ("spike") in U(VI) concentrations downgradient of the treatment zone in systems with insignificant carbonate content. This is due to geochemical changes (carbonate and ferrihydrite concentrations and pH) induced by DMRB which cause desorption of ferrihydrite-complexed U(VI).

Simulations confirm that this is not predicted by empirical adsorption models, likely because they do not account for the variations in pH, carbonate or mineral abundance along the flow path. The increase in downgradient U(VI) appears to be temporary, as desorbed U(VI) is immobilised to U(IV) following this process.

U(VI) bioimmobilisation is predicted to be significantly affected by the presence of dual porosity porous media with bioactivity taking place in the media region of relatively high-velocity ranging flow ("mobile region"). Dual-porosity systems are likely to exhibit delayed U(VI) immobilisation relative to more homogeneous systems due to diffusion limitations on all electron acceptors.

Sensitivity simulations suggest that, when the "mobile"-region of a dual porosity possesses the dominant microbial activity, the rate of mass transfer between the "mobile" and "immobile" regions appears to have little impact on remediation efficiency. However, variation in the each region's fraction of the total porosity resulted in quantitatively different time delays for U(VI) immobilisation. When bioactivity occurs predominantly in the "mobile" region of DP systems, results suggest this delay will be reduced as the "mobile" region porosity approaches that of the single porosity system. Overall, the study underscores (i) the value of relatively comprehensive biogeochemical models (e.g., that include robust surface complexation processes and a database of standard geochemical reactions) and (ii) the time delay anticipated for U(VI) bioimmobilisation due to diffusion limitations in heterogeneous systems.

The presented simulations assumed microbial residence in the "mobile" region in order to minimize the differences between single and dual porosity systems being compared in this work. It is acknowledged that systems with significant bacterial activity in relatively immobile porous media will likely exhibit different behaviour; this is the focus of future work. Further, this work assumes that system biomass has reached a quasi-steady-state and therefore does not grow, and that ferrihydrite is the only surface with which U(VI) complexes. Despite these simplifications, it is expected that the differences outlined between single and dual porosity systems are likely to be broadly representative for systems with predominant bioactivity in more media regions of more mobile (relatively high-velocity) flow. It is acknowledged that this work focuses on one-dimensional simulations; future work that combines the presented model with a multidimensional flow and transport simulator will investigate the expected additional remediation challenges associated with heterogeneous systems such as spatial variability in microbial populations and flow bypassing of injected substrates. Further, reoxidation of immobilised U should be considered in future work in order to assess the long-term success of bioimmobilisation strategies (Suzuki and Suko, 2006).

6. Sensitivity analysis of the biogeochemical reactive transport model for U(VI) immobilisation via immobile-resident DMRB in dual porosity porous media

6.1. Introduction

In this chapter, dimensionless parameter groups are employed to analyze a wide range of system behaviour. An extensive suite of simulations are presented that explore how key processes impact remediation efficiency, and permit identification of the conditions under which processes associated with groundwater transport, dual porosity media phenomena and microbial activity interact.

In this chapter, it is assumed that DMRB reside in regions of low-to-negligible advective flow. Most aquifer bacteria are associated with particle surfaces (Christensen et al., 2001; Tabak et al., 2005), and particularly with the surfaces of the finer sediment such as clay and silt (Albrechtsen, 1994). Some bacteria produce electron-shuttling compounds and/or chelators negating any requirement to make contact with the Fe(III) or Mn(IV) oxides (Newman and Kolter, 2000; Childers et al., 2002; Nevin and Lovley, 2002a,b), however, many bacteria must make contact with an electron acceptor (EA) to reduce it (Nevin and Lovley, 2000c). Indeed, doubt exists as to whether production of electron-shuttling compounds and Fe(III) chelators may be an energetically favourable approach for Fe(III) oxide reduction in nutrient-poor subsurface environments (Childers, 2002; Nevin and Lovley, 2002a). Furthermore, Neal et al. (2004) conducted continuous flow bioreactor experiments in which DMRB colonised hematite surfaces as a biofilm. It is

therefore hypothesized that DMRB are non-motile and predominantly occupy low flow and finer-grained regions where they take advantage of low shear forces and high electron accepting capacity. A conceptual representation of the system is presented in Figure 6.1. The figure displays individual model cells for both the mobile and immobile regions. OC enters the mobile region in which advective-diffusive transport occurs. All aqueous chemical species may transfer into the immobile region, in which pore water is stagnant. Thus aqueous chemical species, such as U(VI), sequestered in the immobile region are essentially rendered immobile.

In this chapter, all microbially mediated redox reactions are implicitly conducted by a single biomass population. This is deemed reasonable in a system which follows the accepted sequence of TEAPs, where the interest is not specifically focused on individual microbial processes, but rather on the net geochemical changes in the system (Postma and Jakobsen, 1996). The biomass population is considered to be in a non-growth, steady state condition. This is because (i) it is likely that biomass populations attain a maximum concentration during the organic carbon stimulation phase (Jaffé and Rabitz, 1988), and (ii) models are typically parameterised using data obtained under non-growth conditions both in the laboratory (Truex et al., 1997; Liu et al., 2002a) and in the field (Schroth et al., 1998; North et al., 2004). The biomass degrades the injected electron donor, dissolved organic carbon (OC) represented by CH_2O, via first-order kinetics (equation 3.1).

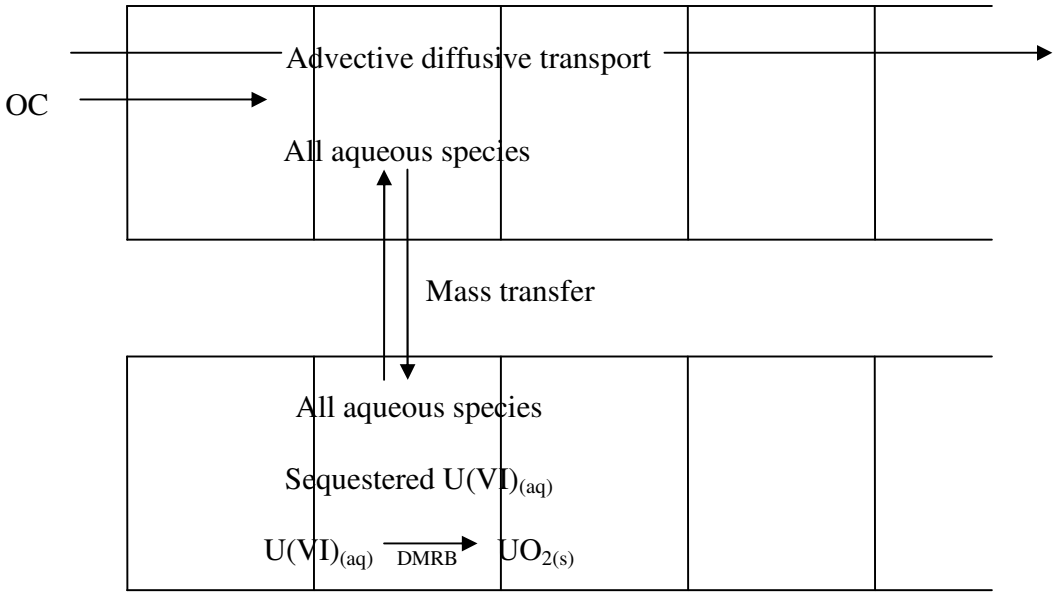

Figure 6.1. Arrangement of dual porosity domain.

The simulations consider U(VI)-contaminated oxic recharge water entering an anaerobic aquifer. Geochemical conditions vary widely in the natural environment and it is impractical to cover the entire range. The geochemical parameters used in the presented numerical simulations were selected based on U-contaminated (and high-nitrate) field site data: the Shiprock U mill tailing site (Elias et al., 2003) and Area 2 of the Oak Ridge Field Research Center, USA (ORNL, 2007). Initial conditions and boundary conditions are presented in Table 6.1. Identical initial geochemical conditions are employed for the mobile and immobile regions. Rhodochrosite, siderite, calcite, mackinawite and uraninite all have the potential to precipitate, but are not initially present. Surface complexation of U(VI) to sandstone or iron hydroxide minerals is insignificant in contaminated sites (e.g., Abdelouas et al., 1998b and 1999) when carbonate concentrations are high (Hsi and Langmuir 1985; Koß 1988; Bond et al., 1991). To

better constrain the system in this parametric study, U(VI)-surface complexation and biomass attachment are ignored.

Table 6.1. Initial and boundary conditions.

Species	Units	Boundary concentration	Initial concentration
OC	mmol l^{-1}	300	0
N(V)	mmol l^{-1}	2.24	2.24
S(VI)	mmol l^{-1}	6.1×10^{-1}	6.1×10^{-1}
Ferrihydrite	mmol dm^{-3}	0	117
Pyrolusite	mmol dm^{-3}	0	76
U(VI)	mmol l^{-1}	8.5×10^{-3}	8.5×10^{-3}
Carbonate	mmol l^{-1}	1.06	1.06
$pO_2(g)$		$10^{-3.55}$	0
pH		7.1	7.15

6.2. Model analysis: dimensionless parameter groups

Biogeochemical transport models encompass multiple complex processes, each of which may require multiple parameter inputs. Such models have the potential to simulate system behaviour over a large parameter space, within which processes may interact differently depending on the chosen point in the multi-parameter space. The remediation efficiency in bioremediated aquifers is dependent on the combined impacts of groundwater transport processes, DMRB activity and geochemical effects.

Mapping system behaviour across a complex, multi-parameter space requires a thorough, extensive approach to results collation; a process associated with substantial computational expense. For this reason, the majority of existing biogeochemical models exploring U(VI) bioremediation instead employ specific parameter sets, typically representing a small number of demonstrative base case scenarios (e.g., Wang and

Papenguth, 2001; Roden and Scheibe, 2005). This approach is applied widely; for example to complex redox models (e.g., Hunter et al., 1998; Smith and Jaffé, 1998; Prommer et al., 1999a). However, this approach may limit the applicability of the results, since remediation efficiency can vary widely depending on the parameter values chosen for each scenario. For example, using 23 references from a variety of environments, Hunter et al. (1998) collected first-order OC oxidation rate values which covered a range of 10 orders of magnitude. Base case scenarios making use of a single rate value cannot cover the range of behaviour that could exist in systems of such widely varying bacterial rates.

Furthermore, uncertainty remains over the validity of sourcing parameters from one environment and transferring them to the modelling scenarios of different environments (Alvarez et al., 1994). Restricting model parameterisation to, for example, biological rate data from experimental laboratory studies may be inappropriate as such data can vastly overestimate in situ bacterial rates (Lovley and Chapelle, 1995). Moreover, microbial kinetic rate experimental data is generally fit to a single mathematical kinetic approach (e.g., simple Monod, Michaelis-Menten with/without inhibition factors), and it is difficult to compare different approaches. For example, kinetic rate data for U(VI) biomineralisation by DMRB have been successfully fitted to non-growth biomass-dependent dual Monod (Roden and Scheibe, 2005), non-growth biomass-explicitly-independent dual Monod (Wang et al., 2003), non-growth biomass-dependent (single) Monod (Truex et al., 1997; Liu et al., 2002a), first-order (Liu et al., 2002a; Gu and Chen, 2003) and zero-order (North et al., 2004) kinetic formulations.

Few U(VI) bioremediation studies explore the parameter sensitivities of the system. Wang et al. (2003) conducted an extensive parameter sensitivity study on primary and secondary redox reaction rates. However, the study did not consider varying groundwater transport or geochemical conditions.

This work addresses the complexity of system mapping bioremediation efficiency in multi-parameter space by making use of dimensionless parameter groups (DPGs). DPGs allow analysis of the relative importance of interacting or competing processes. Additionally, by using DPGs, the system of interest is decoupled from specific space or time scales (Griffioen, 1998). The approach therefore has the potential to cover a wide range of parameter values, scales, and modes of behaviour. In any non-dimensionalisation, several choices are possible, with the physical circumstances providing the basis for the DPGs chosen.

In identifying the DPGs for the dual-porosity first-order-kinetic PEA biogeochemical model outlined in this work, it is convenient to introduce the dimensionless variables

$$T = \frac{v_m t}{L} \tag{6.1}$$

$$X = \frac{x}{L} \tag{6.2}$$

where L is the physical length scale.

Substitution of equations (6.1-6.2) into equations (3.3 and 3.6) give the dimensionless forms

$$\frac{v_m\theta_m\partial C_m}{L\ \partial T} + \frac{v_m\theta_{im}\partial C_{im}}{L\ \partial T} = -\frac{\theta_m v_m\partial C_m}{L\ \partial X} + \frac{\theta_m}{L^2}(D_e + av_m)\frac{\partial^2 C_m}{\partial X^2} - \frac{v_m\partial q}{L\,\partial T} \quad (6.3)$$

$$\frac{v_m\theta_{im}}{L}\left(1 + \frac{\partial q_{im}}{\partial C_{im}}\right)\frac{\partial C_{im}}{\partial T} = \alpha(C_m - C_{im}) - \theta_{im}kC_{im} \quad (6.4)$$

Dimensional analysis yields four dimensionless parameter groups. The first, the Péclet number, is defined by

$$Pe = \frac{v_m L}{D} \quad (6.5)$$

The second DPG is associated with the mobile-immobile mass transfer, defined as

$$\omega = \frac{\gamma L}{\theta_m v_m} = \frac{T_{flux}}{T_{tranfser}} \quad (6.6)$$

where $T_{flux} = L/\theta_m v_m$ and $T_{transfer} = 1/\gamma$. The DPG ω therefore combines the timescales associated with volumetric flux (T_{flux}) and mobile-immobile mass transfer ($T_{transfer}$).

The third DPG is associated with matrix porosities, is defined as

$$\theta_p = \frac{\theta_m}{\theta_{im}} \quad (6.7)$$

and the fourth DPG is associated with microbial activity when DMRB activity is present in the immobile region only:

$$Dk = \frac{kL}{v_m} = \frac{T_{advection}}{T_{microbial}} \tag{6.8}$$

where $T_{advection} = L/v_m$ and $T_{microbial} = 1/k$. The DPG Dk therefore combines the timescales associated with advection ($T_{advection}$) and the microbial fermentation of OC ($T_{microbial}$).

In general, the processes within each of these DPGs compete when the DPG's value approaches unity. For example, both advective and diffusive transport are significant when $Pe = 1$, whereas advective transport dominates when $Pe >> 1$ and diffusive transport dominates when $Pe << 1$. It is important to note also that the chosen DPGs are not independent, with advective velocity, porosity, and length all appearing in multiple DPGs; this is appropriate because of their central influence on key processes examined. Determining the success of remediation through use of DPGs and associated timescales allows for a thorough investigation of the system parameter space.

The simulations explore the full range of parameter values reported in the literature by varying the value of a single DPG while holding all other DPGs constant. This exercise is then repeated until all DPGs have been considered.

The values over which the DPGs were varied were based on data reported in the literature. The values of the DPGs ω and Dk were each varied over 8 orders of magnitude, from 0.0001 to 10 000. This covers the range of fermentation rate (k) values collated by Hunter et al. (1998) and the range of mobile-immobile mass transfer rates

used and reported by numerous authors (Griffioen et al., 1998; Feehley et al., 2000; Harvey and Gorelick, 2000; Kim and Corapcioglu, 2002; Haws et al., 2004 and 2005; Jørgensen et al., 2004; Luo et al., 2005; Roden and Scheibe, 2005). The *Pe* values were varied between 0.1 and 10 000, bracketing the majority of conditions observed at field sites (Gelhar et al., 1992). The DPG θ_p is ranged from 0.09 to 0.99, covering the full range reported by Griffioen et al. (1998) (equivalent $\theta_m/(\theta_m + \theta_i)$ values in that work range 0.55-1).

6.3. Simulation results

6.3.1. Remediation metric

In this study, success of a particular bioremediation strategy is related to the U(VI) concentration flowing out of the remediation zone. The cumulative U(VI) concentration passing at $X = L$ is:

$$M_{remediated} = \int [\mathrm{U(VI)}]\, \mathrm{d}T \tag{6.9}$$

while the equivalent cumulative U(VI) concentration exiting an identical system that is not undergoing bioremediation is defined as $M_{contaminated}$. The upper integration limit of $T = 5$ is chosen to ensure complete temporal coverage. The remediation efficiency of a system, M, is then defined as

$$M = 1 - \frac{M_{\mathrm{remediated}}}{M_{\mathrm{contaminated}}} \tag{6.10}$$

This metric is taken to represent the remediation efficiency of any scenario, providing a basis for comparison. Note that the maximum efficiency cannot reach unity for the system examined here since OC is injected and the initial state of the porous medium is not altered. Thus, about one pore volume must be eluted before the effect of remediation is seen. In this study we wish to determine relative efficiency, so the fact that the maximum efficiency does not reach unity is unimportant.

6.3.2. Remediation efficiency under various conditions

Figure 6.2 illustrates the observed remediation efficiency, M, for $\log(\omega)$ values varied over 6 orders of magnitude. The solid line shows this relation for all other DPGs equal to unity ($Pe = \theta_p = Dk = 1$). Note that volumetric flux dominates when ω is low and mobile-immobile mass transfer dominates when it is high. Meeting expectations, bioremediation is unsuccessful at low ω due to the DMRB's limited access to OC. However, the figure illustrates that when ω is high, the DMRB are not OC-limited and bioremediation is more efficient. A transition zone is evident between the asymptotic results at the two extremes.

Figure 6.2 also presents the sensitivity of this relationship to microbial efficiency, Dk. At reduced microbial efficiency (reduced Dk) the transition zone is unaffected, but the maximum attainable remediation efficiency (asymptote at high Dk) is reduced. Likewise, at an increased microbial efficiency, the range of the transition zone remains unaffected, while the maximum attainable remediation efficiency is increased. Clearly,

the greater the microbial activity the greater the maximum potential level of remediation, but this maximum potential is only attained when the mobile-immobile mass transfer timescale ($T_{transfer}$) is smaller than one-thirtieth the value of the volumetric flux timescale (T_{flux}) ($\omega > 30$ or $\log(\omega) > 1.5$). Furthermore, minimum remediation efficiency always occurs at $\log(\omega) < 1.5$. This suggests that if the mobile-immobile mass transfer timescale ($T_{transfer}$) is larger than approximately 30 times the value of the volumetric flux timescale (T_{flux}) then it is unlikely that remediation will take place.

All results presented in Figure 6.2 consider the geochemical conditions outlined in Table 6.1. However, initial geochemical conditions can modify modelling outcomes significantly (Zhu and Burden, 2001). Figure 6.3 explores the effect of different mineralogy on remediation efficiency for varying $\log(\omega)$ values, with all other DPG's equal to unity. All curves share the same parameter values, except that the level of minerals present is varied as outlined in Table 6.2. The "low" mineral values represent the lowest concentrations reported for Area 2 of the ORFRC field site (ORNL, 2007). The "high" mineral values are well above those encountered at either the ORFRC or Shiprock (Elias et al., 2003) field sites. The results suggest that as mineral presence is reduced, net remediation becomes slightly more efficient. This is because bacteria progress through the redox sequence more rapidly due to reduced EA availability prior to U(VI), and U(VI) reduction then occurs earlier. As the EA presence in the system is reduced the $\log(\omega)$ value at which remediation becomes significant decreases (M near zero). Nevertheless, the point at which optimal remediation takes place remains the same

for the different geochemical conditions, and is consistent with that reported in Figure 6.2 ($\log(\omega) > 1.5$). It is acknowledged that substantially different geochemical conditions may cause greater shifts than the results reported here.

Table 6.2. Simulations varying geochemical conditions: initial conditions.

Species	Units	Low	Intermediate	High
N(V)	mmol l^{-1}	0.1	1	2.2
S(VI)	mmol l^{-1}	0.1	0.3	0.6
Ferrihydrite	mmol dm^{-3}	0.008	0.163	117
Pyrolusite	mmol dm^{-3}	0.001	0.026	76

Figure 6.4 presents remediation efficiency, *M*, for varying log(*Dk*). The solid line shows this relationship when all other DPGs values equal unity. The results indicate that, as expected, remediation is more efficient when the value of the DPG *Dk* is high. The transition zone between the asymptotic values is 2-3 orders of magnitude, which is slightly greater than that for the DPG associated with mobile-immobile mass transfer (Figure 6.2). Thus, U(VI) bioremediation in dual porosity media may be more sensitive to microbial efficiency than immobile-mobile mass transfer rate, all other things being equal. Figure 6.4 further illustrates that remediation effectiveness increases as the value of the mobile-immobile mass transfer DPG, ω, is increased. This suggests that systems with lower mobile-immobile transfer require increased bacterial efficiency to achieve efficient remediation.

Figure 6.5 presents remediation efficiency (*M*) as a function of microbial efficiency DPG (*Dk*) for three different geochemical conditions defined in Table 6.2 (all other DPGs equal to unity). Similar to the results for mobile-immobile mass transfer DPG, ω

(Figure 6.3), reductions in EA presence result in slightly improved remediation efficiency and this is achieved at slightly lower microbial efficiencies. In both cases the DPG value at which optimum remediation occurs remains largely insensitive to the mineral presence ($\log(Dk)$ or $\log(\omega) \approx 1.5$). Further, the range of DPG values at which remediation becomes significant (M near zero) for microbial efficiency is similar to that for mobile-immobile mass transfer efficiency ($-3 < \log(Dk) < -1$ in Figure 6.5 versus $-3 < \log(\omega) < -1$ in Figure 6.3, respectively).

Figure 6.6 reveals how remediation efficiency varies with the Péclet number DPG, Pe. Independent of the Pe value, it is observed that remediation is limited by the DMRB's access to OC transferring into the immobile region. This is demonstrated by the fact that M is relatively constant over the entire Pe range, but that the remediation efficiency increases as the mobile-immobile mass transfer DPG increases. The same phenomenon is observed in Figure 6.7 for the DPG associated with microbial efficiency, Dk. Remediation is here limited by the DMRB's efficiency itself. Since the DMRB are present in the immobile region only, it is unsurprising that changes in solute transport behaviour (represented by the DPG Pe) have no effect on the remediation efficiency.

Figures 6.8-6.10 demonstrate how the remediation efficiency varies with mobile to immobile region porosity ratio, including sensitivity to ω, Dk, and Pe, respectively. The relationship appears to display peak remediation efficiency at an intermediate mobile-immobile region porosity ratio in each case. At peak remediation efficiency, OC and

U(VI) are transferred into the immobile region at a rate that is balanced (accommodated) by the DMRB activity (see equation 3..6). At lower immobile region porosities, efficiency is reduced due to limited transfer of OC and U(VI). At higher immobile region porosities, OC and U(VI) transfer rates exceed the DMRB fermentation rate also resulting in decreased remediation efficiency. In all cases, maximum remediation efficiency generally tends to occur at porosity ratios (as defined in Figures 6.8-6.10) in the range 0.5-0.8. This suggests that, for immobile-resident DMRB systems, optimal remediation tends to occur when the mobile region porosity is between one and four times the magnitude of the immobile region porosity.

Figure 6.8, presenting sensitivity to the mobile-immobile transfer DPG, ω, reveals that maximum remediation occurs when the porosity ratio is approximately 0.7 (all other DPGs equal to unity). Overall, as mobile-immobile mass transfer increases, peak efficiency occurs at higher porosity ratios and the porosity ratio range over which optimal remediation takes places widens. Thus, high mobile-immobile transfer systems may be able to achieve efficient remediation regardless of porosity ratio.

A similar trend is observed for variations in microbial efficiency, as illustrated in Figure 6.9. With high microbial efficiency, remediation is more efficient and high remediation efficiency is maintained over a wide range of porosity ratios. As microbial efficiency reduces, the peak remediation value reduces and the porosity range over which optimum

remediation takes place narrows. Figure 6.10 illustrates that, in agreement with previous results, changes in *Pe* have little influence on remediation efficiency for this model.

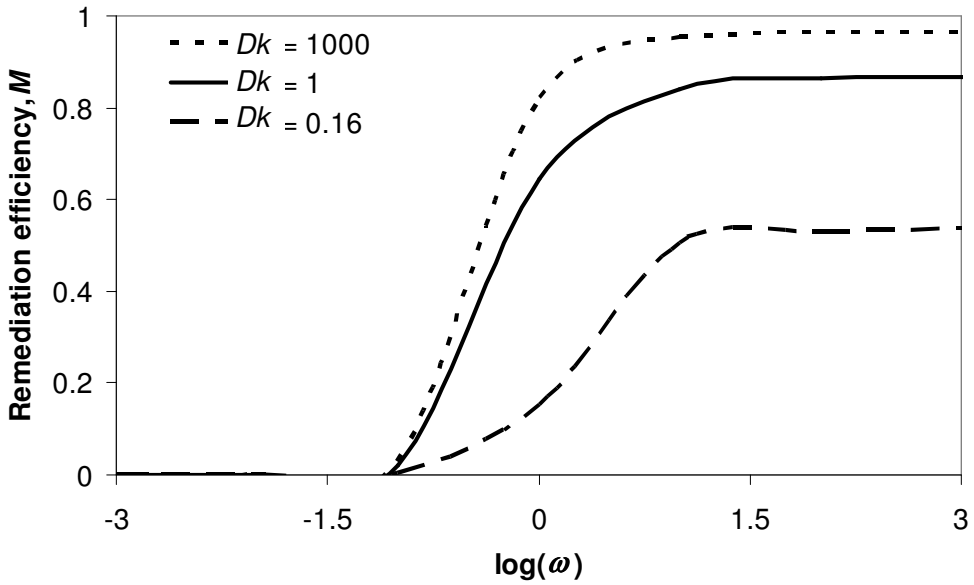

Figure 6.2. Variation in remediation efficiency with DPG ω for various DPG *Dk* values.

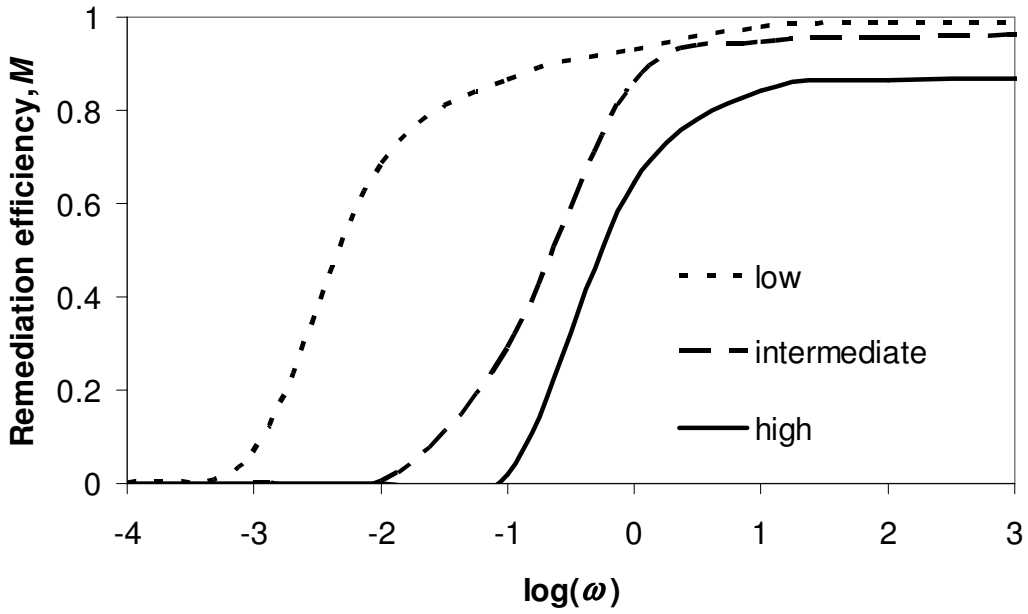

Figure 6.3. Variation in remediation efficiency with DPG ω for various geochemical conditions.

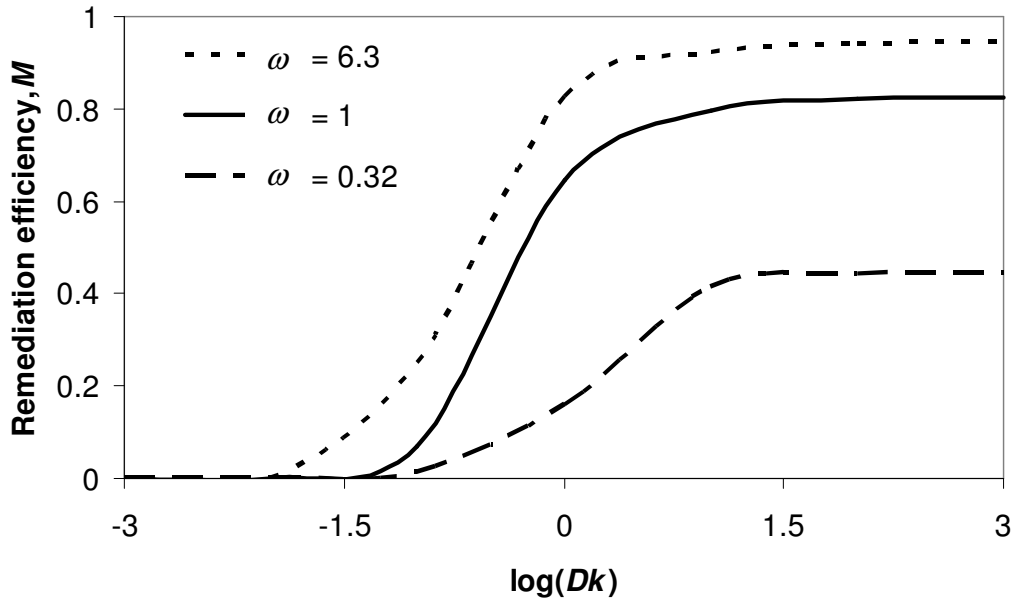

Figure 6.4. Variation in remediation efficiency with DPG *Dk* for various DPG ω values.

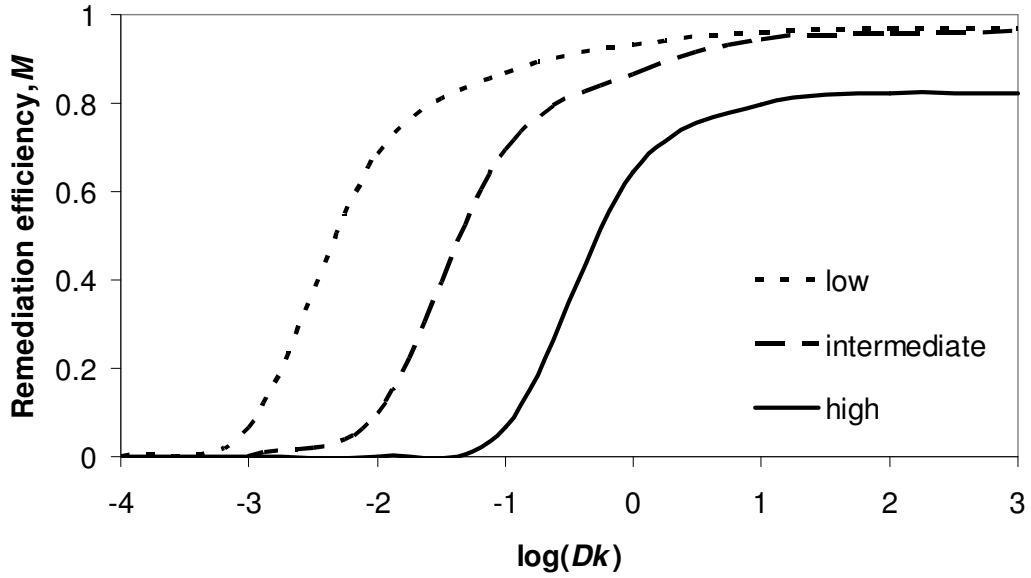

Figure 6.5. Variation in remediation efficiency with DPG *Dk* for various geochemical conditions.

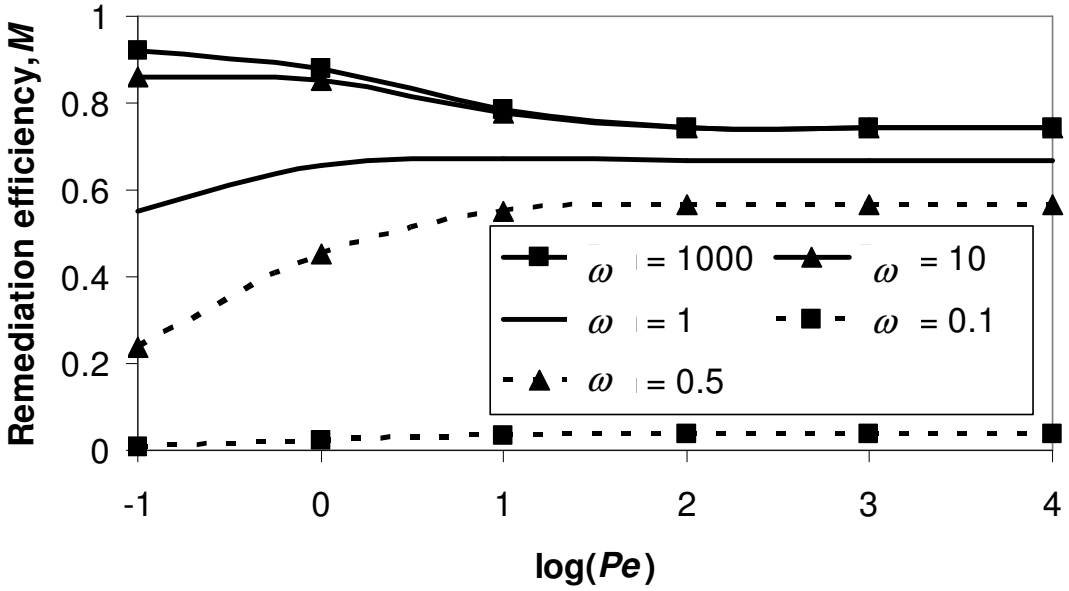

Figure 6.6. Variation in remediation efficiency with DPG Pe for various DPG ω values.

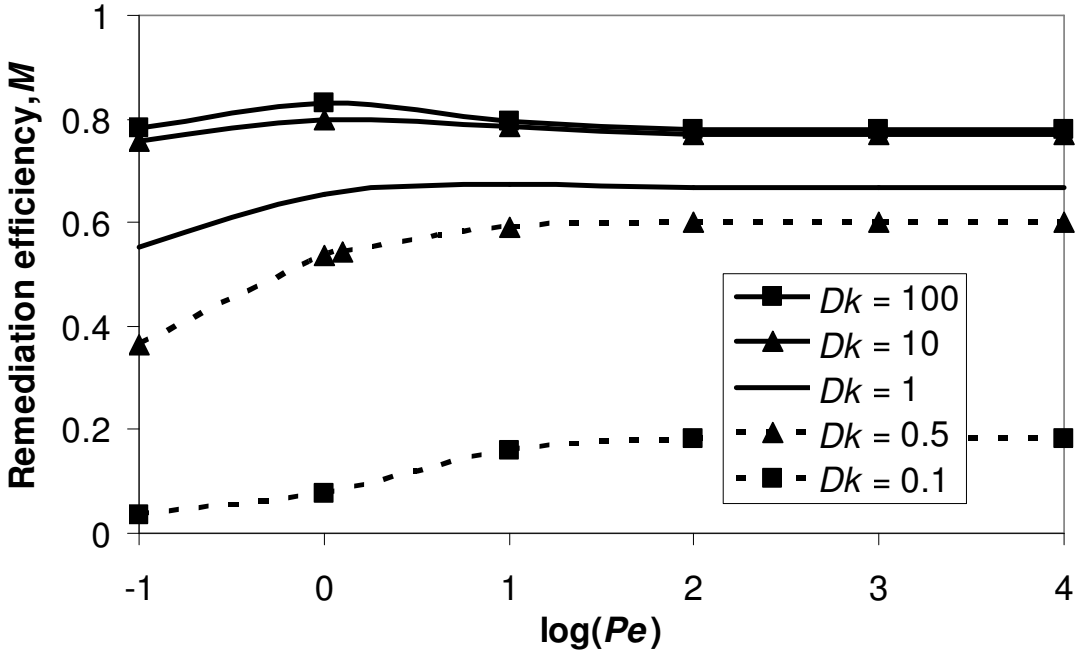

Figure 6.7. Variation in remediation efficiency with DPG *Pe* for various DPG *Dk* values.

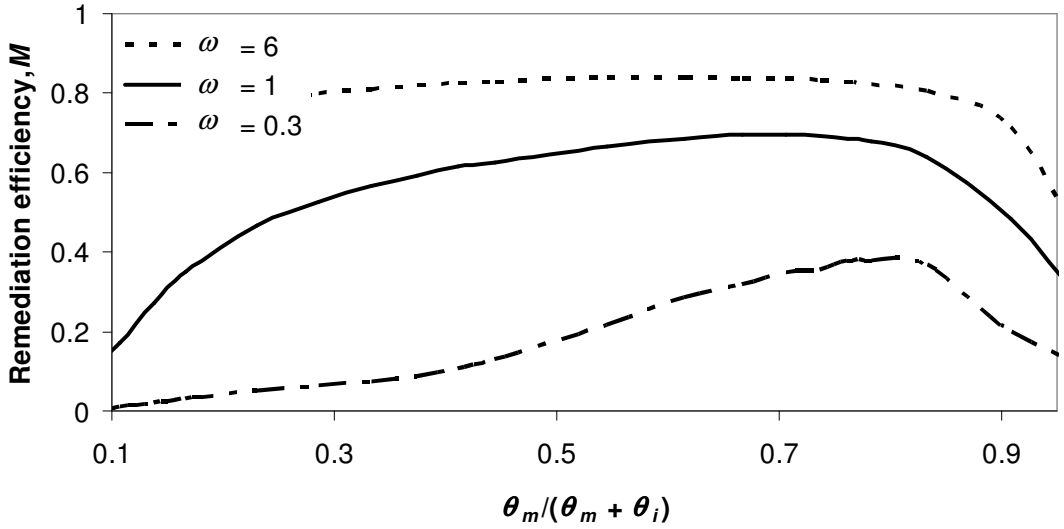

Figure 6.8. Variation in remediation efficiency for varying porosity ratios and ω values.

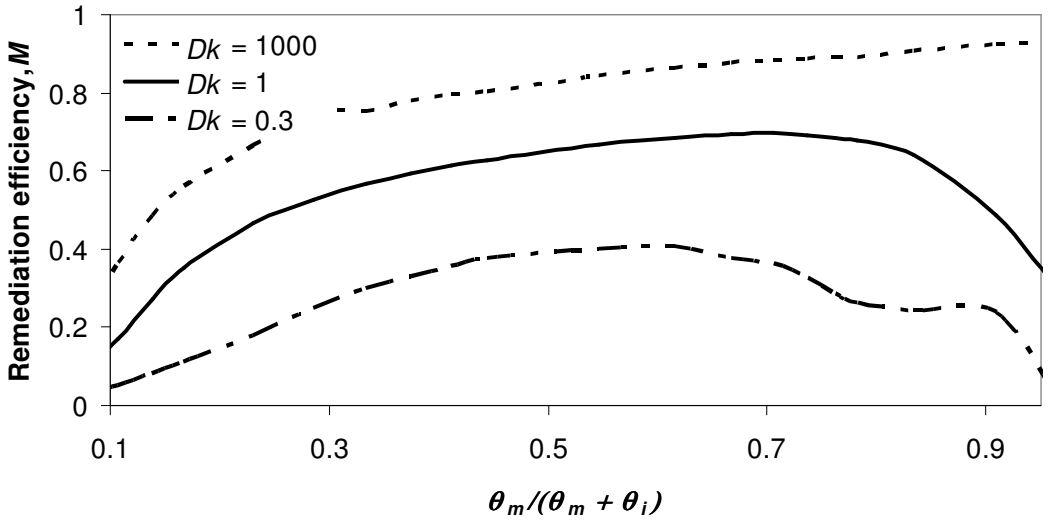

Figure 6.9. Variation in remediation efficiency for varying porosity ratios and *Dk* values.

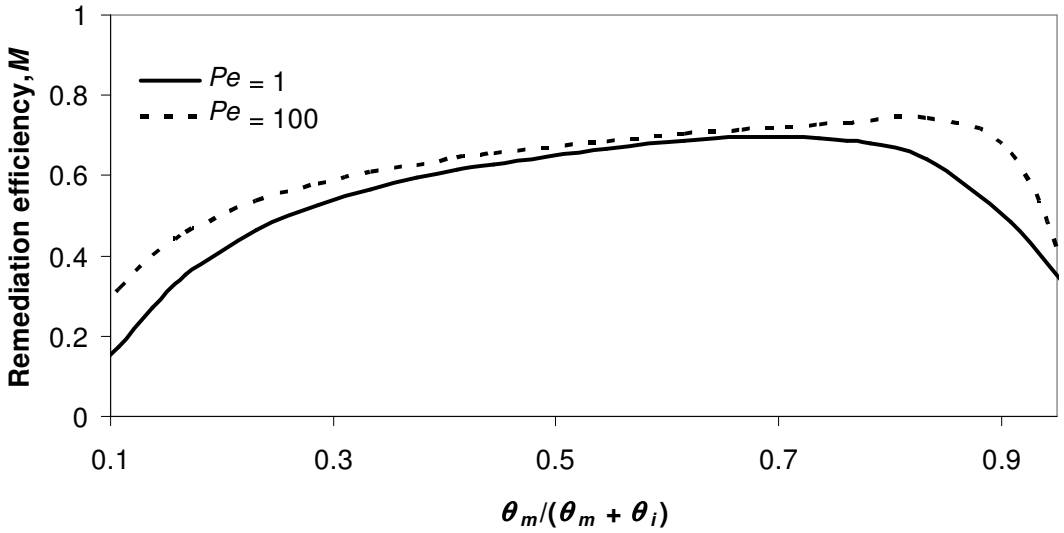

Figure 6.10. Variation in remediation efficiency for varying porosity ratios and *Pe* values.

6.4. Potential application

The insight gained from the DPG analysis in this work may be useful in conceptual remediation design. To illustrate this, an example application scenario motivated by field

site data is discussed. Groundwater transport parameters were obtained from Luo et al. (2005) and microbial parameters from Liu et al. (2002a).

Luo et al. (2005) conducted a bromide tracer test at the Y-12 National Security Complex site in the Oak Ridge Reservation, Oak Ridge, TN (USA). The authors calculated heterogeneous mass transfer properties by successfully fitting the experimental data to dual- and tri-porosity models. The parameter values for pore water velocities, mobile-immobile mass transfer rates, hydrodynamic dispersion and the mobile-immobile porosity ratio they provide (Table 1 of Luo et al., 2005) are assumed representative of U(VI) contaminated porous media exhibiting multi-porosity behaviour. The DPGs for a conservative scenario are calculated using the minimum pore water velocity value (2.8×10^{-4} ms^{-1}), the maximum hydrodynamic dispersion value (1.2×10^{-4} m^2s^{-1}), the minimum (dual porosity equivalent) mobile-immobile mass transfer exchange value (5.1×10^{-6} s^{-1}), and a remediation scheme length scale, L, of 1.8 m (estimated from the tracer pumping plan). This results in the DPG values $Pe = 4$, $\omega = 0.3$, and $\theta_p = 0.9$, providing a conservative case that is likely to yield less efficient remediation.

Liu et al. (2002a) conducted U(VI) reduction experiments by four DMRB species utilizing 3 different electron donors. That work employed a Monod formulation, rather than the first-order kinetic rates used in this work. The values were therefore estimated to reflect this, with a first-order OC fermentation rate (k) value ranging approximately

4000 (minimum) to 2.3×10^5 (maximum) d^{-1} adopted in this work. This yields a DPG value for *Dk* between 0.8 (minimum) and 46 (maximum).

Simulations parameterised accordingly yield a remediation efficiency, *M*, of 0.13 and 0.46 using the minimum and maximum *Dk* values, respectively. The DPG analysis previously discussed gives an indication of the process(es) which may limit remediation efficiency in this scenario. For example, it was noted earlier that for optimum bioremediation to take place, it is preferable that the mobile-immobile mass transfer timescale ($T_{transfer}$) is lower than one-thirtieth the value of the volumetric flux timescale (T_{flux}) (i.e., $\omega > 30$). Therefore, it appears likely that the reduced remediation efficiency experienced by this system is due to, at least in part, the fact that the mobile-immobile mass transfer timescale ($T_{transfer}$) is too high relative to the volumetric flux timescale (T_{flux}). This system might be optimized by adjusting the ratio of these timescales. Reducing the pore water velocity (e.g., by modifying pumping rates in the laboratory or field) value by one tenth accomplishes this goal by subsequently increases the volumetric flux timescale (T_{flux}) by an order of magnitude. The DPG values then become $Pe = 0.4$, $\omega = 3$, $Dk = 8$ (minimum) and 458 (maximum), and $\theta_p = 0.9$. The adjusted scenario yields a remediation efficiency, *M*, of 0.90 and 0.93 for the minimum and maximum *Dk* values used, respectively. When considered in concert with other important features of DMRB bioremediation systems (e.g., complex geochemical conditions), consideration of the timescales associated with interacting processes may improve experimental or field design conditions such that bioremediation is optimized.

6.5. Conclusions

Over relatively wide ranging microbial and geochemical conditions, optimum bioremediation is likely to occur when the mobile-immobile mass transfer timescale and/or microbial timescale is less than one thirtieth the value of the volumetric flux timescale. Furthermore, remediation may be restricted to systems whose mobile-immobile region mass transfer timescale and/or microbial timescale is between approximately 10 and 1000 times the volumetric flux timescale; the exact value may increase or decrease in systems less or more abundant in electron acceptors, respectively.

The study suggests that the ratio of advection to diffusion in the mobile zone exerts little influence on the remediation efficiency in this system, since the mobile-immobile mass transfer and microbial efficiency are the rate limiting parameters in an immobile-DMRB-resident system under conditions in which sufficient electron donor is supplied. This work further suggests that, in dual porosity immobile-resident DMRB systems, optimal remediation is associated with mobile region porosity between equal to and four times greater than the immobile region porosity.

The presented results demonstrate the conditions under which improved U immobilisation might be improved in biostimulated DMRB U(VI) remediation schemes in dual-porosity systems. Influential parameters that can be actively manipulated in the field include advective velocity (e.g., via pumping rates), microbial efficiency (e.g., via

bioaugmentation, nutrient supply, or maturation of the population), and mobile region porosity (e.g., via hydraulic fracturing). The other parameters may be dictated by site conditions and the presented results may suggest scenarios in which bioimmobilisation is unlikely to be efficient.

The results presented are subject, of course, to the assumptions in the model scenarios in this chapter. This chapter has assumed that DMRB are resident only in the immobile region. It is expected that as mobile-resident DMRB increases, the importance of *Pe* will increase. This chapter has also assumed no surface complexation occurs; while complexation may be important in some scenarios it is expected that the relative changes (i.e., sensitivity) with respect to the DPGs presented will not be significantly affected. The model assumes non-limiting OC in the mobile region and is one-dimensional; multi-dimensional modelling is expected to illuminate the large scale issues of dilution, bypassing, and other challenges in delivering remedial fluids to highly heterogeneous systems.

7. Impact of microbial residency on U(VI) immobilisation in dual porosity porous media

7.1. Introduction

Recent numerical models targeted at simulating U bioimmobilisation remediation have been developed in an attempt to gain a better understanding of the complex interaction between the biological, geochemical and solute transport processes involved (Wang and Papenguth, 2001; Wang et al., 2003; Roden and Scheibe, 2005; Luo et al., 2007). A few of these studies account for the heterogeneous physical structure of aquifer porous media by modelling solute transport using a multi- region or porosity approach. This approach is widely accepted for the modelling of media which possess local flow variations and interregional diffusion due to the existence of fractures, contrasting zones of low- and high- hydraulic conductivity, and/or preferential flow paths (Sidle et al., 1998; Feehley et al., 2000; Ryan et al., 2000; Julian et al., 2001; Haws et al., 2004 and 2005). A multi-porosity approach involves characterization of the media by two or more overlapping flow continua (e.g., van Genuchten and Wierenga, 1976; Grisak and Pickens, 1980; Šimůnek et al., 2003; Haws et al., 2004; Jørgensen et al., 2004; Gwo et al., 2005). In a dual-porosity approach a "mobile" region is conceptualized as exhibiting a relatively high-velocity range transport behaviour dominated by interregional diffusive mass transfer, while a second "immobile" region is conceptualized as exhibiting a contrastingly low-velocity range transport behaviour dominated by local mass transfer. Modelling systems with heterogeneous hydraulic conductivity using the two-region approach has successfully reproduced observed solute transport behaviour (e.g., Li et al., 1994; Feehley et al., 2000). The models must therefore consider in which region(s)

microbial activity occurs. This study explores the consequences of different assumptions concerning the region of microbial residence.

Unfortunately, there is very limited data that identifies the residential preferences of microbes in subsurface porous media, especially under remediation schemes. The available data is further distorted by the act of gathering the media, the method of analysis, and the choice of sample media (Lehman et al., 2004). Nevertheless, subsurface studies have found microbial activity correlated with porosity (Musslewhite et al., 2003), media type (Madsen and Ghiorse, 1993), and grain size (Balkwill, 1989; Sinclair and Ghiorse, 1989; Kieft et al., 1995; Albrechtsen, 1994).

There remain some difficulties in interpreting these identified correlations, since the correlated parameters may not be independent: for example, correlations between microbial activity and either organic carbon content or depth may be made, yet a correlation between depth and organic carbon content may itself be made (Kieft et al., 1995). This situation may lead to apparent contradictions in the correlations. For example, in one study Martino et al. (1998) found the microbial activity to be independent of grain size, so the correlation that was previously attributed to this parameter may have actually instead been associated with a different parameter that also happened to vary with grain size in that study. Furthermore, such correlations may depend on bacterial species. For example Martino et al. (1998) found that lithology influenced the abundance of anaerobic heterotroph and sulfate reducing bacteria, but not of aerobic heterotrophs. The study reported in the present chapter presents a first attempt

at understanding the relationship between media-correlated bacterial residence and U immobilisation.

Bacterial growth or movement may be restricted by the porous media physical conditions. Porosity networks with pore throat sizes narrower than the bacterial cell diameter prevent bacterial penetration into these regions (Smith et al., 1985; Champ and Schroeter, 1988; McKay et al., 1993; Fredrickson et al., 1997). The high shear forces often associated with rapid fluid flow may cause biomass sloughing (Applegate and Bryers, 1991), resulting in a bacterial preference for immobile or near-immobile regions in which shear forces are low and flow is dominated by diffusion. Furthermore, biomass starvation of electron acceptors (as opposed to electron donor) may cause significant sloughing events (Applegate and Bryers, 1991). This suggests that porous media regions scarce in electron acceptors may be less likely to harbour significant bacterial populations. Accordingly, Roden and Scheibe (2005) chose to model DMRB presence in only the mid-region of their tri-region model, in part for these reasons.

In the undisturbed subsurface, microbial activity is certainly correlated with higher carbon contents (Kieft et al., 1995). Naturally, it may be expected that microbial distribution correlates well with an electron donor source. In organic-rich sediments, dominant bacterial activity may take place at the interface between different media/porosity regions (Krumholz et al., 1997; Detmers et al., 2001; Ulrich et al., 1998). It is often assumed that this is due to diffusion of existing electron donors from fine-grained, organic-rich sediment. Deep aquifers have also shown OC fermentation

restricted to the clayey confining sediment, with the resulting fermentation acids being transported to the surrounding lower-OC sandy sediment in which the electron acceptors are present (Lovley and Chapelle, 1995). In such cases, complete redox processes are physically separated. However, in bioremediation schemes in which OC is injected into the subsurface, the initial natural OC content may become less significant to the microbial distribution: bacterial communities may instead favour the more mobile (advective dominant flow) regions where electron donor concentrations are higher and therefore more accessible to the bacteria. Regions in which electron acceptor concentrations are higher may also be favoured. Such regions are likely to exist in lower porosity regions where the ratio of solid surface area to pore water volume is high and hydraulic conductivity is low.

Such varied data and conditions make it difficult to generalize how characteristic regional media conditions and microbial residence are linked. Many authors consequently assume that (i) all biological processes are restricted to a chosen region(s) (e.g., Roden and Scheibe, 2005), or (ii) bioactivity occurs in all regions (e.g., Sun et al., 1999; Luo et al., 2007). It is not known what effect such assumptions have on the outcome of modelling calculations. Further, the effect of such assumptions may influence field site characterization decisions.

This chapter provides a preliminary investigation into the affects of different bacterial residence locations in multi-porosity porous media systems. The study considers

multiple conditions typical of field sites and identifies the key distinctions in U immobilisation behaviour imparted by the different bioresidence modelling assumptions.

7.2. Simulation parameterisation

Simulations using the model developed in Chapter 3 were conducted for three different microbial residency conditions: bioactivity present in the immobile region, the mobile region, and both regions. The simulations consider U(VI)-contaminated oxic recharge water entering an anaerobic aquifer. In order to best represent real-site conditions and allow for the influence of U(VI) on the accumulation and stability of both oxidized and reduced U phases (Neal et al., 2004), U(VI) is considered to continually enter the domain. OC is injected into the mobile region. Mass transfer occurs between the mobile and immobile regions. The transport conditions are outlined in Table 7.1.

Geochemical conditions vary widely in the natural environment and it is impractical to cover the full range in numerical simulations. Therefore, the geochemical parameters used in the numerical simulations were selected based on U-contaminated field site data so as to be representative of U-contaminated aquifers in what is deemed to be a typical natural environment. The geochemical conditions used in the simulations were mean values from data reported for Area 2 of the Oak Ridge Field Research Center (ORNL, 2007), and are presented in Table 7.2. A media bulk density of 1.5 kg dm^{-3} was assumed. Rhodochrosite, siderite, calcite, mackinawite and uraninite all have the potential to precipitate, but were not taken to be present initially. The same initial conditions were adopted for both the mobile and immobile domain.

The microbial kinetics of the system were parameterised according to Wang et al. (2003). Values were previously given in Table 4.3.

Table 7.1. Transport conditions used in simulations.

Parameter	Units	Value
Groundwater velocity, v[a]	m yr^{-1}	10
Dispersivity, a[a]	m	0.25
Mobile-immobile mass transfer, γ^c	yr^{-1}	1900 (high value) 280 (mean value) 1.6 (low value)
Δx	m	0.25
Domain length	m	Semi-infinite
Upstream boundary condition	-	Dirichlet

[a]Wang et al. (2003)

[b]Fetter (1994); Griffioen et al. (1998); Kim and Corapcioglu (2002); Haws et al. (2005); Roden and Scheibe (2005).

[c]Feehley et al. (2000); Harvey and Gorelick, 2000; Kim and Corapcioglu (2002); Haws et al. (2004, 2005); Jørgensen et al. (2004); Luo et al. (2005); Roden and Scheibe (2005).

Table 7.2. Initial and boundary geochemical conditions.

Species	Units	Boundary concentration (x=0, t)	Initial concentration (x>0, t=0)
OC	μmol l^{-1}	3000	0
O_2	μmol l^{-1}	200	0
N(V)	μmol l^{-1}	200	200
S(VI)	μmol l^{-1}	300	300
U(VI)	μmol l^{-1}	1	1
Ca^{2+}	mmol l^{-1}	3.5	0
Ferrihydrite	mmol dm^{-3}	0	0.163
Pyrolusite	mmol dm^{-3}	0	0.026
Calcite	mmol dm^{-3}	0	0.804
Carbonate	mmol dm^{-3}	1	1
pH	-	6.5	7.15

7.3. Simulation results

7.3.1. Impact of media porosity

The injected OC is utilized by the bacteria in TEAPs, and the EAs are sequentially reduced in the system in order of the most energetically favourable. This leads to a reductive section in the domain where U(VI) is, when energetically most favourable, reduced. Surface complexation of U(VI) and numerous abiotic reactions also take place in the system. The specifics of these phenomena have been documented elsewhere (Wang and Papenguth, 2001; Wang et al., 2003). Instead, the focus here is on how different bioactivity scenarios affect U(VI) bioimmobilisation. U(VI) migrating from the contaminated site gives an indication of the success of bioimmobilisation. The time at which U(VI) is reduced to less than the existing groundwater protection standard of 0.18 μmol l^{-1} (Federal Register, 1995) in the mobile region at 10 m downstream of the OC injection point is therefore used as the metric for the comparison of different simulation scenarios. In order to compare bioimmobilisation efficiency in different porous media types, the ratio of mobile to total porosities is used:

$$\beta = \frac{\theta_m}{\theta_m + \theta_i} \tag{7.1}$$

This ratio tends to be constant for any given medium type (Li et al., 1994).

Figure 7.1 presents the time at which U(VI) is reduced to the metric level against the porosity ratio (β). When bioactivity occurs in both the mobile and immobile regions the net microbial efficiency is high, resulting in rapid consumption of electron acceptors and

faster U(VI) immobilisation relative to either mobile- or immobile-region isolated bioactivity. Further, the time taken to immobilise the U(VI) is independent of the porosity ratio.

However, when bioactivity occurs in either the immobile or mobile region only, the net microbial efficiency is slower and is demonstrated to vary with β. In the case of immobile-resident bioactivity, mass transfer limitations between the mobile and immobile region limit the bacteria's access to OC, thereby reducing the net microbial efficiency. As a result, U(VI) immobilisation is considerably slower compared to systems in which bioactivity occurs in both regions. As the immobile region porosity becomes smaller relative to the mobile region porosity (increasing β), the reduced relative porosity of the immobile region yields a reduced pore water volume in which microbial activity takes place, thus reducing the net U(VI) immobilisation efficiency. In the case of mobile-resident bioactivity, the reverse situation occurs as β increases: microbially accessible pore water volume increases and the time taken to reduce U(VI) decreases.

Therefore, systems with $\theta_m < \theta_i$ and microbial activity occurring predominantly in porous media regions of more mobile (higher velocity ranging) pore water will tend to exhibit slower U(VI) immobilisation than those with microbial activity occurring predominantly in immobile (low velocity ranging) pore water regions, for systems of comparable biological, geochemical, and transport conditions. In systems in which $\theta_m > \theta_i$, this phenomenon reverses: when predominant microbial activity occurs in the

immobile region, U(VI) immobilisation is more efficient than when microbial activity occurs predominantly in the mobile region.

The majority of porous media exhibiting dual porosity transport behaviour are likely to be characterized by a mobile region porosity of lower value than their immobile region porosity. This is because regions which are of low hydraulic conductivity (e.g., clay) are correlated with high porosity, and vice versa (e.g., Morin, 2006). It is therefore likely that in most systems, if microbial activity is dominant in either one of the mobile or immobile pore water regions only, higher remediation efficiency will occur in the case of the latter. However, it should also be noted that microbial activity in both regions results in greater remediation efficiency than either of these scenarios. This suggests that, under equivalent bacterial, geochemical (including injected OC concentration) and transport conditions, variation in porosity ratio does not affect bioimmobilisation speed when both regions are bioactive.

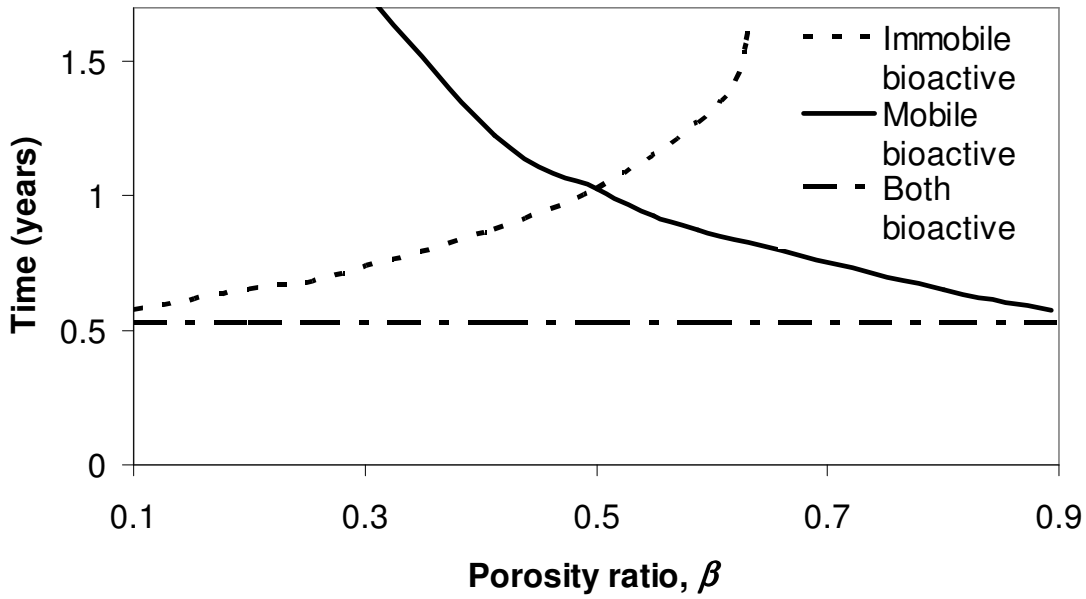

Figure 7.1. Time at which U(VI) is immobilised for bioactivity in different regions at various porosity ratios, with an mean value mobile-immobile mass transfer rate.

The uraninite mineral presence may also vary significantly depending on media conditions. Figures 7.2-7.7 present the spatial uraninite concentration distributions after 1.5 years of biostimulation for systems with a mean value transfer rate (γ = 280 yr^{-1}). This represents a point in time when U(VI) is no longer present (above the 0.18 μmol l^{-1} standard) in the groundwater passing 10 m downgradient of the OC injection point. Two different porosity ratios (β = 0.41 and β = 0.59) are presented to demonstrate the behaviour of different media types. In all simulations, oscillations of uraninite concentration occur. It may be supposed that these have arisen due to a poor numerical discretisation. Figure 7.8 displays the spatial uraninite distribution after 1.5 yrs of biostimulation for a system with a bioactive mobile region only, mean transfer rate (γ= 280 yr^{-1}) and β = 0.41 at three different model discretisations. The results show that even

discretisations as fine as Δx = 0.01 m (Δt = 3.65 days) do not significantly change the results. Nevertheless, the causes of these oscillations are likely due to coarse discretisation. This issue is discussed further in Section 8.3.

Figures 7.2 and 7.3 display systems with bioactivity in the mobile region only. At either porosity ratio (β) of 0.59 (Figure 7.2) or 0.41 (Figure 7.3), the mobile region holds the majority of uraninite in the system. The immobile region in both these systems also holds a small quantity of uraninite. Although the immobile region is not bioactive, both scenarios display a small amount of uraninite present in the immobile region. This is due to the transfer of reduced species such as Fe(II) and HS^- into the immobile region, allowing U(VI) to be abiotically reduced in this region. However, when the mobile-immobile transfer rate is reduced to the low value of 1.5 yr^{-1} this effect is not observed (result not shown), since significant quantities of reduced species do not enter the immobile region. These observations are similar for the two different porosity ratio systems.

Figures 7.4 and 7.5 display systems with bioactivity in the immobile region only. In contrast with mobile-region bioactive systems, these systems instead hold the majority of uraninite in the immobile region. This is the case irrespective of porosity ratio. They also hold a significant amount of uraninite in the non-bioactive mobile region. But, in contrast with mobile-region bioactive systems, the quantity of uraninite in the mobile region varies slightly depending on porosity ratio: the system with the higher porosity ratio (β = 0.59, Figure 7.4) contains less uraninite than the system with the lower

porosity ratio (β = 0.41, Figure 7.5). Furthermore, the uraninite in this system is clustered in a small spatial region (3 m < x < 5 m). Note also that the upgradient front of the reductive region (down gradient of which uraninite precipitates) tends to shift position slightly depending on the porosity ratio.

Figures 7.6 and 7.7 display systems with bioactivity in both regions. At the higher porosity ratio (β = 0.59, Figure 7.6) the system contains twice as much uraninite as held in any of the preceding systems. (Note the different scale on the vertical axis for this figure.) This is to be expected, since bioactivity in both regions increases the net microbial activity within the system. Further, the mobile and immobile regions share the same uraninite content. At the low porosity ratio (β = 0.41, Figure 7.7) the uraninite concentrations and spatial distributions are similar to the system of the same porosity ratio with bioactivity in the immobile region only (Figure 7.5), except that the uraninite in immobile region is distributed somewhat differently (both systems show a similar total quantity in the region).

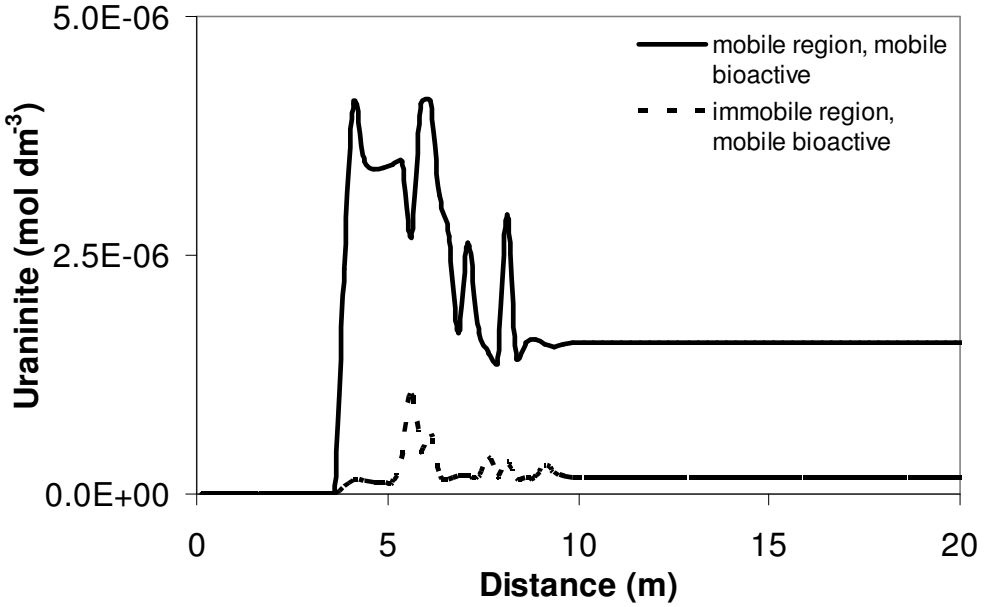

Figure 7.2. Spatial uraninite distribution after 1.5 yrs of biostimulation for bioactive mobile region only, with mean transfer rate and β = 0.59.

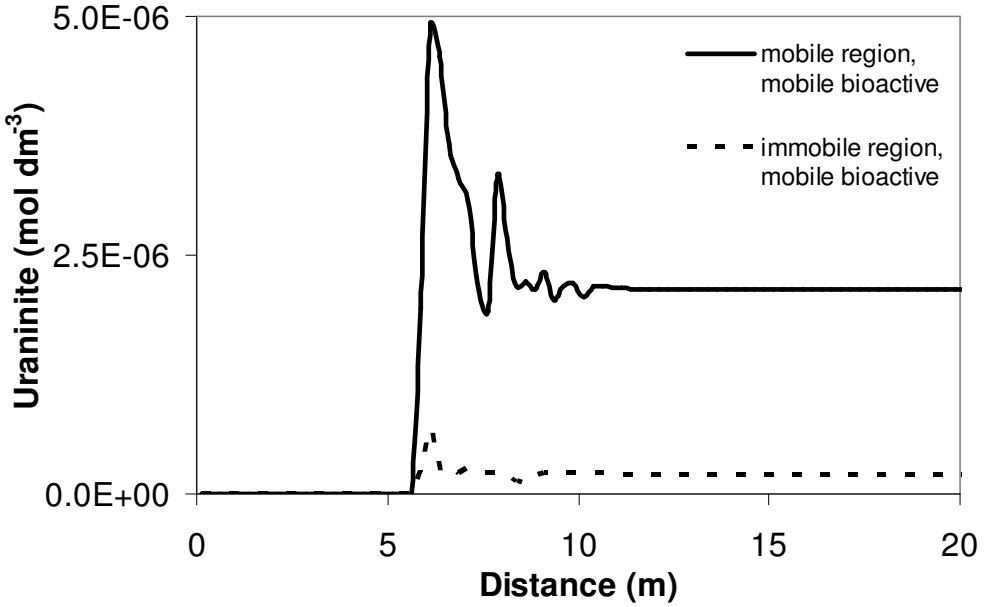

Figure 7.3. Spatial uraninite distribution after 1.5 yrs of biostimulation for bioactive mobile region only, with mean transfer rate and β = 0.41.

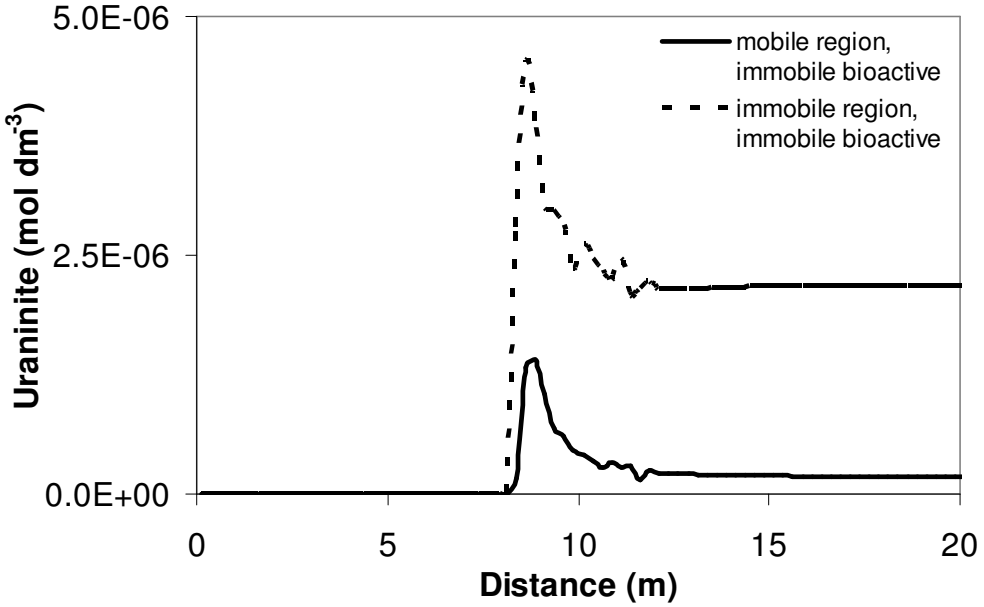

Figure 7.4. Spatial uraninite distribution after 1.5 yrs of biostimulation for bioactive immobile region only, with mean transfer rate and $\beta = 0.59$.

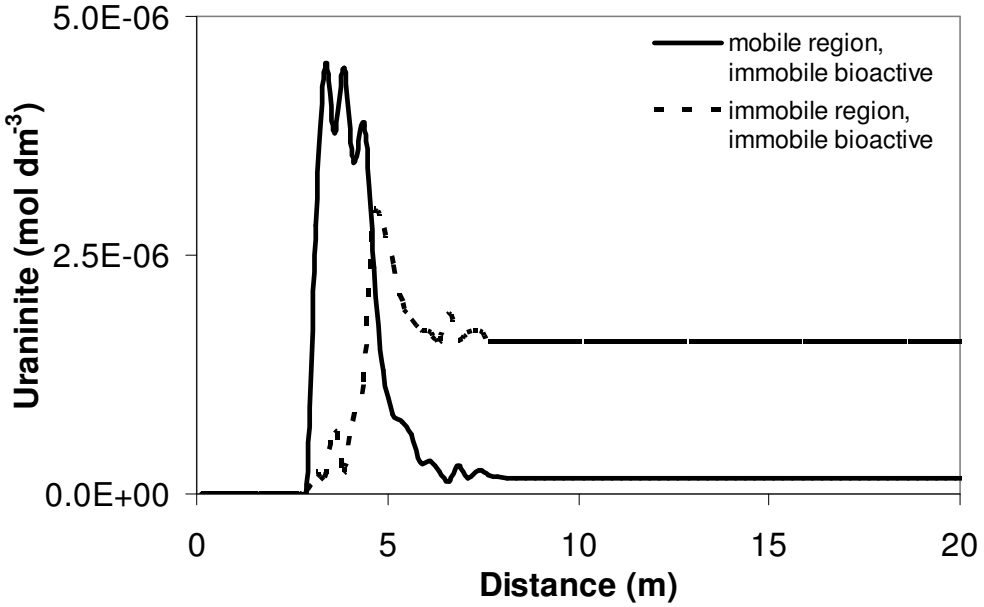

Figure 7.5. Spatial uraninite distribution after 1.5 yrs of biostimulation for bioactive immobile region only, with mean transfer rate and $\beta = 0.41$.

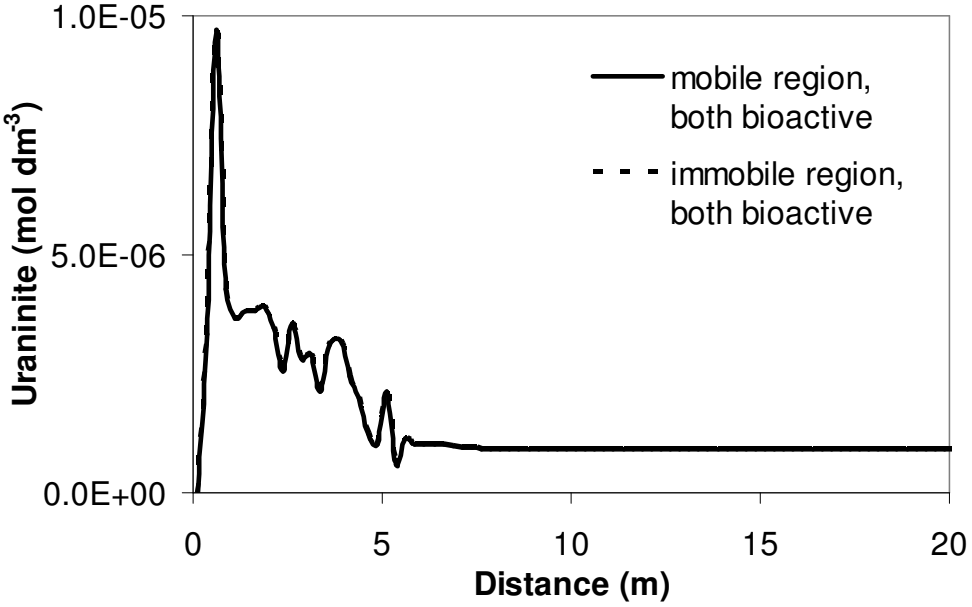

Figure 7.6. Spatial uraninite distribution after 1.5 yrs of biostimulation for both regions bioactive, with mean transfer rate and β = 0.59.

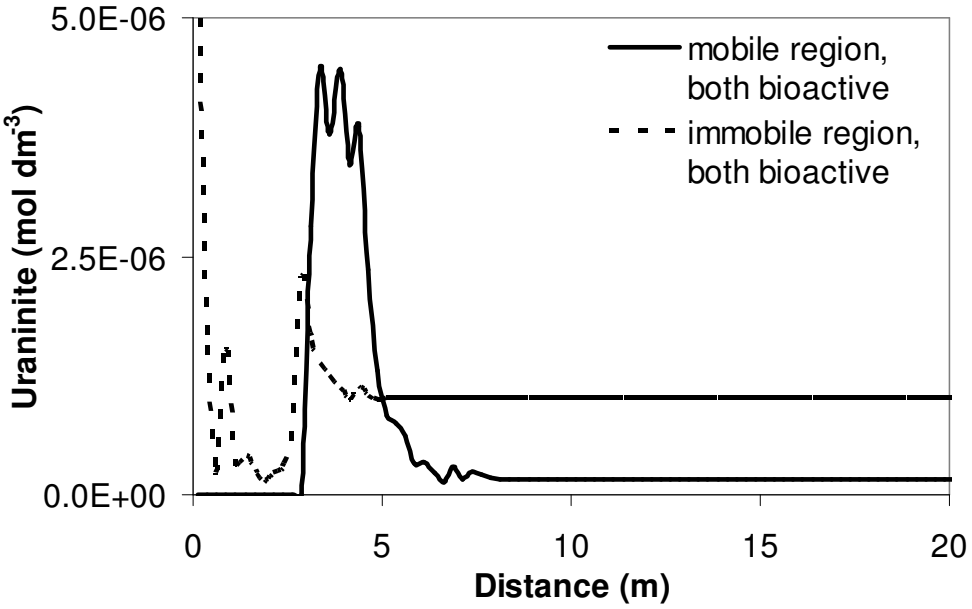

Figure 7.7. Spatial uraninite distribution after 1.5 yrs of biostimulation for both regions bioactive, with mean transfer rate and β = 0.41.

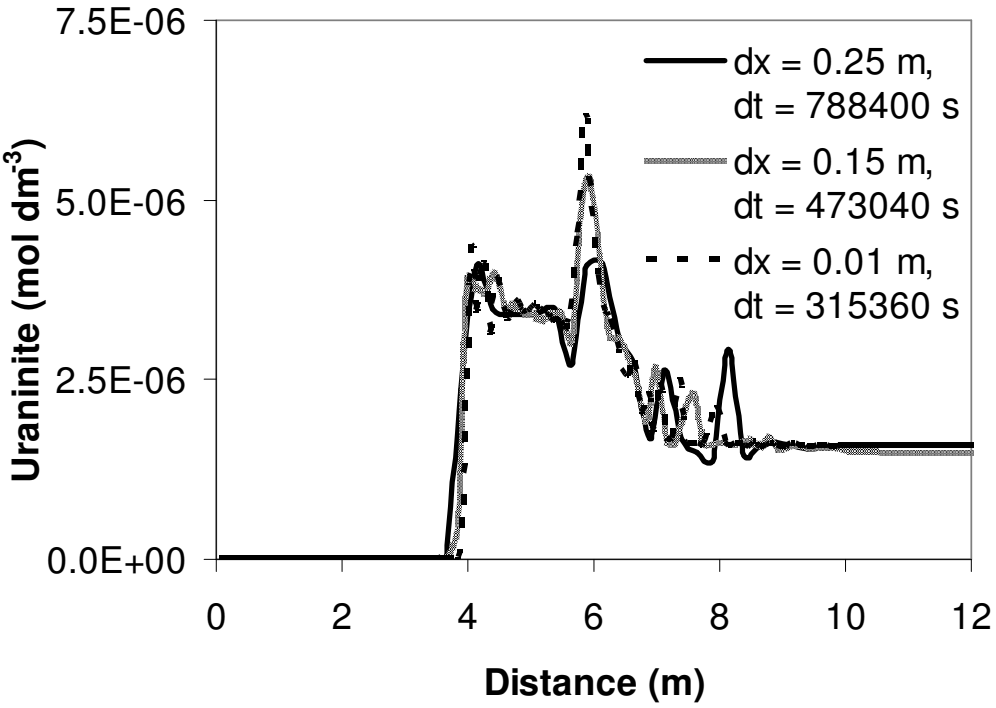

Figure 7.8. Spatial uraninite distribution after 1.5 yrs of biostimulation for bioactive mobile region only, mean transfer rate, β = 0.41 for various model discretisations.

7.3.2. Impact of mass transfer rate

The rate of mass transfer between the mobile and immobile regions may also impact remediation efficiency significantly. For the geochemical and transport conditions used in this Chapter, U(VI) immobilisation at the maximum transfer rate determined from real site data (1900 yr^{-1}) is not significantly different from that at the mean value rate (280 yr^{-1}). However, at a low transfer rate (1.6 yr^{-1}), the impact is significant. Figure 7.9 presents the time at which U(VI) is reduced to the metric value (0.18 μmol l^{-1} at x = 10 m) against the porosity ratio β. These results are complemented by those for the mean value transfer results (previously presented in Figure 7.1) for comparison.

When only the immobile region is bioactive, U(VI) immobilisation efficiency is reduced due to the decreased microbial accessibility to OC. However, when only the mobile region is bioactive, U(VI) immobilisation efficiency is not significantly different to that presented for a mean mobile-immobile transfer rate (mean γ value). This is because the microbial accessibility to OC is not restricted. Furthermore, the geochemical conditions in the immobile region have no significant net impact on the system. When the mobile and immobile regions are both bioactive, the immobilisation efficiency is exactly the same in the low value transfer (low γ value) case as it is for the mean value transfer case (i.e., the same result as shown in Figure 7.1).

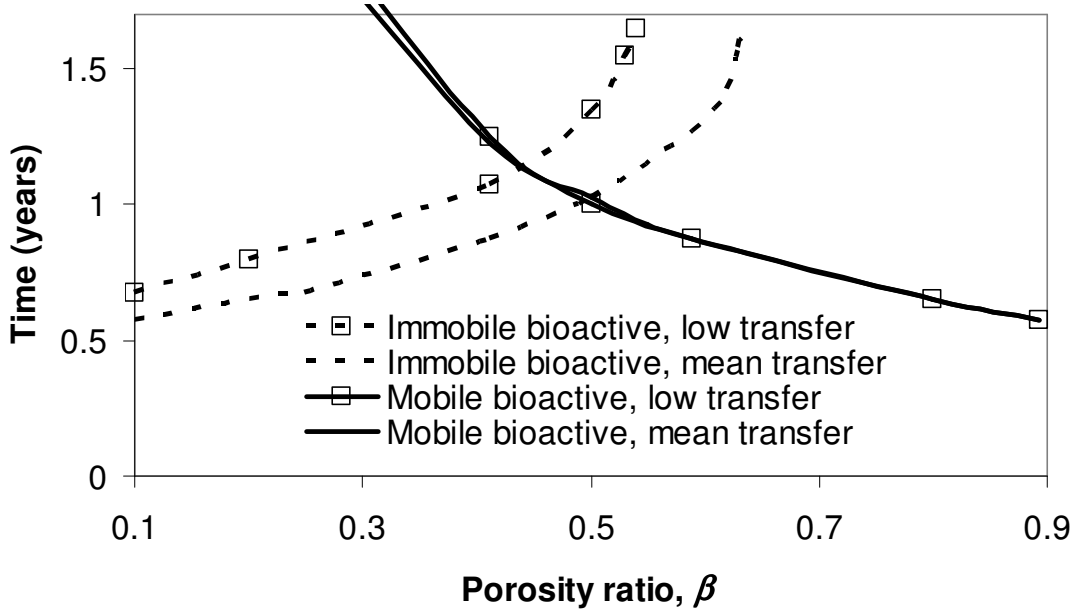

Figure 7.9. Time at which U(VI) is immobilised for bioactivity in different regions at various porosity ratios, for both low and mean value mobile-immobile mass transfer rate.

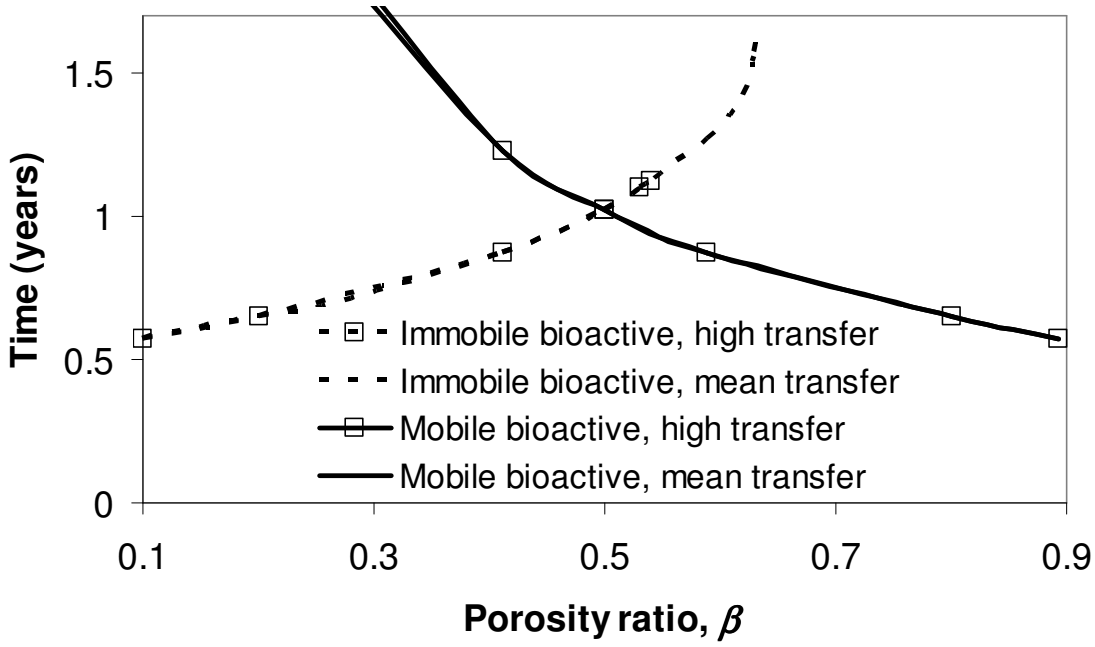

Figure 7.10. Time at which U(VI) is immobilised for bioactivity in different regions at various porosity ratios, for both high and mean value mobile-immobile mass transfer rate.

Figures 7.11-7.16 present the uraninite concentration distributions after 1.5 years of biostimulation in a system with a porosity ratios β of 0.5 for the three transfer rates (γ) of 1900 (high value), 280 (mean value) and 1.6 (low value) yr^{-1}. Whether bioactivity is restricted to the mobile or immobile region, systems possessing this porosity ratio will reach the remediation target (mobile region [U(VI)] < 0.18 μmol l^{-1} at x = 10 m) at the same time (cf. Figures 7.9 and 7.10). This allows such systems to be compared directly. Note, however, that in cases in which bioactivity occurs in both regions, the remediation target will be attained sooner than in either of these single-region bioactive systems.

Figures 7.11-7.13 present the uraninite concentration distributions for the three different transfer rates in the mobile region. Figure 7.11 displays a system with bioactivity in the mobile region only. The concentrations and distributions of uraninite are similar for the three different transfer rates. Figure 7.12 displays a system with bioactivity in the immobile region only. The concentrations and distributions of uraninite are again similar, except when the transfer rate becomes low. In such cases mobile region displays a lower uraninite concentration due to the limited transfer of reduced species from the immobile region into the mobile region. This supports the same result determined from Figure 7.9. Figure 7.13 displays a system with bioactivity in both regions. (Note that the vertical axis scale is different.) The uraninite concentrations in this system are higher than in systems with bioactivity restricted to a single region, yet are again similar for the three different transfer rates. It is worth further noting that the spatial distribution of the uraninite is different in this system, with the majority of uraninite precipitating further upgradient at all three transfer rates compared to that in the mobile only or immobile only bioactive systems.

Figures 7.14-7.16 present the uraninite concentration distributions for the three different transfer rates in the immobile region. In all cases, the different transfer rates do not result in significantly different uraninite concentrations or distributions in each system. When bioactivity occurs in the mobile region only (Figure 7.14), the uraninite concentrations at the low transfer rate are slightly different compared to higher transfer rates. However, as the system contains low uraninite concentrations compared to systems with different residence characteristics, this effect is not considered significant.

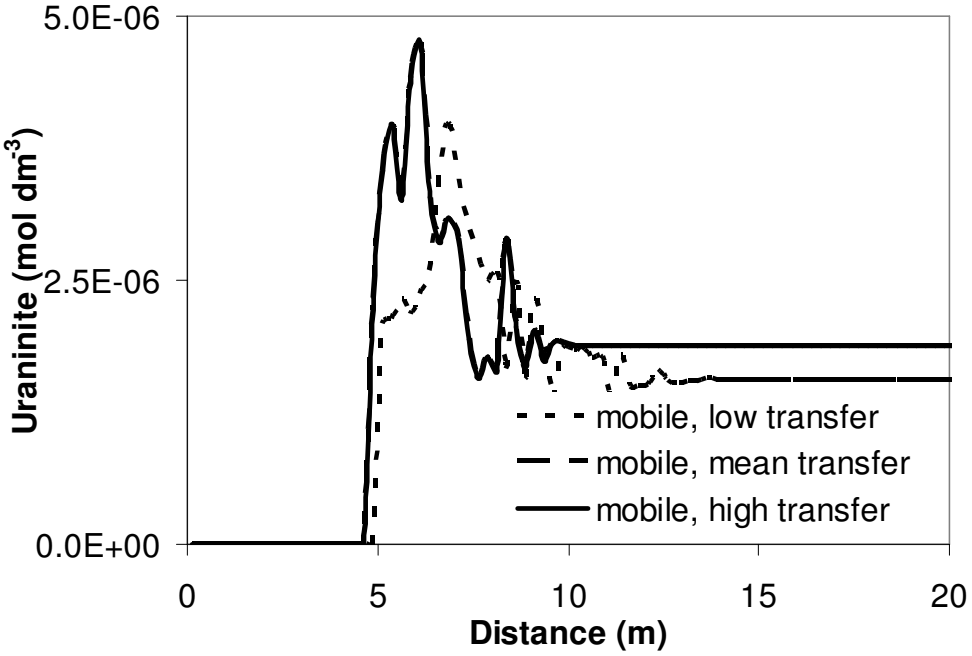

Figure 7.11. Spatial uraninite distribution in the mobile region after 1.5 yrs of biostimulation for bioactive mobile region only and β = 0.5, at three different transfer rates.

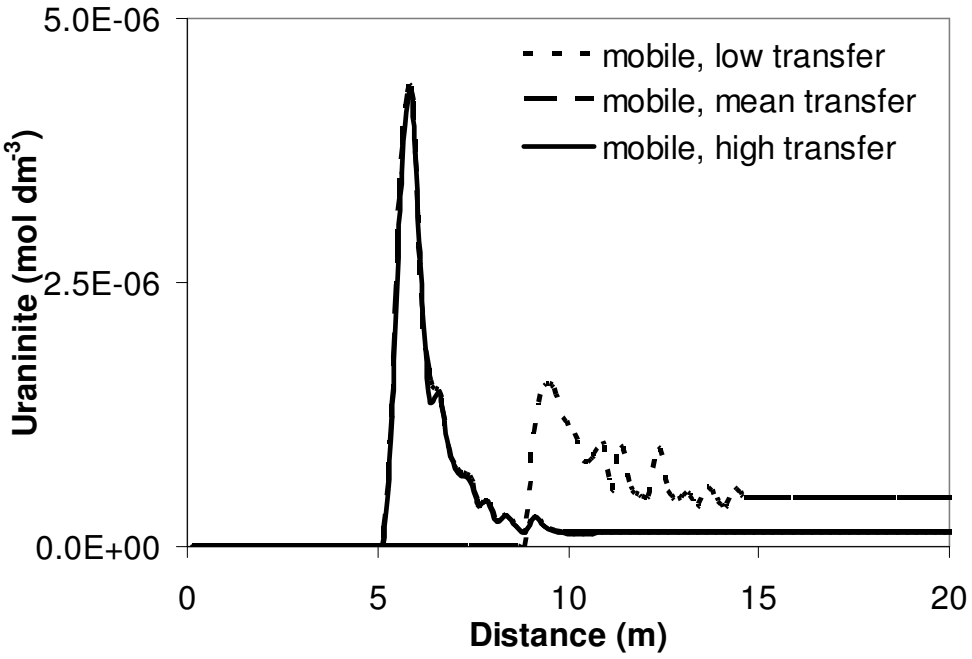

Figure 7.12. Spatial uraninite distribution in the mobile region after 1.5 yrs of biostimulation for bioactive immobile region only and β = 0.5, at three different transfer rates.

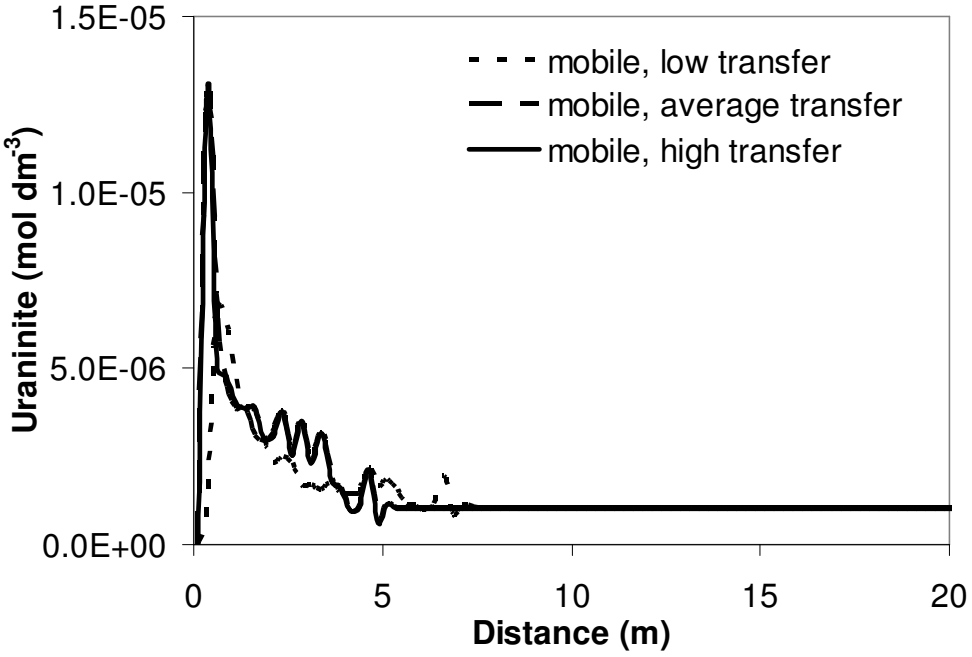

Figure 7.13. Spatial uraninite distribution in the mobile region after 1.5 yrs of biostimulation for bioactivity in both regions and β = 0.5, at three different transfer rates.

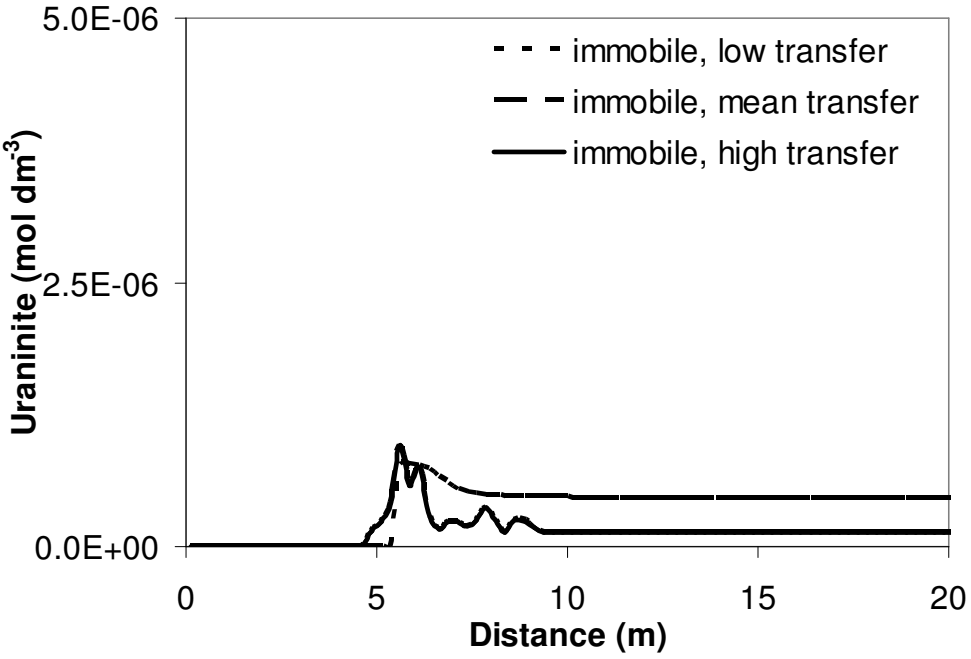

Figure 7.14. Spatial uraninite distribution in the immobile region after 1.5 yrs of biostimulation for bioactive mobile region only and β = 0.5, at three different transfer rate.

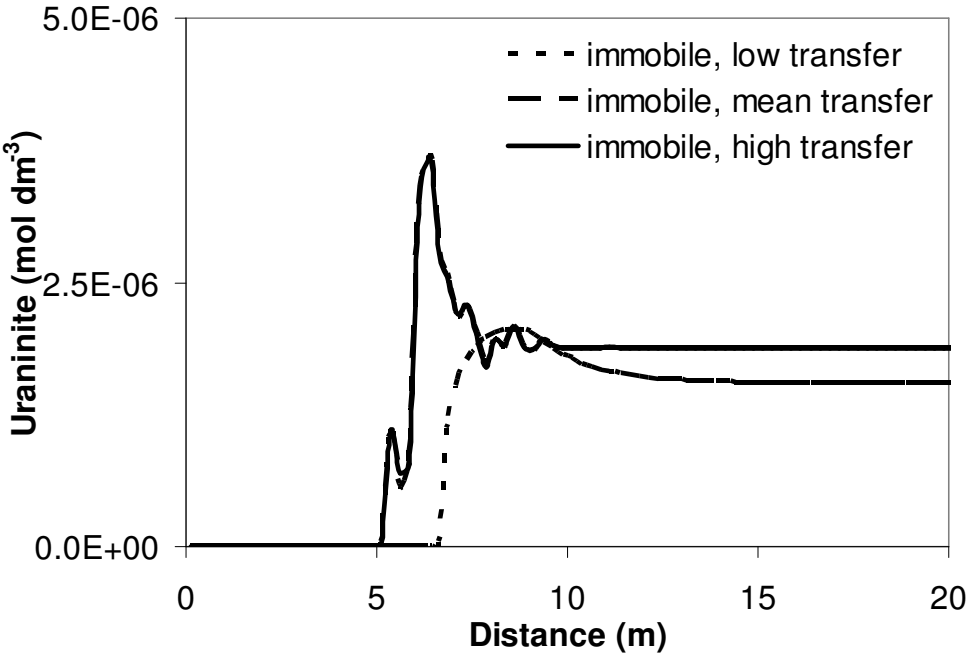

Figure 7.15. Spatial uraninite distribution in the immobile region after 1.5 yrs of biostimulation for bioactive immobile region only and β = 0.5, at three different transfer rates.

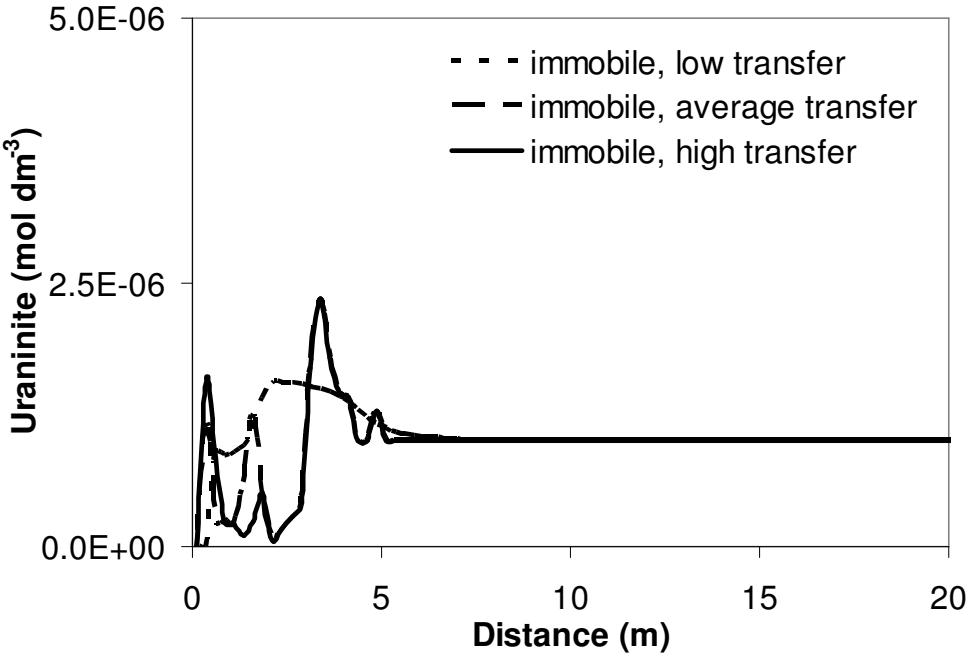

Figure 7.16. Spatial uraninite distribution in the immobile region after 1.5 yrs of biostimulation for bioactivity in both regions and β = 0.5, at three different transfer rates.

7.3.3. Impact of microbial efficiency

Microbial efficiency may, of course, affect U(VI) immobilisation efficiency. In order to determine how immobilisation efficiency varies with porosity when microbial efficiency changes, the results presented in Figure 7.1 is again presented in Figure 7.17 in conjunction with results for which the microbial rates were increased. Increased microbial efficiency was modelled with all rates (μ) in Table 4.3 increased by a factor of two. The results in Figure 7.17 show that the relationship between immobilisation efficiency and porosity holds irrespective of microbial efficiency. Figure 7.17 does not show results for microbial residence in both regions; at the doubled microbial rates the time to U(VI) immobilisation shows the same relationship with porosity, except that the

value is 0.275 years instead of 0.525 years. Clearly, at increased microbial efficiency, U(VI) immobilisation is simply more rapid.

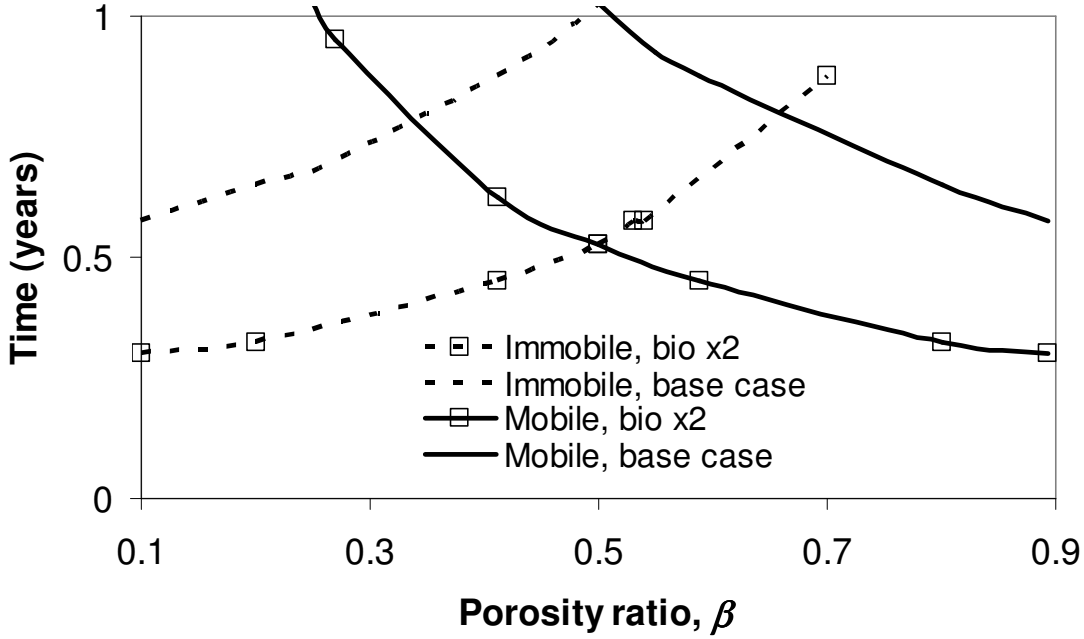

Figure 7.17. Increased microbial efficiency.

7.3.4. Impact of mineralogy

Variations in mineral concentrations may result in significantly different modelling outcomes, even when pore water chemistry is accurately described (Zhu and Burden, 2001). Therefore, understanding the impact which varying mineral assemblages have on the system is important for the effective operation of any bioremediation scheme. The lack of known mineralogy variations within different regions of heterogeneous porous media mean that uncertainties exist over the realism of regionally varying mineralogical conditions. Nevertheless, systems are certainly sensitive to mineralogy, indicating that

this area should be investigated further to explore its potential impact on remediation systems.

The model was used to explore the effect which varying mineral concentrations had on the time taken to reduce the mobile region U(VI) concentration to less than 10^{-11} mol l^{-1} at x = 10 m (the "target" U(VI) reduction metric). Glassley et al. (2002) showed that representation of complex heterogeneous mineral distributions by averaged mineral properties is a valid method for use in reactive transport simulations.

Table 7.3 shows the results of 12 simulations. The "base case" data represent the mineralogies and bioactivity scenarios already presented (mineralogies given in Table 7.2). Further to these, the initial ferrihydrite and pyrolusite concentrations were reduced to 5×10^{-6} and 1×10^{-6} mol dm^{-3}, respectively, in each of (i) the mobile region only, (ii) the immobile region only, and (iii) both regions. These concentrations are approximately the minimum reported for Area 2 of the Oak Ridge Field Research Center site. For each of these three cases, simulations were conducted in which the bioactivity was present in (i) the mobile region only, (ii) the immobile region only, and (iii) both regions. Thus, data for 9 further scenarios is presented. A number of observations can be made from the results. In all cases the reduced initial mineral presence results in a shorter time taken for U immobilisation to occur. The reduced presence of electron acceptors means U-reducing microbial activity can occur relatively sooner.

Table 7.4 displays the time taken for each mineral-reduced system to reach the target U(VI) bioreduction as a percentage of the base case. The table shows that a reduction in time to attain the U(VI) reduction target occurs irrespective of the region(s) in which mineral presence has been reduced, or the region in which microbial activity takes place. The time taken to attain the U(VI) reduction target is reduced with (i) a reduced mineral presence in the immobile region (relative to that present in the mobile region), when bioactivity is restricted to a single region, and (ii) a reduced mineral presence in the mobile region (relative to that present in the immobile region) when both regions are bioactive.

Due to the lack of data concerning mineralogy within heterogeneous porous media, it is uncertain what kind of real scenarios specific mineral distributions represent. Nevertheless, these results not only confirm that mineral presence can exert a significant impact of U(VI) bioreduction efficiency, but also demonstrate that the efficiency is dependent on the combination of spatial mineral distribution and spatial microbial distribution. The results highlight the potential significance of spatially varying mineralogical and biological conditions within heterogeneous porous media and suggest that future research into the sensitivities of systems to mineralogy may prove to bring valuable insight to remediation efficiency.

Table 7.3. Bioimmobilisation time (years, rounded to nearest 0.025 year) for various mineralogy and bioactivity scenarios.

Bioactive region	Base case	Mobile mineralogy reduced	Immobile mineralogy reduced	Both mineralogies reduced
mobile	1.700	1.200	0.875	1.200
immobile	0.525	0.375	0.325	0.375
both	0.725	0.375	0.525	0.525

Table 7.4. Percentage (to nearest 5%) of base case scenario time taken for bioimmobilisation in reduced mineralogy scenarios.

Bioactive region	Mobile mineralogy reduced	Immobile mineralogy reduced	Both mineralogies reduced
mobile	70	50	70
immobile	70	60	70
both	50	70	70

7.4. Conclusions

The biogeochemical transport model developed in Chapter 3 was used to explore the effects of different microbial residence locations on the success of biostimulated U(VI) immobilisation in a dual-porosity porous media system. Three microbial residence scenarios were compared in which bioactivity was present in (i) a predominantly low-velocity ranging (diffusive dominated) "mobile" flow region, (ii) a predominantly high-velocity ranging (advective dominated) "immobile" flow region, and (iii) both these regions. The speed of U(VI) immobilisation was compared for each of the three microbial residence scenarios.

For the typical U(VI) contaminated field site geochemical, microbial and transport conditions used, the predictions suggest that when bioactivity is dominant in only one of the mobile and immobile regions, U(VI) immobilisation efficiency is dependent on the

ratio of the mobile region porosity to the total porosity. However, when both regions are bioactive, the ratio of the region porosities has significantly less impact on U(VI) immobilisation. The mass transfer rate between the mobile and immobile regions may significantly impact U(VI) immobilisation efficiency when only the immobile region is bioactive. However, when the mobile region only or both regions are bioactive, U(VI) immobilisation efficiency is less affected by the transfer rate. In systems with equivalent porosities and bioresidency characteristics, mass transfer rate will not generally cause significantly different uraninite concentrations. An exception to this exists when the mass transfer is low, and the region in which uraninite precipitates is not the region in which bioactivity takes place. In all cases, U(VI) immobilisation is faster in a system with bioactivity in both regions than it is in a system with bioactivity in only one of either the mobile or immobile regions. These conclusions are valid irrespective of the microbial efficiency of the system.

When the predominant bioactive region is the mobile region, the majority of uraninite tends to accumulate in the mobile region. This occurs irrespective of the porosity ratio of the media. When the mass transfer rate between the mobile and immobile regions is high enough, some uraninite also precipitates in the immobile region due to mass transfer of reductive chemical species into that region. However, when the predominant bioactive region is the immobile region, significant quantities of uraninite may precipitate in both the mobile and immobile regions. The quantity precipitating in the immobile region may increase as the porosity ratio decreases, and the location at which uraninite predominantly precipitates may vary depending on porosity ratio and the region of

microbial residence. These observations may be valuable in the context of U remediation schemes, since DMRB tend to form nano-sized particles of uraninite (Suzuki et al., 2002) which may undergo oxidative dissolution (Kelly et al., 2001). The presence of such uraninite particles in less accessible porous media regions of low flow velocity may prevent reoxidation or transportation of the mineral. In such cases, the results presented here would suggest that systems with bioactive immobile regions may hold advantages over those without. Whilst U(VI) immobilisation efficiency in systems with bioactivity in both regions is the same irrespective of the porosity ratio, the distribution of uraninite in the media may nevertheless vary depending on this porosity ratio. Furthermore, systems with bioactivity in both regions tend to exhibit uraninite precipitation further upgradient compared to those with bioactivity in the mobile region only or immobile region only.

Simulations revealed that spatially varying mineral presence can exert a significant impact of U(VI) bioreduction efficiency. Efficiency was found to be dependent on the combination of spatial mineral distribution and spatial microbial distribution. The results highlight the potential significance of spatially varying mineralogical and biological conditions within heterogeneous porous media and suggest that future research into the sensitivities of systems to mineralogy may prove to bring valuable insight to remediation efficiency.

Multi-regional models that assume microbial residence in both “mobile” and “immobile” conceptual flow regions may significantly overestimate microbial efficiency

and thereby exaggerate predicted remediation effectiveness if biomass is restricted to specific media regions. This highlights the importance of characterizing the bioresidency status of field sites if biogeochemical models are to accurately predict remediation schemes in physically heterogeneous media.

8. Reoxidation of bioimmobilised U(IV) in dual porosity media

This chapter details an investigation into the effects of U(IV) reoxidation in porous media after cessation of biostimulation.

8.1. Introduction

As discussed in Chapter 2, the long-term stability of U(IV) following the biostimulation of U-contaminated sites is of some concern (Suzuki and Suko, 2006). Experimental evidence suggests that U(IV) may reoxidise after biostimulation ceases in environments where either oxic groundwater enters the reduced zone (Zhou and Gu, 2005), or under anaerobic conditions by nitrate-reduction products (Senko et al., 2002; Elias et al., 2003; Istok et al., 2004). However, the presence of iron-sulfide minerals may protect bioreduced U(IV) from reoxidation by providing a reductive barrier (Abdelouas et al., 1999; Senko et al., 2005).

Uncertainties exist over the likelihood and extent of reoxidation in previously bioimmobilised U in porous media. This chapter explores the affects of reoxidation on a previously biostimulated domain in dual porosity porous media, in the context of different bioresidency scenarios and in the presence or absence of iron-sulfide minerals.

8.2. Simulation scenarios

The simulations presented in Chapter 7 were used as a basis for exploration. The model developed in Chapter 3 was utilised, with a Michaelis-Menten/Monod kinetic approach to modelling OC oxidation rate (equation 3.2) and inclusion of surface complexation (see Section 3.5). Simulations used the transport conditions outlined in Table 7.1, with β = 0.41. The microbial kinetics parameterisations given in Table 4.3, were used. As in previous simulations (Chapter 7), OC injection proceeded for 1.5 years. The geochemical conditions given in Table 7.2 are used. As in Chapter 7, rhodochrosite, siderite, calcite, and uraninite all have the potential to precipitate, but were not taken to be present initially. In these simulations, however, OC injection was terminated at that time. The same initial conditions were adopted for both the mobile and immobile domain. The domain influent therefore remains as reported in Table 7.2, except that after 1.5 years the influent OC concentration is zero. As the influent water is oxic, after 1.5 years the domain will therefore be exposed to oxic water capable of reoxidising U(IV) in the absence of OC.

It is acknowledged that secondary redox reactions such as the reoxidation of U(IV) may be modelled using a kinetic approach (e.g. Wang and Papenguth, 2001; Wang et al., 2003). Unfortunately, these models do not use kinetic oxidation rates based on observed data. While numerous studies report observed reoxidation of bioimmobilised U (e.g., Abdelouas et al., 1999; Senko et al., 2002, Elias et al., 2003; Sani et al., 2005; Senko et al., 2005; Wan et al., 2005), data concerning the kinetic reoxidation of bioimmobilised U is not available. Data for more general U(IV) reoxidation exists, but such data appears to

be restricted to the oxidative dissolution of spent fuel (e.g., De Windt et al., 2003) rather than to the reoxidation of bioimmobilised U. The relevance of the available data to the reoxidation of bioimmobilised U is therefore questionable.

Simulations considered microbial presence in the mobile region only, the immobile region only, and both regions. Simulations also considered the presence and absence of the iron-sulfide mineral mackinawite in order to assess the impact such minerals might have on U(IV) oxidation.

As discussed further in Section 8.3, model discretisation was an issue in these simulations. Unless otherwise stated, the discretisation used is the simulations in this chapter is $\Delta x = 0.5$ m and $\Delta t = 0.05$ yr.

8.3. Simulation results

Figure 8.1 presents the spatial uraninite concentration in the mobile region at different times for a system with bioactivity in both regions. All times presented are after OC injection has ceased (i.e., > 1.5 years); the domain is therefore experiencing inflowing oxic water. As oxic water enters the domain, uraninite is progressively oxidised and dissolved, and the reductive front moves downgradient. It is also worth noting that the uraninite concentration at the front soon begins to spike. Figure 8.2 presents the spatial U(VI) concentration in this system. The U(VI) concentration profiles reflect the redox zonation with U(VI) present in the oxidised region of the domain. The inflowing U(VI)

concentration of 1 μM can be seen to progressively permeate the domain. Some of the U(VI) entering the domain is abiotically reduced by reduced species. However, the net system effect is that of oxidation. Significantly, oxidised uraninite dissolves at the oxidative front and consequently increases well above that of the influent U(VI) concentration creating a U(VI) concentration spike at the redox front. This U(VI) concentration spiking behaviour should be of serious concern in remediated sites, as it may result in downgradient U(VI) concentrations even higher than prior to bioimmobilisation.

It should be noted that the magnitude of the uraninite and U(V) spikes was observed to vary depending on simulation discretisation. Attempts to refine the mesh in order to negate these instabilities (at, or finer than, Δx = 0.25 m, Δt = 0.025 yr) resulted in numerical convergence problems which caused the code to crash. Reducing the convergence tolerance for the element mole-balance equations by up to 4 orders of magnitude did not alleviate this problem. This does not invalidate the observations made above, since the qualitative observation of spiking behaviour occurs irrespective of the discretisation. However, as uncertainty remains over the exact magnitude of the concentration spikes, it is not possible to compare the magnitude of the spike under different scenarios.

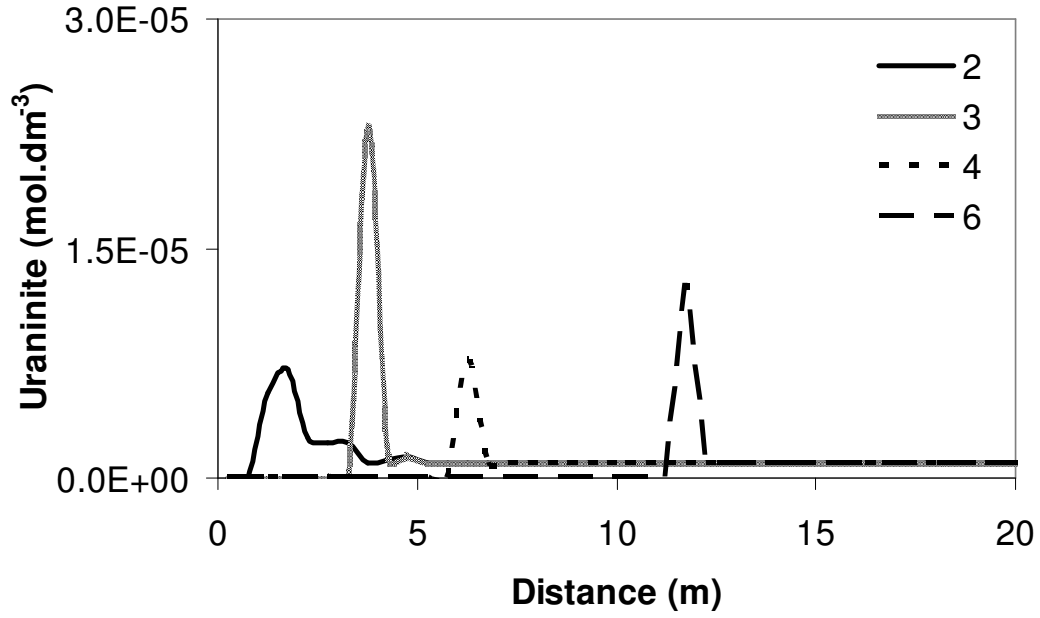

Figure 8.1. Spatial uraninite distribution in the mobile region at *t* = X years for system with both regions bioactive.

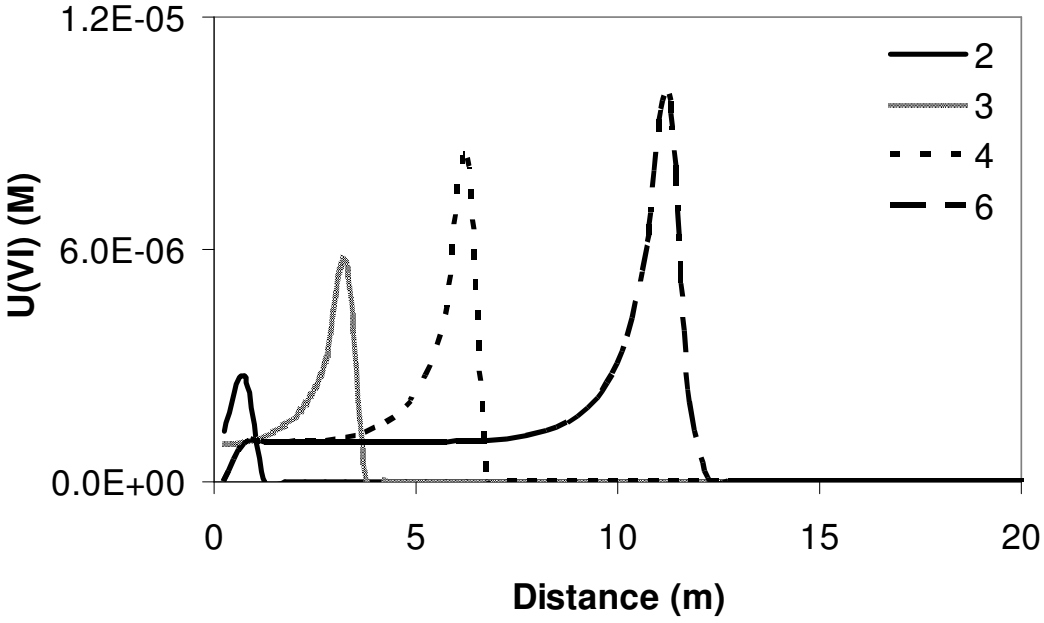

Figure 8.2. Spatial U(VI) distribution in the mobile region at *t* = X years for system with both regions bioactive.

Systems lacking, or with minimised, iron-sulfide mineral presence are likely to be more prone to this effect. This is because such minerals protect the reduced U in the domain (Abdelouas et al., 1999; Senko et al., 2005). Figures 8.3 and 8.4 present the same system as presented in Figures 8.1 and 8.2, except that the iron-sulfide mineral mackinawite is neither formed nor initially present. The uraninite front is observed to move downgradient more rapidly (Figure 8.3) relative to the system with mackinawite present (Figure 8.1), and the U(VI) concentration profiles follow this pattern with even higher U(VI) concentration spikes (Figure 8.4). This behaviour was found to occur regardless of which region(s) is (are) bioactive. Figures 8.5 and 8.6 compare simulations with and without mackinawite for systems with bioactivity restricted to the mobile region only and the immobile region only, respectively.

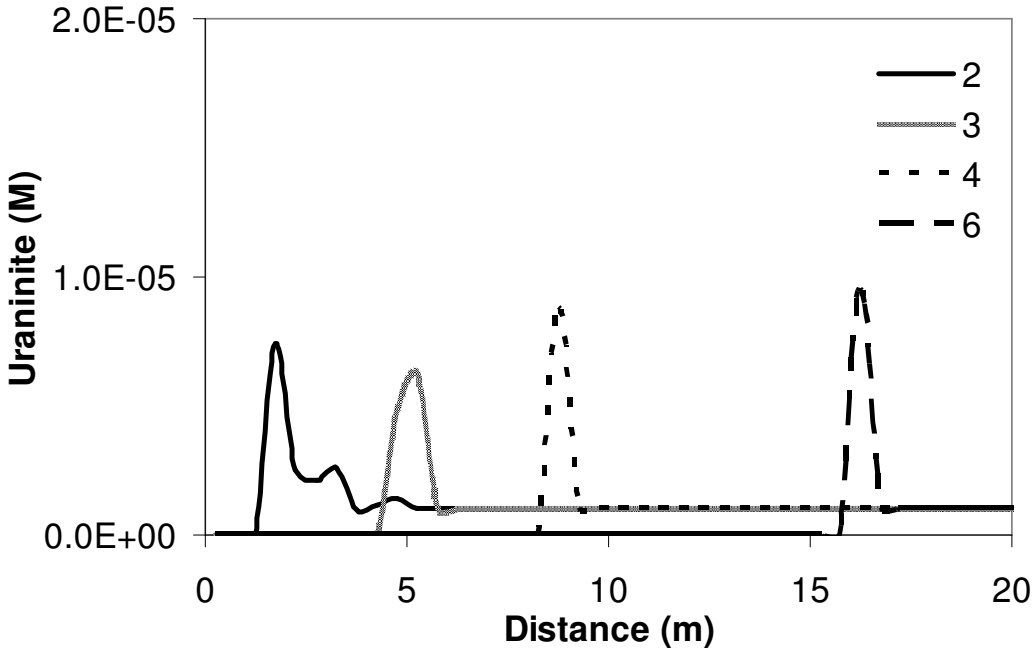

Figure 8.3. Spatial uraninite distribution in the mobile region at *t* = X years for system with both regions bioactive and without mackinawite.

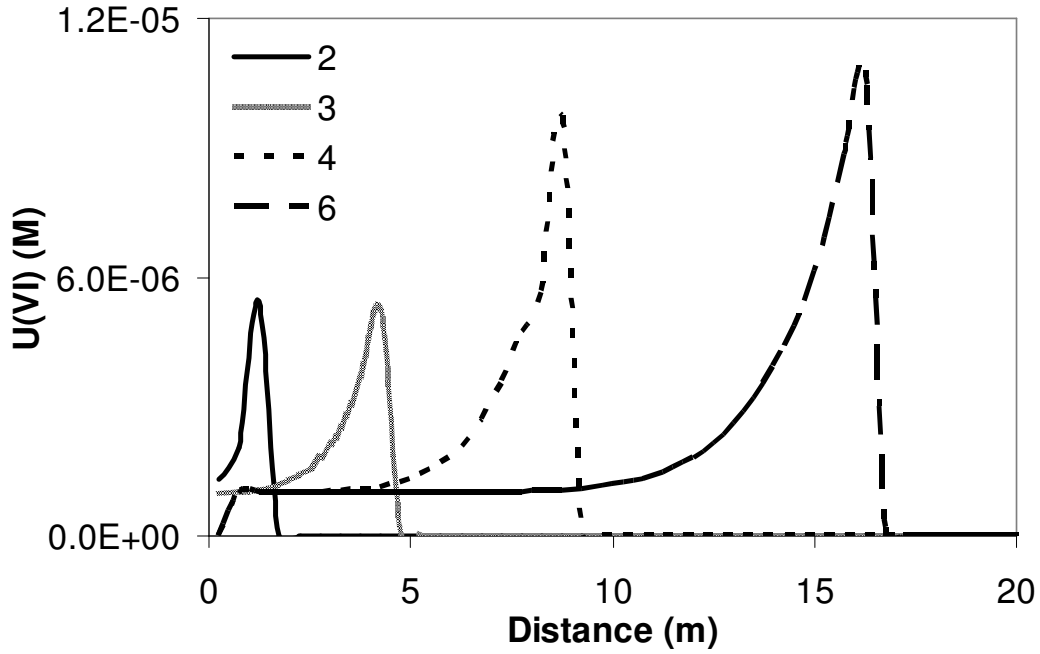

Figure 8.4. Spatial U(VI) distribution in the mobile region at *t* = X years for system with both regions bioactive and without mackinawite.

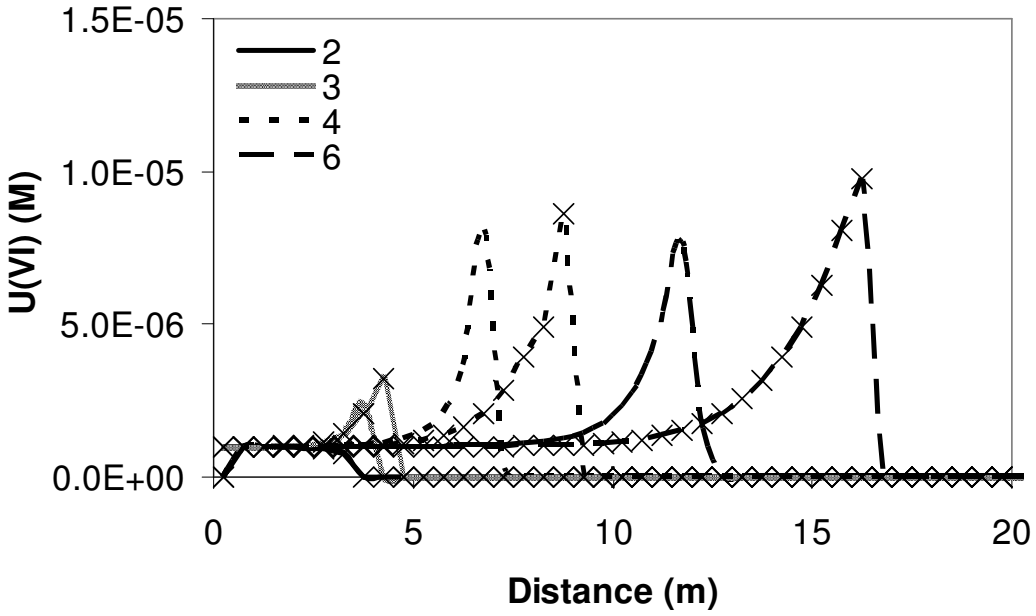

Figure 8.5. Spatial U(VI) distribution in the mobile region at *t* = X years for system with bioactivity in the mobile region only: comparison of system with mackinawite (no crosses) to that without mackinawite (crosses).

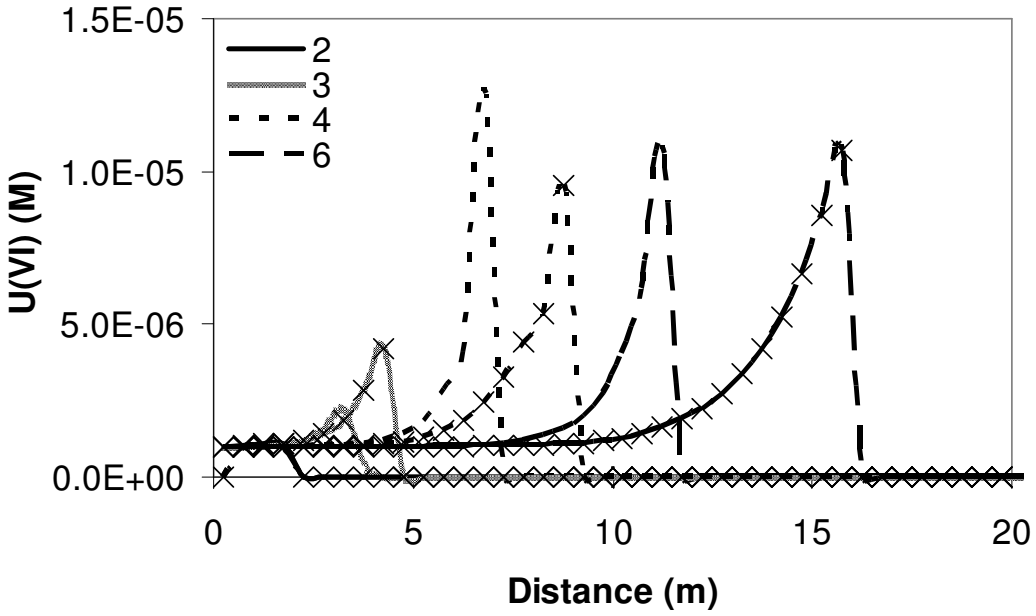

Figure 8.6. Spatial U(VI) distribution in the mobile region at *t* = X years for system with bioactivity in the immobile region only: comparison of system with mackinawite (no crosses) to that without mackinawite (crosses).

In order to compare the progressive reoxidation of U(IV) in systems with and without mackinawite, the following metric is used to represent the total uraninite in the domain:

$$F = \int_{0\text{ m}}^{40\text{ m}} [\text{Uraninite}]dx \tag{8.1}$$

Figure 8.7 displays *F* for the mobile region against time for the scenario in which bioactivity is present in both regions. Data for both with and without mackinawite are presented. The value of *F* for the mobile region is observed to oscillate significantly with time. This is due to numerical instability within the model. Note that these oscillations tend to be more drastic in the simulation with mackinawite present. It is likely that the highly nonlinear geochemical processes in this model exaggerate the chemical

sensitivity of the system to the presence of an additional mineral (i.e. mackinawite). The model discretisation for this simulation is Δx = 0.5 m and Δt = 0.05 yr. Mesh refinement to Δx = 0.3 m and Δt = 0.03 yr yielded the result presented in Figure 8.8. (Note the range on the axes in Figures 8.7 and 8.8 are comparable, but do not begin at zero.) The finer discretisation yields slightly different results, however the general trends remain the same. These results nevertheless demonstrate that while the specific quantitative stability of these results is uncertain, qualitative insight may still be gleaned from them. As a consequence of the numerical instability, an 8-point moving average of the data is used in the figures. This gives an average approximation to the data in general, allowing system trends to be highlighted.

Further simulations at yet finer discretisations of Δx = 0.25 m and Δt = 0.025 yr and Δx = 0.1 m and Δt = 0.01 yr were conducted for bioactivity in only the mobile region and with mackinawite present. The results of the simulations conducted at these discretisations are presented Figure 8.9, and may be compared to the similar results (for a discretisation of Δx = 0.5 m and Δt = 0.05 yr) presented in Figure 8.11. The amplitude of each oscillation was measured, as shown in the figure, for each discretisation simulation. The sum of all oscillation amplitudes in the range was then averaged for each discretisation simulation and the two averages compared. The finer (Δx = 0.1 m and Δt = 0.01 yr) discretisation yielded a 19% reduction in oscillation amplitude compared to the coarser (Δx = 0.25 m and Δt = 0.025 yr) discretisation. This suggests that the oscillations reduce at finer simulation discretisations, and that numerical stability could be maintained if the

discretisation was small enough. Unfortunately, simulations at finer discretisations exhibit prohibitively long run times and are therefore not presented here. Future modelling might utilise other codes, for example PHAST (Parkhurst et al., 2004) in which the cell size and time step are not coupled and a Crank-Nicholson scheme (centered in both time and space) is likely to further minimise numerical dispersion. The parallel version of PHAST can make use of multiple processors, allowing computational times to be reduced significantly.

Figure 8.7 shows that, on average, the system with mackinawite present tends to retain higher quantities of uraninite in the mobile region compared with the system without mackinawite. This further confirms the ability for iron-sulfide minerals to help protect uraninite against oxidation. In addition to Figure 8.7, Figures 8.10 and 8.11 present the same simulations except with the immobile region-only and the mobile region-only bioactive, respectively. Note that the uraninite content in the region immediately after OC injection ceases (1.5 years) may not be the same in each of the different bioresidency scenarios (as shown in Chapter 7). To aid comparison of the different systems, the vertical axes on Figures 8.7-8.11 (excluding Figure 8.9) have been adjusted such that they possess different range values, but that the total range over the axis is the same in each (4×10^{-5} mol.dm^{-2}). The variation in the magnitude of F in each figure is therefore comparable to the other figures.

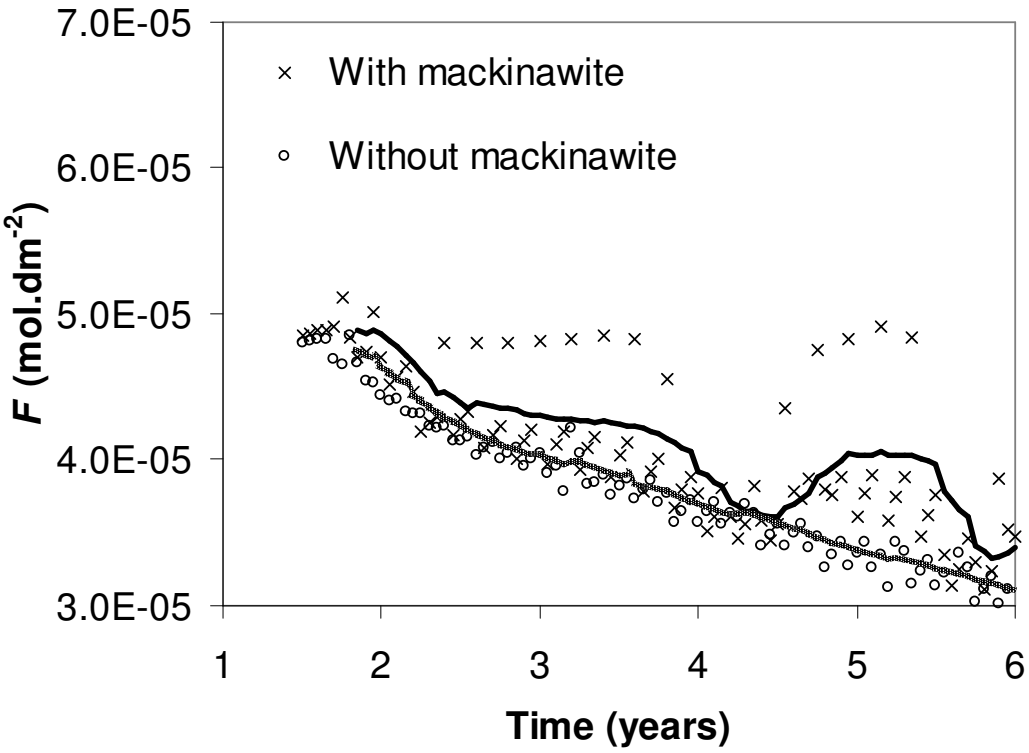

Figure 8.7. Total uraninite, *F*, in mobile region for systems with and without mackinawite. Both regions bioactive, with discretisation Δx = 0.5 m and Δt = 0.05 yr. (Solid dark line – 8-point moving average for with mackinawite data, solid pale line – 8-point moving average for without mackinawite data.)

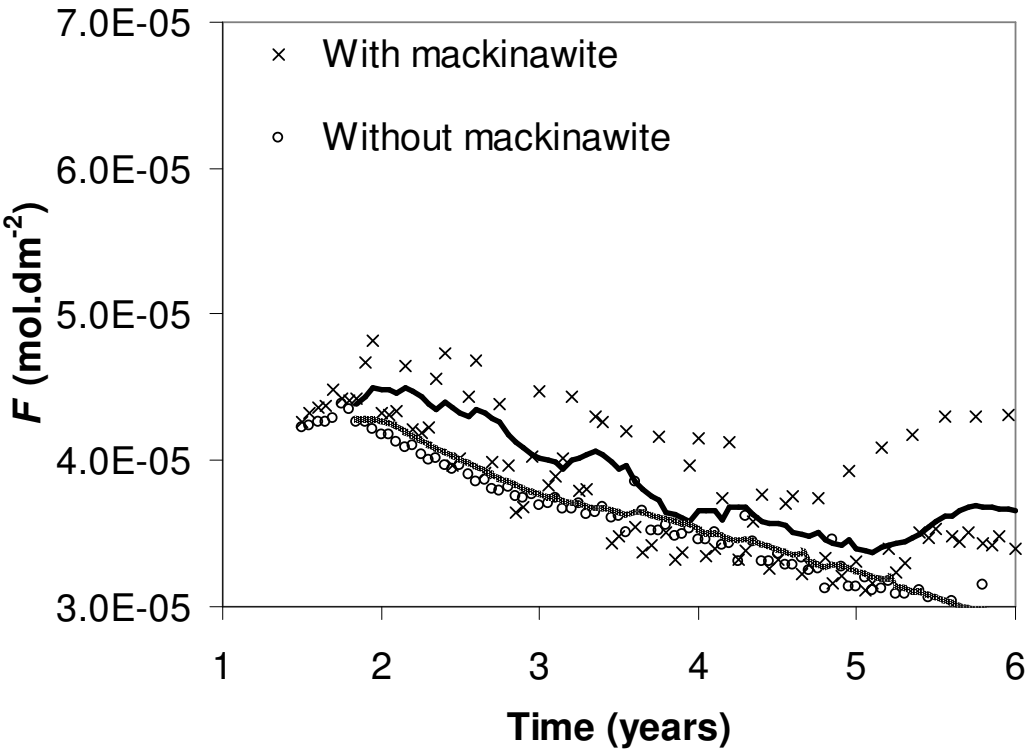

Figure 8.8. Total uraninite, *F*, in mobile region for systems with and without mackinawite. Both regions bioactive, with discretisation Δx = 0.3 m and Δt = 0.03 yr. (Solid dark line – 8-point moving average for with mackinawite data, solid pale line – 8-point moving average for without mackinawite data.)

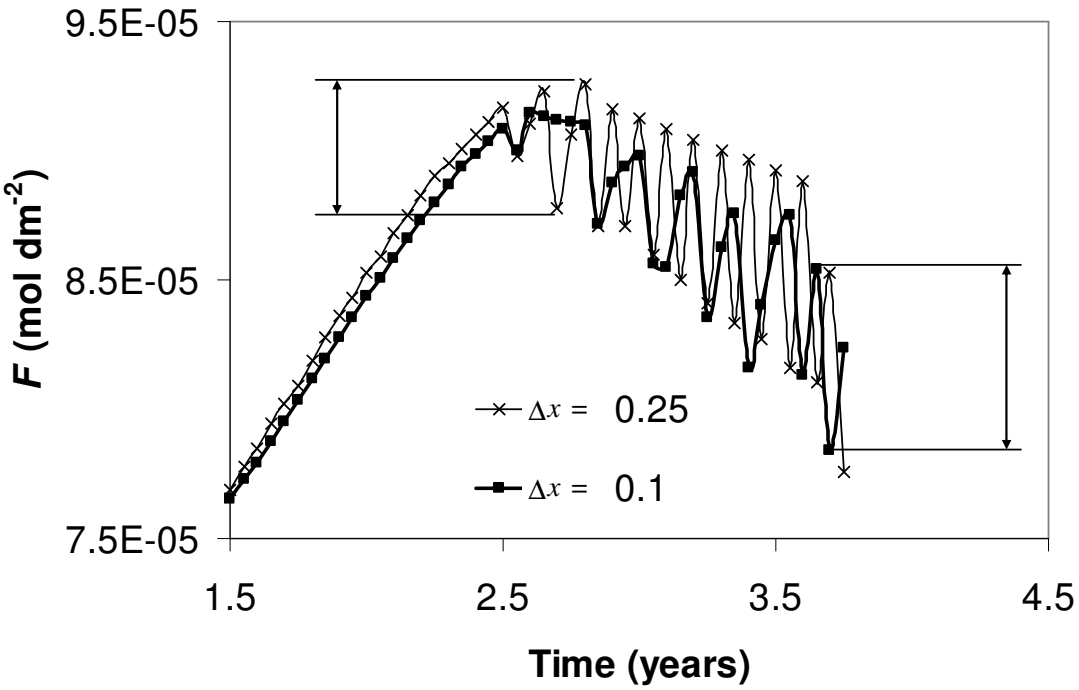

Figure 8.9. Total uraninite, *F*, in mobile region for system with mackinawite and the mobile region only bioactive. Two different discretisations are presented.

In all three bioresidency scenarios the system with mackinawite present tends to retain uraninite more efficiently. This supports the existing experimental evidence (Abdelouas et al., 1999; Senko et al., 2005) suggesting that iron-sulfide mineral presence will help protect uraninite against reoxidation independent of the spatial microbial distribution or the spatial uraninite distribution. When bioactivity is restricted to the immobile region only (Figure 8.10), the system with mackinawite generally maintains a higher uraninite concentration. However, relative to the system with bioactivity in both regions (Figure 8.7) and the system with bioactivity in the mobile region only (Figure 8.10), the total uraninite content remains fairly stable. Uraninite mineral loss is both most significant and most rapid (cf. gradient of slopes) in the system in which bioactivity is restricted to

the mobile region only (Figure 8.11). It is also the system in which mackinawite presence (or absence) impacts uraninite stability most significantly. Interestingly, the uraninite content in this system is also observed to initially increase after cessation of OC injection.

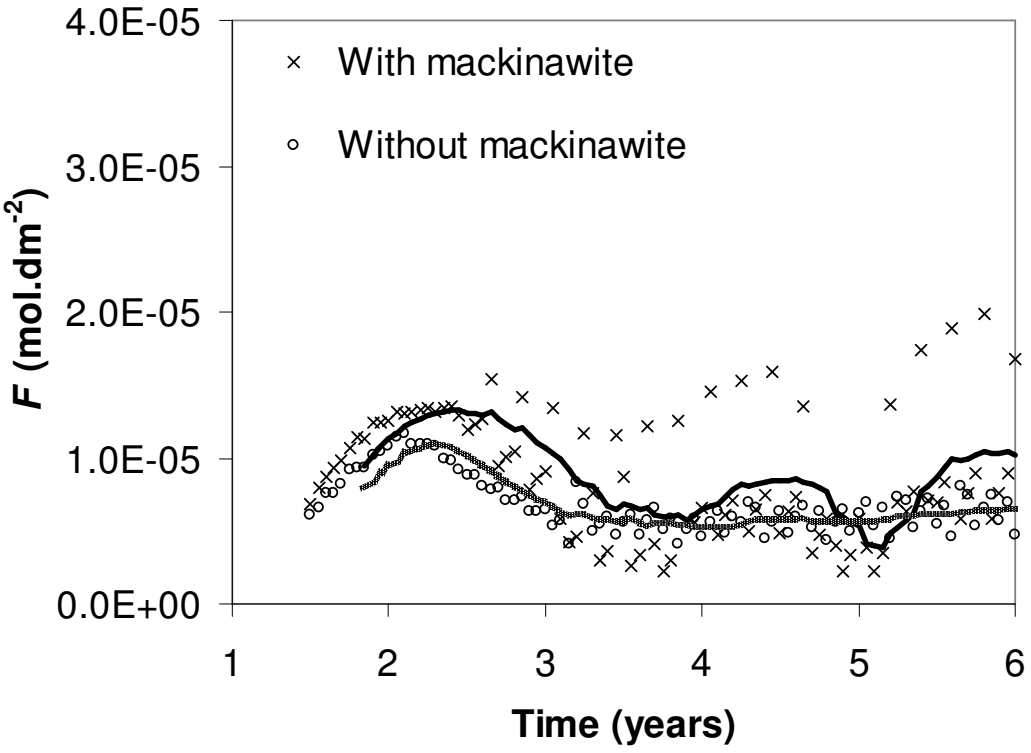

Figure 8.10. Total uraninite, *F*, in mobile region for systems with and without mackinawite. Immobile region only bioactive. (Solid dark line – 8-point moving average for with mackinawite data, solid pale line – 8-point moving average for without mackinawite data.)

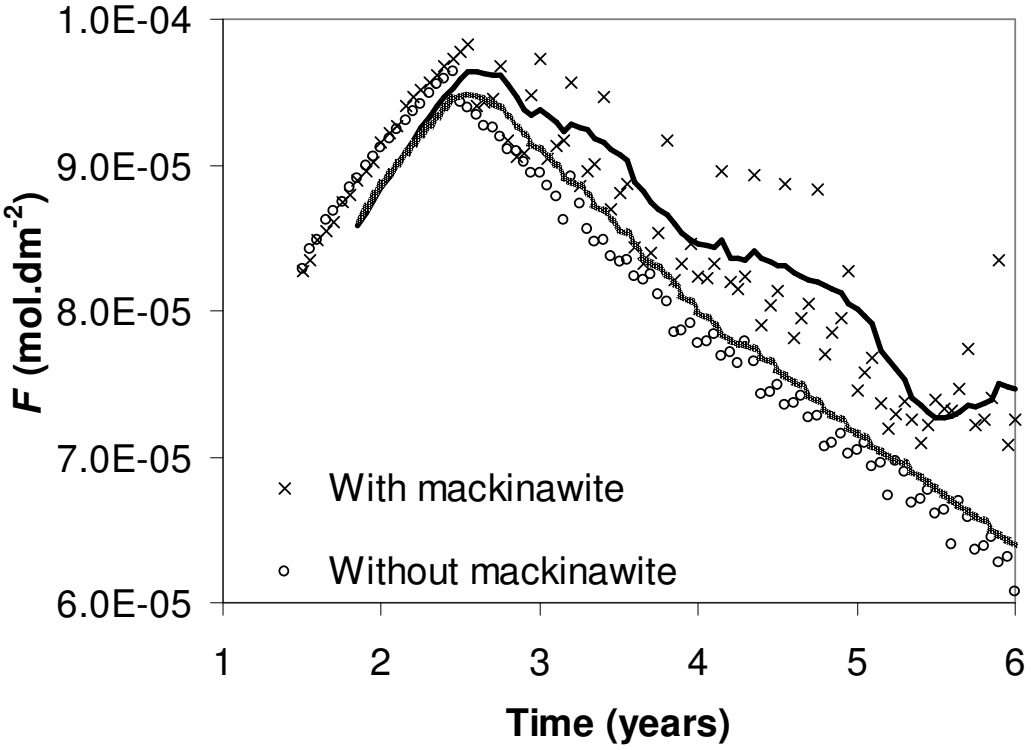

Figure 8.11. Total uraninite, *F*, in mobile region for systems with and without mackinawite. Mobile region only bioactive. (Solid dark line – 8-point moving average for with mackinawite data, solid pale line – 8-point moving average for without mackinawite data.)

Figures 8.12-8.14 show the total uraninite content in the immobile region for the system with bioactivity in (i) both regions, (ii) the immobile region only and (iii) mobile region only, respectively. (Again note that the vertical axes on these figures may possess different range values, but that the total range over the axis is the same in each (4×10^{-5} mol.dm^{-2}), allowing a visual comparison to be made in magnitudes.) As in the mobile region, the system with bioactivity in both regions (Figure 8.12) experiences significant uraninite loss and the impact of mackinawite presence on the system is significant. With bioactivity in the immobile region (Figure 8.13), the immobile region exhibits similar

behaviour to the mobile region with bioactivity in the mobile region. That is, the region with bioactivity will display a high uraninite content after biostimulation (as shown in Chapter 7), but this uraninite will be lost more rapidly than the region in which microbes are not active. Figure 8.14, which presents uraninite content for the immobile region in a system with a bioactive mobile region only, therefore displays a low uraninite content relative to other systems (as shown in Chapter 7), but this uraninite remains relatively stable during reoxidation of the domain.

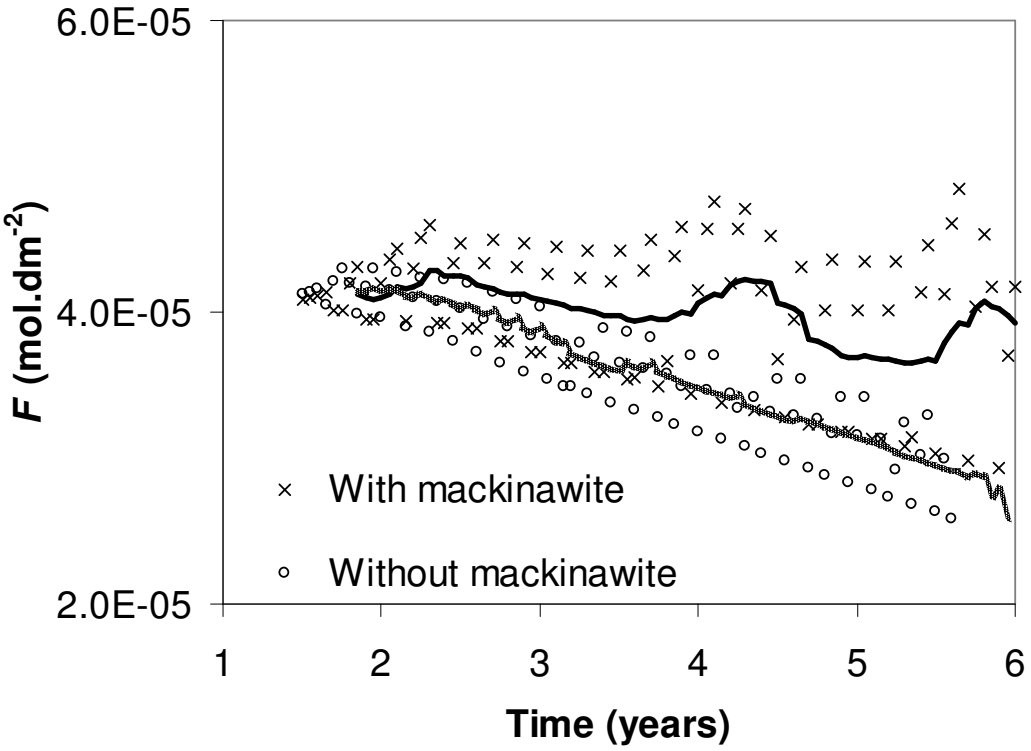

Figure 8.12. Total uraninite, *F*, in immobile region for systems with and without mackinawite. Both regions bioactive. (Solid dark line – 8-point moving average for with mackinawite data, solid pale line – 8-point moving average for without mackinawite data.)

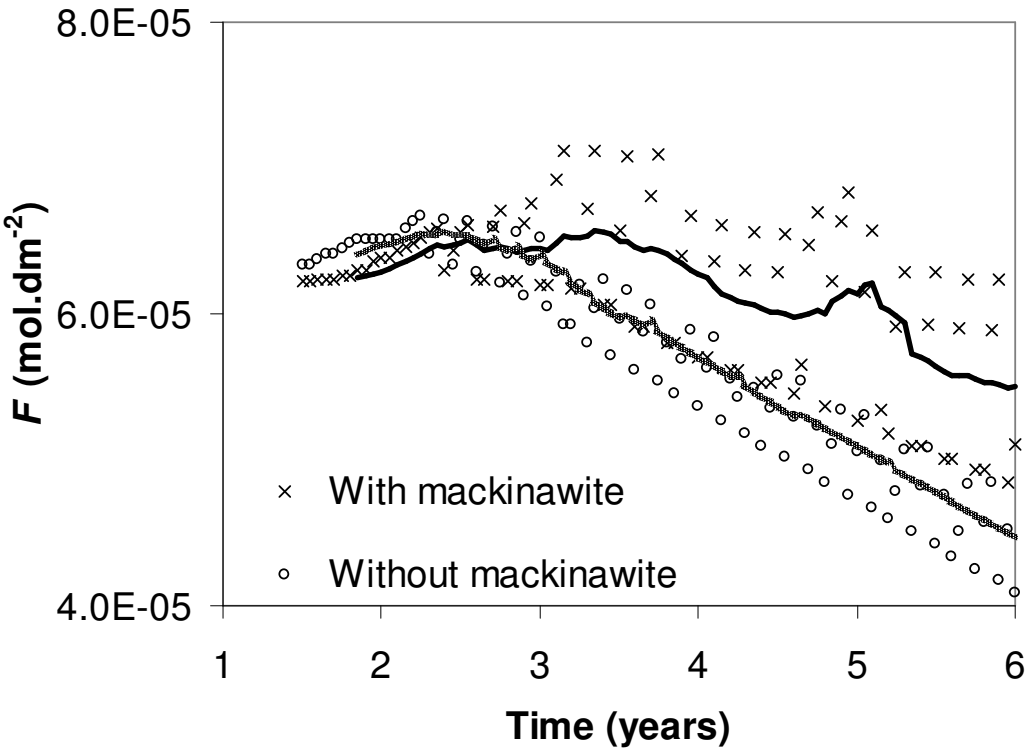

Figure 8.13. Total uraninite, *F*, in immobile region for systems with and without mackinawite. Immobile region only bioactive. (Solid dark line – 8-point moving average for with mackinawite data, solid pale line – 8-point moving average for without mackinawite data.)

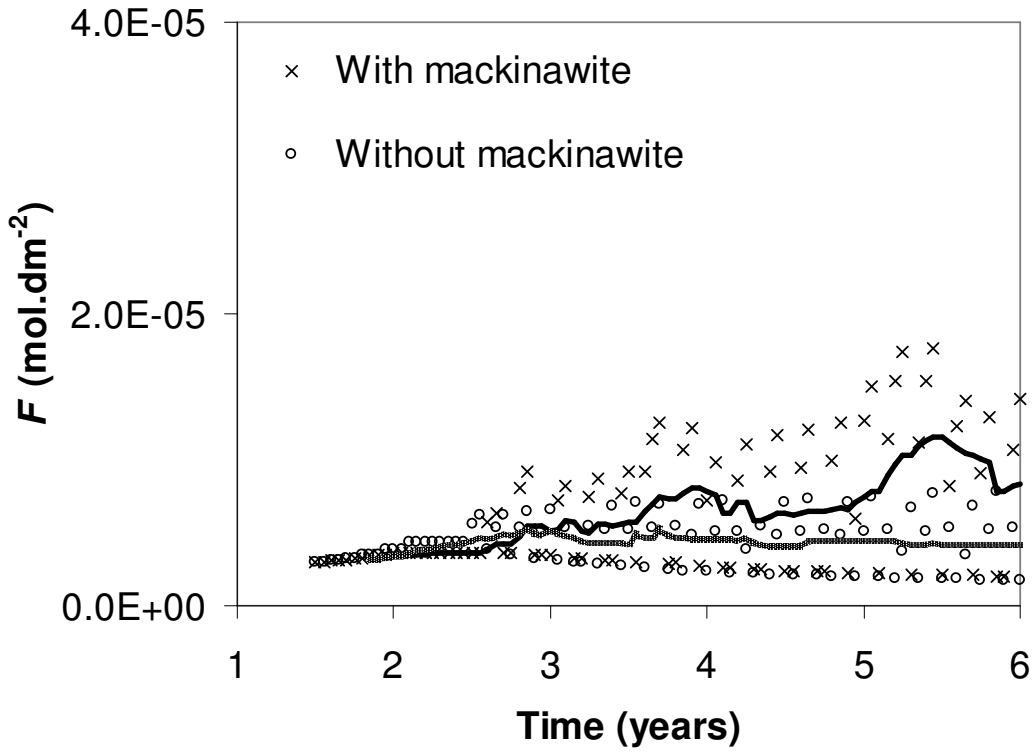

Figure 8.14. Total uraninite, *F*, in immobile region for systems with and without mackinawite. Mobile region only bioactive. (Solid dark line – 8-point moving average for with mackinawite data, solid pale line – 8-point moving average for without mackinawite data.)

The uraninite content, *F*, of the mobile and immobile regions were added together to give insight into the trends occurring within the entire domain for the three different bioresidency scenarios. These results are presented in Figures 8.15-8.17. When bioactivity is restricted to either the mobile region (Figure 8.15) only or the immobile region only (Figure 8.16), the total uraninite content in the domain is observed to initially increase following cessation of OC injection, but soon begins to oxidise and reduce following this. Significantly, all systems experience a similar loss of uraninite. This suggests that the active microbial distribution under biostimulation is unlikely to

affect the system's resistance to any later uraninite oxidation. Furthermore, all bioresidency scenarios show a similar difference between systems with and without mackinawite. Thus, the results suggest that the protection offered by mackinawite is the same in each of the different bioresidency scenarios, and no particular bioresidency scenario offers greater protection over another. However, it is acknowledged that these results are subject to numerical instability and therefore cannot ultimately be deemed authoritative.

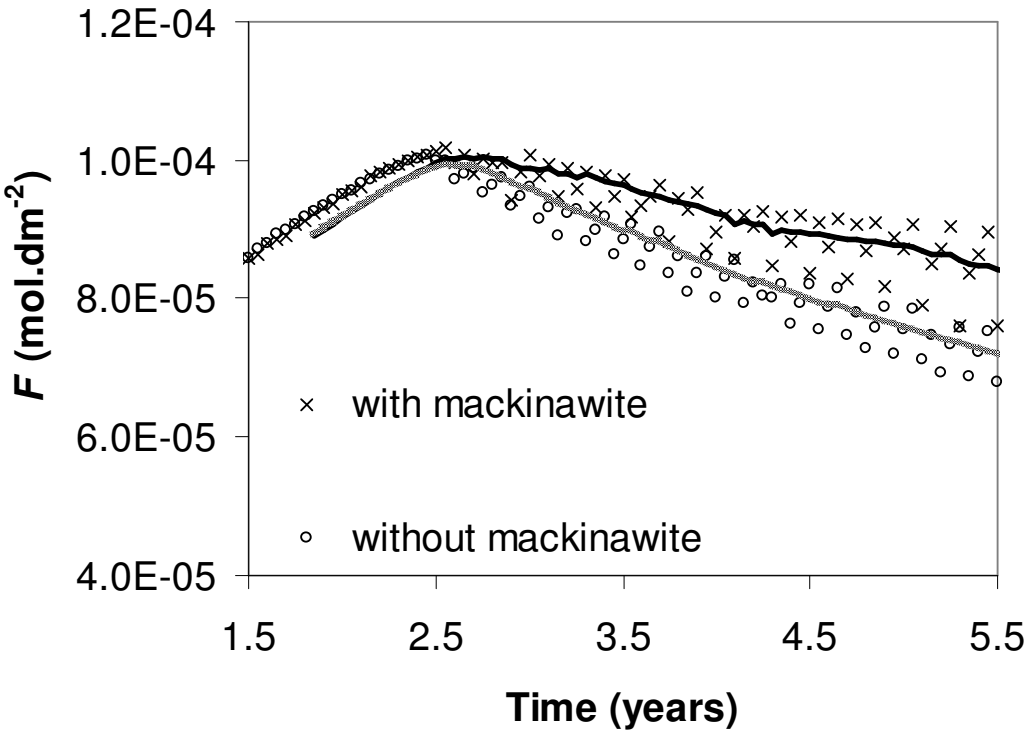

Figure 8.15. Total uraninite in both regions (*F* for mobile + *F* for immobile) for systems with and without mackinawite. Mobile region only bioactive. (Solid dark line – 8-point moving average for with mackinawite data, solid pale line – 8-point moving average for without mackinawite data.)

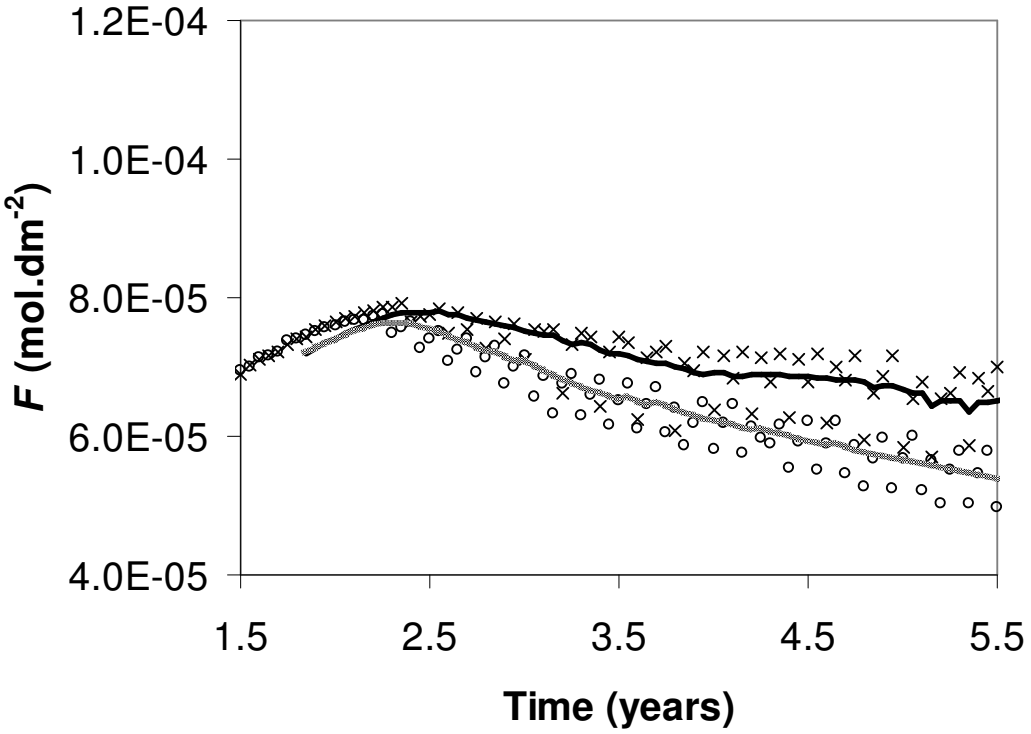

Figure 8.16. Total uraninite in both regions (*F* for mobile + *F* for immobile) for systems with and without mackinawite. Immobile region only bioactive. (Solid dark line – 8-point moving average for with mackinawite data, solid pale line – 8-point moving average for without mackinawite data.)

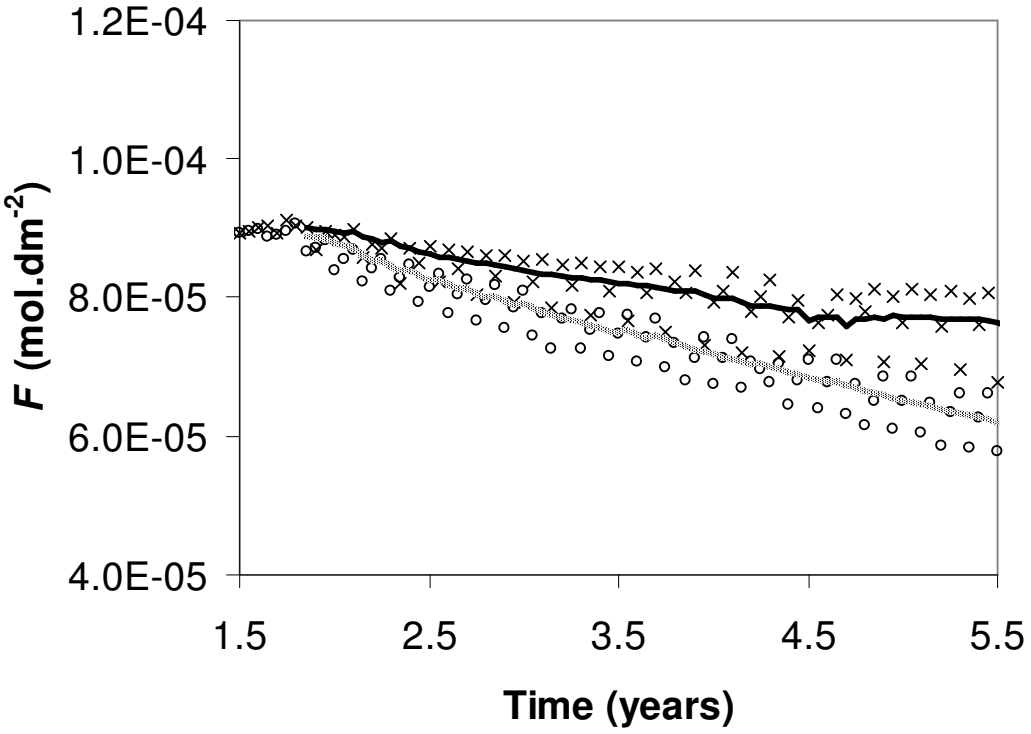

Figure 8.17. Total uraninite in both regions (*F* for mobile + *F* for immobile) for systems with and without mackinawite. Both regions bioactive. (Solid dark line – 8-point moving average for with mackinawite data, solid pale line – 8-point moving average for without mackinawite data.)

8.4. Conclusions

This chapter examined the affects of reoxidation on a previously biostimulated domain. The influence of different bioresidency scenarios and the iron-sulfide mineral mackinawite was explored.

The presence of the iron-sulfide mineral mackinawite was found to offer significant protection against U(IV) oxidation, supporting the existing experimental evidence. In so far as the employed geochemical conditions were representative of real site conditions

(see Section 7.2), these results are considered relevant. However, it is acknowledged that geochemical conditions may vary. The results further suggest that the active microbial distribution in the media is unlikely to affect the system's resistance to U(IV) oxidation. However, it should be noted that this particular conclusion is based upon quantitative analysis that is not definitive due to the absence of numerical stability.

9. Parameter and process significance in mechanistic modelling of cellulose hydrolysis

This chapter illustrates the importance of the biological degradation of cellulose in landfill, and outline the value of modelling of this process. A brief review of the cellulose degradation modelling in the literature will be provided and potential inadequacies in current modelling approaches identified. The chapter will detail the development of a model to overcome the identified inadequacies and explore the validity of the assumptions made in existing models. Model results explore the impact of diffusion biomass transfer on cellulose degradation and show the significance of processes and the assumptions behind them.

9.1. Introduction

Cellulose is a sizeable component of the material deposited into municipal solid waste (MSW) and low level radioactive waste (LLW) disposal sites (BNFL, 2002). It is present in the form of paper, cardboard, wood and fabrics and undergoes enzymatic hydrolysis in situ by microbes in such anaerobic environments, the products of which become substrates for subsequent microbial groups such as methanogen, acetogen and acidogen (El Fadel et al., 1997). These processes could cause changes in a site's geochemical environment. In LLW sites, such changes can affect the solubility of radionuclides which, once mobilized, may then migrate in the groundwater (Humphreys et al., 1997). In addition, the microbial degradation processes result in methane and carbon dioxide gas production, both greenhouse gases (Khalil and Rasmussen, 1989;

Rodhe, 1990). On the other hand, methane can be collected at MSW sites and subsequently used as an energy source (Lay et al., 1999), making desirable both the maximization of gas volume produced and the acceleration of the degradation process itself. Enhanced cellulose hydrolysis leads to more rapid stabilization of the landfill site and a decrease in the leaching of organic acids. The rate of cellulose hydrolysis, and that of the subsequent microbial processes, is therefore important in determining the stability of landfill sites and their potential impact on the environment (Eleazer et al., 1997). Additionally, the anaerobic digestion of the organic fraction of MSW is now a common ex situ treatment for landfill waste/leachate (de Baere, 2000; Mata-Alvarez et al., 2000; O'Keefe and Chynoweth, 2000). The key processes occurring at the microscale in such digesters are identical to those occurring in landfill.

The goal of this work is to evaluate the importance of parameters and processes in the modelling of cellulose degradation. To achieve this, a robust, process-based model of the microbial system at the microscale relevant to cellulose degradation in landfill sites and anaerobic digesters has been developed. Confidence in the model was achieved by comparison to an existing model. This chapter presents the developed model and a sensitivity analysis that investigates the significance of each of the processes commonly used to model cellulose degradation. A number of the novel concepts introduced in this chapter are potentially applicable to microbial degradation of particulate matter in general, and are therefore relevant to waste water treatment applications in addition to MSW and LLW disposal sites; thus, base case simulations are presented for both of

these widely contrasting scenarios. In addition, the developed model is compared with an alternative (simpler) model.

9.2. Process based cellulose degradation model

9.2.1. Existing models

The presence of cellulose-bound cellulolytic bacteria in landfill sites is significant. For example, Lockhart (2004) found numerous cellulolytic clostridia strains in an LLW site and noted that conditions in the site were suitable for a wide diversity of clostridia, and Lockhart et al. (2006) found the highly effective cellulose degrader Neocallimastigales in two landfill sites, one of which contained LLW. The clostridia are well known for their extracellular multi-enzyme complex called cellulosome (Schwarz, 2001) which binds the cells to crystalline cellulose particles (Bayer et al., 1983; Lamed et al., 1987; Mayer et al., 1987). The most common approach to modelling cellulose hydrolyzing bacteria involves approximating the hydrolysis as a zero- or first-order, biomass-independent reaction (e.g., Gusakov and Sinitsyn, 1985; Humphreys et al., 1997; Bezerra and Dias, 2004). A number of assumptions are made in using this approach and these may result in an inadequate representation of reality. First, this approach ignores the impact of the growth of bacteria on the hydrolysis reaction itself. Second, it assumes that both the cellulose particles and the biomass responsible for producing hydrolysis enzymes are available in excess for immediate and spontaneous contact with each other (note that the term ‘particle’ is used to refer to cellulose, while the terms ‘cell’ or ‘biomass’ are used for microbes). This may represent an oversimplification, since (1)

biomass might not have direct access to cellulose particles and (2) biomass/enzyme-cellulose binding is essential for the microbially mediated cellulose hydrolysis process to proceed (Schwarz, 2001; Lynd et al., 2002).

Subsequently, models have explored methods for incorporating the effects of biomass-substrate binding in the cellulose hydrolysis process. Nopharatana et al. (2003) developed a model which recognized the association between biomass and hydrolysis rate. Lai et al. (2005) presented a model in which biomass grew until it approached a limiting value at which substrate coverage was reached. However, the approach used in both of these models neglects the size of the cellulose particles and of the biomass and neglects the spatial separation between them. In systems of low substrate and/or low biomass loading (e.g., landfill or subsurface environments), it is hypothesized that this spatial separation may be large enough to slow hydrolysis significantly. The validity of neglecting such effects has not previously been investigated.

Vavilin et al. (1996) developed a model that incorporated colonisation of cellulose particles by a pre-existing cellulose-bound bacterial population, with the associated progressive reduction in particle size as the cellulose hydrolyzed. However, the model did not distinguish between a cellulose-bound bacterial population and a free-floating (hereon referred to simply as free) bacterial population. Instead, it assumes that the pre-existing cellulose-bound biomass population is solely responsible for particle colonisation. Whilst the authors acknowledge that biomass can slough off into solution, the possibility for free bacteria to colonise cellulose by attachment through contact in

solution was disregarded, and the reattachment process was not modeled explicitly. It is hypothesized that these processes may be significant when biomass is either transported into the system from elsewhere, or is injected into the system as part of an enhanced remediation/treatment strategy.

Other models have investigated the hydrolysis process on an enzymatic level (e.g., Movagarnejad et al., 2000; Gan et al., 2003; Movagarnejad et al., 2003), considering the binding mechanisms of enzymes to the cellulose substrate. However, models working solely at this scale do not explicitly account for the bacterial enzyme source (i.e., biomass) involved in this process.

Here the simplifying assumptions of existing models noted above are addressed by considering that free bacteria can colonise particles by attachment in solution and the hydrolyzing biomass population is that which is substrate-bound. The attachment process accounts for the spatial separation of cellulose particles and biomass using a pseudo-probabilistic based diffusion approach. The cellulose-bound biomass is directly linked to the hydrolysis reaction and thereby controls the rate of hydrolysis.

9.2.2. CHAMP model: Conceptual framework

The CHAMP (Cellulose Hydrolysis Accommodating Microbial Processes) model presented in this work is a microscale process-based model relevant to the saturated zone of anaerobic landfill (MSW, LLW) and anaerobic digesters. Hydrolysis is carried out by

acidogenic bacteria, which are additionally responsible for the production of gases and acids. The bacteria exist as two separate populations: the first is bound to cellulose as a biofilm and the second exists as a free population in the surrounding liquid. The bound biomass may colonise any fraction (between 0 and 100%) of the surface of the cellulose particles. These processes are conceptually illustrated in Figure 9.1. Biomass transfer between the two populations can occur by two routes:

(1) Transfer from the free population to the biofilm (i.e., attachment); as detailed in Section 2.3, attachment depends on both the average spatial separation and the probable contact between cellulose particles and free biomass cells. The movement of cells and particles follows Brownian diffusion and the bacteria are assumed to be non-motile;

(2) Transfer from the biofilm to the free-floating population (i.e., sloughing) due to (i) the growth of excess acidogens on fully covered particles, and (ii) the cellulose particles reducing in size as they hydrolyze.

The free-floating population does not grow, following the assumption that the glucose that the acidogenic population requires for growth is monopolized by the bound cells and that no other glucose sources are available. In this, it is reasoned that the hydrolyzing bacterial population would not waste energy (enzyme production) in obtaining food (glucose) which they would subsequently fail to consume. As the focus of this work is on the cellulose hydrolysis process itself, the model does not consider the presence of acetogenic or methanogenic populations. It should be noted that pH souring

and H_2 accumulation are considered to be negligible in the modeled system and consequently, their impact on cellulose hydrolysis inhibition is not considered. However, it is recognised that systems in which cellulose hydrolysis rates are altered by acetogenic- and methanogeic-induced pH changes should consider these populations. In its present form the model could, if need be, include growth on externally added or initially present glucose. As the model does not consider the presence of acetogenic or methanogenic bacterial population, free-floating biomass is entirely represented by acidogenic bacteria. Therefore, the use of non-glucose bacterial substrates is not considered.

Shearing and hydrodynamic sloughing effects on the biofilm are ignored, as their significance in landfill is likely to be low given the low hydrodynamic forces present. In this work, the system is assumed to be fully saturated.

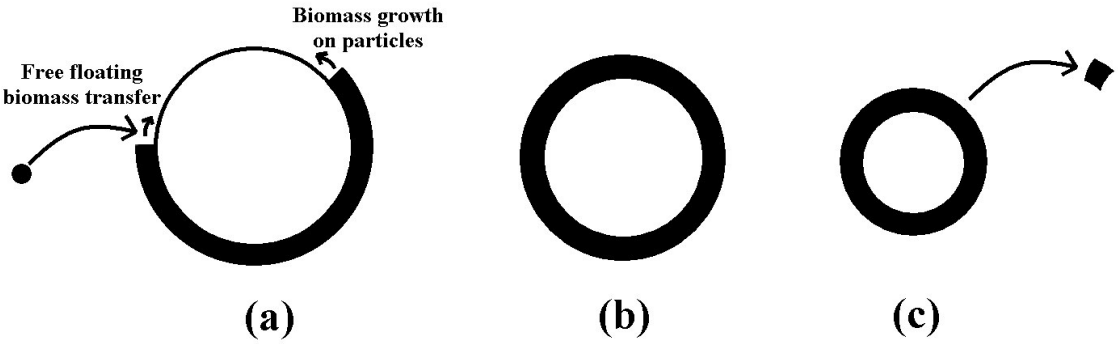

Figure 9.1. Transfer and growth of biomass and associated particle shrinkage. The circles represent cellulose particles which (a) are colonised by biomass (black band surrounding circular particles) from both the free-floating biomass population and the growth of existing particle-bound biomass, (b) have undergone particle shrinkage and are fully colonised and (c) have undergone further particle shrinkage and experience sloughing of bound-biomass into solution.

9.2.3. Model formulation

The model has been developed in PHREEQC (Parkhurst, 1999).

Cellulose is considered to be an anhydroglucose polymer which is hydrolyzed to glucose. While the degree of crystallinity of the cellulose may have an impact on the hydrolysis process (Walker and Wilson, 1991; Ramos et al., 1993), there is a lack of data concerning the role of cellulose crystallinity and it is therefore ignored.

The cellulose hydrolysis process is mathematically modelled according to standard Monod kinetics after Monod (1942, 1949) and McCarty and Mosey (1991):

$$\frac{dC}{dt} = -\frac{V_b C X_b}{K_b + C} \tag{9.1}$$

where C is the concentration of cellulose (see Notation for units used in this work; M denotes units of mass), V_b is a maximum substrate utilization rate, X_b is the concentration of cellulose-bound acidogens, K_b is a half-saturation constant and t is time. By assuming K_b to be small, the growth of biofilm on the cellulose surface is dependent only on X_b until the surface is fully colonised. Thus, in keeping with standard practise for solid substrates (Pavlostathis and Gomez, 1991), the degradation rate of cellulose is essentially first-order with respect to the cellulose, since the population of X_b is itself dependent on the quantity of cellulose present. However, existing models (Vavilin et al., 2001, 2004; Nopharatana et al., 2003) use a Monod kinetics approach and, as the present model is an extension of existing modelling work, the Monod kinetic formulation is used within this work.

The acidogen catabolise the hydrolyzed glucose (indirectly) to produce acetic acid, and hydrogen and carbon dioxide gases. The change in concentration of acidogen-produced acids and gases is given by:

$$\frac{\mathrm{d}R}{\mathrm{d}t} = J(1\text{-}Y_b)\frac{\mathrm{d}C}{\mathrm{d}t} \tag{9.2}$$

where R represents products such as acetic acid, hydrogen and carbon dioxide, J is a stoichiometric coefficient relevant to a respective product, and Y_b is the yield coefficient (i.e. the fraction of substrate consumed in the anabolic reaction).

Table 9.1. Summary of chemical equations.

Process	Stoichiometry	Equation	References
Cellulose hydrolysis	$C_6H_{10}O_5 + H_2O \rightarrow C_6H_{12}O_6$	9.3	Humphreys et al. (1997), Askarieh et al. (2000)
Hydrolyzing glucose acidogen: Catabolism	$3(1-Y_b)C_6H_{12}O_6 + 12(1-Y_b)H_2O \rightarrow 3(1-Y_b)CH_3COOH + 24(1-Y_b)H_2 + 12(1-Y_b)CO_2$	9.4	Humphreys et al. (1997)
Hydrolyzing glucose acidogen: Anabolism	$5Y_bC_6H_{12}O_6 + 6Y_bNH_3 \rightarrow 6Y_bC_5H_7O_2N + 18Y_bH_2O$	9.5	Humphreys et al. (1997), Nopharatana et al. (2003)
Biomass recycle	$279Y_dC_5H_7O_2N + 172Y_dH_2O \rightarrow 20Y_dC_{46}H_{77}O_{17}N_{12} + 155Y_dCO_2 + 39Y_dNH_3$	9.6	Graham et al. (2001), Foree and McCarty (1969)

The stoichiometries of the reactions for biomass growth, cellulose hydrolysis and biomass recycle are given in Table 9.1. Note that equation (9.6) incorporates a fraction, Y_d, of dead acidogen cells that are recycled in the system as protein, carbon dioxide and ammonia. Furthermore, equation (9.6) takes the molar ratio of fixed fatty acids (FFA) to protein in recycled biomass as 2 (Foree and McCarty, 1969). The average number of carbons in the average FFA is taken as 7 as defined by Graham et al. (2003a,b).

Moreover, acetate is assumed to be the predominant acid in the anaerobic digestion system.

Therefore, equations (9.3)-(9.5) therefore may be reduced to:

$$C_6H_{10}O_5 + H_2O + Yb\frac{6}{5}NH_3 \rightarrow C_6H_{12}O_6 \text{ (implicit glucose)} \rightarrow Yb\frac{6}{5}C_5H_7O_2N + 4H_2O$$
$$+ (1\text{-}Yb)CH_3COOH + 8(1\text{-}Yb)H_2 + 4(1\text{-}Yb)CO_2 + \frac{38}{5}YbH_2O \qquad (9.7)$$

Glucose is not explicitly modelled as it is assumed that all glucose produced will be utilized by the bound biomass that produced it. Due to the fact that acetogenic and methanogenic bacteria are not considered in this model, acidic products and H_2 presence may result in souring which may not occur in systems considering the presence of these bacteria. The effect of pH and H_2 concentration on the rate of the hydrolyzing biomass is therefore ignored.

9.2.4. Biomass transfer

Biomass transfer between the free-floating and bound acidogen populations is modelled by first considering the probability of a free-floating acidogen cell coming in contact with a cellulose particle. For this calculation, the characteristic distance between the cellulose particles and the biomass cells must be determined. The particles are considered to diffuse according to Brownian motion. The capabilities of their movement must also be determined.

The number of cellulose particles, N_c, is dependent on the quantity and characteristic size of the cellulose particles. The number of free-floating biomass cells, N_b, is calculated by converting the free-floating biomass concentration, assuming a mass of 10^{-15} g/cell (Elert, 2003).

Assuming a 3D modelling space and a uniform particle distribution, the average distance (A) between one biomass cell and another is:

$$A = \frac{10}{N_b^{1/3}} \tag{9.8}$$

and the average distance (B) between one cellulose particle and another is:

$$B = \frac{10}{N_c^{1/3}} \tag{9.9}$$

where A and B are in centimetres and a one litre unit volume is assumed here (10^{-3} m^3). Note that in 2D modelling space, equations (9.8) and (9.9) would require the cube roots to be replaced with square roots.

The model considers the characteristic distance between the centers of cellulose particles and biomass cells, in meters, to be:

$$s = \frac{\text{minimum } (A, B)}{100} \tag{9.10}$$

Alternatively, the absolute difference between A and B may provide an improved alternative for calculating s.

The diffusion capability of a cellulose particle or biomass cell is calculated using the Stokes-Einstein equation (e.g., Rogak and Flagan, 1992):

$$d = \frac{k_B T_K}{3\pi\mu\phi} \tag{9.11}$$

where k_B is the Boltzmann constant (1.38×10^{-23} m^2 kg s^{-2} K^{-1}), T_K is the temperature (K), μ is the liquid viscosity (8.9×10^{-4} Pa.s at 25°C; temperature is assumed to be constant) and ϕ is either the characteristic diameter of either the cellulose particles or the biomass cells, depending on which respective distance (of A and B) is smaller.

The model does not explicitly consider variations in the diameter of individual particles, but instead employs the average (characteristic) diameter of all the cellulose particles present.

The probability of contact between characteristic free biomass cells and cellulose particles is:

$$P = \text{erfc}\left(\frac{x_s}{\sqrt{4\pi d_1 t}}\right) + 1 - \text{erfc}\left(\frac{x_s - s}{\sqrt{4\pi d_2 t}}\right) \quad (9.12)$$

where d_1 and d_2 are the diffusion capabilities of the biomass cells and the cellulose particles, and t is the model time-step. The derivation of equation (9.12) and the parameter, x_s, are given in Appendix A, Section 1. An approximation is used for the erfc function. Details of the approximation can be found in Appendix A, Section 2. The potential amount of transferable free-floating biomass is equal to P multiplied by the free biomass concentration, X_f.

The transfer rate from the floating cells to the cellulose particles may then be modelled according to the concept of the "sticking efficiency" (α) of the cells. This is defined as the probability of adsorption of a colony forming unit (CFU), once it has been transported (Escher and Characklis, 1990). In this approach, the transfer of free-floating biomass to the cellulose-bound biofilm is calculated as:

$$\frac{dq}{dt} = \alpha P X_f \quad (9.13)$$

where q is the concentration of transferred biomass. Since the "sticking efficiency" is essentially a rate, it may also be termed the diffusive biomass transfer rate. This limits the rate at which biomass is available for transfer in accordance with the expectation that some resistance to binding exists. Indeed, Characklis (1990) suggests from published

data (Fletcher, 1977; Powell and Slater, 1983) that sticking efficiency can range from 83% to 0.6% due to variations in flow conditions and bacteria type.

9.2.5. Cellulose particles

Cellulose particles are modelled as a single group. However, the quantity of cellulose and the characteristic diameter of cellulose particles can be adjusted as parameter input values. The hydrolysis of cellulose and its conversion to glucose results in a corresponding reduction in cellulose particle diameter.

Previous models (e.g., Vavilin et al., 1996) have assumed that cellulose particles take a spherical shape. However, cellulose is a fibrous solid and recent work suggests that the particles typically have a more cylindrical shape at the microscale (Movagarnejad et al., 2000; Gan et al., 2003; Xiang et al., 2003). In the present work, cellulose particle sizes have been parameterised to data in these microscale studies (see Table 9.3) and therefore represent realistic cellulose particle surface areas. Thus, CHAMP has been developed to allow the particles to either be modelled as spheres or cylinders.

The surface area and volume of the spherical cellulose particles are given by, respectively:

$$Surface\ area = \pi\phi^2 \tag{9.14}$$

$$Volume = \frac{\pi\phi^3}{6} \tag{9.15}$$

while for cylindrical particles the corresponding formulas are:

$$\text{Surface area} = \frac{\pi\phi^2}{2} + \pi\phi L_c \tag{9.16}$$

$$Volume = \frac{\pi\phi^2 L_c}{4} \tag{9.17}$$

where L_c is the cylinder length.

The coverage of the cellulose particles by the bound acidogen population is limited. The maximum number of moles of biomass (per litter of water) on the collective group of spherical cellulose particles is:

$$X_{max} = \frac{\phi^2 \pi N_c \rho_b h}{GFW_b} \tag{9.18}$$

where h is the biofilm thickness, ρ_b is the density of biofilm layer (assumed to be as water) and GFW_b is the gram formula weight of biofilm. Acetogenic and methanogenic organisms are known to thicken the biofilm layer with time (Song et al., 2005). However, it is reasoned here that the bacteria capable of hydrolyzing cellulose are those in immediate contact with the cellulose particles. The effective hydrolyzing biofilm is therefore just one cell thick, and this thickness does not change.

The change in X_{max} in a given time step, derived from equation (9.18), is:

$$\frac{dX_{max}}{dt} = \frac{2\phi\pi N_c \rho_b h}{GFW_b} \frac{d\phi}{dt} \tag{9.19}$$

For cylindrical particles, equations (9.18) and (9.19) are respectively:

$$X_{max} = \frac{\left(\frac{\phi^2}{2} + \phi L\right)\pi N_c \rho_b h}{GFW_b} \tag{9.20}$$

$$\frac{dX_{max}}{dt} = \frac{(\phi + L)\pi N_c \rho_b h}{GFW_b} \frac{d\phi}{dt} \tag{9.21}$$

where L is assumed to be constant. As cellulose is hydrolyzed and converted to glucose, the diameter of the cellulose particles correspondingly reduces.

The number of moles of cellulose (per litre of water), C, can be related to the particle volume of spheres:

$$C = \frac{\pi\phi^3 N_c \rho_c}{6GFW_c} \tag{9.22}$$

where ρ_c is the cellulose particle density and GFW_c is the gram formula weight of cellulose.

For cylindrical particles, equation (9.22) is instead:

$$C = \frac{\pi\phi^2 L N_c \rho_c}{4GFW_c} \tag{9.23}$$

The calculation of the bound acidogen population, X_b, involves components for growth, decay and biomass transfer. Step function terms are incorporated to ensure that the amount transferred is never larger than can be accepted by the cellulose surface, given the limited coverage available (X_{max}). When $X_b > X_{max}$ the excess growth on the cellulose particles detaches from the particles and becomes part of the free-floating biomass population. The rate of change of the bound acidogen population, X_b, is:

$$\frac{dX_b}{dt} = H(X_{max} - X_b)\left(Y_b\frac{dC}{dt} - D_bX_b + \frac{dq}{dt}\right) - H(X_b - X_{max})\frac{dX_{max}}{dt} \qquad (9.24)$$

where H is the Heaviside step function.

The PHREEQC ODE solver had numerical difficulties with this step function and equation (9.24) was therefore further refined to allow a smoother transition than a step (see Appendix A, Section 3). The, H is replaced by W and equation (9.24) becomes:

$$\frac{dX_b}{dt} = W\left(Y_b\frac{dC}{dt} - D_bX_b + \frac{dq}{dt}\right) - (1 - W)\frac{dX_{max}}{dt} \qquad (9.25)$$

9.2.6. Calculation of change in free acidogen population

Calculation of the free acidogen population, X_f, involves both its decay and its transfer (to or from cellulose). The rate of change of the free acidogen population is:

$$\frac{dX_f}{dt} = (1 - W)\left(Y_b\frac{dC}{dt} - D_bX_b + \frac{dq}{dt} + \frac{dX_{max}}{dt}\right) - D_fX_f - \frac{dq}{dt} \quad (9.26)$$

where the same step-function approximation as in equation (9.26) is used.

9.3. Model comparison

9.3.1. Introduction

For model verification, base case simulations were conducted to examine model behaviour and examine the mass balance of system components. Model validation remains challenging since experimental data measuring bacterial colonisation and transfer between biofilms and free populations is not available. Therefore, a comparison study (pseudo-validation) between the presented model and an existing verified model is conducted. These steps are undertaken to build confidence that CHAMP correctly solves the governing equations and adequately simulates the expected outcomes in such systems.

9.3.2. Base case data set

Literature data sets were examined to obtain the expected averages and ranges of model parameters for relevant systems. The majority of studies presenting cellulose degradation rates involve anaerobic digestion rather than landfill sites, with the former often directly measured and the latter typically inferred through the analysis of monitoring data. Overall, landfill waste degradation rates are observed to be significantly lower than those for anaerobic digesters. Table 9.2, summarizing the mean minimum, mean maximum and mean average values for documented substrate degradation rates, reveals that the process rate is significantly lower in landfills than in

anaerobic digesters. It is deemed reasonable to consider mean average values to represent these systems for the purposes of this study. In particular, the maximum landfill waste degradation rates are observed to be two orders of magnitude less than the minimum digestion rate.

Table 9.2. Degradation rates for waste in landfill and anaerobic digestion.

Situation	Minimum (s^{-1})	Maximum (s^{-1})	Average (s^{-1})
Landfill[a]	2.2×10^{-11}	2.2×10^{-8}	3.1×10^{-9}
Digestion[b]	3.5×10^{-6}	5.0×10^{-5}	5.6×10^{-6}

[a]Beadle (2002), Young (1989), Hoeks (1983)

[b]Andrews and Pearson (1965), Ghosh and Pohland (1974), Gosh and Poland (1974), Gosh et al. (1975), Hill and Barth (1977), Ghosh and Klass (1978),Gosh and Klass (1978), Russell and Baldwin (1979), Sinechal et al. (1979), Ghosh et al. (1980), Eastman and Ferguson (1981), Zoetmeyer et al. (1982a, b), Gujer and Zehnder (1983), Huang (1983), Lee and Donaldson (1984), Moletta et al. (1986), Llabres-Leungo et al. (1987), Denac et al. (1988), Dinopoulou et al. (1988), Pavlostathis et al. (1988), Lynd et al. (1989), Jones et al. (1992), Owens and Chynoweth (1993).

The likely reasons for the significantly higher rates in digesters include:

(i) Digesters are typically run at higher temperatures than those in landfills,

(ii) Digesters typically possess high nutrient loadings, in contrast to (possibly) nutrient-limited landfills,

(iii) Sections of landfill are often under-saturated, operating at less than 60% moisture content (Chugh et al., 1999), and therefore bacterial action may be limited over large sections of the site.

For these reasons, it is expected that landfills exhibiting saturated, nutrient-rich environments and higher operating temperatures (e.g., engineered systems) would likely be associated with significantly higher rates than those presented here, perhaps approaching those of anaerobic digesters.

Table 9.3 presents a complete set of CHAMP base case parameters that were compiled from the literature. The table footnotes identify references for each value or, in the absence of data, indicate where values were assumed. Table 9.3 outlines both a "fast" base case and a "slow" base case. The fast base case parameters are considered representative for non-limited processes (e.g., a saturated system without nutrient limitation, and operating at a temperature of 20-35°C) while the slow base case parameters are considered representative of limited processes (e.g., a typical, non-engineered landfill). Further sources of parameter values, while not exploited in the present work, may be found in IWA (2002) and IAWPRC (1986).

Table 9.3. Base case parameter set.

Parameter	Base Case	Base Case Value
Initial bound biomass population, X_{bi} (mol/l)[a]	Slow and Fast	1×10^{-8}
Maximum substrate utilization rate, V_b (s^{-1})[b]	Fast	5.6×10^{-6}
	Slow	3.1×10^{-9}
Microbial yield coefficient, Y_b (-)[c]	Slow and Fast	0.34
Bound biomass death rate, D_b (s^{-1})[d]	Fast	3.0×10^{-7}
	Slow	3.0×10^{-12}
Half saturation constant, K_b (mol/l)[e]	Slow and Fast	1×10^{-6}
Initial free biomass population, X_{fi} (mol/l)[f]	Slow and Fast	1×10^{-5}
Free biomass death rate, D_f (s^{-1})[g]	Fast	3.0×10^{-6}
	Slow	3.0×10^{-11}
Fraction of recycled dead biomass cells, Y_d (-)[h]	Slow and Fast	0.8
Biofilm thickness, h (m)[i]	Slow and Fast	1×10^{-6}
Initial cellulose particle diameter, ϕ_i (μm)[j]	Slow and Fast	42
Initial cellulose concentration, C_i (mol/l)[k]	Slow and Fast	2.87
Sticking efficiency, α (-)[l]	Slow and Fast	0.8
$\rho_{cellulose}$ (kg/m^3)[m]	Slow and Fast	1500

[a]Assumed value << X_f

[b]See Table 9.2

[c]Andrews and Pearson (1965), Bauchop and Elsden (1960), Denac et al. (1988), Eastman and Ferguson (1981), Gosh and Klass (1978), Gosh and Poland (1974), Gosh et al. (1975), Hill and Barth (1977), Jones et al. (1992), Lee and Donaldson (1984), Lee et al. (1993), Lynd et al. (1989), Matsumoto et al. (1981), McCarty (1971a,b), Pavlostathis and Gossett (1988), Speece and McCarty (1964), Vavilin et al. (1995), Yaguchi (1982), Young and McCarty (1967), Zoetmeyer et al. (1982a)

[d]Andrews and Pearson (1965), Bauchop and Elsden (1960), Costello et al. (1991), Denac et al. (1988), Dinopoulou et al. (1988), Eastman and Ferguson (1981), El-fadel et al. (1989), Gosh and Poland (1974), Gosh et al. (1975), Hill and Barth (1977), Lee and Donaldson (1984), Lee et al. (1993), Matsumoto et al. (1981), Pavlostathis and Gossett (1988), Pavlostathis et al. (1988), Speece and McCarty (1964), Yaguchi (1982)

[e]Assumed

[f]Cahan (2005) found viable biomass populations of 1×10^{-5} to 4×10^{-5} mol biomass per gram of dry waste on LLW waste simulants. Assuming cells are 90% water and a dry waste density of 687 kg/m^3 this equates to concentrations of 7.35×10^{-3} to 2.46×10^{-2} mol/l of biomass. BNFL (2002) reported biomass concentrations of 6.13×10^2 and 8.38×10^2 g/m^3 in simulations. Additionally assuming a cell weight of 1×10^{-15} g/cell, this equates to a concentration of 1.49×10^{-5} mol/l. This data is in agreement with concentrations observed on landfill material by Palmisano et al. (1993), who found maximum concentrations around 6.03×10^{-5} mol/l

[g]Assumed as one order of magnitude greater than D_b

[h]Foree and McCarty (1969) found that the anaerobic degradation of algal biomass 20% COD and 18% VSS remaining after a 613 d period. An average of 19% therefore remained, giving a degradable fraction of 80%. Algal biomass is used as an analogue of acidogen biomass and the percentage of biomass recycled is taken as 80%

[i]Assumed to be one cell thick

[j]Gan et al. (2003), Movagarnejad et al. (2000), Xiang et al. (2003)

[k]Waste has density 1500 kg/m^3 and is 31%/weight cellulose (BNFL, 2002) which yields 465 kg/m^3 cellulose which is 2.87 mol/l cellulose

[l]Characklis (1990), Powell and Slater (1983), Fletcher (1977), Tong et al. (2005)

[m]Assumed

Literature observations of death rates for bacteria and biomass yield are largely absent, especially for those bacteria associated with landfill sites. Therefore, Table 9.3 includes

values based on a wide range of studies. However, these data are expected to be relevant to landfill applications since their values do not vary significantly; for example, biomass yield is not significantly influenced by culture age, substrate chemical form, or initial concentration (Panikov, 1995).

9.3.3. Base case results

The two base case simulations demonstrate the key process interactions of the developed model. Figures 9.2 and 9.3 show model results for the fast base case. Figure 9.2 presents the free and the cellulose-bound biomass (biofilm) populations and the biomass transfer rate between these two populations. Note that the transfer rate is positive when transfer occurs from X_f to X_b, and negative when transfer occurs from X_b to X_f. Figure 9.3 shows principle geochemical components and cellulose particle diameter. The figures demonstrate that system behaviour changes at the time corresponding to complete cellulose particle coverage. At early time, Figure 9.2 illustrates that the biofilm population (X_b) is observed to grow as colonisation of the cellulose particle takes place. During this phase, net biomass transfer from the free to the bound phase is observed (slightly positive transfer rate value, Figure 9.2) indicating that colonisation of the biofilm is occurring due to the attachment of diffused biomass from the bulk liquid. Simultaneously, the average cellulose particle diameter is decreasing as cellulose degrades (Figure 9.3), reducing the maximum possible coverage ($X_{max,}$ Figure 9.2).

The time at which the particles are completely covered is identified by the convergence of X_b and X_{max} on Figure 9.2. Beyond this time, biomass transfer is observed to reverse in direction (negative transfer rate value, Figure 9.2) and the biofilm population reduces as cellulose particle size continues to decrease. The free biomass population (X_f) is simultaneously observed to grow as biomass sloughs off the biofilm (Figure 9.2). Sloughing continues as the particle size continues to diminish (Figure 9.3). As the cellulose nears complete degradation, the production of carbon dioxide and acetic acid is seen to slow and approach a final value (Figure 9.3).

Figure 9.4 presents model results for the slow base case, revealing that its behaviour is consistent with that of the fast base case. However, note that the slow base case requires on the order of 500 years to achieve complete degradation versus approximately 100 days for the fast base case. The slow base case differs from the fast base case in that all of the free-floating biomass has attached to the cellulose well before full colonisation of the cellulose occurs (figure not shown). Additionally, at approximately t = 444 y, the death rate of the free biomass exceeds its rate of increase due to sloughing, as evidenced by that population's net decrease.

These model results show that the model is operating as expected, in a realistic and consistent manner. Mass balance on cellulose/products and on bacterial populations is maintained.

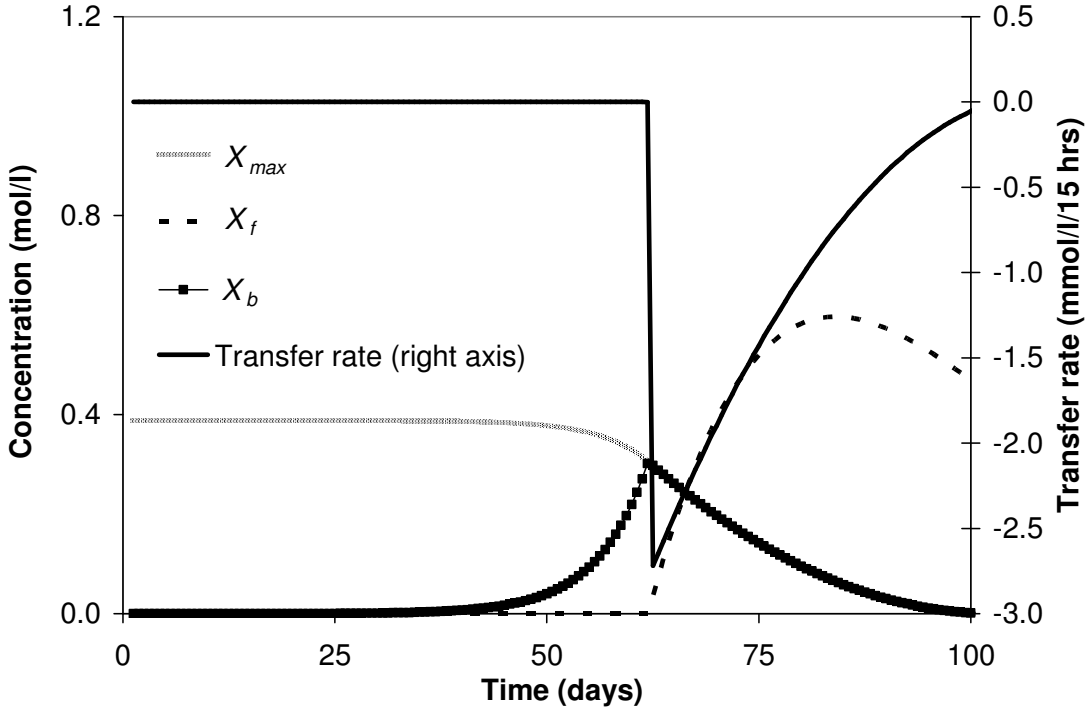

Figure 9.2. Results for fast base case: Biomass and transfer.

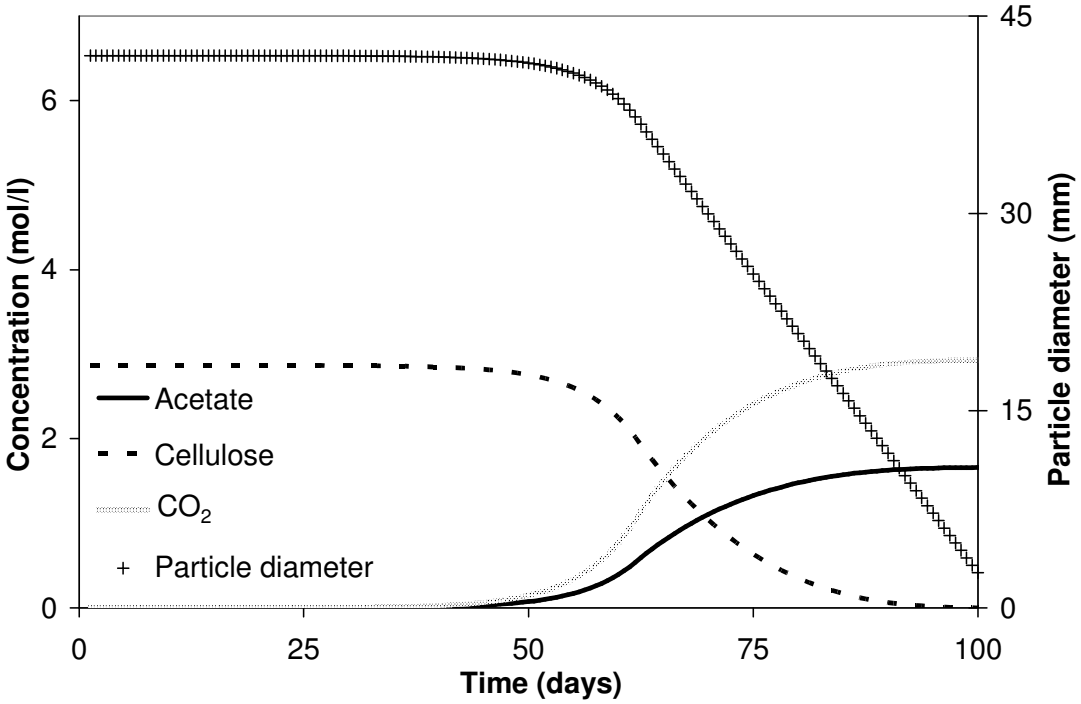

Figure 9.3. Biochemical parameter results for fast base case.

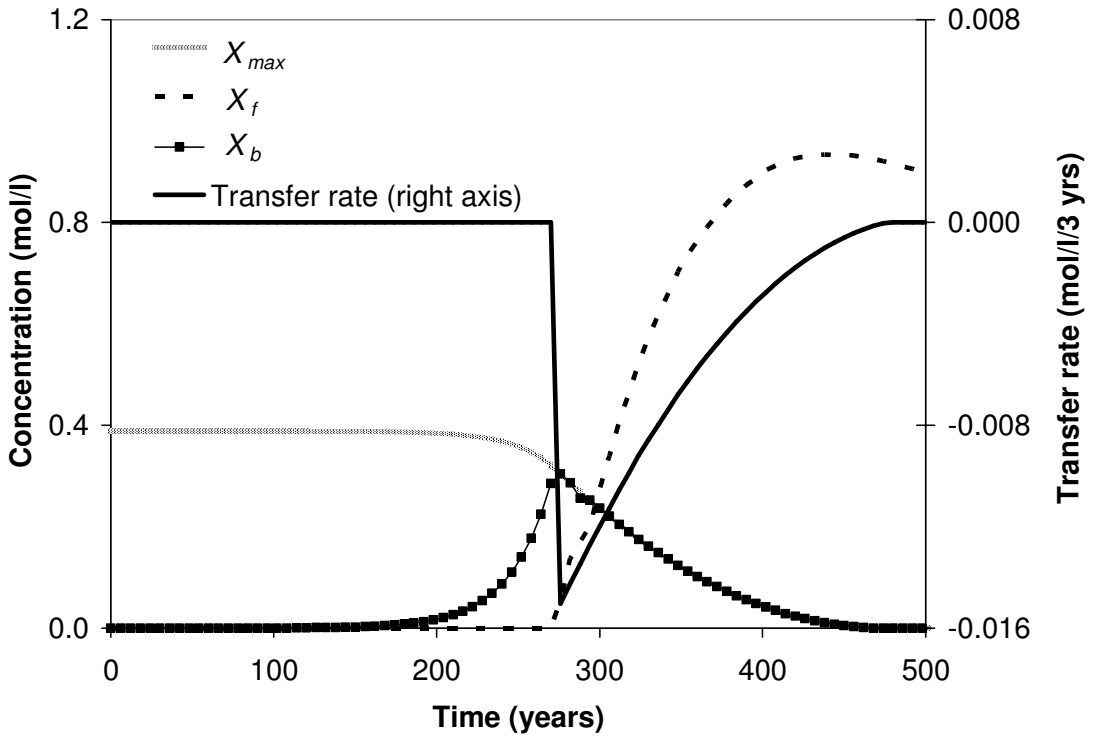

Figure 9.4. Biomass results for slow base case: Biomass and transfer.

9.3.4. GRM model comparison

The General Repository Model (GRM) was developed by British Nuclear Fuels Ltd (Graham et al., 2003a,b) as an expanded and generalized (non-site-specific) version of their DRINK model (Humphreys et al., 1995; Manton et al., 1995; Humphreys et al., 1997). This model is a complex biogeochemical transport code which considers a host of microbial processes and associated chemistry. The model has been fully verified through a strict protocol comprising peer review and model testing. This verification was thorough, including coverage of the model formulation, mathematical fitness-for-purpose, benchmarking against analytical solutions and other codes, experimental test cases, use of analogues, field trials and uncertainty and sensitivity analysis (Graham et

al., 2003a,b). As such, it provides a reliable benchmark against which to evaluate CHAMP.

Figure 9.5 presents the results of both the CHAMP model and the GRM employing parameter values similar to the fast base case (Table 9.3). The relevant GRM parameters are given in Table 9.4. As the approaches to cellulose hydrolysis are somewhat different in the two models, these differences were minimized for the purposes of model comparison. For example, the GRM simulates the conversion of cellulose to glucose (hydrolysis) and the conversion of glucose to microbial products as two distinct processes with different rates. The hydrolysis step in the GRM (cellulose hydrolyzed to glucose) is first-order with respect to cellulose concentration and does not consider bacterial populations. It is the acidogens which then consume glucose, and this consumption rate is dependent on biomass concentration. Contrastingly, in the CHAMP model, the hydrolysis of cellulose and consumption of glucose are linked as a single process (see equation 9.7).

Table 9.4. GRM model parameter set.

Parameter	Value
Initial (type 1) cellulose concentration (mol/l)	2.87
Inventory density ($\rho_{cellulose}$) (kgm^{-3})	1500
Fraction of recycled dead biomass cells (-)	0.8
Type 1 cellulose hydrolysis rate constant (s^{-1})	1×10^{3}
Glucose acidogen	
Initial biomass population (gm^{-3})	1.14
Maximum substrate utilization rate (s^{-1})	5.5×10^{-4}
Microbial yield coefficient (-)	0.34
Biomass death rate (s^{-1})	3.0×10^{-7}
Half saturation constant (mol/l)	1×10^{-6}
Aerobic bacteria	
Initial biomass population (gm^{-3})	1.14×10^{-3}
Maximum substrate utilization rate (s^{-1})	1
Microbial yield coefficient (-)	0.58
Biomass death rate (s^{-1})	4.8×10^{-6}
Half saturation constant (gm^{-3})	0

Thus, for comparison purposes, the GRM hydrolysis rate was set to excess and the GRM parameters associated with acidogens were set to match the CHAMP model acidogens parameters. This approach results in cellulose being represented as glucose in the GRM. Glucose would not accumulate in such real systems, and the glucose in Figure 9.5 should be considered as cellulose. In addition, new features of CHAMP that are not present in the GRM were switched off, including the shrinkage of cellulose particles and biomass transfer from bulk liquid to biofilm.

The evolving concentrations of both cellulose and total biomass for both the GRM and the CHAMP model are presented in Figure 9.5. A comparison between the models may be made for both biomass and cellulose concentration by temporally integrating the concentration profile over the time shown in the figure. Such an analysis yields a 5%

difference between the CHAMP cellulose presence and the GRM cellulose presence, and a 13% difference between the calculated biomass concentration profile. This comparison enhances confidence in the microbiological approach used in the CHAMP model. The small differences observed are due to the presence in the GRM of further microbial processes (i.e., aerobic bacteria) that exhibit minor activity in the case examined. Exclusion of these processes from the code may improve the comparison. As the diffusive biomass transfer process modelled in this work has not been quantified experimentally, validation of this aspect of the model remains unachievable. Validation of the model with diffusive biomass switched off is, however, possible and may be conducted for select data sets listed as references for Table 9.2.

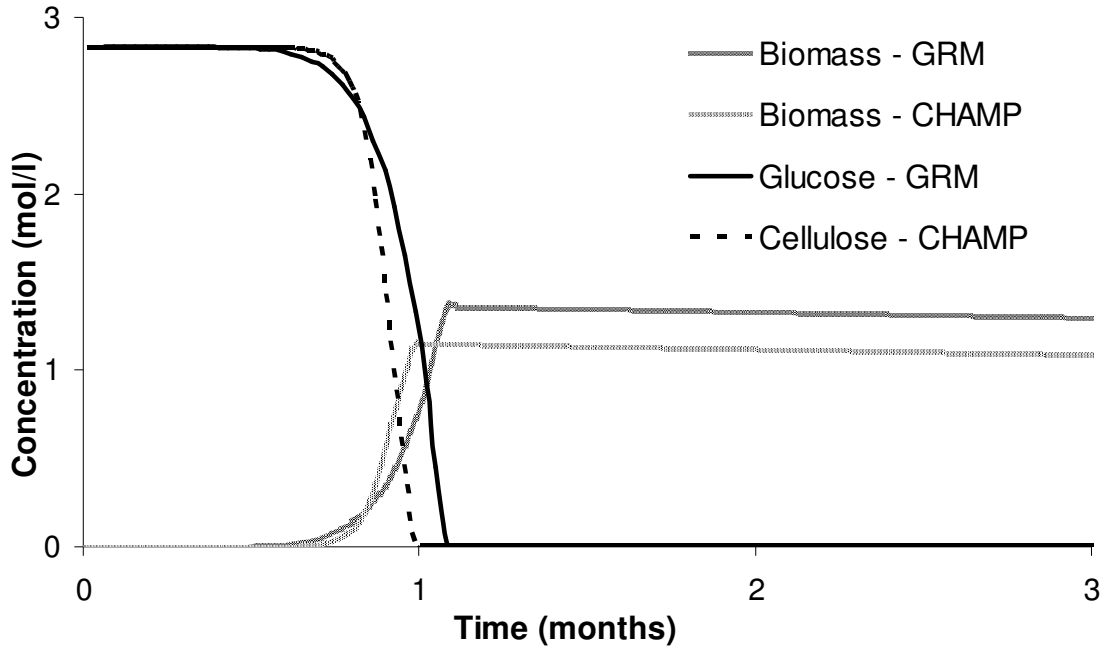

Figure 9.5. Comparison of GRM and CHAMP model results.

9.4. Parameter and process significance

9.4.1. Influence of diffusive biomass transfer

The effect of diffusion-transported free-floating biomass onto the cellulose was explored by comparing simulations where this process was either included or excluded. Two such simulations using the parameters of the slow base case (Table 9.3) are presented in Figure 9.6a, and two simulations using the parameters of the fast base case (Table 9.3) are presented in Figure 9.6b. For the base case ("with transfer"), a pre-existing cellulose-bound biomass population as well as biomass transfer to the cellulose from the bulk liquid present the sources of biomass for cellulose colonisation. For the "without transfer" case, the biomass transfer is neglected and growth of a pre-existing cellulose-bound biomass population is solely responsible for the colonisation of the cellulose particles. The results demonstrate that accounting for biomass transfer predicts significantly faster particle coverage, as shown in Figure 9.6c for the slow base case. Consequently, cellulose is predicted to degrade more rapidly with biomass transfer included. This result is unsurprising, since increased biomass transfer to the particle will result in enhanced colonisation that, due to the increased cellulose-bound biomass population, subsequently increases the amount of cellulose hydrolyzed.

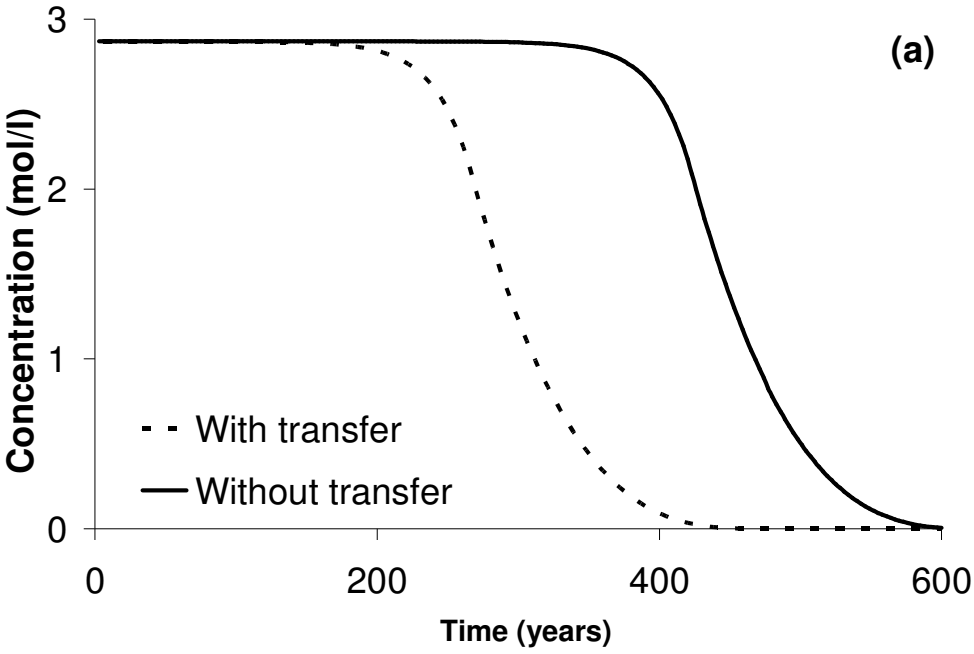
(a)
Concentration (mol/l)
3
2
1
0
With transfer
Without transfer
0
200
400
600
Time (years)

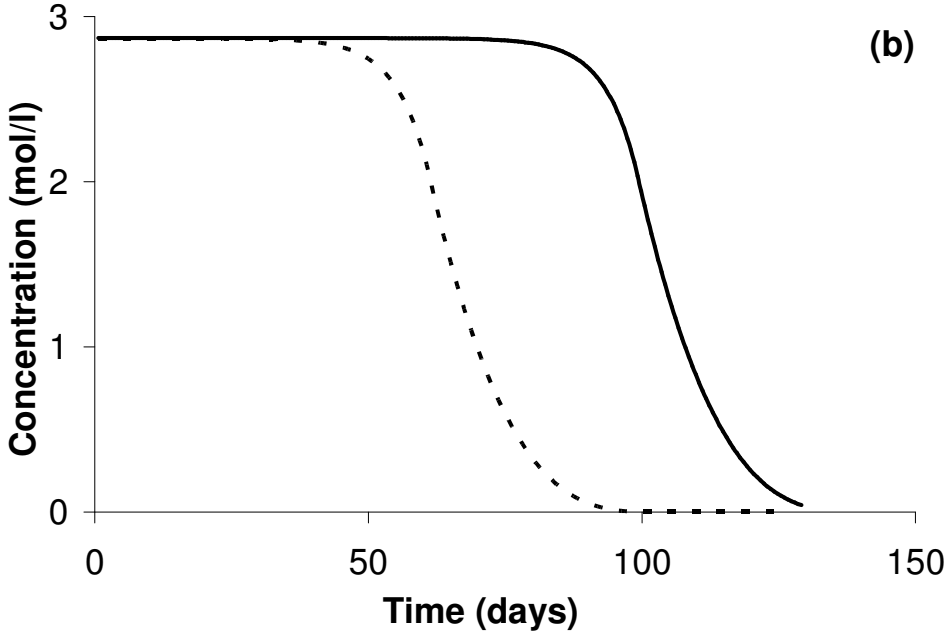
(b)
Concentration (mol/l)
3
2
1
0
0
50
100
150
Time (days)

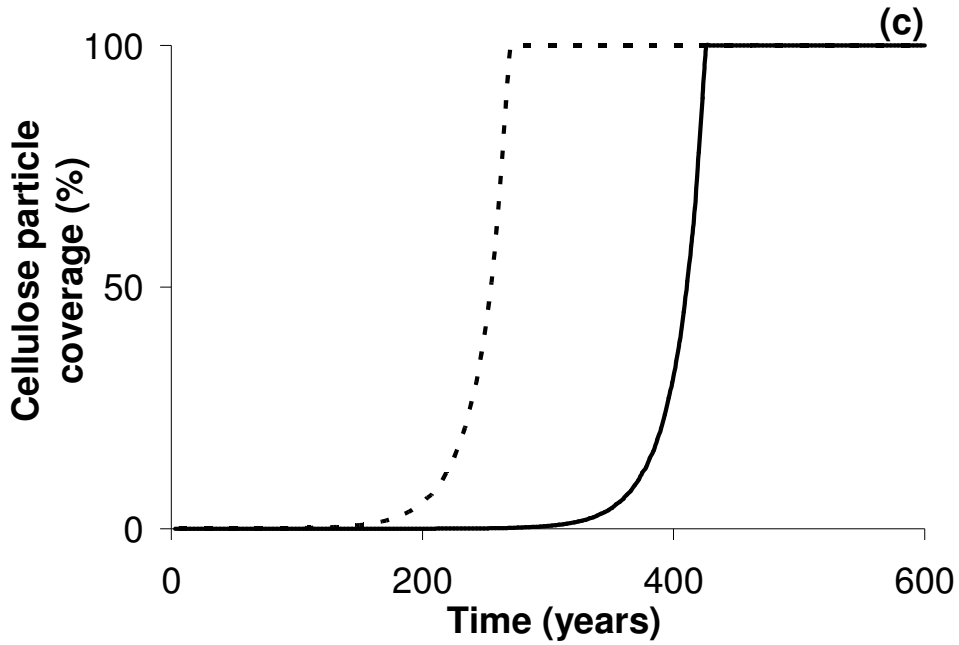

Figure 9.6(a-c). Influence of transfer on cellulose colonisation and degradation for (a) the slow base case (V_b = 3.12 × 10^{-9} s^{-1}), (b) a faster rate between the fast and slow base case rates (V_b = 3.12 × 10^{-8} s^{-1}), and (c) the fast base case (V_b = 5.48 × 10^{-4} s^{-1}).

9.4.2. Influence of biomass transfer: free population

The initial free biomass concentration was varied to explore the effect this parameter had on the system. Using the fast base case parameters, the initial X_f value (X_{fi}) was increased from 10^{-5} mol/l to (a) a realistically high natural level (10^{-3} mol/l) and (b) a level representative of an engineered system (10^{-2} mol/l). Varying X_f does not affect system behaviour when transfer is disregarded, of course, because the model assumes that free biomass does not degrade cellulose. However, when biomass transfer is accounted for, the results for both the fast base case (Figure 9.7) and the slow base case (not shown) indicate that higher initial free biomass concentrations cause more rapid

cellulose degradation (Figure 9.7a). This is as expected, since a higher concentration of biomass in the bulk liquid increases the rate of biomass transfer, and thus cause an earlier colonisation of the cellulose (Figure 9.7b).

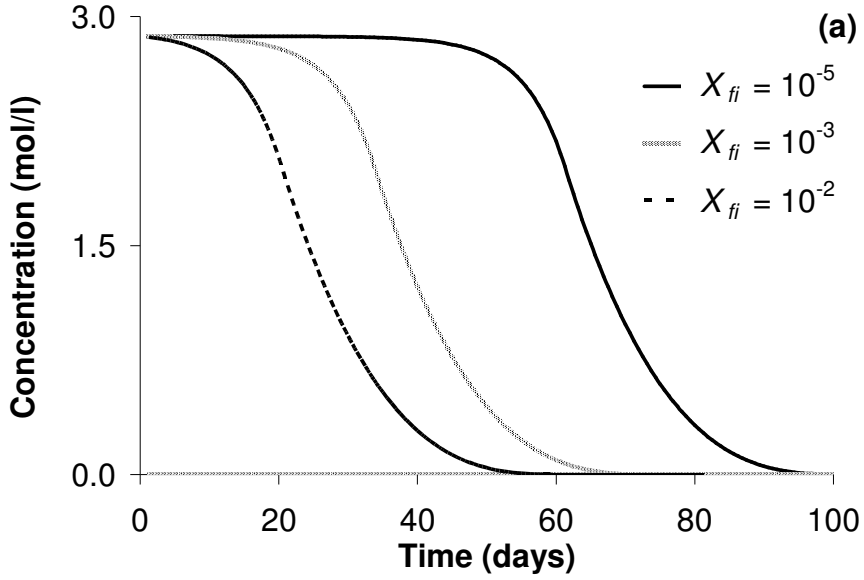

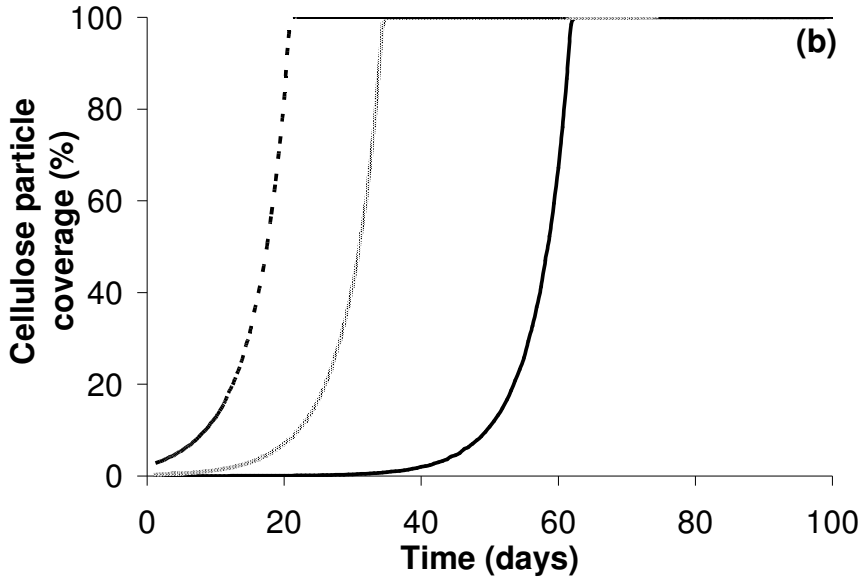

Figure 9.7(a-b). The influence of initial free biomass concentration for simulations using the fast base case parameters on (a) cellulose degradation, (c) cellulose colonisation.

9.4.3. Influence of initial cellulose particle size

The impact of different initial cellulose particle sizes on the system was evaluated using three different particle diameters (20, 42 and 64 μm) typical of those reported in the literature (Movagarnejad et al., 2000; Gan et al., 2003; Xiang et al., 2003).

It is clear that a decrease in initial cellulose particle size significantly increases the rate of cellulose degradation for both the slow and fast base cases (Figure 9.8a and b, respectively). Note that a constant concentration of substrate is assumed; therefore specifying a smaller particle diameter corresponds to an increased number of particles and an increased total particle surface area for potential bound biomass colonisation, X_{max} (Figure 9.8c). Increased surface area corresponds to increased bound biomass

concentrations (Figure 9.8d) that subsequently yield a more rapid hydrolysis of the cellulose.

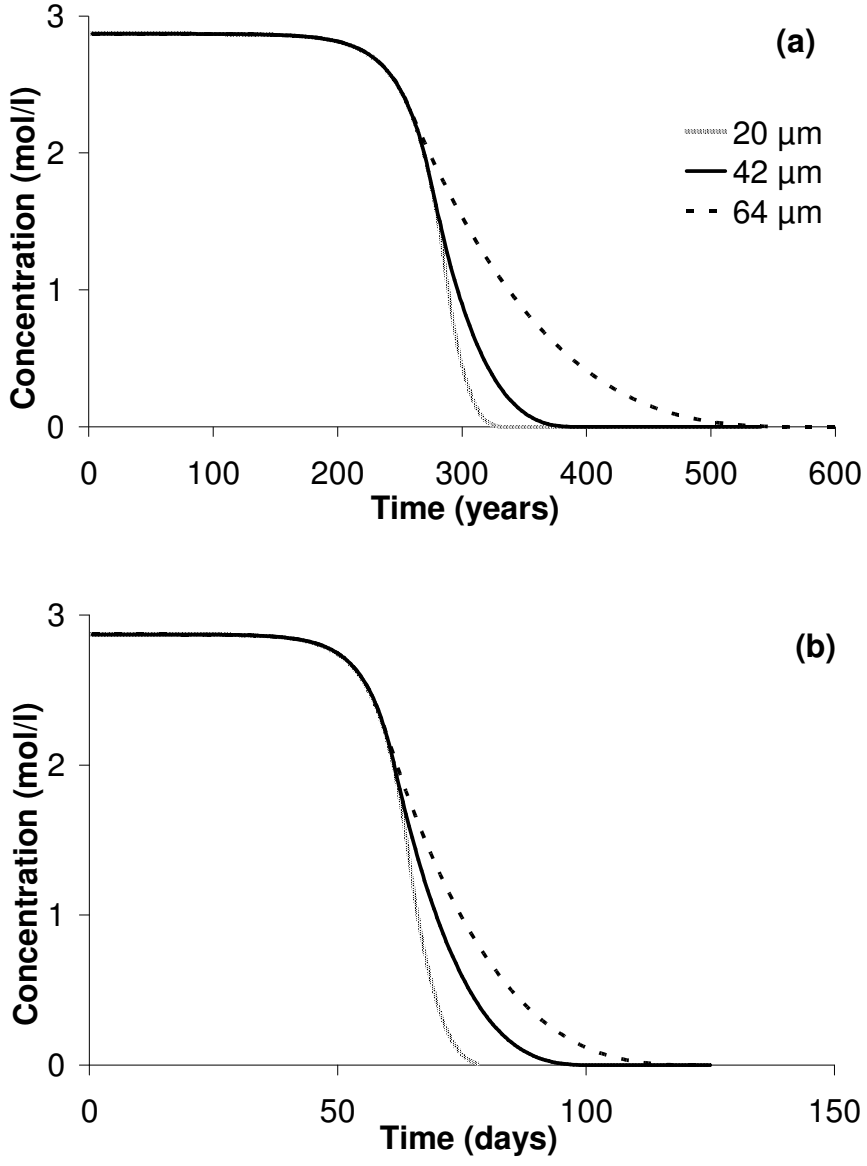

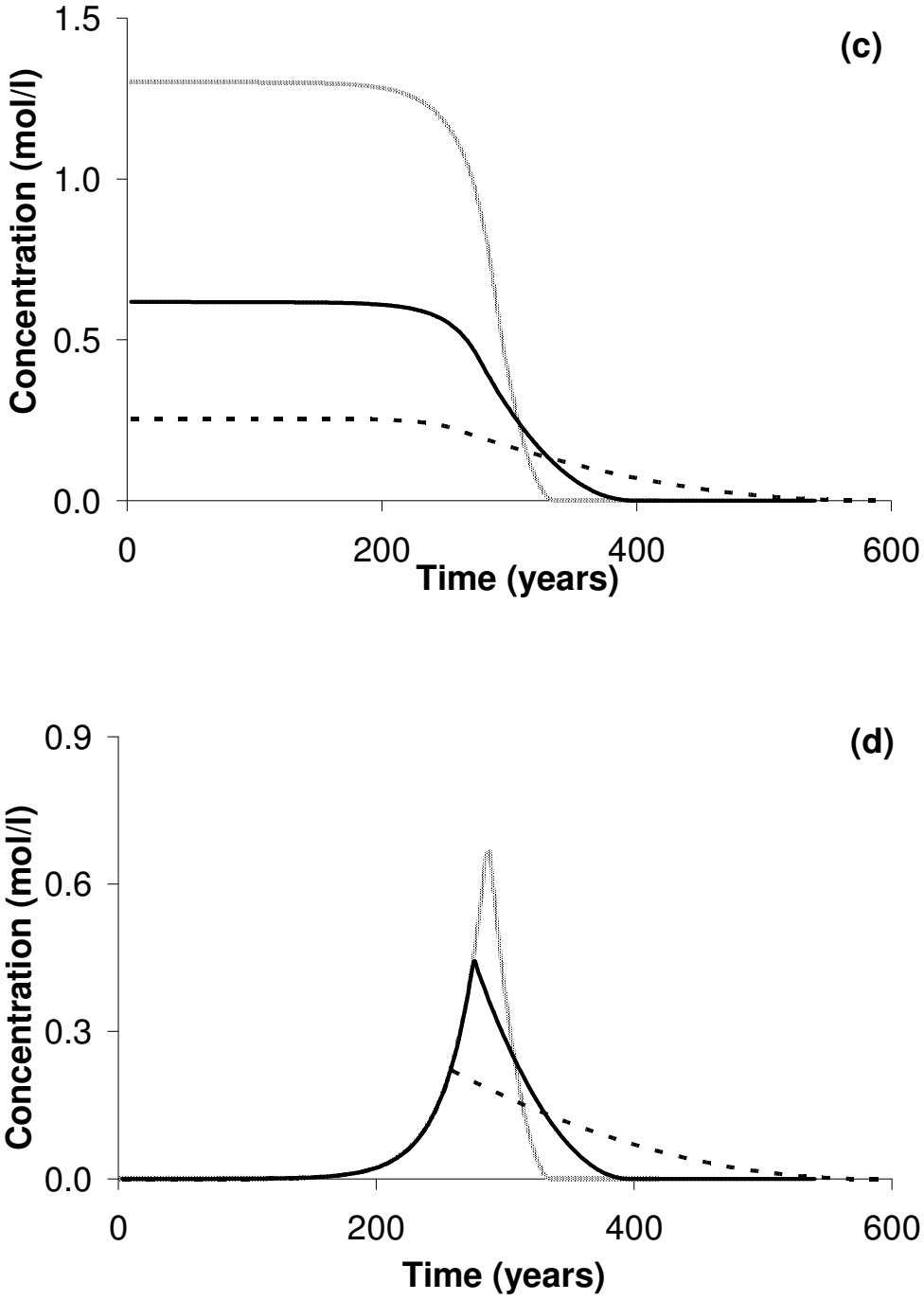

Figure 9.8(a-d). The influence of initial cellulose particle diameter on (a) cellulose degradation for the slow base case, (b) cellulose degradation for the fast base case, (c) maximum possible biofilm concentration for the slow base case, and (d) bound biomass for the slow base case.

9.4.4. Influence of cellulose particle shape

Simulations were conducted with cellulose particles modelled as both spheres and cylinders (see Section 2.5 for differences in the approach of the numerical model for this comparison study) in order to determine the influence of particle shape. Simulations with varying bacterial growth rates, initial cellulose concentrations and number of cellulose particles were examined with the initial surface area of the spheres and cylinders matched by adjusting the number of particles present. In all cases, no significant differences where witnessed between the degradation of particles of cylindrical shape and those of spherical shape when the particles have the same characteristic surface area. This is because the phenomena related to bacterial growth (such as cellulose degradation) correlate to the surface area of substrate per unit volume available.

9.5. Sensitivity to parameters

The sensitivity of the system to changes in a wide range of model parameters was quantified systematically. Parameters included the initial bound biomass concentration (X_{bi}), the initial free biomass concentration (X_{fi}), the maximum substrate utilization rate (V_b), the yield coefficient (Y_b), the death rates of both the bound and free biomasses (D_b and D_f), the half-saturation constant (K_b), the biofilm thickness (h) and the initial cellulose particle diameter (ϕ_i). The parameters for each base case (Table 9.3) were each independently both increased by both 10% and 1%. Consistent with the focus in this work on the resultant rates of cellulose degradation, the model-dependent variable

examined is taken to be the time at which the cellulose has degraded to 90% of its initial concentration (denoted T_{c90}).

By varying parameter β_n by a small increment, $\Delta\beta_n$, the model output of interest in the system:

$$O = O(\beta_1, \beta_2, \beta_3 \ldots \beta_m) \tag{9.27}$$

is given by:

$$O(\beta_n + \Delta\beta_n) = O(\beta_n) + \frac{\partial O}{\partial \beta_n}\Delta\beta_n \tag{9.28}$$

Thus, the sensitivity of the chosen model output to $\Delta\beta_n$ may be constructed as:

$$\varsigma_n = \frac{\partial O}{\partial \beta_n} \tag{9.29}$$

To permit comparison of parameters with different dimensions, the sensitivity, ς_n, is non-dimensionalised as follows:

$$\sigma_n = \varsigma_n \frac{\beta_n}{O} \tag{9.30}$$

Such sensitivities are, therefore, a measure of the relative importance of parameters on a system for a chosen initial condition. Parameter value changes of both 10% and 1%

yielded similar results. Table 9.5 shows the results of applying this procedure to the model independent variables listed above for both the fast and slow base cases.

Table 9.5. Sensitivity matrix of T_{c90} values[a].

Base case	D_b	D_f	h	K_b	V_b	X_b	X_{fi}	Y_b	ϕ_i	α
Fast	0.80	0.01	2.18	0.00	9.92	0.00[b]	0.74	7.08	3.51	0.38
Slow	0.30	0.19	2.10	0.36	8.81	0.36	0.30	5.60	3.75	0.32

[a]values rounded to nearest 0.01.

[b]actual value 0.002.

Using the values in Table 9.5, the ranked importance of the parameters for these systems (in order of descending influence) are:

$V_b > Y_b > \phi_i > h > D_b > X_{fi} > \alpha > D_f > X_{bi} > K_b$ for the fast base case, and

$V_b > Y_b > \phi_i > h > X_{bi} > K_b > \alpha > X_{fi} > D_b > D_f$ for the slow base case.

The table reveals that, unsurprisingly, both the maximum substrate utilization rate and the yield coefficient of the bound (hydrolyzing) biomass population dominate in terms of impact on the time required for degradation. These two properties are followed in importance by the physical properties of both the cellulose and the hydrolyzing biomass (i.e., cellulose particle and biofilm thickness) and both the initial free and the bound biomass populations. This suggests that cellulose degradation is more sensitive to the microbial efficiency than the physical properties of the system at the microscale. Thus, selection of a more efficient bacterial strain may be of greater effect to a remediation

strategy than simply increasing the quantity of biomass initially inoculated into the system.

In addition, cellulose degradation appears to be more sensitive to the initial free biomass population for the fast base case than for the slow base case (0.74 versus 0.30 for the fast and slow base cases, respectively, see Table 9.5). The reverse is true for the initial bound biomass population (0.002 versus 0.357 for the fast and slow base cases, respectively, see Table 9.5). This suggests that the initial free microbial biomass has significant influence on cellulose degradation in a digester (or nutrient rich, high temperature) system. In landfill/natural systems, the free biomass population is of reduced importance. The application of existing cellulose degradation models to naturally fast systems such as digesters (working in nutrient rich environments at optimal temperatures) may result in erroneous cellulose degradation behaviour if diffusive-driven biomass transfer is not considered. However, this risk is reduced when these same models are applied to naturally slower systems such as landfill environments. This finding additionally implies that digester/engineered systems may generally require more complex models and more extensive parameter measurements than landfill sites.

9.6. Dimensionless parameter analysis

The preceding section examined the relative effects of changes in individual parameters. Here, the effect of parameter variation based on dimensionless parameter groups is examined. Dimensionless parameter groups were selected using process-relevant

independent model parameters. A systematic approach towards obtaining relationships between these chosen parameter groups and T_{c90} values was taken. A total of approximately 150 runs were conducted varying the following parameters in a number of parameter groups: V_b, α, C_i, K, X_{bi}, X_{fi}, D_b and D_f. Additionally, the difference between the T_{c90} value when transfer is not considered (transfer off) and the T_{c90} value when transfer is considered (transfer on), ΔT_{c90}, was evaluated for each of these runs. The ΔT_{c90} value is therefore a measure of the significance that biomass transfer has on cellulose degradation behaviour. Several parameter groups that contribute novel insight into system behaviour are discussed below.

The impact that the ratio of the diffusive biomass transfer rate (α) to the cellulose-hydrolyzing biomass substrate utilization rate (V_b) had on both T_{c90} and ΔT_{c90} values was investigated. The ΔT_{c90} values show the influence that diffusive biomass transfer has on cellulose degradation for various α/V_b ratios, whilst the T_{c90} values show the influence the α/V_b ratio has on the time to 90% cellulose degradation. The α/V_b ratio is used to ascertain when the diffusive biomass transfer becomes significant on cellulose degradation behaviour. Figures 9.9a and 9.9b present $\log(\Delta T_{c90})$ values for varying α/V_b ratios for systems with low substrate utilization rates. As the α/V_b ratio increases, ΔT_{c90} is observed to increase. Interestingly, the value of ΔT_{c90} begins to plateau when the α/V_b ratio increases beyond approximately 0.4. These figures reveal that the relationship between α/V_b and ΔT_{c90} is quantitatively different for different substrate utilization rates (compare ΔT_{c90} values in Figure 9.9a against those in Figure 9.9b at the same α/V_b ratio

and D_b value) and for different bound biomass death rates (Figures 9.9a and 9.9b). It may be noted that as the bound biomass death rate, D_b, decreases, the ΔT_{c90} value increases for the same α/V_b ratio. This is to be expected, since a slower death rate coupled with the same growth rate will result in faster net biomass growth and therefore faster cellulose degradation.

Figures 9.9c and 9.9d present $\log(T_{c90})$ values (with transfer on) for varying α/V_b ratios for systems working at slow substrate utilization rates. Note that the order of magnitude of results requires the figures to use log values on both axes. The figures reveal that when the α/V_b ratio is small the T_{c90} value varies only slightly (values are within 1% of each other) but that diffusive biomass transfer begins to impact upon the system when the α/V_b ratio increases above approximately 10^{-4}, after which T_{c90} reduces significantly as the influence of biomass transfer on the system increases. At a deceased bound biomass death rate, D_b, the T_{c90} value decreases for the same α/V_b ratio. Again, this is to be expected, since a slower death rate coupled with the same growth rate will result in faster net biomass growth and therefore faster cellulose degradation.

The impact on cellulose degradation behaviour due to the ratio of the initial concentration of bound biomass to the initial concentration of free-floating biomass, X_{bi}/X_{fi}, was also explored. With all other parameters being equal, this dimensionless parameter group shows no direct correlation with T_{c90} values. Whilst the X_{fi} value can have significant impact on the system when diffusive biomass transfer occurs, the

influence of X_{bi} is clearly dominant in the system (data not shown). Likewise, the ratio of the bound-biomass death rate to the cellulose-hydrolyzing biomass substrate utilization rate, D_b/V_b, shows no direct correlation with T_{c90} values. T_{c90} values vary due to both D_b and V_b values, and this variance occurs for each of these two parameters independently of the other. This is further supported by the evidence from Figures 9.9(a-d) which show that T_{c90} values vary depending, independently, on both D_b and V_b values. Naturally, as the K/C ratio is increased equation (9.1) no longer shows a zero order dependence on the substrate resulting in an increase in T_{c90}.

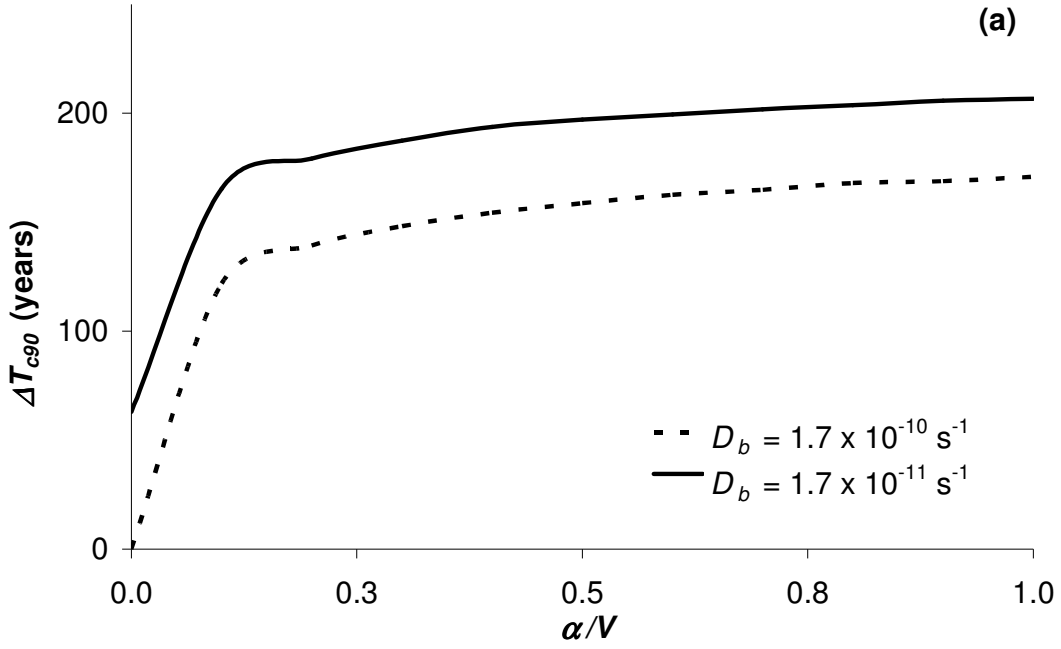

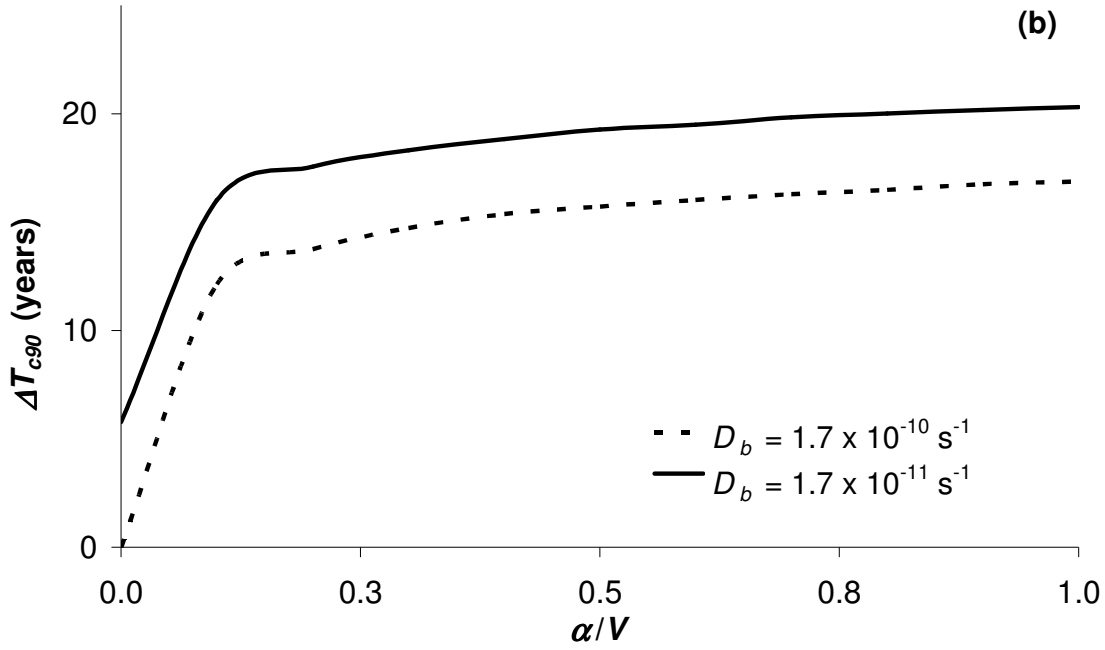
(b)
20
10
0
ΔT_{c90} (years)
D_b = 1.7 x 10^{-10} s^{-1}
D_b = 1.7 x 10^{-11} s^{-1}
0.0
0.3
0.5
0.8
1.0
α/V

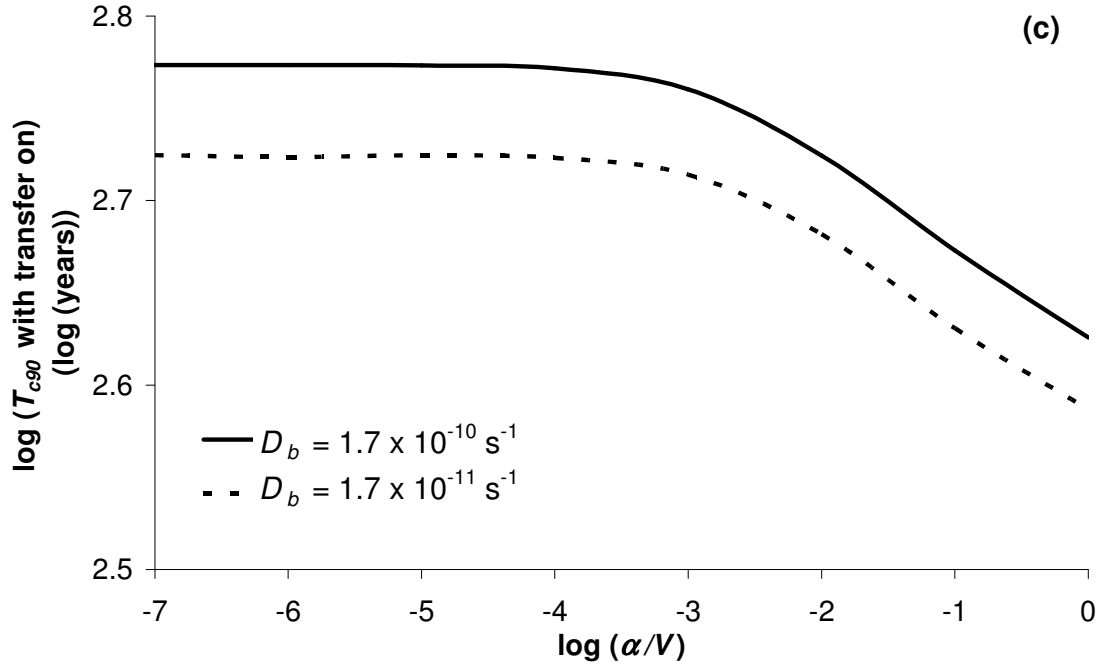
(c)
2.8
2.7
2.6
2.5
log (T_{c90} with transfer on) (log (years))
D_b = 1.7 x 10^{-10} s^{-1}
D_b = 1.7 x 10^{-11} s^{-1}
-7
-6
-5
-4
-3
-2
-1
0
log (α/V)

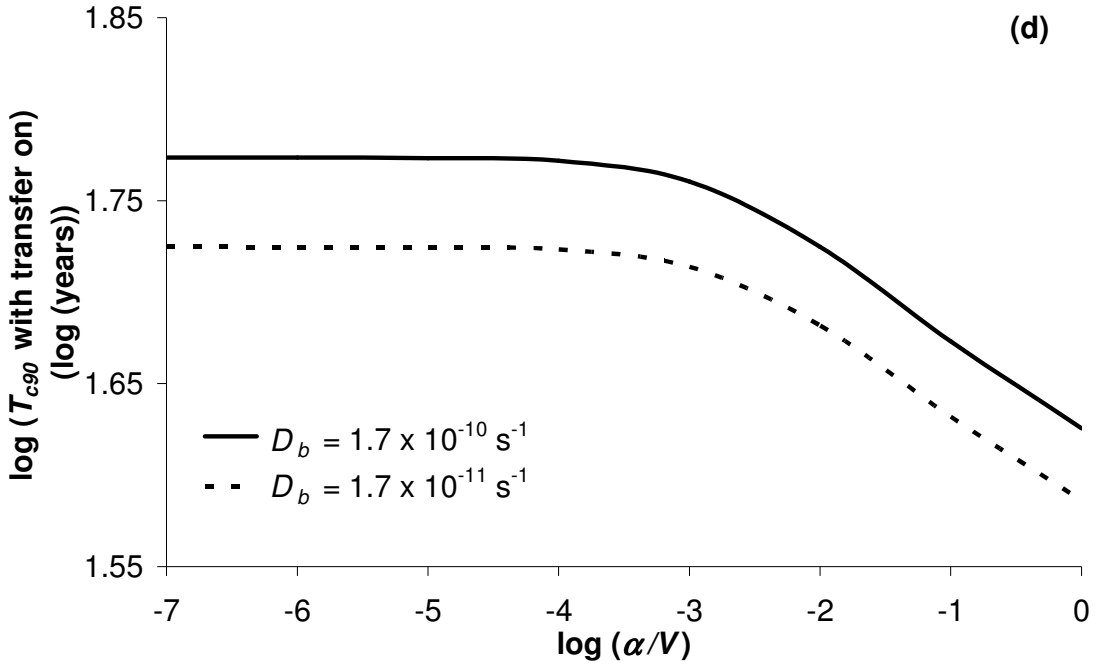

Figure 9.9(a-d). Impact of the dimensionless parameter α/V_b on (a) ΔT_{c90} for V_b = 3.08×10^{-9} s^{-1}, (b) ΔT_{c90} for V_b = 3.08×10^{-8} s^{-1}, (c) ΔT_{c90} with transfer on for V_b = 3.08×10^{-9} s^{-1} and (d) Tc_{90} with transfer on for V_b = 3.08×10^{-8} s^{-1}.

9.7. Conclusions

A new model was developed for simulating cellulose hydrolysis in natural and engineered systems such as landfills and anaerobic digesters. Uniquely, the model incorporates the ability of free-floating bacteria to colonise cellulose particles by attachment through contact in solution, thus accounting for the spatial separation of cellulose particles and biomass. The model considers an evolving substrate-bound acidogenic biomass to be the hydrolyzing population. Other bacterial populations are not considered. Additionally included are the processes of particle shrinkage during hydrolysis and cellulose-bound biomass sloughing.

Sensitivity simulations with the model revealed that accounting for cellulose colonisation via biomass transfer from the bulk liquid is of significance in degrading systems such as digesters and landfill environments.

Analysis of the model's effective dimensionless parameters further revealed that, for the defined base case parameter space, the diffusive biomass transfer becomes significant when the ratio of diffusive biomass transfer rate to the cellulose-hydrolyzing biomass substrate utilization rate (α/V_b) becomes larger than 10^{-4}. Above this value the time taken for cellulose to degrade to 10% of its original concentration is significantly reduced by the impact of diffusive biomass transfer on the system. This reduction in time remains quantitatively constant above a α/V_b ratio of approximately 0.4. Therefore, more specifically, models which neglect to account for diffusive biomass transfer in systems where the cellulose-hydrolyzing biomass has a growth rate 10^4 greater than the diffusive biomass transfer rate are likely to significantly over-predict the time taken for cellulose to substantially degrade.

The spatially separated nature and size of the cellulose particles appear to have a significant effect on cellulose degradation. Smaller cellulose particles were shown to cause more rapid cellulose degradation due to the increased surface area made available for colonisation, resulting in larger populations of cellulose-bound bacteria actively participating in hydrolysis. The relation of system degradation behaviour to particle surface area is emphasized by insensitivity to the shape of the modelled particles as long

as surface area is maintained. These results confirm the expectation that the physical reduction of cellulose particle size before disposal may be an effective option for reducing the overall degradation period of the waste.

In addition, increased concentrations of biomass in the bulk liquid surrounding the cellulose result in increased colonisation rates, thereby significantly accelerating cellulose degradation. This underscores the knowledge that increased free-floating bacterial populations, either via the transportation of biomass into the system from elsewhere or the bacterial inoculation of such systems, might enhance degradation rates. Moreover, it further emphasizes the need to account for such biomass transfer processes to accurately predict the overall rate of substrate degradation.

A sensitivity study of the parameters used in the model revealed that the (biological) rate and yield properties of the hydrolyzing bacteria are of most significance with regards to degradation in the system. The physical properties of both the cellulose and the hydrolyzing biomass, and the initial population of biomass in liquid surrounding the cellulose particles are of secondary importance to these. In cases where biomass is injected into the system as part of an enhanced remediation/treatment scheme, selection of a microbial strain with superior performance may be more important than the physical properties of that strain or the initial cellulose particle size.

This work focuses on processes at the microscale. Further work is required to explore the importance of the investigated processes at the macroscale. Additionally, there

remains a need to conduct experiments in order to properly validate the biomass transfer phenomena examined in this work.

10. Summary and conclusions

10.1. Research motivation and goals

The motivation of this research was the risk posed by radionuclide transport from contaminated mining, ore extraction, nuclear fuel reprocessing, ammunitions manufacture facilities, mill tailings, and LLW repositories. The goal of this research was to improve understanding of how the dominant interacting microbial, geochemical and physical transport processes in porous media affect radionuclide immobilisation efficiency. In order to investigate this, a one-dimensional biogeochemical transport model was developed for biostimulated U immobilisation by dissimilatory metal reducing bacteria in dual-porosity heterogeneous porous media was developed. The effectiveness of U bioimmobilisation efficiency was explored with simulations spanning a range of interacting geochemical, microbial, and transport processes and porous media characteristics.

10.2. Developed model

The model utilised a dual-porosity (two-region) approach with a mobile (advective-dominant) region and an immobile (diffusive-dominant) region. This approach accounts for media variability in hydraulic conductivity thereby implicitly accounts for the heterogeneous nature of porous media. The model included surface complexation of U(VI) to iron hydroxide minerals and the extensive geochemical reactions listed within the MINTEQ database. A partial equilibrium approach was used to model microbially mediated redox reactions, and either a first-order or a Michaelas-Menten/Monod

formulation was used for microbial OC degradation. The model is limited to one-dimension and assumes bioclogging and microbial-facilitated U transport to be insignificant, biomass to be at steady state (i.e., no explicitly growth or decay), and ideal mixing in each of the media regions. The dual-porosity approach implicitly accounts for porous media heterogeneity. The coupling of this approach to microbially mediated redox reactions, including uranium geochemistry, is unique and has not been employed elsewhere. Additionally, the inclusion of U(VI) surface complexation in such a model has not previously been exploited.

10.3. Model evaluation

The model was partially evaluated against experimental data and compared to a published model. Evaluation against a U immobilisation experiment in a biostimulated heterogeneous sediment column demonstrated that the model's ability to qualitatively capture the U(VI) bioreductive process. Further, a one-dimensional simulation of a single porosity domain compared well with the Wang et al. (2003) model without any model or special adjustment of this model. These model evaluation exercises built confidence in the ability of the model to capture the relevant U(VI) reduction and U immobilisation processes occurring in U(VI) bioimmobilisation remediation strategies. However, quantitative evaluation was not possible due to insufficient data.

10.4. Impact of dual porosity porous media

Simulations explored the potential impact that spatial heterogeneity might exert on U(VI) immobilisation efficiency. The impacts of porous media characteristics such as porosity and regional mass transfer, as well as biological and geochemical conditions were investigated. Significantly different U(VI) immobilisation efficiency behaviour observed between porous media systems characterized by dual porosity transport behaviour and those exhibiting more homogeneous flow behaviour. It was demonstrated that systems exhibiting regions of contrastingly low- and high- pore water velocities are likely to exhibit delayed U(VI) immobilisation relative to more homogeneous systems. This is due to diffusive limitations on electron donor(s) and acceptors. This finding is consistent with expectations and with studies of other remediation strategies for aqueous phase contamination of fractured rock and clay systems.

10.5. Impact of microbial distribution in dual-porosity media

The physical distribution of bioactive microorganisms in dual-porosity media is uncertain and may impact the success of remediation strategies. The impact of spatially-distributed microbial activity in the context of radionuclide containment and remediation has not previously been explored. Hence, further simulations explored the affects of different bacterial residence locations in dual-porosity porous media systems. The study considered multiple conditions typical of field sites and identified the key distinctions in U immobilisation behaviour imparted by the different bioresidence modelling assumptions.

For the conditions examined, sensitivity simulations suggest that when bioactivity is dominant in only one of the two dual porosity regions, U(VI) immobilisation efficiency – particularly with respect to time – is dependent on the porosity ratio. Efficiency is found to be proportional to the porosity-associated volume in which microbial activity takes place. Consequently, when bioactivity occurs in both regions, the net remediation efficiency is increased. Holding the total porosity-associated volume constant, findings match expectations that the time taken to immobilise U(VI) was found to be independent of the porosity ratio under such conditions. These results suggest that the DMRB remediation efficiency is more sensitive to variations in physical porous media properties (e.g., porosity, hydraulic conductivity) when microbial activity is heterogeneous within dual porosity media. This highlights the importance of characterizing the bioresidency status of field sites if biogeochemical models are to accurately predict remediation schemes in physically heterogeneous media. Additionally, multi-region models that unwittingly assume microbial residence to be homogeneous throughout a porous media may significantly overestimate microbial efficiency and thereby exaggerate predicted remediation effectiveness.

10.6. Impact of inter-regional mass transfer

Modelling results further revealed that U(VI) immobilisation efficiency may be significantly affected by inter-regional mass transfer rates when bioactivity is restricted to regions of diffusion-dominated solute transport. However, when bioactivity is either restricted to advection dominated flow regions or is active uniformly throughout the

media, U(VI) immobilisation efficiency is less affected by the transfer rate. In agreement with expectations, this suggests that the significance of diffusion-limited processes in dual porosity porous media increases as microbial activity becomes dominant in the diffusion-limited region.

Heterogeneous media exhibiting mass transfer limitations may hold some advantages over more homogeneous media in the post-biostimulation maintenance of remediated sites. Migration of reduced species from bioactive advective-dominated flow regions into diffusive-dominated flow regions which are not bioactive (or exhibit low bioactivity) may instigate uraninite precipitation in the non-bioactive region. Due to mass transfer limitations, it may be that these diffusion-dominant flow regions better retain reduced U if the sediment experiences reoxidising conditions.

10.7. Impact of mineral presence

Simulations additionally revealed that spatially varying mineral presence may exert a significant impact on U(VI) bioreduction efficiency. Efficiency was found to be dependent on the combined spatial distributions of minerals and microbial activity. Reduced mineral presence in diffusion-dominant flow regions offered increased efficiency across the range of bioactivity scenarios, but otherwise similar increases in efficiency were observed over the range of bioactivity scenarios. This suggests that spatially varying mineralogy may significantly impact remediation schemes making use

of DMRB, and that the impact of mineral variations should not be considered in isolation, but rather in concert with the impact of spatial biological distributions.

10.8. Conditions for optimum remediation efficiency

Further sensitivity analyses using dimensionless parameter groups analyzed a wide range of system behaviour for scenarios in which microbial activity was confined to the less mobile regions of the media. An extensive suite of simulations explored how key processes impact remediation efficiency, and permit identification of the conditions under which processes associated with groundwater transport, dual porosity media phenomena and microbial activity interact. A relatively wide range of microbial and geochemical conditions were explored for bacterial presence limited to diffusion-dominated flow regions. The results suggest the following conditions apply to systems in which the microbial activity is confined to the diffusion-dominant flow regions of the media:

- Optimum bioremediation is likely to occur when:
    - the timescale associated with inter-regional mass transfer between regions of advection-dominant and diffusive-dominant flow is less than one thirtieth of the value of the volumetric flux timescale.
    - the organic carbon fermentation timescale is less than one thirtieth of the value of the volumetric flux timescale.

- the advective-dominant flow region porosity is between equal to and four times greater than the diffusion-dominant flow region porosity.

- Remediation may be restricted to systems whose interregional mass transfer timescale and/or organic carbon fermentation timescale is between approximately 10 and 1000 times the volumetric flux timescale.
- Based on typical field data these conditions are attainable, but engineering of the system may be required in order to achieve them. The exact value may increase or decrease in systems less or more abundant in electron acceptors, respectively.

The presented results provide insights into how to improve biostimulated DMRB U(VI) immobilisation remediation schemes in porous media exhibiting dual-porosity flow behaviour. The present work showed how influential parameters can be actively manipulated in the field to optimize U(VI) immobilisation efficiency.

10.9. Impact of reoxidation

Reoxidation of previously bioreduced U(IV) is a concern in U(VI) bioimmobilisation schemes. This process was explored under different bioresidency scenarios and in the presence or absence of iron-sulfide minerals. The results demonstrated that reoxidation of bioreduced U(IV) causes U(VI) concentration "spikes" at concentrations higher than the influent U(VI) concentration. These "spikes" move downgradient in the domain and present a significant risk to the success of U immobilisation remediation schemes. The

results suggest that iron-sulfide mineral presence can offer significant protection against U(IV) oxidation, supporting the existing experimental evidence. Model results further suggest that microbial heterogeneity in the media was unlikely to affect the system's resistance to U(IV) oxidation, however numerical instability in the model renders this particular finding inconclusive.

10.10. Cellulose hydrolysis

A further study was devoted to the process of cellulose hydrolysis, an important process in determining the stability of low level radioactive waste disposal and municipal solid waste landfill sites, and their potential impact on the environment. A second, process-based model relevant to landfill and anaerobic digesters was developed, which includes a novel approach to biomass transfer between a cellulose-bound biofilm and biomass in the bulk liquid. Model results highlight the significance of the bacterial colonisation of cellulose particles by attachment through contact in solution. Simulations reveal that both enhanced colonisation and cellulose degradation are associated with reduced cellulose particle size, increased biomass populations in solution and increased cellulose-binding ability of the biomass. This suggests that transportation of biomass into the system from elsewhere and/or bacterial inoculation of such systems could enhance degradation significantly. A sensitivity analysis of the system parameters revealed that the biological rate and yield properties of the hydrolyzing bacteria are most significant with regard to cellulose degradation in the system. As LLW sites containing

significant quantities of cellulose can affect radionuclide transport, these findings may be relevant to such sites.

10.11. Sites amenable to U bioimmobilisation

Based upon this work, it is possible to infer the types of sites amenable to U bioimmobilisation. These include:

- Porous media which does not exhibit dual porosity transport behaviour
- Porous media in which bioactive porosity is large relative to total system porosity
- Pore water possessing low electron acceptor concentrations
- Porous media likely to produce Fe-S minerals during biostimulation
- Porous media exhibiting smaller (more rapid) timescales for mass transfer between regions of advection-dominant and diffusive-dominant flow
- Systems exhibiting rapid cellulose hydrolysis, possibly enhanced via diffusive biomass transfer processes
- Specifically in systems in which DMRB are predominantly active in diffusion-dominant flow region:
    - Porous media in which the timescale associated with inter-regional mass transfer between regions of advection-dominant and diffusive-dominant flow is less than one thirtieth of the value of the volumetric flux timescale.
    - Porous media in which the organic carbon fermentation timescale is less than one thirtieth of the value of the volumetric flux timescale.

- Porous media in which the advective-dominant flow region porosity is between equal to and four times greater than the diffusion-dominant flow region porosity.

10.12. Engineering approaches to increased U bioimmobilisation effectiveness

Furthermore, based upon this work, it is possible to infer engineering approaches that may result in the increased effectiveness of bioimmobilisation strategies. These include:

- Hydraulic fracturing to reduce diffusion distances between advective flow paths.
- Stimulating bioactivity in both advection- and diffusion-dominated regions by pulsed OC injection, where quiescent periods between pumping times permits diffusion into the matrix.
- Adjustment of injected ED concentration to account for media mineralogy (EA concentrations).
- Addition of iron filings (e.g., in permeable reactive barriers) or injection of sulphate into the subsurface in order to encourage Fe-S mineral formation, manipulate redox conditions and thereby delay U(VI) rebound.
- In systems with bioactivity restricted to diffusion-dominant flow regions: injection of active biomass into the subsurface to increase U(VI) immobilisation efficiency. This technique is further likely to result in efficiency being less sensitive to the porosity ratio of the media.

- Adjusting pumping rates and locations in order to modify pore water velocity and consequently manipulate the advective transport timescale relative to diffusive and microbial timescales.
- Injection of free-floating biomass into systems with cellulose presence in order to encourage biomass attachment onto cellulose particles and thereby increase cellulose hydrolysis rates.
- Processing of cellulosic waste in order to reduce cellulose particle size and therby encourage more rapid cellulose hydrolysis.

It is acknowledged that such possibilities are suggested by simulations conducted in one-dimension and consisting of the numerous numerical, physical, chemical, and biological assumptions as outlined in this research. The feasibility and effectiveness of these options needs to be investigated further, both in experimental and multi-dimensional simulations. Further work is discussed in more detail in Chapter 11.

10.13. Summary

This thesis presented a general background to radionuclide-contaminated sites and their potential remediation. A developed multicomponent reactive transport model was employed to aid understanding of how heterogeneous porous media might affect radionuclide containment and remediation through interactions with the dominant geochemical, microbial and transport processes. The studies identified the conditions under which remediation efficiency is affected and suggested engineering approaches

that may result in increased effectiveness of bioimmobilisation strategies. It is hoped that this research be applied to future experimental and field site work in order to optimise U-immobilisation and avoid potential difficulties associated with remediation strategies.

11. Future research directions and needs

This chapter proposes research needs identified in this work.

11.1. Experimental research work

Improved experimental data is needed to adequately validate biogeochemical reactive transport models dealing with U(VI) bioreduction.

In particular, experiments that (i) provide detailed data analyses of media characteristics, both physical and chemical mineralogy, and (ii) provide both spatial and temporal tracking of both oxidized and reduced U concentrations and all important EAs during biostimulation of the experiment would be most valuable. Accurate characterization of the pore water chemistry is essential for understanding the multiple geochemical processes occurring in such systems. Given the advantages of flushing and conditioning of the sediment/pore water in U contaminated sites prior to biostimulation, experiments focused on the competing processes occurring under recirculated porewater flushing and conditioning in contaminated site sediment would prove useful.

Macro-scale data is perhaps of more practical use than field scale, given that the uncertainties of maco-scale data may be reduced significantly in experimental work.

Furthermore, the present work has revealed that spatially varying mineral presence may exert a significant impact on U(VI) bioreduction efficiency. Assessing the impact that

mineralogy heterogeneity has on the success of U(VI) bioimmobilisation would be beneficial.

In order to assess the long-term success of bioimmobilisation strategies, there is a serious need to investigate both the inhibition of U(VI) reduction and the reoxidation of U(IV) under varying geochemical conditions (Suzuki and Suko, 2006). Future work should consider both the geochemical and physical conditions under which uraninite reoxidation occurs, since both geochemical conditions and the uraninite particle size appear to influence U(IV) reoxidation. Further work that identifies the geochemical conditions under which U(VI) reduction is inhibited is also required.

11.2. Research on microorganisms

Microbial distributions within the subsurface are poorly understood, particularly those related to remediation schemes. The present work has demonstrated the significant impact that different bacterial distributions may exert on the efficiency of bioimmobilisation remediation strategies. This supports existing work in this area (e.g., Tompson et al., 1996). As modelling of bioremediation strategies is an important method for determining their effectiveness (National Research Council, 1993), data that may be directly applied to modelling applications is valuable. Increased knowledge of microbial residence preferences in heterogeneous media, microbial growth processes, and microbial transport within the subsurface environment are all key areas expected to improve the understanding of, and predictive capabilities for, regarding bioremediation

schemes in general. Research in these areas is particularly important due to the difficulty and high cost involved in obtaining subsurface samples, particularly undisturbed samples.

The use of new non-invasive technologies to observe temporal and spatial microbial dynamics, as well as microbial spatial patterns and their correlations with media or chemical properties are likely to prove particularly useful in this regard. For example, resistivity and acoustic wave propagation may be used to understand how microorganisms influence geochemical processes within the subsurface and the related geophysical properties (Williams et al., 2005). Experimental techniques such as bioluminescence and fibre optic detection may be used to track bacterial transport and aid the understanding of bacterial transport phenomena (Dorn et al., 2005; Oates et al., 2005).

Future work should specifically focus on active microorganisms during the biostimulation phase of in situ remediation strategies. Use of RNA (as opposed to DNA) promises to identify active microbial groups (e.g., North et al., 2004).

Intermediate-scale experiments supported by modelling work are most likely to prove useful in elucidating microbial related phenomena. For example, Murphy et al. (1997) found that that unexpected processes, such as buoyancy effects and biological dynamics (e.g., growth, respiration, cell division, and adhesion/detachment) contributed to biodegradation in heterogeneous media.

With regard to DMRB specifically, future work should continue to identify the differences between the different DMRB strains involved in radionuclide remediation.

11.3. Modelling research work

Future biogeochemical modelling of radionuclide bioremediation schemes that considers porous media heterogeneity in 2D or 3D would be of value, particularly that which explicitly represents heterogeneity in hydraulic conductivity and mineralogy. A comparison between such an approach and multi-porosity approaches is likely to reveal the strengths and weaknesses of each. Comparison of microbial kinetic modelling approaches, such as partial equilibrium and fully kinetic, as well as modelling formulations such as first-order, Monod and Michaelis-Menten should also be explored for their relevance to different scenarios and applications. Future models might further consider the impact of bioclogging and mineral precipitation on porous media hydraulic conductivity, explicit representation of bacterial biofilms or microcolonies, different OC fractions, gas bubble evolution, and surface complexation to a variety of different minerals (e.g., different iron oxides).

Modelling work on upscaling hydrogeological parameters relevant to reactive transport models is scarce (de Marsily et al., 2005). Considerable work is required at large scales to ascertain whether upscaling is possible, and under what conditions it is relevant for reactive transport modelling.

In the hope that further experimental data on microbial transport becomes available, models that consider this process may be of value in radionuclide remediation modelling. As transport of bacteria may be influenced by cell size (Fontes et al., 1991), motility (Camesano and Logan, 1998; Camper et al., 1993), surface chemistry (Scholl and Harvey, 1992), and shape (Weiss et al., 1995), models which consider bacterial transport and account for bacteria–surface interactions and motility traits may show most promise.

PHREEQC's transport model seriously limits user discretisation of simulations. The code enforces conditions that result in this limitation in order to maintain numerical stability and minimise numerical dispersion. The code might be modified in future to allow enough flexibility in time step and discretisation to allow more straight forward exploration of the reasons for instability.

11.4. Issues related to U immobilisation strategies

This research has identified a number of potential problems related to the successful application of U immobilisation strategies and future avenues of research which might aid in solving such problems.

The flushing of pore water through sediments in order to remove nitrate and aluminium and create a favourable pH condition for DMRB has been conducted in both the laboratory (Gu et al., 2005) and in the field (Wu et al., 2006a,b). This technique provides

an effect strategy for dealing with U-contaminated sediment unfavourable for DMRB activity prior to biostimulation. However, the laboratory study conducted by Gu et al. (2005) appeared to lack bioactivity following flushing. The authors considered that the flushing and conditioning of the system had killed or removed the bacteria required and subsequently injected biomass into the system, after which U(VI) reduction was successful. Thus, it is possible that under certain conditions, flushing and conditioning of contaminated sediments may lead to repercussions which inhibit the success of the strategy. Future work might explore the impact of changing geochemical conditions and biomass transport under such circumstances to identify the inhibitory factors.

The results of work conducted in Chapter 8 demonstrated that under reoxidation of previously immobilised U, a U(VI) concentration spike higher than the upgradient concentration is likely to migrate downgradient. In certain situations, this may be used to advantage by assisting in the removal of U(VI) from the site. Alternatively, advanced treatments might be used to maintain the reduced redox state within the remediated zone. Future research might investigate the potential for injection strategies to foster a geochemical environment that encourages the formation of iron sulphide minerals in order to maintain immobilised U within the site.

Research has pointed out that as Fe(III) oxides become depleted near the point of OC injection, sulfate reducers can become the dominant DMRB species (Anderson et al., 2003). This appears to cause fouling near field site wells, resulting in U(VI) circumventing the biostimulated zone (Jaffé, 2007). As a consequence, an increasing

proportion of OC may be consumed by non-U reducing bacteria leading to a net decrease in remediation efficiency. This emphasises the need to identify strategies able to maintain the dominance of Fe-reducing bacteria (Anderson et al., 2003). It is possible that injection of Fe into the treatment zone may alleviate this problem.

Further research on radioactive decay products, and the influence of geochemical conditions on the solubility of daughter products would be valuable.

12. References

Abdelouas, A., L. Yongming, W. Lutze, and H. E. Nuttall (1998a). Reduction of U(VI) to U(IV) by indigenous bacteria in contaminated ground water. J. Contam. Hydrol., 35, 217–233.

Abdelouas, A., Lutze, W., Nuttall, E. (1998b). Chemical reactions of uranium in ground water at a mill tailings site. J. Contam. Hydrol., 34, 343-361.

Abdelouas, A., W. Lutze, W. Gong, E. H. Nuttall, B. A. Strietelmeier, and B. J. Travis (2000). Biological reduction of uranium in groundwater and subsurface soil. Sci. Total Environ., 250, 21-35.

Abrams, R. H., K. Loague, and D. B. Kent (1998). Development and testing of a compartmentalized reaction network model for redox zones in contaminated aquifers. Water Resour. Res., 34, 1531– 1542.

Abrams, R.H., and K. Loague (2000a). A compartmentalized solute transport model for redox zones in contaminated aquifers: 1: Theory and development. Water Resour. Res., 36, 2015–2030.

Abrams, R.H., and K. Loague (2000b). A compartmentalized solute transport model for redox zones in contaminated aquifers: 2. Field-scale simulations. Water Resour. Res., 36, 2015–2030.

Ahmadi, A., M. Quintard, and S. Whitaker (1998). Transport in chemically and mechanically heterogeneous porous media V: two-equation model for solute transport with adsorption. Adv. Water Resour., 22, 59–86.

Ahmann D., A.L. Roberts, H.F. Krumholz, and F.M.M. Morel (1994). Microbe grows by reducing arsenic. Nature, 371, 750.

Albrechtsen, H.-J. (1994). Distribution of bacteria, estimated by a viable count method, and heterotrophic activity in different size fractions of aquifer sediment. Geomicrobiol. J., 12, 253-264.

Alcacio, T.E., D. Hesterberg, J.W. Chou, J.D. Martin, S. Beauchemin, and D.E. Sayers (2001). Molecular scale characteristics of Cu(II) bonding in goethite-humate complexes. Geochim. Cosmochim. Acta, 65, 1355–1366.

Allison, J.D., D.S. Brown, K.J. Novo-Gradec (1991). MINTEQA2/PRODEFA2, A geochemical assessment model for environmental systems: Version 3.0 user's manual. U.S. EPA: Athens, GA.

Amirbaham, A., R. Schöneberger, C.A. Johnson, L. Sigg (1998). Aqueous- and solid-phase biogeochemistry of a calcareous aquifer system downgradient from a municipal solid waste landfill (Winterthur, Switzerland). Environ. Sci. Technol., 32, 1933-1940.

Amos, R.T., Mayer, K.U., Blowes, D.W., Ptacek, C.J. (2004). Reactive transport modelling of column experiments for the remediation of acid mine drainage. Environ. Sci. Technol., 38, 3131–3138.

Amos, R.T., and Mayer, K.U. (2006). Investigating the role of gas bubble formation and entrapment in contaminated aquifers: Reactive transport modelling. J. Contam. Hydrol., 87, 123–154.

Amter, S. (1989). Natural analogues. *In:* Ross, B. (Ed.), Models of Nuclear Waste Repository Performance, Eng. Geol., 26, 431-440.

Anderson, R.T., H.A. Vrionis, I. Ortiz-Bernad, C.T. Resch, A. Peacock, R. Dayvault, S. Marutzky, D.R. Metzler, K. Karp, M. Lowe, D.C. White, P.E. Long, and D.R. Lovley (2003). Stimulating the in situ activity of Geobacter species to remove uranium from the groundwater of a uranium-contaminated aquifer. Appl. Environ. Microbiol., 69, 5884–5891.

Appelo, C., and D. Postma (1993). Geochemistry, Groundwater and Pollution. A.A. Balkema, Rotterdam, Holland.

Applegate, D.H., and J.D. Bryers (1991). Effects of carbon and oxygen limitations and calcium concentrations on biofilm removal processes. Biotechnol. Bioeng., 37, 17–25.

Askarieh, M.M., A.V. Chambers, F.B.D. Daniel, P.L. FitzGerald, G.J. Holtom, N.J. Pilkington, and J.H. Rees (2000). The chemical and microbial degradation of cellulose in the near field of a repository for radioactive wastes. Waste Manage., 20, 93-106.

Baedecker, M.J., and W. Back (1979). Hydrogeological processes and chemical reactions at a landfill. Ground Water, 17, 429–437.

Bajracharya K., and D.A. Barry (1997). Nonequilibrium solute transport parameters and their physical significance: numerical and experimental results. J. Contam. Hydrol., 24, 185–204.

Balkwill, D.L. (1989). Numbers, diversity, and morphological characteristics of aerobic chemoheterotrophic bacteria in deep subsurface sediments from a site in South Carolina. Geomicrobiol. J., 7, 33–52.

Barenblatt, G.E., I.P. Zheltov, and I.N. Kochina (1960). Basic concept of the theory of seepage of homogeneous liquids in fissured rocks. J. Appl. Math. Mech., Eng. Transl., 24, 1286–1303.

Bargar, J.R., R. Reitmeyer, J.J. Lenhart, and J.A. Davis (2000). Characterization of U(VI)-carbonato ternary complexes on hematite: EXAFS and electrophoretic mobility measurements. Geochim. Cosmochim. Acta, 64, 2737–2749.

Barnett, M.O., P.M. Jardine, S.C. Brooks, and H.M. Selim (2000). Adsorption and transport of uranium(VI) in subsurface media. Soil Sci. Soc. Am. J., 64, 908-917.

Barnett, M.O., P.M. Jardine, and S.C. Brooks (2002). U(VI) adsorption to heterogeneous subsurface media: application of a surface complexation model. Environ. Sci. Technol., 36, 937-942.

Barry, D.A., J.L. Starr, J.-Y. Parlange, and R.D. Braddock (1983). Numerical analysis of the snowplow effect. Soil Sci. Soc. Am. J., 47, 862-868.

Barry, D.A., H. Prommer, C.T. Miller, P. Engesgaard, A. Brun, and C. Zheng (2002). Modeling the fate of oxidizable organic contaminants in groundwater. Adv. Water Resour., 25, 945-983.

Basberg, L., and P. Engesdaard (1999). A sequential partial equilibrium approach to mulit-component reactive transport modelling of redox processes in groundwater impacted by landfill leachate, Chapter 5. *In:* Field and numerical investigations of landfill leachate in the Gardermoen glaciofluvial aquifer, Norway (pp. 64-106) Ph.D thesis by Leif Basberg, Faculty of Applied Earth Sciences, Department of Geology and Mineral Resources Engineering, The Norwegian University of Science and Technology.

Batstone, D.J., J. Keller, R.B. Newell, and M. Newland (2000). Modelling anaerobic degradation of complex wastewater. I: model development. Bioresource Technol., 75, 67-74.

Baveye, P., and A. Valocchi. (1989). An evaluation of mathematical models of the transport of biologically reacting solutes in saturated soil and aquifers. Water Resour. Res., 25, 1413-1421.

Baveye, P., and A. Valocchi. (1991). Reply. Water Resour. Res., 27, 1379-1380.

Baveye, P., P. Vandevivere and D. De Lozada (1992). Comment on “Biofilm growth and the related changes in the physical properties of a porous media, 1, Experimental investigation” by S.W. Taylor and P.R. Jaffé. Water Resour. Res., 28, 1481-1482.

Bayer, E.A., R. Kenig, and R. Lamed (1983). Adherence of Clostridium thermocellum to cellulose. J. Bacteriol., 156, 818–827.

Beadle, I.B., 2002. Long term trench experiment, progress report, DTP 01/03 TN102 Internal report, British Nuclear Fuels plc, U.K.

Becker, U., K.M. Rosso, and M.F. Hochella (2001). The proximity effect on semiconducting mineral surfaces: A new aspect of mineral surface reactivity and surface complexation theory? Geochim. Cosmochim. Acta, 65, 2641–2649.

Benner, R., A.E. Maccubbin, and R.E. Hodson (1984a). Preparation, characterisation, and microbial degradation of specifically radiolabelled 14C lignocelluloses from marine and freshwater macrophytes, Appl. Environ. Microb., 47, 381-389.

Benner, R., A.E. Maccubbin, and R.E. Hodson (1984b). Anaerobic biodegradation of the lignin and polysaccharide components of lignocellulose and synthetic lignin by sediment microflora. Appl. Environ. Microb., 47, 998-1004.

Berkowitz, B. (2002). Characterizing flow and transport in fractured geological media: A review. Advances in Water Resources, 25, 861–884.

Berner, R.A. (1980). Early Diagenesis – A Theoretical Approach. Princeton Univ. Press.

Berner, R.A. (1981a), A new geochemical classification of sedimentary environments, J. Sed. Petrol., 51, 359–365.

Berner R.A. (1981b). Authigenic mineral formation resulting from organic matter decomposition in modern sediments. Fortschr. Miner., 59, 117–135.

Bernhard, G., G. Geipel, V. Brendler, and H. Nitsche (1996). Speciation of uranium in seepage waters of a mine tailing pile studied by time-resolved laser-induced fluorescence spectroscopy (TRLFS). Radiochim. Acta, 74, 87–91.

Bernhard, G., G. Geipel, T. Reich, V. Brendler, S. Amayri, and H. Nitsche (2001). Uranyl(VI) carbonate complex formation: validation of the $Ca_2UO_2(CO_3)$_{3(aq)}species. Radiochim. Acta, 89, 511–518.

Bethke, C.M., and P.V. Brady (2000). How the Kd Approach Undermines Group Water Cleanup. Ground Water, 38, 435–443.

Beveridge TJ, Makin SA, Kadurugamuwa JL & Li Z (1997a) Interactions between biofilms and the environment. FEMS Microbiol. Rev., 20, 291–303

Beveridge, T.J., M.N. Hughes, H. Lee, K.T. Leung, P.K. Poole, I. Savvaidis, S. Silver, and J.T. Trevors (1997b). Metal–microbe interactions: contemporary approaches. Adv. Microbial. Physiol., 38, 177–243.

Beyenal, H., R.K. Sani, B.M. Peyton, A.C. Dohnalkova, J.E. Amonette, and Z. Lewandowski (2004). Uranium Immobilisation by Sulfate-Reducing Biofilms. Environ. Sci. Technol., 38, 2067-2074.

Bezerra, R.M.F., and A.A. Dias (2004). Discrimination among eight modified Michaelis-Menten kinetics models of cellulose hydrolysis with a large range of substrate/enzyme ratios. Appl. Biochem. Biotech., 112, 173-184.

BNFL (2002). Drigg post-closure safety case: near-field biogeochemistry. British Nuclear Fuels plc, U.K., September.

Bolte, J.P., and D.T. Hill (1993). A comprehensive dynamic model of attached growth anaerobic fermenters. Transactions of the ASAE, 36, 1805-1814.

Bond, K.A., J.E. Cross, and F.T. Ewart (1991). Thermodynamic modelling of the effect of organic complexants on sorption behaviour. Radiochim. Acta, 52/53, 433–437.

Bookter, T.J., and R.K.J. Ham (1982). Stabilization of solid waste landfill. Journal Environ. Eng. Div. (Am. Soc. Civ. Eng.), 108, 1089-1100.

Borden, R.C. and P.B. Bedient (1986a). Transport of dissolved hydrocarbons influenced by oxygen-limited biodegradation, 1. Theoretical development. Water Resour. Res., 22, 1973-1982.

Borden, R.C., P.B. Bedient, M.D. Lee, C.H. Ward, and J.T. Wilson (1986b). Transport of dissolved hydrocarbons influenced by oxygen-limited biodegradation, 2. Field application. Water Resour. Res., 22, 1973-1982.

Boudreau, B.P., and B.R. Ruddick (1991). On a reactive continuum representation of organic matter diagenesis. Amer. J. Sci., 291, 507-538.

Bouwer, E.J. and P.L. McCarty (1984). Modelling of trace organics biotransformation in the subsurface. Ground Water, 22, 433-440.

Bouwer, E.J. and G.D. Cobb (1987). Modelling of biological processes in the subsurface. Water Sci. Technol., 19, 769-779.

Boyle, V. (1993) Soils washing. *In:* Pratt, M. (Ed.) Remedial Processes for Contaminated Land (pp 33–53). Institution of Chemical Engineers, Warwickshire.

Bredehoeft, J.D., and L.F. Konikow (1993). Ground-water models: Validate or invalidate. Ground Water, 31, 178–179.

Brooks, S.C., J.K. Fredrickson, S.L. Carroll, D.W. Kennedy, J.M. Zachara, A.E. Plymale, S.D. Kelly, K.M. Kemner, and S. Fendorf (2003). Inhibition of bacterial U(VI) reduction by calcium. Environ. Sci. Technol., 37, 1850–1858.

Brown, G.E., and G.A. Parks (2001). Sorption of Trace Elements on Mineral Surfaces: Modern Perspectives from Spectroscopic Studies and Comments on Sorption in the Marine Environment. Intnl. Geol. Rev., 43, 963–1073.

Brun, A., P. Engesgaard, T. H. Christensen, and D. Rosbjerg (2002). Modelling of transport and biogeochemical processes in pollution plumes: Vejen landfill, Denmark. J. Hydrol., 256, 228-247.

Brusseau, M.L., Z. Gerstl, D. Augustijn, and P.S.C. Rao (1993). Simulating solute transport in an aggregated soil with the dual-porosity model: Measured and optimized parameter values. J. Hydrol., 163, 187–193.

Caccavo, F. Jr., D.J. Lonergan, D.R. Lovley, M. Davis, J.F. Stolz, and M.J. McInerney (1994). Geobacter sulfurreducens sp. nov., a hydrogen and acetate-oxidizing dissimilatory metal reducing microorganism. Appl. Environ. Microbiol., 60, 3752-3759.

Camesano, T.A., and B.E. Logan (1998). Influence of fluid velocity and cell concentration on the transport of motile and nonmotile bacteria in porous media. Environ. Sci. Technol., 32, 1699– 1708.

Camper, A.K., J.T. Hayes, P.J. Sturman, W.L. Jones, and A.B. Cunningham (1993). Effects of motility and adsorption rate coefficient on transport of bacteria through saturated porous media. App. Environ. Microbiol., 59, 3455– 3462.

Canfield, D.E., B. Thamdrup, and J.W. Hansen (1993). The anaerobic degradation of organic matter in Danish coastal sediments: Iron reduction, manganese reduction and sulfate reduction. Geochim. Cosmochim. Acta, 57, 3867-3883.

Cederberg, G.A., R.L. Street, and J.O. Leckie (1985). A groundwater mass transport and equilibrium chemistry model for multicomponent systems. Water Resour. Res., 21, 1095– 1104.

Champ, D.R., and J. Schroeter (1988). Bacterial transport in fractured rock—a field scale tracer test at the Chalk River Nuclear Laboratories. *In:* International Conference on Water and Waste Management, Newport Beach, CA, pp. 1–7.

Chandratillake, M., D.P. Trivedi , M.G. Randall , P.N. Humphreys , and E.J. Kelly (1998). Criteria for compilation of a site-specific thermodynamic database for geochemical speciation calculations. J. Alloy Compd., 271–273, 821–825.

Chaney, R.L. (1997). Phytoremediation of soil metals. Cur. Opin. Biotechnol., 8, 370-384.

Chang, J.R., G.T. Yeh, and T.E. Short (1993). Modelling two-dimensional subsurface flow, fate and transport of microbes and chemicals. Paper presented at International Symposium of Engineering Hydrology, Am. Soc. Civ. Eng., San Francisco, 25– 30 July.

Chang, Y.-J. (2005). In situ biostimulation of uranium reducing microorganisms at the Old Rifle UMTRA site. Ph.D thesis. The University of Tennessee, Knoxville, USA.

Chapelle, F.H., and D.R. Lovley (1992). Competitive exclusion of sulfate reduction by Fe(III)-reducing bacteria: a mechanism for producing discrete zones of high-iron ground water. Ground Water, 30, 29-36.

Chapelle, F.H. (1993). Ground-Water Microbiology and Geochemistry. Wiley, New York, 424 pp.

Chapman, S.W., and B.L. Parker (2005). Plume Persistence Due to Aquitard Back Diffusion Following Dense Nonaqueous Phase Liquid Removal or Isolation. Water Resour. Res., 41, W12411.

Characklis, W.G. (1990). Biofilm processes. *In:* Characklis, W.G., and K.C. Marshall (Eds.), Biofilms, John Wiley and Sons, Inc.

Chen, B., and L. Yaqing (2002). Simulation of thick biofilm growth at the microscale. Appl. Numer. Math., 40, 261–271.

Chen, J.P., and S. Yiacoumi (2002). Modelling of depleted uranium transport in subsurface systems. Water, Air and Soil Poll., 140, 173-201.

Chen, Y.M., L.M. Abriola, P.J.J. Alvarez, P.J. Anid, and T.M. Vogel (1992). Modelling transport and biodegradation of benzene and toluene in sandy aquifer material: Comparison with experimental measurements. Water Resour. Res., 28, 1833-1847.

Chen-Charpentier, B. (1999). Numerical simulation of biofilm growth in porous media. J. Comput. Appl. Math., 103, 55—66.

Cheng, H.-P. (1995) Development and application of a three-dimensional finite element model of subsurface flow, heat transfer, and reactive chemical transport. Ph.D. thesis, Dep. of Civ. and Environ. Eng., Pa. State Univ., University Park.

Cheng, J.R., and G.T. Yeh (1994). Modelling three-dimensional subsurface flow, fate and transport of microbes and chemicals (3DFATMIC). Paper presented at Xth International Conference on Numerical Methods in Water Resources, Univ. of Heidelberg, Heidelberg, Germany, 19–22 July 1994.

Cherblanc, F., A. Ahmadi, and M. Quintard (2003). Two-medium description of dispersion in heterogeneous porous media: calculation of macroscopic properties. Water Resour. Res., 39, 1154–73

Chilakapati, A. (1995). RAFT: A Simulator for ReActive Flow and Transport of Groundwater Contaminants. PNL Report, 10636.

Chilakapati, A., T.R. Ginn, and J.E. Szecsody (1998). An analysis of complex reaction networks in groundwater modelling. Water Resour. Res., 34, 1767–1780.

Chilakapati, A., S. Yabusaki, J. Szecsody, and W. MacEvoy (2000). Groundwater flow, multicomponent transport and biochemistry: development and application of a coupled process model. J. Contam. Hydrol., 43, 303–325.

Childers, S.E., S. Ciufo, and D.R. Lovley (2002). Geobacter metallireducens accesses Fe(III) oxide by chemotaxis. Nature, 416, 767-769.

Chisholm-Brause, C.J., J.M. Berg, R.A. Matzner, and D.E. Morris (2001). Uranium(VI) sorption complexes on montmorillonite as a function of solution chemistry. J. Coll. Inter. Sci., 233, 38–49.

Christensen, T.H., P. Kjeldsen, P.L. Bjerg, D.L. Jensen, J.B. Christensen, A. Baun, H.-J. Albrechtsen, and G. Heron (2001). Biogeochemistry of landfill leachate plumes. Appl. Geochem., 16, 659-718.

Chugh, S., D.P. Chynoweth, W. Clarke, P. Pullammanappallil, and V. Rudolph (1999). Degradation of unsorted municipal solid waste by a leach-bed process. Bioresource Technol., 69, 103-115.

Chynoweth, D.P., J. Owens, D. O'Keefe, J.F.K. Earle, G. Bosch, and R. Legrand (1992). Sequential batch anaerobic composting of the organic fraction of municipal solid waste. Water Sci. Technol., 25, 327–339.

Clement, T.P. (1997). "RT3D - A Modular Computer Code for Simulating Reactive Multi-Species Transport in 3-Dimensional Groundwater Aquifers", Pacific Northwest National Laboratory, Richland, Washington. (http://bioprocess.pnl.gov/rt3d_pubs.htm#fund)

Clement, T.P., B.S. Hooker, and R.S. Skeen (1996a). Macroscopic models for predicting changes in 3-dimensional groundwater aquifers. Technical report, Pacific Northwest National Laboratory, Richland.

Clement, T.P., Hooker, B.S., Skeen, R.S., (1996b). Macroscopic models for predicting changes in saturated porous media properties caused by microbial growth. Ground Water, 34, 934–942.

Clement, T.P., B.M. Peyton, R.S. Skeen, D.A. Jennings, and J.N. Petersen (1997). Microbial growth and transport in porous media under denitrification conditions: experiments and simulations. J. Contam. Hydrol., 24, 269-285.

Coats, K.H., and B.D. Smith (1964). Dead end pore volume and dispersion in porous media. Soc. Pet. Eng. J., 4, 73-84.

Colberg, P.J., and L.Y. Young (1982). Biodegradation of lignin-derived molecules under anaerobic conditions. Can. J. Microbiol., 28, 886-889.

Colberg, P.J. (1988). Anaerobic microbial degradation of cellulose, lignin, oligolignols, and monoaromatic lignin derivates. *In:* A.J.B. Zehnder (Ed.), Biology of anaerobic microorganisms (pp. 333-372), John Wiley and Sons, UK.

Contois, D.E. (1959). Kinetics of bacterial growth. Relationship between population density and specific growth rate of continuous cultures. J. Gen. Microbiol., 21, 40-50.

Costello, D.J., P.F. Greenfield, and P.L. Lee (1991). Dynamic modelling of a single stage reactor - I. Model derivation. Water Res., 25, 847-858.

Cozzarelli, I.M., J.S. Herman, and M.J. Baedecker (1995). Fate of microbial metabolites of hydrocarbons in a coastal plain aquifer: the role of electron acceptors. Environ. Sci. Technol., 29, 458–469.

Cummings, D.E., O.L. Snoeyenbos-West, D.T. Newby, A.M. Niggemyer, D.R. Lovley, L.A. Achenbach, and R.F. Rosenzweig (2003). Diversity of Geobacteraceae species inhabiting metal-polluted freshwater lake sediments ascertained by 16S rDNA analyses. Microb. Ecol., 46, 257–269.

Cummins, S.P., and C.S. Stuart (1994). Newspaper as a substrate for cellulolytic landfill bacteria. J. Appl. Bacteriol., 76, 195-202.

Cunningham, S.D., W.R. Berti, and J.W. Huang (1995). Phytoremediation of contaminated soils. Trends Biotechnol., 13, 393–397.

Cunningham, J.A., and I. Mendoza-Sanchez (2006). Equivalence of two models for biodegradation during contaminant transport in groundwater. Water Resour. Res., 42, W02416.

Curtis, G.P., J.A. Davis, and D.L. Naftz (2004). Simulation of reactive transport of uranium(VI) in groundwater with variable chemical conditions. Water Res. Res., 42 W04404, doi:10.1029/2005WR003979.

Damköhler, G. (1936). Einflüsse der Strömung, Diffusion und des Wärmeübergangs auf die Leistung von Reaktionsöfen. Ztschr. Elektrochem., 42, 846– 862.

Davis, J.A. (2001). Surface Complexation Modelling of Uranium(VI) Adsorption on Natural Mineral Assemblages. Report NUREG/CR- 6708. U. S. Nuclear Regulatory Commission, Rockville, MD.

Davis, J.A., T.E. Payne, and T.D. Waite (2002). Simulating the pH and pCO2 Dependence of Uranium(VI) Adsorption by a Weathered Schist with Surface Complexation Models. *In:* Geochemistry of Soil Radionuclides, Special Pub. 59 (pp. 61–86). Soil Science Society America, Madison, WI.

de Baere, L. (2000). Anaerobic digestion of solid waste: state-of-the-art. Water Sci. Technol., 41, 283–290.

de Marsily, G., F. Delay, J. Gonçalvès, Ph. Renard, V. Teles, and S. Violette (2005). Dealing with spatial heterogeneity. Hydrogeol. J., 13, 161–183.

De Windt, L., A. Burnol, P. Montarnal, and J. van der Lee (2003). Intercomparison of reactive transport models applied to UO_2 oxidative dissolution and uranium migration. J. Contam. Hydrol., 61, 303– 312.

De Windt, L., D. Pellegrini, and J. van der Lee (2004). Coupled modeling of cement/claystone interactions and radionuclide migration. J. Contam. Hydrol., 68, 165–182.

Deans, H. A. (1963). A mathematical model for dispersion in the direction of flow in porous media. Trans. Soc. Pet. Eng., March, 49–52.

Denac, M., A. Miguel, and I. J. Dunn (1988). Modelling dynamic experiments on the anaerobic degradation of molasses wastewater. Biotechnol. Bioeng., 31, 1-10.

Dentz M, and B. Berkowitz (2003). Transport behaviour of a passive solute in continuous time random walks and multirate mass transfer. Water Resour. Res., 39, 1111. doi:10.1029/2001WR001163.

Detmers, J., U. Schulte, H. Strauss, and J. Kuever (2001). Sulfate reduction at a lignite seam: microbial abundance and activity. Microb. Ecol., 42, 238–247.

DiChristina, T. J. (1992). Effects of nitrate and nitrite on dissimilatory. Fe(III) reduction by Shewanella putrefaciens. J. Bacteriol., 174, 1891–1896.

Dinipoulou, G., R.M. Sterritt, and J.N. Lester (1988). Anaerobic acidogenesis of a complex wastewater: II. Kinetics of growth inhibition, and product formation. Biotechnol. Bioeng., 31, 969-978.

DOE (1991). Subsurface Science Program: Program overview and research abstracts. US Department of Energy, Office of Energy Research, Office of Health and Environmental Research.

DOE (2007a). http://www.er.doe.gov/OBER/ERSD/ersd_nabir.html. Last accessed August 2007.

DOE (2007b). http://www.er.doe.gov/OBER/ERSD/ersd_nabir.html. Last accessed August 2007.

Dorn, J.G., M.L. Brusseau, and R.M. Maier (2005). Real-time, in situ monitoring of bioactive zone dynamics in heterogeneous systems. Environ. Sci. Technol. 39, 8898-8905.

Doyle, O.P., J.D. O'Malley, E.C. Clausen, and J.L. Gaddy (1983). Kinetic improvements in the production of methane from cellulosic residues, *In:* Energy from Biomass and Wastes, VII (pp. 534-545), Institute of Gas Technology, Chicago IL.

Dutton, M.V., and P.N. Humphreys (2005). Assessing the potential of short rotation coppice (SRC) for cleanup of radionuclide-contaminated sites. International Journal of Phytoremediation, 7, 279-293.

Dykhuizen, R.C. (1990). A new coupling term for dual-porosity models. Water Resour. Res., 26, 351–6.

Dykhuizen, R.C. (1987). Transport of solutes through unsaturated fractured media. Water Res., 21, 1531–1539.

Dzombak, D.A. and F.M.M. Morel (1990). Surface complexation modelling: hydrous ferric oxide. John Wiley & Sons Inc.

Eastman, J.A., and J.F. Ferguson (1981). Solubilization of particulate organic carbon during the acid phase of anaerobic digestion. J. Water Pollut. Con. F., 53, 353-367.

El Fadel, M., A.N. Findikakis, and J.O. Leckie (1997). Gas simulation models for solid waste landfills, Critical Reviews in Environmental Science and Technology, 27, 237-283.

Eleazer, W.E., W.S. Odle, Y.-S. Wang, and M.A. Barlaz (1997). Biodegradability of municipal solid waste components in laboratory-scale landfills. Environ. Sci. Technol., 31, 911-917.

Elert, G. (2003). Mass of a Bacterium, The Physics Factbook, accessed 21 March 2006, http://hypertextbook.com/facts/2003/LouisSiu.shtml.

Elias, D.A., L.R. Krumholz, D. Wong, P.E. Long, and J.M. Suflita (2003). Characterization of microbial activities and U reduction in a shallow aquifer contaminiated by uranium mill tailings. Microb. Ecol., 46, 83-91.

El-Fadel, M., A.N. Findikakis, and J.O. Leckie (1989). A numerical model for methane production in managed sanitary landfills. Waste Manage. Res., 7, 31-42.

Escher, A., and W.G. Characklis (1990). Modelling the initial events in biofilm accumulation. *In:* Characklis, W.G. and K.C. Marshall (Eds.), Biofilms, John Wiley and Sons, Inc.

Essaid, H.I., B.A. Bekins, E.M. Godsy, E. Warren, M.J. Baedecker, and I.M. Cozarelli (1995). Simulation of aerobic and anaerobic biodegradation processes at a crude-oil spill site. Water Resour. Res., 31, 3309-3327.

Fang, Y., G.-T. Yeh, and W.D. Burgos (2003). A general paradigm to model reaction-based biogeochemical processes in batch systems. Water Resour. Res., 39, 1083 doi:10.1029/2002WR001694.

Farquhar, G.J., J.F. Sykes (1982). Control of leachate organics in soil. Conserv. Recycling, 5, 55-68.

Federal Register. Environmental Protection Agency EPA, CFR 40 Part 192, groundwater standards for remedial actions at inactive uranium processing sites. Table 1, November 1995, 2866.

Feehley, C.E., C. Zheng, and F.J. Molz (2000). A dual-domain mass transfer approach for modelling solute transport in heterogeneous aquifers: Application to the macrodispersion experiment (MADE) site. Water Resour. Res., 36, 2501-2515.

Felmy, A.R. (1990). GMIN: A computerized chemical equilibrium model using a constrained minimization of the Gibbs free energy. PNL-7281. Technical report, Pacific Northwest National Laboratory, Richland.

Felmy, A.R., D. Girvin, and E.A. Jenne (1984). MINTEQ: A computer program for calculating aqueous geochemical equilibria. Technical report, U.S. Environmental Protection Agency.

Fendorf, S., B.W. Wielinga, and C.M. Hansel (2000). Chromium transformations in natural environments: the role of biological and abiological processes in chromium(VI) reduction. Intl. Geol. Rev., 42, 691–701

Fetter, C. W. (1994). Applied Hydrogeology, 3rd Ed. Upper Saddle River, NJ: Prentice Hall, Inc.

Finneran, K.T., R.T. Anderson, K.P. Nevin, and D.R. Lovley (2002a). Potential for Bioremediation of uranium-contaminated aquifers with microbial U(VI) reduction. Soil Sediment. Contam., 11, 339–357.

Finneran, K.T., M.E. Housewright, and D.R. Lovley (2002b). Multiple influences of nitrate on uranium solubility during bioremediation of uranium-contaminated subsurface sediments. Environ. Microbiol., 4, 510-516.

Fletcher, M., 1977. The effects of culture concentration and age, time, and temperature on bacterial attachment to polystyrene, Can. J. Microbiol., 23:1, 1-6.

Folger, M.T. (1994). Overview of the repository programme. Nucl. Energy, 33, 15.

Fontes, D.E., A.L. Mills, G.M. Hornberger, and J.S. Herman (1991). Physical and chemical factors influencing transport of microorganisms through porous media. Appl. Environ. Microbiol., 57, 2473–2481.

Foree, E.G., and P.L. McCarty (1969). The rate and extent of algal decomposition in anaerobic waters. Proceedings of the 24th Industrial Waste Conference Purdue University, pp. 13-35.

Francis, A.J., C.J. Dodge, F. Lu, G.P. Halada, and C.R. Clayton (1994). XPS and XANES studies of uranium reduction by clostridium sp.. Environ. Sci. Technol., 28, 636-639.

Fredrickson, J.K., J.P. McKinley, B.N. Bjornstad, P.E. Long, D.B. Ringelberg, D.C. White, L.R. Krumholz, J.M. Suflita, F.S. Colwell, R.M. Lehman, and T.J. Phelps (1997). Pore-size constraints on the activity and survival of subsurface bacteria in a late Cretaceous shale-sandstone sequence, northwestern New Mexico. Geomicrobiol. J., 14, 183-202.

Fredrickson, J.K., J.M. Zachara, D.W. Kennedy, M.C. Duff, and Y.A. Gorby (2000). Reduction of U(VI) in goethite (α-FeOOH) suspensions by a dissimilatory metal-reducing bacterium. Geochimica et Cosmochimica Acta, 64, 3085–3098.

Fredrickson, J.K., J.M. Zachara, D.W. Kennedy, C. Liu, M.C. Duff, D.B. Hunter, and A. Dohnalkova (2002). Influence of Mn oxides on the reduction of uranium(VI) by the metal-reducing bacterium *Shewanella putrefaciens*. Geochim. Cosmochim. Act., 66, 3247–3262.

Gadd, G.M., and C. White (1989). Heavy metal and radionuclide accumulation and toxicity in fungi and yeasts. *In:* Metal–Microbe Interactions (pp 19–38) by Poole, R.K. and G.M. Gadd (Eds.). Society for General Microbiology. IRL Press, Oxford, England.

Gan, Q., S.J. Allen, and G.Taylor (2003). Kinetic dynamics in heterogeneous enzymatic hydrolysis of cellulose: an overview, an experimental study and mathematical modelling. Process Biochem., 38, 1003-1018.

Ganesh, R., K.G. Robinson, L. Chu, D. Kucsmas, and G.D. Reed (1999). Reductive precipitation of uranium by *Desulfovibrio desulfuricans*: evaluation of cocontaminant effects and selective removal. Water Res., 33, 3447-3458.

Gardner, W.R., and R.H. Brooks (1957). A descriptive theory of leaching. Soil Sci., 83, 295–304.

Gasol, J.M., and C.M. Duarte (2000). Comparative analyses in aquatic microbial ecology: how far do they go? FEMS Microb. Ecol., 31, 99–106.

Gaudet, J.P., H. Jégat, G. Vachaud, and P.J. Wierenga (1977). Solute transfer, with exchange between mobile and stagnant water, through unsaturated sand. Soil Sci. Soc. Am. J., 41, 665–71.

Gelhar, L.W., C. Welty, and K.R. Rehfeldt (1992). A critical review of data on field-scale dispersion in aquifers. Water Resour. Res., 28, 1955-1974.

Gerke, H.H., and M.T. van Genuchten (1993). A dual-porosity model for simulating the preferential movement of water and solutes in structured porous media. Water Resour. Res., 29, 305–19.

Gerke, H.H., and M.T. van Genuchten (1996). Macroscopic representation of structural geometry for simulating water and solute movement in dual-porosity media. Adv. Water Resour., 19, 343–57.

Ghosh, S., and D. L. Klass (1978). Two phase anaerobic digestion. Proceedings in Biochemistry, 13, 15.

Ghosh, S., and F. G. Pohland (1974). Kinetics of substrate assimilation and product formation in anaerobic digestion. J. Water Poll. Con. F., 46, 748-749.

Ghosh, S., M.P. Henry, and D.L. Klass (1980). Bioconversion of water hyacinth - coastal Bermuda grass-MSW-sludge blends to methane. Biotechnology and Bioengineering Symposium, 10, 163-187.

Gillow, J.B., A.J. Francis, C.J. Dodge, R. Harris, T.J. Beveridge, P.V. Brady, and H.W. Papenguth (1999). Actinide biocolloid formation in brine by halophilic bacteria. Sci. Basis Nucl. Waste Manage. XXII, MRS, 556, 1133–1140.

Glassley, W.E., A.M. Simmons, and J.R. Kercher (2002). Mineralogical heterogeneity in fractured, porous media and its representation in reactive transport models. Appl. Geochem., 17, 699–708.

Glynn, P.D. (2003). Modelling Np and Pu transport with a surface complexation model and spatially variant sorption capacities: implications for reactive transport modelling and performance assessments of nuclear waste disposal sites. Comp. Geosci., 29, 331–349.

Goltz, M.N., and P.V. Roberts (1986). Interpreting organic solute transport data from a field experiment using physical non-equilibrium models. J. Contam. Hydrol., 1, 77–93.

Goltz, M.N., and P.V. Roberts (1988). Simulations of physical nonequilibrium solute transport models: application to a large-scale field experiment. J. Contam. Hydrol., 3, 37–63.

Gorby, Y.A., and D.R. Lovley (1992). Enzymatic uranium precipitation. Environ. Sci. Technol., 26, 205–207.

Gorby, Y.A., F.Jr. Caccavo, H.Jr. Bolton (1998). Microbial reduction of cobalt(III)EDTA in the presence and absence of manganese(IV) oxide. Environ. Sci. Technol., 32, 244–250.

Graham, J., R. Plant, J. Small, and D. Smalley (2003a). Program User's Guide for the code GRM, Version 4.1. BNFL Report 00/EN00127/7/1, Drigg Post-Closure Safety Case Report DTP/150.

Graham, J., G. Towler, P. Abraitis, and J. Small (2003b). Program Verification Report for GRM, Version 4.1. BNFL Report 00/EN00127/7/2, Drigg Post-Closure Safety Case Report DTP/151.

Grenthe, I., J. Fuger, R.J.M. Konings, R.J. Lemire, A.B. Muller, C. Nguyen-Trung, and H. Wanner (Eds.), 1992. Chemical Thermodynamics of Uranium. Nuclear Energy Agency OECD. Elsevier Science Publishers.

Griffioen, J. (1993). Multicomponent cation exchange including alkalinization/ acidification following flow through a sandy sediment. Water Resour. Res., 29, 3005–3019.

Griffioen, J., P. Engesgaard, A. Brun, D. Rodak, I. Mucha, and J.C. Refsgaard (1995). Nitrate and Mn-chemistry in the alluvial Danubian Lowland aquifer, Slovakia, Groundwater Quality, Remediation, and Protection. Proceedings of the Praque Conference, May, IAHS Publ. 225, 87-96.

Griffioen, J.W., D.A. Barry, and J.-Y. Parlange (1998). Interpretation of two-region model parameters. Water Resour. Res., 34, 373-384.

Grisak, G.E., and J.F. Pickens (1980). Solute transfer through fractured media: 1. The effect of matrix diffusion. Water Resour. Res., 16, 719–730.

Grisak, G.E., J.F. Pickens, and J.A. Cherry (1980). Solute transport through fractured media. 2. Column study of fractured till. Water Resour. Res., 16, 731-739.

Gu, B., and J. Chen (2003). Enhanced microbial reduction of Cr(VI) and U(VI) by different natural organic matter fractions. Geochim. Cosmochim. Act., 67, 3575-3582.

Gu, B., W.-M. Wu, M.A. Ginder-Vogel, H. Yan, M.W. Fields, J. Zhou, S. Fendorf, C.S. Criddle, and P.M. Jardine (2005). Bioreduction of Uranium in a Contaminated Soil Column. Environ. Sci. Technol., 39, 4841 -4847.

Guha, H., J.E. Saiers, S. Brooks, P. Jardine, and K. Jayachandran (2001). Chromium transport, oxidation, and adsorption on manganese- coated sand. J. Contam. Hydrol., 49, 311 –334.

Gujer, W. and A.J.B. Zehnder (1983). Conversion processes in anaerobic digestion. Water Sci. Technol., 15, 127-167.

Gurban, I., M. Laaksoharju, B. Madé, and E. Ledoux (2003). Uranium transport around the reactor zone at Bangombe, and Okelobondo (Oklo): examples of hydrogeological and geochemical model integration and data evaluation. J. Contam. Hydrol., 61, 247–264.

Gusakov, A.V., and A.P. Sinitsyn (1985). Kinetics of the enzymatic hydrolysis of cellulose: 1. A mathematical model for a batch reactor process. Water Sci. Technol., 7, 346-352.

Gwo, J.P., P.M. Jardine, G.T. Yeh, and G.V. Wilson (1994). MURF user's guide: a finite element model of multiple-pore-region flow through variably saturated subsurface media. ORNL/GWPO- 011, Oak Ridge National Laboratory, Oak Ridge, Tennessee.

Gwo, J.P., P.M. Jardine, G.V. Wilson, and G.T. Yeh (1995). A multiple-pore-region concept to modelling mass transfer in subsurface media. J. Hydrol., 164, 217–237.

Gwo, J.P., P.M. Jardine, G.V. Wilson, and G.T. Yeh (1996). Using a multiregion model to study the effects of advective and diffusive mass transfer on local physical nonequilibrium and solute mobility in a structured soil. Water Resour. Res., 32, 561–570.

Gwo, J.-P., R. O'Brien, and P.M. Jardine (1998). Mass transfer in structured porous media: embedding mesoscale structure and microscale hydrodynamics in a two-region model. J. Hydrol., 208, 204–22.

Gwo, J.-P., P.M. Jardine, and W. Sanford (2005). Effect of advective mass transfer on field scale fluid and solute movement: Field and modelling studies at a waste disposal site in fractured rock at Oak Ridge National Laboratory, Tennessee, USA. Hydrogeol. J., 13, 565–583.

Haggerty, R., and S. Gorelick (1995). Multiple-rate mass transfer for modelling diffusion and surface reactions in media with pore-scale heterogeneity. Water Resour. Res., 31, 2383–400.

Haggerty, R., and S. M. Gorelick (1998). Modelling mass transfer processes in soil columns with pore-scale heterogeneity. Soil Sci. Soc. Am. J., 62, 62–74.

Haggerty, R., S. McKenna, and L. Meigs (2000). On late-time behaviour of tracer test breakthrough curves. Water Resour. Res., 36, 3467–79.

Hamm, S.-Y., and P. Bidaux (1996). Dual-porosity fractal models for transient flow analysis in fissured rocks. Water Resour. Res., 32, 2733–2745.

Hantush, M.M., and M.A. Marino (1998). Interlayer diffusive transfer and transport of contaminants in stratified formation. I: Theory. J. Hydrol. Eng., 3, 232-240.

Harvey, C., and S.M. Gorelick (2000). Rate-limited mass transfer or macrodispersion: Which dominates plume evolution at the Macrodispersion Experiment (MADE) site? Water Resour. Res., 36, 637-650.

Haselow, J.S., and R.A. Greenkorn (1991). An experimental investigation of the effect of idealized heterogeneity on the dispersion of miscible fluids. Water Resour. Res., 27, 2473–2482.

Hassanizadeh, M., and W.G. Gray (1979a). General conservation equations for multi-phase systems. 1. Averaging procedure. Adv. Water Resour., 2, 131-144.

Hassanizadeh, M. and W.G. Gray (1979b). General conservation equations for multi-phase systems. 2. Mass, momenta, energy, and entropy equations. Adv. Water Resour., 2, 191-203.

Haws, N.W., B.S. Das, P.S.C. Rao (2004). Dual-domain solute transfer and transport processes: Evaluation in batch and transport experiments. J. Contam. Hydrol., 75, 257-280.

Haws, N.W., P.S.C. Rao, J. Šimůnek, and I.C. Poyer (2005). Single-porosity and dual-porosity modelling of water flow and solute transport in subsurface-drained fields using effective field-scale parameters. J. Hydrol., 313, 257-273.

Hazen, T.C., and H.H. Tabak (2005). Developments in bioremediation of soils and sediments polluted with metals and radionuclides: 2. Field research on bioremediation of metals and radionuclides. Reviews in Environmental Science and Bio/Technology, 4, 157–183.

Hebert, H.J. (2003). "Congressional investigators say nuclear cleanup needs overhaul after $18 billion spent". Associated Press, 17 July.

Istok, J.D., J.M. Senko, L.R. Krumholz, D. Watson, M.A. Bogle, A. Peacock, Y.-J. Chang, and D.C. White (2004). In Situ Bioreduction of Technetium and Uranium in a Nitrate-Contaminated Aquifer. Environ. Sci. Technol., 38,468-475.

Heron, G., and T.H. Christensen (1995). Impact of sediment-bound iron on redox buffering in a landfill leachate polluted aquifer Vejen, Denmark. Environ. Sci. Technol., 29, 187–192.

Herr, M., G. Schafer, and K. Spitz (1989). Experimental studies of mass transport in porous media with local heterogeneities. J. Contam. Hydrol., 4, 127–137.

Heukelekian, H. (1927). Decomposition of cellulose in fresh sewage solids, Industrial and Engineering Chemistry, 19, 8.

Hill, D.T., and C.L. Barth (1977). A dynamic model for simulation of animal waste digestion. Journal of Water Pollut. Control Fed., 49, 2129-2143.

Hoeks, J. (1983). Significance of biogas production in waste tips. Waste Management, 1, 323-335.

Holm, J. (1999). Effect of biomass growth on the hydrodynamic properties of groundwater aquifers. Institute of Hydrodynamics and Hydraulic Engineering. Technical University of Denmark, Lyngy. Ph.D Thesis.

Holmes, D.E., K.T. Finneran, R.A. O'Neil, and D.R. Lovley (2002). Enrichment of members of the family Geobacteraceae associated with stimulation of dissimilatory metal reduction in uranium-contaminated aquifer sediments. Appl. Environ. Microb., 68, 2300-2306.

Hostetler, J.C., and R.L. Erickson (1989). FASTCHEM Package 5, Rep. EA- 5870-CCM, Battelle Pac. Northwest Lab., Richland, Wash..

Hsi, C.-K.D., and D. Langmuir (1985). Adsorption of uranyl onto ferric oxyhydroxides: application of the surface complexation site-binding model. Geochim. Cosmochim. Ac., 49, 1931–1941.

Hu, Q., and M.L. Brusseau (1996). Transport of rate-limited sorbing solutes in an aggregated porous medium: A multiprocess non-ideality approach. J. Contam. Hydrol., 24, 53–73.

Huang, C.J. (1983). The effects of dilution rate on the kinetics of anaerobic acidogenesis, Proc. 13th Annual Biochemical Engineering Symposium, P.J. Reilly (Ed.), Iowa State University.

Huang, C.P., and W. Stumm (1973). Specific adsorption of cations on hydrous a-Al2O3. J. Colloid Interface Sci., 22, 231-1941.

Humphreys, P.N., T. Johnstone, D. Trivedi, and A. Hoffman (1995). The biogeochemical transport code DRINK: a mechanistic description. Materials Research Society Symposium Proceedings, 353, 211-218.

Humphreys, P.N., R. McGarry, A. Hoffmann, and P. Binks (1997). DRINK: A biogeochemical source term model for low level radioactive waste disposal sites. FEMS Microbiol. Rev., 20, 552-571.

Hunter, K.S., Y. Wang, and P. Van Cappellen (1998). Kinetic modelling of microbially-driven redox chemistry of subsurface environments: coupling transport, microbial metabolism and geochemistry. J. Hydrol., 209, 53–80.

Huyakorn, P.S., B.H. Lester, and J.W. Mercer (1983). An efficient finite element technique for modelling transport in fractured media, 1, Single-species transport. Water Resour. Res., 19, 841–854.

Istok, J.D., J.M. Senko, L.R. Krumholz, D. Watson, M.A. Bogle, A. Peacock, Y.J. Chang, and D.C. White (2004). In situ bioreduction of technetium and uranium in a nitrate-contaminated aquifer. Environ. Sci. Technol., 38, 468–475.

IWA Task Group for Mathematical Modelling of Anaerobic Digestion Processes (2002). Anaerobic Digestion Model No.1 (ADM1). IAW Publishing. Febrauary 2002.

IAWPRC (International Association on Water Pollution Research and Control) (1986). Scientific and Technical Reports No. 1: Activated sludge model No.1. IAWPRC (now IAWQ) Task Group, July 1986.

Jaffé, P.R. (2007). Personal communication.

Jaffé, P.R., and H.A. Rabitz (1988). NABIR Systems Integration Workshop, Summary of Proceedings. Department of Energy, Office of Biological and Environmental Research, Washington, DC, December 18th.

Jakobsen, R., and D. Postma (1994). In situ rates of sulfate reduction in an aquifer Romo, Denmark and implications for the reactivity of organic matter. Geology, 22, 1103–1106.

Jakobsen, R. and D. Postma (1999). Redox zoning, rates of sulfate reduction and interactions with Fe-reduction and methanogenesis in a shallow sandy aquifer, Rømø, Denmark. Geochim. Cosmochim. Act., 63, 137–151.

Jardine, P.M., G.K. Jacobs, and G.V. Wilson (1993). Unsaturated transport processes in undisturbed heterogenous porous media: I. Inorganic contaminants. Soil Sci. Soc. Am. J., 57, 945–953.

Jarvis, N.J., P.-E. Jansson, P.E. Dik, and I. Messing (1991). Modelling water and solute transport in macroporous soil. I. Model description and sensitivity analysis. J. Soil Sci., 42, 59–70.

Jeon, B.-H., S.D. Kelly, K.M. Kemner, M.O. Barnett, W.D. Burgos, B.A. Dempsey, and E.E. Roden (2004). Microbial reduction of U(VI) at the solid-water interface. Environ. Sci. Technol., 38, 5649-5655.

Johnson G., K. Gupta, D. Putz, Q. Huc, and M. Brusseau (2003). The effect of local-scale physical heterogeneity and nonlinear, rate-limited sorption/ desorption on contaminant transport in porous media. J. Contam. Hydrol., 64, 35–58.

Jones, R.M., J.F. MacGregor, K.L. Murphy, and E.R. Hall (1992). Towards a useful dynamic model of the anaerobic wastewater treatment process: a practical illustration of process identification. Water Sci. Technol., 25, 61-71.

Jørgensen, P.R., T. Helstrup, J. Urup, and D. Seifert (2004). Modelling of non-reactive solute transport in factured clayey till during variable flow rate and time. J. Contam. Hydrol., 68, 193-216.

Julian, H.E., J.M. Boggs, C. Zheng, and C.E. Feehley (2001). Numerical simulation of a natural gradient tracer experiment for the natural attenuation study: flow and physical transport. Ground Water, 39, 534-545.

Jurjovec, J., D.W. Blowes, C.J. Ptacek, and K.U. Mayer (2004). Multicomponent reactive transport modelling of acid neutralization reactions in mill tailings. Water Resour. Res., 40, W11202. doi:10.1029/2003WR002233.

Kabala, Z.J., and G. Sposito (1991). A stochastic model of reactive solute transport with time-varying velocity in a heterogeneous aquifer. Water Resour. Res. 27, 341-350.

Kalmykov, S.N., and G.R. Choppin (2000). Mixed Ca2/UO2/CO2 complex formation at different ionic strengths. Radiochim. Acta 88, 603–606.

Keating E.H., and J.M. Bahr (1998). Reactive transport modelling of redox geochemistry: Approaches to chemical disequilibrium and reaction rate estimation at a site in northern Wisconsin. Water Resour. Res., 34, 3573-3584.

Kelly, S.D., M.I. Boyanov, B.A. Bunker, J.B. Fein, D.A. Fowle, N. Yee, and K.M.J. Kemner (2001). XAFS determination of the bacterial cell wall functional groups responsible for complexation of Cd and U as a function of pH. Synchrotron Radiat. 8, 946-948.

Kent, D.B., J.A. Davis, L.C.D. Anderson, B.A. Rea, and T.D. Waite (1994). Transport of chromium and selenium in the suboxic zone of a shallow aquifer: influence of redox and adsorption reactions. Water Resour. Res., 30, 1099–1114.

Kent, D.B., R.H. Abrams, J.A. Davis, J.A. Coston, and D.R. LeBlanc (2000). Modelling the influence of variable pH on the transport of zinc in a contaminated aquifer using semi-empirical surface complexation models. Water Resour. Res., 36, 3411–3425.

Khalil, M.A.K., and R.A. Rasmussen (1989). Climate-induced feedbacks for the global cycles of methane and nitrous oxide. Tellus, Series B, 41B:5, 554-559.

Kieft, T.L., J.K. Fredrickson, J.P. McKinley, B.N. Bjornstad, S.A. Rawson, T.J. Phelps, F.J. Brockman, and S.M. Pfiffner (1995). Microbiological comparisons within and across contiguous lacustrine, paleosol, and fluvial subsurface sediments. App. Environ. Microbiol., 61, 749-757.

Kim, S-B., and M. Y. Corapcioglu (2002). Contaminant transport in dual-porosity media with dissolved organic matter and bacteria present as mobile colloids. J. Contam. Hydrol., 59, 267– 289.

Kindred, J.S., and M.A. Celia (1989). Contaminant transport and biodegradation, 2. Conceptual model and test simulation. Water Resour. Res., 25, 1149-1160.

Kinzelbach, W., W. Schäfer, and J. Herzer (1991). Numerical modelling of natural and enhanced denitrification processes in aquifers. Water Resour. Res., 27, 1123-1135.

Kjeldsen, P. (1986). Attenuation of landfill leachate in soil and aquifer material. Ph.D. thesis. Technical University of Denmark. Dept. of Environmental Engineering, Lyngby.

Kjeldsen, P. and T. H. Christensen (1984). Soil attenuation of acid phase landfill leachate. Waste Management Resources, 2, 247-263.

Kohler, M., G.P. Curtis, D.B. Kent, and J.A. Davis (1996). Experimental investigation and modelling of uranium(VI) transport under variable chemical conditions. Water Res. Res., 32, 3539–3551.

Kohler, M., B.D. Honeyman, and J.O. Leckie (1999). Neptunium(V) Sorption on Hematite (α-Fe2O3) in Aqueous Suspension: The effect of CO_2. Radiochim. Acta, 85, 33–48.

Konikow, L.F., and J.D. Bredehoeft (1992). Ground-water models cannot be validated. Adv. Water Resour., 15, 75– 83.

Koretsky, C. (2000). The significance of surface complexation reactions in hydrologic systems: A geochemist's perspective. J. Hydrol., 230, 127–171.

Koß, V. (1988). Modelling of uranium VI sorption and speciation in a natural sediment-groundwater system. Radiochim. Acta, 44/45, 403–406.

Kräutle, S., and P. Knabner (2005). A new numerical reduction scheme for fully coupled multicomponent transport-reaction problems in porous media. Water Resour. Res., 41, W09414.

Krumholz, L.R., J.P. McKinley, G.A. Ulrich, and J.M. Suflit (1997). Confined subsurface microbial communities in Cretaceous rock. Nature, 386, 64-66.

Kuivila, K.M., J.W. Murray, A.H. Devol, and P.C. Novelli (1989). Methane production, sulfate reduction and competition for substrates in the sediments of Lake Washington. Geochim. Cosmochim. Acta., 53, 409–416.

L. de Baere (2000). Anaerobic digestion of solid waste: state-of-the-art. Water Sci. Technol., 41, 283–290.

De Windt, L., A. Burnol, P. Montarnal, J. van der Lee. 2003. Intercomparison of reactive transport models applied to UO_2 oxidative dissolution and uranium migration. J. Contam. Hydrol., 61, 303– 312.

Lai, T.E., P. Pullammanappallil, and W.P. Clarke (2005). A model to predict the effect of buffer on the start-up of slurry and leach-bed anaerobic digestion of MSW, Proceedings of Sardinia 2003, the Ninth International Waste Management and Landfill Symposium, October 2003.

Lamed, R., J. Naimark, E. Morgenstern, and E.A. Bayer (1987). Specialized surface structure in cellulolytic bacteria. J. Bacteriol., 169, 3792–3800.

Landa, E.R., and J.R. Gray (1995). US Geological Survey – Research on the environmental fate of uranium mining and milling wastes. Environ. Geol., 26, 19-31.

Landa, E.R. (2004). Uranium mill tailings: nuclear waste and natural laboratory for geochemical and radioecological investigations. J. Environ. Radioactiv., 77, 1–27.

Langmuir, D. (1978). Uranium solution-mineral equilibria at low temperatures with applications to sedimentary ore deposits. Geochim. Cosmochim. Acta, 42, 547-569.

Langmuir, D. (1997). Aqueous Environmental Geochemistry. Prentice Hall. 600 pp.

Larsson, M., and N. Jarvis (1999). Evaluation of a dual-porosity model to predict field-scale solute transport in a macroporous soil. J. Hydrol., 215, 153–71.

Lay, J.-J., Y.-J. Lee, and T. Noike (1999). Feasibility of biological hydrogen production from organic fraction of municipal solid waste. Water Resour., 33, 2579-2586.

Lee, D.D., and T.L. Donaldson (1984). Dynamic simulation model for anaerobic digestion of cellulose. Biotechnology and Bioengineering Symposium, 14, 503-508.

Lee, Y.-H., and L.T. Fan (1982). Kinetic studies of enzymatic hydrolysis of insoluble cellulose: analysis of the initial rates. Biotechnol. Bioeng., 124, 2383-2406.

Lee, J.J., I.H. Jung, W.B. Lee, J.O. Kim (1993). Computer and experimental simulations of the production of methane gas from municipal solid waste. Water Sci. Technol., 27, 224-35.

Lehman, R.M., S.P. O'Connell, A. Banta, J.K. Fredrickson, A.-L. Reysenbach, T.L. Kieft, and F.S. Colwell (2004). Microbiological comparison of core and groundwater samples collected from a fractured basalt aquifer with that of dialysis chambers incubated in situ. Geomicrobiol. J., 21, 169–182.

Lenhart, J.J., and B.D. Honeyman (1999). Uranium(VI) sorption to hematite in the presence of humic acid. Geochim. Cosmochim. Acta, 63, 2891–2901.

Lensing, H.J., M. Vogt, and B. Herrling (1994). Modelling of biologically mediated redox-processes in the subsurface. J. Hydrol., 159, 125-143.

Li, L., D.A. Barry, P.J. Culligan-Hensley, and K. Bajracharya (1994). Mass transfer in soils with local stratification of hydraulic conductivity. Water Resour. Res., 30, 2891-2900.

Lichtner, P.C., 1996a. Continuum formulation of multicomponent– multiphase reactive transport. Ch. 1. *In:* Lichtner, P.C., C.I. Steefel, and E.H. Oelkers (Eds.), Reactive

Transport in Porous Media, Reviews in Mineralogy, vol. 34. Mineralogical Society of America, Washington, DC.

Liu, M.-X., and Z.-X. Chen (1990). Exact solution for flow of slightly compressible fluids through multipleporosity, multiple-permeability media. Water Resour. Res., 26, 1393-1400.

Liu, C., and T. Narasimhan (1989a)., Redox-controlled multiple-species reactive chemical transport, 1, Model development. Water Resour. Res., 25, 869–882.

Liu, C., and T. Narasimhan (1989b). Redox-controlled multiple-species reactive chemical transport, 2, Verification and application. Water Resour. Res., 25, 883–910.

Liu, C., Y.A. Gorby, J.M. Zachara, J.K. Fredrickson, and C.F. Brown (2002a). Reduction Kinetics of Fe(III), Co(III), U(VI), Cr(VI), and Tc(VII) in Cultures of Dissimilatory Metal-Reducing Bacteria. Biotechnol. Bioeng., 80, 637-649.

Liu, C., J.M. Zachara, J.F. Fredrickson, D.W. Kennedy, and A. Dohnalkova (2002b). Modelling the Inhibition of the Bacterial Reduction of U(VI) by -$MnO_{2(s)}$. Environ. Sci. Technol., 36, 1452-1459.

Llabres-Luengo, P., and J. Mata-Alvarez (1987). Kinetic study of the anaerobic digestion of straw-pig manure mixtures. Biomass, 14, 129-142.

Lloyd, J.R. (2003). Microbial reduction of metals and radionuclides. FEMS Microbiol. Rev., 27, 411–425

Lloyd, J.R., and L.E. Macaskie (1996). A novel phosphorImager based technique for monitoring the microbial reduction of technetium. Appl. Environ. Microbiol., 62, 578–582

Lloyd, J.R., and L.E. Macaskie (2000). Bioremediation of radioactive metals. *In:* Lovley, D.R. (Ed.) Environmental Microbe–Metal Interactions (pp 277–327). ASM Press, Washington, D.C.

Lloyd, J.R., and L.E. Macaskie (2002). The biochemical basis of radionuclide-microbe interaction. *In:* Livens, F.R., and M. Keith-Roach (Eds.), Microbiology and Radioactivity, Elsevier.

Lloyd, J.R., and J.C. Renshaw (2005). Microbial transformations of radionuclides: fundamental mechanisms and biogeochemical implications. Met. Ions Biol. Syst., 44, 205-40.

Lloyd, J.R., V.A. Sole, C.V. Van Praagh, and D.R. Lovley (2000). Direct and Fe(II)-mediated reduction of technetium by Fe(III)-reducing bacteria. Appl. Environ. Microbiol., 66, 3743–3749

Lockhart, R. (2004). Molecular biological characterisation of a low level radioactive waste disposal site. Ph.D thesis, University of Liverpool, U.K., submitted February 2004.

Lockhart, R.J, M.I. Van Dyke, I.R. Beadle, P. Humphreys, and A.J. McCarthy (2006). Molecular Biological Detection of Anaerobic Gut Fungi (Neocallimastigales) from Landfill Sites. Appl. Environ. Microb., 72, 5659–5661.

Lovley, D.R. (1993). Dissimilatory metal reduction. Ann. Rev. Microbiol., 47, 263-290.

Lovley, D.R. (1995). Bioremediation of organic and metal contaminants with dissimilatory metal reduction. J. Ind. Microbiol., 14, 85-93.

Lovley, D.R., and F.H. Chapelle (1995). Deep subsurface microbial processes. Rev. Geophys., 33, 365-381.

Lovley, D.R., and S. Goodwin (1988). Hydrogen concentrations as an indicator of predominant terminal electron accepting reactions in aquatic sediments. Geochim. Cosmochim. Acta., 52, 2993-3003.

Lovley, D.R., and E.J.P. Phillips (1988). Novel mode of microbial energy metabolism: organic carbon oxidation coupled to dissimilatory reduction of iron or manganese. Appl. Environ. Microbiol., 54, 1472–1480.

Lovley, D.R., and E.J.P. Phillips (1992a). Bioremediation of uranium contamination with enzymatic uranium reduction. Environ. Sci. Technol., 26, 2228–2234.

Lovley, D.R., and E.J.P. Phillips (1992b). Reduction of uranium by Desulfovibrio desulfuricans. Appl. Environ. Microbiol., 58, 850–856.

Lovley, D.R., E.J.P. Phillips, Y.A. Gorby, and E.R. Landa (1991). Microbial reduction of uranium. Nature, 350, 413–416.

Lovley, D.R., E.E. Roden, E.J.P. Phillips, and J.C. Woodward (1993). Enzymatic iron and uranium reduction by sulfate-reducing bacteria. Mar. Geol., 113, 41-53.

Luo, J., O.A. Cirpka, W. Wu, M.N. Fienen, P.M. Jardine, T.L. Mehlhorn, D.B. Watson, G.S. Criddle, and P.K. Kitanidis (2005). Mass-transfer limitations for nitrate removal in a uranium-contaminated aquifer. Environ. Sci. Technol., 39, 8453-8459.

Luo, J., F.-A. Weber, O.A. Cirpka, W.-M. Wu, J.L. Nyman, J. Carley, P.M. Jardine, C.S. Criddle, and P.K. Kitanidis (2007). Modelling in-situ uranium(VI) bioreduction by sulfate-reducing bacteria. J. Contam. Hydrol., doi:10.1016/j.jconhyd.2007.01.004.

Lynd, L.R., H.E. Grethlein, and R.H. Wolkin (1989). Fermentation of cellulosic substrates in batch and continuous cultures by Clostridium therocellum. Appl. Environ. Microbiol., 55, 3131-3139.

Lynd, L.R., P.J. Weimer, W.H. van Zyl, and I.S. Pretorius (2002). Microbial Cellulose Utilization: Fundamentals and Biotechnology. Microbiol. Mol. Biol. R., 66, 506-577.

Macaskie, L.E. (1991). The application biotechnology to the treatment of wastes produced from the nuclear fuel cycle: biodegradation and bioaccumulation as a means of treating radionuclide-containing streams. Crit. Rev. Biotechnol., 11, 41–112

Macaskie, L.E., P. Yong, T.C. Doyle, M.G. Roig, M. Diaz, and T. Manzano (1997). Bioremediation of uranium-bearing wastewater: Biochemical and chemical factors influencing bioprocess application. Biotechnol. Bioeng., 53, 100-109.

MacQuarrie, K.T.B., and K.U. Mayer (2005). Reactive transport modelling in fractured rock: A state-of-the-science review. Earth-Science Reviews, 72, 189–227.

MacQuarrie, K.T.B., E.A. Sudicky, and E.O. Frind (1990). Simulation of biodegradable organic contaminants in groundwater: 1. Numerical formulation in principle directions. Water Resour. Res., 26, 207-222.

Madsen, E.L., and W.C. Ghiorse (1993). Groundwater microbiology: subsurface ecosystem processes. *In:* T.E. Ford (Ed.), Aquatic microbiology: an ecological approach (pp. 167–213). Blackwell, Oxford.

Manton, S.T., T. Johnston, D. Trivedi, S.M.A. Hoffman, and P.M. Humphreys (1995). Modelling radionuclide migration in the near surface environment with the coupled geochemical/microbiological code DRINK. Radiochim. Acta, 68, 75-79.

Mao, X., H. Prommer, D.A. Barry, C.D. Langevin, B. Panteleit, and L. Li (2006). Three-dimensional model for multi-component reactive transport with variable density groundwater flow. Environ. Modell. Softw., 21, 615-628.

Maraga, M. (2001). Prediction of mass-transfer coefficient for solute transport in porous media. J. Contam. Hydrol., 50, 1–19.

Martino, D.P., E.L. Grossman, G.A. Ulrich, K.C. Burger, J.L. Schlichenmeyer, J.M. Suflita, and J.W. Ammerman (1998). Microbial Abundance and Activity in a Low-Conductivity Aquifer System in East-Central Texas. Microb. Ecol., 35, 224–234.

Mata-Alvarez, J., S. Macé, and P. Llabrés (2000). Anaerobic digestion of organic solid wastes. An overview of research achievements and perspectives. Bioresour. Technol., 74, 3-16.

Mayer, K.U. (1999). A numerical model for multicomponent reactive transport in variably saturated porous media, Ph.D thesis, Department of Earth Sciences, University of Waterloo.

Mayer, F., M.P. Coughlan, Y. Mori, and L.G. Ljungdahl (1987). Macromolecular organization of the cellulolytic enzyme complex of Clostridium thermocellum as revealed by electron microscopy. Appl. Environ. Microbiol., 53, 2785–2792.

Mayer, K.U., E.O. Frind, and D.W. Blowes (2002). A numerical model for the investigation of reactive transport in variably saturated media using a generalized formulation for kinetically controlled reactions. Water Resour. Res., 38, 1301–1321.

McCarty, P.L. (1975). Stoichiometry of biological reactions. Progress in Water Technology, 7, 157-172.

McCarty, P.L., and F.E. Mosey (1991). Modelling of anaerobic digestion processes. Water Sci. Technol., 24, 17-33.

McHale, A.P., and S. McHale (1994). Microbial biosorption of metals: potential in the treatment of metal pollution. Biotechnol. Adv., 12, 647–652.

McKay, L.D., J.A. Cherry, R.C. Bales, M.T. Yahya, and C.P. Gerba (1993). A field example of bacteriophage as tracers of fracture flow. Environ. Sci. Technol., 27, 1075–1079.

McMahon, P.B., and F.H. Chapelle (1991). Microbial production of organic acids in aquitard sediments and its role in aquifer geochemistry. Nature, 349, 233-235.

McNab, W.W., and T.N. Narasimhan (1994). Modelling reactive transport of organic compounds in groundwater using a partial redox disequilibrium approach. Water Resour. Res., 30, 2619-2636.

McNab Jr, W.W., and T.N. Narasimhan (1995). Reactive transport of petroleum hydrocarbon constituents in a shallow aquifer: modelling geochemical interactions between organic and inorganic species. Water Resour. Res., 31, 2027-2033.

Meile, C., K. Tuncay, and P. Van Cappellen (2003). Explicit representation of spatial heterogeneity in reactive transport models: application to bioirrigated sediments. J. Geochem. Explor., 78-79, 231-234.

Michalsen, M.M., B.A. Goodman, S.D. Kelly, K.M. Kemner, J.P. McKinley, J.W. Stucki, and J.D. Istok (2006). Uranium and Technetium Bio-Immobilisation in Intermediate-Scale Physical Models of an In Situ Bio-Barrier. Environ. Sci. Technol., 40, 7048 -7053.

Middelburg, J.J. (1989). A simple rate model for organic matter decomposition in marine sediments. Geochim. Cosmochim. Acta., 53, 1577-1581.

Miller, C.W., and L.V. Benson (1983)., Simulation of solute transport in a chemical reactive heterogeneous system: Model development and application. Water Resour. Res., 19, 381– 391.

Moletta, R., D. Verrier, and G. Albagnac (1986). Dynamic modelling of anaerobic digestion. Water Res., 20, 427-434.

Molins, S., J. Carrera, C. Ayora, and M.W. Saaltink (2004). A formulation for decoupling components in reactive transport problems. Water Resour. Res., 40, W10301.

Monod, J. (1942). Recherches sur la croissance des culture bacteriennes. Herman et Cie, Paris.

Monod, J. (1949). The growth of bacterial cultures. Annual Reviews of Microbiology, 3, 371-394.

Morin, R.H. (2006). Negative correlation between porosity and hydraulic conductivity in sand-and-gravel aquifers at Cape Cod, Massachusetts, USA. J. Hydrol., 316, 43-52.

Movagarnejad, K., M. Sohrabi, T. Kaghazchi, and F. Vahabzadeh (2000). A model for the rate of enzymatic hydrolysis of cellulose in heterogeneous solid–liquid systems. Biochem. Eng. J., 4, 197–206.

Movagarnejad, K., M. Sohrabi, T. Kaghazchi, and F. Vahabzadeh (2003). A model for the rate of enzymatic hydrolysis of some cellulose waste materials in solid-liquid systems. Biochem. Eng. J., 14, 1-8.

Murphy, E.M., J.A. Schramke, J.K. Fredrickson, H.W. Bledsoe, A.J. Francis, D.S. Sklarew, and J.C. Linehan (1992). The influence of microbial activity and sedimentary organic carbon on the isotope geochemistry of the Middendorf aquifer. Water Resour. Res., 28, 723–740.

Murphy, E.M., T.R. Ginn, A. Chilakapati, C.T. Resch, J.L. Phillips, T.W. Wietsma, and C.M. Spadoni (1997). The influence of physical heterogeneity on microbial degradation and distribution in porous media. Water Resour. Res., 33, 1087-1103.

Musslewhite, C., M.J. McInerney, H. Dong, T.C. Onstott, M. Green-Blum, D. Swift, S. MacNaughton, D.C. White, C. Murray, J.-Y. Chien (2003). The factors controlling microbial distribution and activity in the shallow subsurface. Geomicrobiol. J., 20, 245-261.

Narasimhan, T.N., A.F. White, and T. Tokunaga (1986). Groundwater contamination from an inactive uranium mill tailings pile, 2, Application of a dynamic mixing model. Water Resour. Res., 22, 1820– 1834.

Narasimhan, T.N. (1995). Models and modelling of hydrogeologic processes. Soil Sci. Soc. Am. J., 59, 300– 306.

National Research Council (1993). In Situ Bioremediation: When Does It Work? National Academy Press, Washington, DC.

NationalResearchCouncil, 2000. Research needs in subsurface science. National Academy Press, Washington, DC.

Neal, A.L., J.E. Amonette, B.M. Peyton, and G.G. Geesey (2004). Uranium complexes formed at hematite surfaces colonised by sulfate-reducing bacteria. Environ. Sci. Technol., 38, 3019-3027.

Nelson, R.H. (2001). From Waste to wilderness: maintaining biodiversity on nuclear-bomb-building sites. Competitive Enterprise Inst.,Washington, DC.

Nevin, K.P., and D.R. Lovley (2000). Lack of production of electron-shuttling compounds or solubilization of Fe(III) during reduction of insoluble Fe(III) oxide by Geobacter metallireducens. Appl. Environ. Microbiol., 66, 2248–2251.

Nevin, K.P., and D.R. Lovley (2002a). Mechanisms for Fe(III) oxide reduction in sedimentary environments. Geomicrobiol. J., 19, 141-159.

Nevin, K.P., and D.R. Lovley (2002b). Mechanisms for accessing insoluble Fe(III) oxide during dissimilatory Fe(III) reduction by Geothrix fermentans. Appl. Environ. Microbiol., 68, 2294–2299.

Newman, D.K., and R. Kolter (2000). A role for excreted quinones in extracellular electron transfer. Nature, 405, 94–97.

Nitzsche, O., G. Meinrath, and B. Merkel (2000). Database uncertainty as a limiting factor in reactive transport prognosis. J. Contam. Hydrol., 44, 223–237.

Nkedi-Kizza, P., J.W. Biggar, H.M. Selim, M.T. van Genuchten, P.J. Wierenga, J.M. Davison, and D.R. Nielsen (1983). Modelling tritium and chloride 36 transport through an aggregated oxisol. Water Resour. Res., 19, 691–700.

Noike, T., G. Endo, J. Chang, J. Yaguchi, and J. Matsumoto (1985). Characteristics of carbohydrate degradation and the rate limiting step in anaerobic digestion. Biotechnol. Bioeng., 24, 1482-1489.

Nopharatana, A., P.C. Pullammanappallil, and W.P. Clarke (2003). A dynamic mathematical model for sequential leach bed anaerobic digestion of organic fraction of municipal solid waste. Biochem. Eng. J., 13, 21–33.

North, N.N., S.L. Dollhopff, L. Petrie, J.D. Istok, D.L. Balkwill, and J.E. Kostka (2004). Change in bacterial community structure during in situ biostimulation of subsurface sediment cocontaminated with uranium and nitrate. Appl. Environ. Microbiol., 70, 4911–4920.

Nyman, J.L., T.L. Marsh, M.A. Ginder-Vogel, M. Gentile, S. Fendorf, and C. Criddle (2006). Heterogeneous response to biostimulation for U(VI) reduction in replicated sediment microcosms. Biodegradation, 17, 303-316.

Oates, P.M., C. Castenson, C.F. Harvey, M. Pola, and P. Culligan (2005). Illuminating reactive microbial transport in saturated porous media: Demonstration of a visualization method and conceptual transport model. J. Contam. Hydrol., 77, 233– 245.

Odencrantz, J.E. (1992). Modelling of biodegradation kinetics of dissolved organic contaminants in a saturated heterogeneous two-dimensional aquifer. Dept. of Civ. Eng., University of Illinois, Urbana, IL., unpublished Ph.D thesis. www.tri-s.com/articles/dissertation.pdf, Accessed 9th July 2007.

O'Keefe, D.M. and D.P. Chynoweth (2000). Influence of phase separation, leachate recycle and aeration on treatment of municipal solid waste in simulated landfill cells. Bioresource Technol., 72, 55-66.

Oremland, R., J.S. Blum, C. Culbertson, P. Visscher, L. Miller, P. Dowdle, and F. Strohmaier (1994). Isolation, growth and metabolism of an obligately anaerobic, selenate-respiringbacterium, strain SES-3. Appl. Environ. Microbiol., 60, 3011–3019.

Oreskes, N., K. Shrader-Frechette, and K. Belitz (1994). Verification, validation, and confirmation of numerical models in the Earth Sciences. Science, 263, 641–646.

ORNL (1999). http://hbgc.esd.ornl.gov/hbgc123d-1.0/main.shtml. Last accessed July 2007.

ORNL (2007). http://www.esd.ornl.gov/nabirfrc/. Last accessed July 2007.

Ortiz-Bernad, I., R.T. Anderson, H.A. Vrionis, and D.R. Lovley (2004a). Vanadium respiration by *Geobacter metallireducens*: a novel strategy for the in situ removal of vanadium from groundwater. Appl. Environ. Microbiol., 70: 3091–3095.

Ortiz-Bernard, I., R.T. Anderson, H.A. Vrionis, and D.R. Lovley (2004b). Resistance of solid-phase U(VI) to microbial reduction during in situ bioremediation of uranium-contaminated groundwater. Appl. Environ. Microbiol., 70, 7558–7560.

Owens, J.M., and D.P. Chynoweth (1993). Biochemical methane potential of municipal solid waste (MSW) components. Water Sci. Technol., 27, 1-14.

Pabalan, R.T., D.R. Turner, F.P. Bertetti, and J.D. Prikryl (1998). Uranium(VI) Sorption onto Selected Mineral Surfaces: Key Geochemical Parameters. *In:* Adsorption of Metals by Geomedia (p. 99–130), Academic Press.

Palmisano, A.C., D.A. Maruscik, and B.S. Schwab (1993). Enumeration of fermentative and hydrolytic microorganisms from three sanitary landfills. J. Gen. Microbiol., 139, 387-391.

Panikov, N.S. (1995). Microbial Growth Kinetics, Chapman and Hall, U.K.

Papini, M.P., Y.D. Kahie, B. Troia, and M. Majone (1999). Adsorption of Lead at Variable pH onto a Natural Porous Medium: Modelling of Batch and Column Experiments. Env. Sci. Tech., 33, 4457–4464.

Parkes R.J., B.A. Cragg, J.C. Fry, R.A. Herbert, and J.W.T. Wimpenny (1990). Bacterial biomass and activity in deep sediment layers from the Peru margin. Phil. Trans. R. Soc. Lond., A331, 139–153.

Parkhurst, D.L. (1995). User's guide to PHREEQC – A computer program for speciation, reaction-path, advective-transport, and inverse geochemical calculations. Technical Report 4227, U.S. Geological Survey Water-Resources Investigations Report.

Parkhurst, D.L., and C.A.J. Appelo (1999). User's guide to PHREEQC (version 2) - A computer program for speciation, batch-reaction, one-dimensional transport, and inverse geochemical calculations. U.S. Geological Survey Water-Resources Investigations Report, 99-4259.

Parkhurst, D.L., D.C. Thorstenson, and L.N. Plummer (1980). PHREEQE – A computer program for geochemical calculations. Technical report, U.S. Geological Survey techniques of Water-Resources Investigations Report 80-96.

Parkhurst D.L., K.G. Stollenwerk, and J.A. Colman (2003). Reactivetransport of phosphorus in the sewage plume at the Massachusetts Military Reservation, Cape Cod,

Massachusetts. Water-Resources Investigations Report 03-4017, U.S. Geological Survey.

Parkhurst, D.L., K.L. Kipp, P. Engesgaard, and S.R. Charlton (2004). PHAST—A program for simulating ground-water flow, solute transport, and multicomponent geochemical reactions. U.S. Geological Survey Techniques and Methods 6–A8, 154 p.

Pasternak, D. and P. Carey (1992). U.S. News World Rep., 14 December, p. 34.

Pastres, R., and S. Ciavatta (2005). A comparison between the uncertainties in model parameters and in forcing functions: its application to a 3D water quality model. Environm. Modell. Softw., 20, 981-989.

Pavlostathis, S.G., and J.M. Gossett (1988). Preliminary conversion mechanisms in anaerobic digestion of biological sludges. J. Environm. Eng., 114, 575-592.

Pavlostathis, S.G., T.L. Miller, and M.J. Wollin (1988). Kinetics of insoluble cellulose fermentation by continuous cultures of Rumincoccus albus. Appl. Environ. Microbiol., 54, 2660-2663.

Pavlostathis., S.G., T.L. Miller, and M.J. Wollin (1990). Cellulose fermentation by continuous cultures of Rumincoccus albus and Methanobrevibacter smithii. Appl. Environ. Microbiol., 33, 109-116.

Petrie, L., N.N. North, S.L. Dollhopf, D.L. Balkwill, and J.E. Kostka (2003). Enumeration and characterization of iron(III)-reducing microbial communities from acidic subsurface sediments contaminated with uranium(VI). Appl. Environ. Microbiol., 69, 7467-7479.

Postma, D., and R. Jakobsen (1996). Redox zonation: Equilibrium constraints on the Fe(III)/SO-reduction interface. Geochim. Cosmochim. Act., 60, 3169-3175.

Postma, D., and C.A.J. Appelo (2000). Reduction of Mnoxides by ferrous iron in a flow system: column experiment and reactive transport modelling. Geochim. Cosmochim. Acta, 64, 1237– 1247.

Pavlostathis, S.G., and E. Giraldo Gomez (1991). Kinetics of Anaerobic Treatment. Water Sci. Tech., 24, 35-59.

Powell, M.S., and N.K.H. Slater (1983). The deposition of bacterial cells from laminar flows onto solid surfaces. Biotechnol. Bioeng., 25, 891-900.

Prikryl, J.D., A. Jain., D.R. Turner, and R.T. Pabalan (2001). Uranium(VI) Sorption Behaviour on Silicate Mineral Mixtures. J. Contam. Hydrol., 47, 241–253.

Prommer, H. (2000). Modelling reactive multicomponent transport in contaminated aquifers. Ph.D thesis. University of Western Australia, March.

Prommer, H., D.A. Barry, G.B. Davis (1999a). A one-dimensional reactive multi-component transport model for biodegradation of petroleum hydrocarbons in groundwater. Environ. Model. Softw., 14, 213-223.

Prommer, H., G.B. Davis, and D.A. Barry (1999b). Geochemical changes during biodegradation of petroleum hydrocarbons: Field investigations and biogeochemical modelling. Org. Geochem., 30, 423-435.

Pulford, I.D., and C. Watson (2003). Phytoremediation of heavy metyal-contaminated land by trees: a review. Environ. Int., 29, 539–560.

Quinton, G.E., R.J. Buchanan, D.E. Ellis, and S.H. Shoemaker (1997). A method to compare groundwater cleanup technologies. Remediation, Autumn, 7–16.

Ramos, L.P., C. Breuil, J.N. Saddler (1993). The use of enzyme recycling and the influence of sugar accumulation on cellulose hydrolysis by Trichoderma cellulases. Enzyme Microb. Technol., 15, 19-25.

Raskin, I., R.D. Smith, and D.E. Salt (1997). Phytoremediation of metals: Using plants to remove pollutants from the environment. Curr. Opin. Biotechnol., 8, 221–226.

Rao, P.S.C., J.M. Davidson, R.E. Jessup, and H.M. Selim (1979). Evaluation of conceptual models for describing non-equilibrium adsorption- desorption of pesticides during steady-flow in soils. Soil Sci. Soc. Am. J., 43, 22–28.

Rao, P.S.C., D.E. Rolston, R.E. Jessup, and J.M. Davidson (1980). Solute transport in aggregated porous media: Theoretical and experimental evaluation. Soil Sci. Soc. Am. J., 44, 1139–1146.

Read, D. and P. Hooker (1992). Using data from natural environments to improve models of uranium speciation in groundwaters. J. Geochem. Explor., 46, 63-81.

Read, D., D. Ross, and R.J. Sims (1998). The Migration of uranium through Clashach Sandstone: the role of low molecular weight organics in enhancing radionuclide transport. J. Contam. Hydrol., 35, 235–248.

Riba, O., C. Walker, and K. Vala Ragnarsdottir (2005). Kinetic Studies of Synthetic Metaschoepite under Acidic Conditions in Batch and Flow Experiments. Environ. Sci. Technol., 39, 7915-7920.

Riley, R.G., J.M. Zachara, and F.J. Wobber (1992). Chemical contaminants on DOE land and selections of contaminant mixtures for subsurface science research. DOE/ER-0547T, U.S. Department of Energy: Washington, DC.

Rittman, B.E. and P.L. McCarty (1980). Model of steady-state biofilm kinetics. Biotech. Bioeng., 22, 2343-2357.

Robertson, W.D., B.M. Russell, and J.A. Cherry (1996). Attenuation of nitrate in aquitard sediments of southern Ontario. J. Hydrol., 180, 267–281.

Robinson, B.A., H.S. Viswanathan, and A.J. Valocchi (2000). Efficient numerical techniques for modelling multicomponent ground-water transport based upon simultaneous solution of strongly coupled subsets of chemical components. Adv. Water Resour., 23, 307–324.

Roden, E.E., and T.D. Scheibe (2005). Conceptual and numerical model of uranium(VI) reductive immobilisation in fractured subsurface sediments. Chemosphere, 59, 617-628.

Rodhe, H. (1990). A comparison of the contribution of various gases to the greenhouse effect. Science, 248, 1217-1219.

Rogak, S.N., and R.C. Flagan (1992). Coagulation of aerosol agglomerates in the transition regime. J. Colloid Interf. Sci., 151, 1.

Röling, W.F.M., B.M. van Breukelen, M. Braster, B. Lin, and H.W. van Verseveld (2001). Relationships between microbial community structure and hydrochemistry in a landfill leachatepolluted aquifer. Appl. Environ. Microbiol., 67:, 4619–4629.

Russell, J.B., and R.L. Baldwin (1979). Comparison of substrate affinities among several rumen bacteria: a possible determinant of rumen bacterial competition. Appl. Environ. Microbiol., 37, 531-536.

Ryan, M.C., K.T.B. MacQuarrie, J. Harman, and J. McLelland (2000). Field and modelling evidence for a "stagnant flow" zone in the upper meter of sandy phreatic aquifers. J. Hyd., 233, 223-240.

Saaltink, M.W., C. Ayora, and J. Carrera (1998). A mathematical formulation for reactive transport that eliminates mineral concentrations. Water Resour. Res., 34, 1649–1656.

Saiers, J.E., H. Guha, P. Jardine, and S. Brooks (2000). Development and evaluation of a mathematical model for the transport and oxidation– reduction of CoEDTA. Water Resour. Res., 36, 3151– 3165.

Salas, J. and C. Ayora (2004). Groundwater chemistry of the Okélobondo uraninite deposit area (Oklo, Gabon): two-dimensional reactive transport modelling. J. Contam. Hydrol., 69, 115– 137.

Salt, D.E., R.D. Smith, and I. Raskin (1998). Phytoremediation. Ann. Rev. Plant Phys. Plant Mol. Biol., 49, 643–668.

Salvage, K., and G. T. Yeh (1998). Development and application of a numerical model of kinetic and equilibrium microbiological and geochemical reactions (BIOKEMOD). J. Hydrol., 209, 27– 52.

Salvage, K.M., G.T. Yeh, H.P. Cheng, and J.R. Cheng (1996). Development of a model of subsurface hydrologic transport and biogeochemical reactions (HYDROBIOGEOCHEM), *In:* Computational Methods in Water Resources XI, vol. 2, Computation Methods in Surface Flow and Transport Problems (pp. 517–524), Comput. Mech., Boston, Mass.

Sánchez-Vila, X., and J. Carrera (2003). On the striking similarity between the moments of breakthrough curves for a heterogeneous medium and a homogeneous medium with a matrix diffusion term. J. Hydrol., 294, 164–75.

Sani, R.K., B.M. Peyton, J.E. Amonette, and G.G. Geesey (2004). Reduction of uranium(VI) under sulfate-reducing conditions in the presence of Fe(III)-(hydr)oxides. Geochim. Cosmochim. Act., 68, 2639-2648.

Schäfer, W. (1992). Numerische Modellierung mikrobiell beeinflusster Stofftransprotvorgänge im Wasser. Oldernbourg Verlag, München, Wien.

Schäfer, W., and R. Therrien (1995). Simulating transport and removal of xylene during remediation of a sandy aquifer. J. Contam. Hydrol., 19, 205-236.

Schäfer, D., W. Schäfer, and W. Kinzelbach (1998a). Simulation of reactive processes related to biodegradation in aquifers. 1. Structure of the three-dimensional reactive transport model. J. Contam. Hydrol., 31, 167-186.

Schäfer, D., W. Schäfer, and W. Kinzelbach (1998b). Simulation of reactive processes related to biodegradation in aquifers. 2. Model application to a column study on organic carbon degradation. J. Contam. Hydrol., 31, 187-209.

Schwitzguebel, J.P., D. van der Lelie, A. Baker, D. Glass, and J. Vangrosweld (2002). Phytoremediation: european and american trends, successes, obstacles and needs. J. Soils Sediments, 2, 91–99.

Scholl, M.A., and R.W. Harvey (1992). Laboratory investigations on the role of sediment surface and groundwater chemistry in transport of bacteria through a contaminated sandy aquifer. Environ. Sci. Technol., 26, 1410–1417.

Schroth, M.H., J.D. Istok, G.T. Conner, M.R. Hyman, R. Haggerty, and K.T. O'Reilly (1998). Spatial variability in situ aerobic respiration and denitrification rates in a petroleum-contaminated aquifer. Ground Water, 36, 924–937.

Schwarz, W.H. (2001). The cellulosome and cellulose degradation by anaerobic bacteria. Appl. Microbiol. Biotech., 56, 634–649.

Schwarze, H., U. Jaekel, and H. Vereecken (2001). Estimation of macrodispersion by different approximation methods for flow and transport in randomly heterogeneous media. Transp. Porous Media, 43, 265–87.

Selim, H.M., J.M. Davidson, and P.S.C. Rao (1977). Transport of reactive solutes through multilayered soils. Soil Sci. Soc. Am. J., 41, 3–10.

Senko, J.M., J.D. Istok, J.M. Suflita, and L.R. Krumholz (2002). In-situ evidence for uranium immobilisation and remobilization. Environ. Sci. Technol., 36, 1491-1496.

Senko, J.M., J.M. Suflita, and L.R. Krumholz (2005). Geochemical controls on microbial nitrate-dependent U(IV) oxidation. Geomicrobiol. J., 22, 371–378.

Shelobolina, E.S., S.A. Sullivan, K.R. O'Neill, K.P. Nevin and D.R. Lovley (2004). Isolation, characterization, and U(VI)-reducing potential of a facultatively anaerobic, acid-resistant bacterium from low-pH, nitrate- and U(VI)-contaminated subsurface sediment and description of *Salmonella subterranea* sp. Nov. Appl. Environ. Microbiol., 70, 2959–2965.

Sidle, R.C., B. Nilsson, M. Hansen, and J. Fredericia (1998). Spatially varying hydraulic and solute transport characteristics of a fractured till determined by field tracer tests, Funen, Denmark. Water Resour. Res., 34, 2515-2527.

Šimůnek, J., N.J. Jarvis, M.T. van Genuchten, and A. Gardenas (2003). Review and comparison of models for describing nonequilibrium and preferential flow and transport in the vadose zone. J. Hydrol., 272, 14– 35.

Sinclair, J.L., and W.C. Ghiorse (1989). Distribution of aerobic bacteria, protozoa, algae, and fungi in deep subsurface sediments. Geomicrobiol. J., 7, 15–31.

Sinechal, X.J, M.J. Installe, and E.J. Nyans (1979). Differentiation between acetate and higher volatile acids in the modelling of the anaerobic biomethanation process. Biotechnol. Lett., 1, 309-314.

Skopp, J., and A.W. Warrick (1974). A two-phase model for the miscible displacement of reactive solutes in soils. Soil Sci. Soc. Am. J., 38, 525–550.

Skopp, J., W.R. Gardner, and E.J. Tyler (1981). Solute movement in structured soils: two-region model with small interaction. Soil Sci. Soc. Am. J., 45, 837–42.

Smith, S.L., and P.R. Jaffé (1998). Modelling the transport and reaction of trace metals in water-saturated soils and sediments. Water Resour. Res., 34, 3135-3147.

Smith, A.C., D. Balkwill, A.S. Madden, and T.J. Phelps (2006). Microbial community responses to nitrate-indifferent uranium bioreduction, poster presented at AGU Fall Meeting, 2006, San Francisco, Calif., Eos Trans. AGU, 87(52), Fall Meet. Suppl., Abstract B53C-0356.

Snoeyenbos-West, O., K.P. Nevin, R.T. Anderson, and D.R. Lovley (2000). Enrichment of Geobacter species in response to stimulation of Fe(III) reduction in sandy aquifer sediments. Microbiol. Ecol., 39, 153–167.

Song, H., W.P. Clarke, and L.L. Blackall (2005). Concurrent Microscopic Observations and Activity Measurements of Cellulose Hydrolyzing and Methanogenic Populations During the Batch Anaerobic Digestion of Crystalline Cellulose. Biotechnol. Bioeng., 91, 369-378.

Spear, J.R., L.A. Figueroa, and B.D. Honeyman (2000). Modelling reduction of uranium U(VI) under variable sulfate concentrations by sulfate-reducing bacteria. Appl. Environ. Microbiol., 66, 3711–3721.

Sposito, G. (1994). Chemical equilibria and kinetics in soils. Oxford Univ. Press.

Sposito, G., and D. A. Barry (1987). On the Dagan model of solute transport in groundwater: Foundational aspects. Water Resour. Res., 23, 1867-1875.

Spycher, N.F., E.L. Sonnenthal, and J.A. Apps (2003). Fluid flow and reactive transport around potential nuclear waste emplacement tunnels at Yucca Mountain, Nevada. J. Contam. Hydrol., 62–63, 653– 673.

Srivastava, R. and M.L. Brusseau (1996). Nonideal transport of reactive solutes in heterogeneous porous media: 1. Numerical model development and moments analysis. J. Contam. Hydrol., 24, 117-143.

Stagnitti, F., L. Li, D.A. Barry, G. Allinson, J.-Y. Parlange, T. Steenhuis, and E. Lakshmanan (2001). Modelling solute transport in structured soils: Performance evaluation of ADR and TRM models. Math. Comput. Model., 34, 433-440.

Starr, J.L. and J.-Y. Parlange (1979), Dispersion in soil columns: The snow plow effect. Soil Sci. Soc. Am. J., 43, 448-450.

Steefel, C.I., and A.C. Lasaga (1994). A coupled model for transport of multiple chemical species and kinetic precipitation/dissolution reactions with application to reactive flow in single phase hydrothermal systems. Am. J. Sci., 294, 529–592.

Steefel, C.I., Lichtner, P.C. (1998). Multicomponent reactive transport in discrete fractures: II. Infiltration of hyperalkaline groundwater at Maqarin, Jordan, a natural analogue site. J. Hydrol. 209, 186–199.

Steefel, C.I. and S.B. Yabusaki (1996). OS3D/GIMRT Software for modelling multicomponent-multidimensional reactive transport. User manual and programmer's guide. Pacific Northwest National Lab., Richland, WA, USA. May 6th.

Stollenwerk, K.G. (1998). Molybdate Transport in a Chemically Complex Aquifer; Field Measurements Compared with Solute-transport Model Predictions. Water Res. Res., 34, 2727–2740.

Stumm, W. and J.J. Morgan (1996). Aquatic chemistry: Chemical equilibria and rates in natural water, 3rd Ed. Wiley-Interscience, John Wiley & Sons Inc, NY, USA.

Stumm, W., C.P. Huang, and S.R. Jenkins (1970). Specific chemical interactions affecting the stability of dispersed systems. Croat. Chem. Acta, 42, 223-244.

Suarez, D., and J. Šimunek (1996). Solute transport modelling under variably saturated water flow conditions, *In:* Lichtner, P.C., C.I. Steefel, and E.H. Oelkers (Eds.), Reactive Transport in Porous Media, Rev. Mineral., vol. 34, (pp. 229–268), Mineral. Soc. of Am., Washington, D. C.

Sudicky, E.A., and R.G. McLaren (1992). The Laplace Transform Galerkin technique for large-scale simulation of mass transport in discretely fractured porous formations. Water Resour. Res., 28, 499–514.

Sudicky, E.A., R.W. Gillham, and E.O. Frind (1985). Experimental Investigations of Solute Transport in Stratified Porous Media 1: The Non Reactive Case. Water Resour. Res., 21, 1035-1041.

Sun, Y., J.N. Petersen, J. Bear, T.P. Clement, and B.S. Hooker (1999). Modelling microbial transport and biodegradation in a dual-porosity system. Transport in Porous Med., 35, 49-65.

Suzuki, Y., and J.F. Banfield (1999). Geomicrobiology of uranium. *In:* Burns, P.C. and R. Finch (Eds.), Uranium: mineralogy, geochemistry and the environment, Reviews in Mineralgoy, Mineralogical Scoeity of America, Washington, D.C., 38, 393-432.

Suzuki, Y., and T. Suko (2006). Geomicrobiological factors that control uranium mobility in the environment: Update on recent advances in the bioremediation of uranium-contaminated sites. J. Miner. Petrol. Sci., 101, 299-307.

Suzuki, Y., S.D. Kelly, K.M. Kemner, and J.F. Banfield (2002). Nanometre-size products of uranium bioreduction. Nature, 419, 134.

Suzuki, Y., S.D. Kelly, K.M. Kemner, and J.F. Banfield (2003). Microbial populations stimulated for hexavalent uranium reduction in uranium mine sediment. Appl. Environ. Microbiol., 69, 1337–1346.

Sverjensky, D.A. (2001). Interpretation and prediction of triple-layer model capacitances and the structure of the oxide-electrolyte-water interface. Geochim. Cosmochim. Acta, 65, 3643–3655.

Sylwester, E.R., E.A. Hudson, and P.G. Allen (2000). The structure of uranium (VI) sorption complexes on silica, alumina, and montmorillonite. Geochim. Cosmochim. Acta, 64, 2431–2438.

Szecsody, J.E., J.M. Zachara, A. Chilakapati, P.M. Jardine, and A.S. Ferrency (1998). Importance of flow and particle-scale heterogeneity on Co(II/ III)EDTA reactive transport. J. Hydrol., 209, 112– 136.

Tabak, H.H., P. Lens, E.D. Van Hullebusch, and W. Dejonghe (2005). Developments in bioremediation of soils and sediments polluted with metals and radionuclides - 1. Microbial processes and mechanisms affecting bioremediation of metal contamination and influencing metal toxicity and transport. Reviews in Environmental Science and Biotechnology, 4, 115-156.

Tang, D.H., E.O. Frind, and E.A. Sudicky (1981). Contaminant transport in fractured porous media: analytical solution for a single fracture. Water Resour. Res., 17, 555–564.

Taylor, S.W., and P.R. Jaffé (1990). Biofilm growth and the related changes in the physical properties of a porous medium, experimental investigation. Water Resour. Res., 26, 2153-2159.

Taylor, S.W., P.C.D. Milly, and P.R. Jaffé (1990). Biofilm growth and the related changes in the physical properties of a porous media, 2, Permeability. Water Resour. Res., 26, 2161-2169.

Tebes-Stevens, C., A.J. Valocchi, J.M. VanBriesen, and B.E. Rittmann (1998). Multicomponent transport with coupled geochemical and microbiological reactions: Model description and example simulations. J. Hydrol., 209, 8–26.

Tebo, B.M., and A.Y. Obraztsova (1998). Sulfate-reducing bacterium grows with Cr(VI), U(VI), Mn(IV), and Fe(III) as electron acceptors. FEMS Microbiol. Lett., 162, 193-198.

Theis, T.L., D.J. Kirkner, and A.A. Jennings (1982). Multi-solute subsurface transport modelling for energy solid wastes. Tech. Progress Rep. C00- 10253-3, Dep. of Civ. Eng., Univ. of Notre Dame, Notre Dame.

Therrien, R., and E.A. Sudicky (1996). Three-dimensional analysis of variably-saturated flow and solute transport in discretely fractured porous media. J. Contam. Hydrol., 23, 1–44.

Thullner, M., J. Zeyer, and W. Kinzelbach (2002). Influence of microbial growth on hydraulic properties of pore networks. Transp. Porous Media, 49, 99–122.

Thullner, M., M.H. Schroth, J. Zeyer, and W. Kinzelbach (2004). Modelling of a microbial growth experiment with bioclogging in a two-dimensional saturated porous media flow field. J. Contam. Hydrol., 70, 37– 62.

Thullner, M., P. Van Cappellen, and P. Regnier (2005). Modelling the impact of microbial activity on redox dynamics in porous media. Geochim. Cosmochim. Acta, 69, 5005–5019.

Tobin, J.M., C. White, and G.M. Gadd (1994). Metal accumulation by fungi: applications in environmental biotechnology. J. Ind. Microbiol., 13, 126–130.

Tokunaga, T.K., J. Wan, J. Pena, E.L. Brodie, M.K. Firestone, T.C. Hazen, S.R. Sutton, A. Lanzirotti, and M. Newville (2005). Uranium Reduction in Sediments under Diffusion-Limited Transport of Organic Carbon. Environ. Sci. Technol., 39, 7077 -7083.

Tompson, A.F.B., A.L. Schafer, and R.W. Smith (1996). Impacts of physical and chemical heterogeneity on contaminant transport in a sandy porous medium. Water Resour. Res., 32, 801-818.

Tompson, A.F.B., E.G. Vomvoris, and L.W. Gelhar (1988). Numerical solution of solute transport in randomly heterogeneous porous media: Motivation, model development, and application. Rep. 316, 114 pp., Ralph M Parsons Lab., Civil Eng. Dep., Mass. Inst. Of Technol., Cambridge.

Tong, M., X. Li, C.N. Brow, and W.P. Johnson (2005). Detachment-influenced transport of an adhesion-deficient bacterial strain within water-reactive porous media. Environ. Sci. Technol., 39, 2500-2508.

Truex, M.J., B.M. Peyton, N.B. Valentine, and Y.A. Gorby (1997). Kinetics of U(VI) reduction by a dissimilatory Fe(III)-reducing bacterium under non-growth conditions. Biotechnol. Bioeng., 55, 490-496.

Turner G.D., J.M. Zachara, J.P. McKinley, and S.C. Smith (1996). Surface-charge Properties and UO_2^{2+} Adsorption of a Subsurface Smectite. Geochim. Cosmochim. Acta, 60, 3399–3414.

Ulrich, G., A.D. Martino, K. Burger, J. Routh, E.L. Grossman, J.W. Ammerman, and J.M. Suflita (1998). Sulfur Cycling in the Terrestrial Subsurface: Commensal Interactions, Spatial Scales, and Microbial Heterogeneity. Microb. Ecol., 36, 141–151.

UMTRCA (1978). Uranium Mill tailings Radiation Control Act, enacted by American Congress on November 8, 1978, Public Law 95-604.

USEPA (1999). Understanding Variation in Partition Coefficient, Kd, Values. Vol. 1, Report EPA 402-R-99–0044A, Washington, DC.

van Breukelen, B.M., C.A.J. Appelo, and T.N. Olsthoorn (1998). Hydrogeochemical transport modelling of 24 years of Rhine water infiltration in the dunes of the Amsterdam Water Supply. J. Hydrol., 209, 281-296.

Van der Lelie, D., J.P. Schwitzguebel, D.J. Glass, and A. Baker (2001). Assessing phytoremediation's progress in the United States and Europe. Environ. Sci. Technol., 35, 447A–452A.

Van Cappellen, P., and J.-F. Gaillard (1996). Biogeochemical dynamics in aquatic sediments. *In:* Lichtner, P.C., Steefel, C.I., Oelkers, E.H. (Eds.), Reactive Transport in Porous Media, Rev. Mineral., vol. 34. Mineralogical Society of America, Washington, DC.

van Genuchten, M.T. (1981). Non-Equilibrium Transport Parameters From Miscible Displacement Experiments. Research Report No. 119. U.S. Department of Agriculture. Science and Education Administration. U.S. Salinity Lab, Riverside, California.

van Genuchten, M.T., and W.J. Alves (1982). Analytical solution of the onedimensional convective – dispersive solute transport equation. U.S. Department of Agriculture, Washington, D.C.

van Genuchten, M.T., and F.N. Dalton (1986). Models for simulating salt movement in aggregated field soils. Geoderma, 38, 165–83.

van Genuchten, M.T., and P.J. Wierenga (1976). Mass transfer studies in sorbing porous media, I, Analytical solutions. Soil Sci. Soc. Am. J., 40, 473–481.

van Genutchen, M.T., and P.J. Wierenga (1977). Mass transport studies in sorbing porous media, 2, Experimental evaluation with tritium ($3H_2O$). Soil Sci. Soc. Am. J., 41.

Vandevivere, P., and P. Baveye (1992a). Saturated hydraulic conductivity reduction caused by aerobic bacteria in sand column. J. Soil Sci. Soc. Am., 56, 1-13.

Vandevivre, P., and P. Baveye (1992b). Effect of bacterial extracellular polymers on the saturated hydraulic conductivity of sand columns. Appl. Environ. Microbiol., 58, 1690-1698.

VanGulcka, J.F., and R.K. Rowe (2004). Evolution of clog formation with time in columns permeated with synthetic landfill leachate. J. Contam. Hydrol., 75, 115-139.

Vavilin, V.A., S.V. Rytow, and L.Y. Lokshina (1995). Modelling hydrogen partial pressure change as a result of competition between the butyric and propionic groups of acidogenic bacteria. Bioresource Technol., 54, 171-177.

Vavilin, V.A, S.V. Rytov, and L.Y. Lokshina (1996). A description of hydrolysis kinetics in anaerobic degradation of particulate matter. Bioresource Technol., 56, 229-237.

Vavilin, V.A., S.V. Rytov, L.Y. Lokshina, J.A. Rintala, and G. Lyberatos (2001). Simplified hydrolysis models for the optimal design of two-stage anaerobic digestion. Water Research, 35, 4247-4251.

Vavilin, V.A., L.Y. Lokshina, J.P.Y. Jokela, and J.A. Rintala (2004). Modelling solid waste decomposition. Bioresource Technol., 94, 69-81.

Vogel, T., H. Gerke, R. Zhang, and M.Van Genuchten (2000). Modelling flow and transport in a two-dimensional dual-permeability system with spatially variable hydraulic properties. J. Hydrol., 238, 78–89.

Volesky, B., and Z.R. Holan (1995). Biosorption of heavy metals. Biotechnol. Prog., 11, 235–250

Vrionis, H.A., R.T. Anderson, I. Ortiz-Bernard, K.R. O'Neill, C.T. Resch, A.D. Peacock, R. Dayvault, D.C. White, P.E. Long, and D.R. Lovley (2005). Microbiological and Geochemical Heterogeneity in an In Situ Uranium Bioremediation Field Site. Appl. Environ. Microbiol., 71, 6308-6318.

Vroblesky, D.A., and F.H. Chapelle (1994). Temporal and spatial changes of terminal electron-accepting processes in a petroleum hydrocarbon-contaminated aquifer and the significance for contaminant biodegradation. Water Resour. Res., 30, 1561–1570.

Waite, T.D., J.A. Davis, T.E. Payne, G.A. Waychunas, and N. Xu (1994). Uranium(VI) adsorption to ferrihydrite: Application of a surface complexation model. Geochim. Cosmochim. Act., 58, 5465-5478.

Walker, L.P., and D.B. Wilson (1991). Enzymatic hydrolysis of cellulose: an overview. Bioresource Technol., 36, 3-14.

Walter, A.L., E.O. Frind, D.W. Blowes, C.J. Ptacek, and J.W. Molson (1994). Modelling of multicomponent reactive transport in groundwater: 1. Model development and evaluation. Water Resour. Res., 30, 3137– 3148.

Wan, J., T.K. Tokunaga, E. Brodie, Z. Wang, Z. Zheng, D. Herman, T.C. Hazen, M. K. Firestone, S.R. Sutton (2005). Reoxidation of bioreduced uranium under reducing conditions. Environ. Sci. Technol., 39, 6162-6169.

Wang, Y., and P. Van Cappellen (1996). A multicomponent reactive transport model of early diagenesis: application of redox cycling in coastal marine sediments. Geochim. Cosmochim. Acta, 60, 2993–3014.

Wang, Y. and H.W. Papenguth (2001). Kinetic modelling of microbially-driven redox chemistry of radionuclides in subsurface environments: coupling transport, microbial metabolism and geochemistry. J. Contam. Hydrol., 47, 297–309.

Wang, S., P.R. Jaffé, G. Li, S.W. Wang, and H.A. Rabitz (2003). Simulating bioremediation of uranium-contaminated aquifers; uncertainty assessment of model parameters. J. Contam. Hydrol., 64, 283– 307.

Weber, K.A., F.W. Picardal, and E.E. Roden (2001). Microbially catalyed nitrate-dependent oxidation of biogenic solid-phase Fe(II) compounds. Environ. Sci. Technol., 35, 1644-1650.

Weiss, T.H., A.L. Mills, G.M. Hornberger, and J.S. Herman (1995). Effect of bacterial cell shape on transport of bacteria in porous media. Environ. Sci. Technol., 29, 1737–1740.

Wersin, P., P. Höhener, R. Giovanoli, and W. Stumm (1991). Early diagenetic influences on iron transformations in a freshwater lake sediment. Chem. Geol., 90, 233–252.

Westall, J. (1986). MINEQL — a computer program for the calculation of the chemical equilibrium composition of aqueous systems. Technical Report, 86-01, Department of Chemistry, Oregon State University.

Westrich, J.T. and R.A. Berner (1984). The role of sedimentary organic matter in bacterial sulfate reduction: The G model tested, Limnol. Oceanogr., 29, 236-249.

Wheatcraft, S.W., and S.W. Tyler (1988). An explanation of scale-depdendent dispersivity in heterogeneous aquifers using concepts form fractal geometry. Water Resour. Res., 24, 566-578.

Whicker, F.W., T.G. Hinton, M.M. MacDonell, J.E. Pinder, and L.J. Habegger (2004). Avoiding destructive remediation at DOE sites.Science, 303, 1615-1616.

Widdowson, M.A. (1991). Comment on An evaluation of mathematical models of the transport of biologically reacting solutes in saturated soils and aquifers by Phillipe Baveye and Albert Valocchi. Water Resour. Res., 27, 1375-1378.

Wielinga, B., B. Bostick, C.M. Hansel, R.F. Rosenzweig, and S. Fendorf (2000). Inhibition of bacterially promoted uranium reduction: Ferric (hydr)oxides as competitive electron acceptors. Environ. Sci. Technol., 34, 2190-2195.

Williams, K.H., D. Ntarlagiannis, L.D. Slater, A. Dohnalkova, S.S. Hubbard, and J.F. Banfield (2005). Geophysical imaging of stimulated microbial biomineralization. Environ. Sci. Technol., 39, 7592-600.

Williamson, K., and P. L. McCarty (1976). A model of substrate utilisation by bacterial films. Journal of Water Pollution Control Federation, 48, 9-25.

Wilson, G.V., P.M. Jardine, J.D. Odell, and M. Collineau (1993). Field-scale transport from a buried line source in variably saturated soil. J. Hydrol., 145, 83–109.

Wolery, T.J. (1979). Calculation of chemical equilibrium between aqeous solution and minerals: the EQ3/6 software package. Technical Report URCL-52658, Lawrence Livermore National Laboratory.

Wood, S.A. (1996). The role of humic substances in the transport and fixation of metals of economic interest (Au, Pt, Pd, U, V). Ore Geology Reviews, 11, 1-31.

Wood, B.D., C.N. Dawson, J.E. Szecsody, and G.P. Streile (1994). Modelling contaminant transport and biodegradation in a layered porous media system. Water Resour. Res., 30, 1833–1845.

Wu, W.-M., J. Carley, M. Fienen, T. Mehlhorn, K. Lowe, J. Nyman, J. Luo, M.E. Gentile, R. Rajan, D. Wagner, R.F. Hickey, B. Gu, D. Watson, O.A. Cirpka, P.K. Kitanidis, P.M. Jardine, and C.S. Criddle (2006a). Pilot-Scale in Situ Bioremediation of Uranium in a Highly Contaminated Aquifer. 1. Conditioning of a Treatment Zone. Environ. Sci. Technol., 40, 3978 -3985.

Wu, W.-M., J. Carley, T. Gentry, M.A. Ginder-Vogel, M. Fienen, T. Mehlhorn, H. Yan, S. Caroll, M.N. Pace, J. Nyman, J. Luo, M.E. Gentile, M.W. Fields, R.F. Hickey, B. Gu,

D. Watson, O.A. Cirpka, J. Zhou, S. Fendorf, P.K. Kitanidis, P.M. Jardine, and C.S. Criddle (2006b). Pilot-Scale in Situ Bioremedation of Uranium in a Highly Contaminated Aquifer. 2. Reduction of U(VI) and Geochemical Control of U(VI) Bioavailability. Environ. Sci. Technol., 40, 3986-3995.

Xiang, Q., Y.Y. Lee, P.O. Petterson, and R.W. Torget (2003). Heterogeneous aspects of acid hydrolysis of α-cellulose. Appl. Biochem. Biotechnol.. 105-108, 505-514.

Xu, T., E. Sonnenthal, and G. Bodvarsson (2003). A reaction-transport model for calcite precipitation and evaluation of infiltration fluxes in unsaturated fractured rock. J. Contam. Hydrol., 64, 113– 127.

Xu, T., S.P. White, K. Pruess, and G.H. Brimhall (2000). Modelling of pyrite oxidation in saturated and unsaturated subsurface flow systems. Transp. Porous Media, 39, 25– 56.

Yeh, G.T., and V.S. Tripathi (1989). A critical evaluation of recent developments in hydrogeochemical transport models of reactive multichemical components. Water Resour. Res., 25, 93-108.

Yeh, G.T., and V.S. Tripathi (1991). A model for simulating transport of reactive multispecies components: Model development and demonstration. Water Resour. Res., 27, 3075–3094.

Yeh, G.T., K.M. Salvage, J.P. Gwo, Z.M. Zachara, and J.E. Szecsody (1998). "HYDROBIOGEOCHEM: a coupled model of HYDROlogic Transport and Mixed BIOGEOCHEMical Kinetic/Equilibrium Reactions in Saturated-Unsaturated Media" Report ORNL/TM-13668. Oak Ridge National Laboratory, Oak Ridge, TN.

Yeh, G.T., K. Salvage, and W.H. Choi (2001a). Reactive multispecies-multicomponent chemical transport controlled by both equilibrium and kinetic reactions, paper presented at XIth Internatioanl Conference on Numerical Methods in Water Resources, Mexican Inst. of Water Technol., Canquan, Mexico, 22 –26 July 1996.

Yeh, G.T., M.D. Siegel, and M.H. Li (2001b). Numerical modelling of coupled fluid flows and reactive transport including fast and slow chemical reactions. J. Contam. Hydrol., 47, 379–390.

Young, A. (1989). Simulating Methanogenesis in Landfills, A Presentation at the Landfill Microbiology Workshop, edited by Lawson and Alison, UK Dept. of Energy.

Zhang, Z., and M.L. Brusseau (1999). Nonideal transport of reactive solutes in heterogeneous porous media, 5, Simulating regional-scale behaviour of a trichloroethene plume during pump-and-treat remediation. Water Resour. Res., 35, 2921–2935.

Zhang, F., G.-T. Yeh, J.C. Parker, S.C. Brooks, M.N. Pace, Y.-J. Kim, P.M. Jardine, and D.B. Watson (2007). A reaction-based paradigm to model reactive chemical transport in groundwater with general kinetic and equilibrium reactions. J. Contam. Hydrol., 92, 10–32.

Zheng, C. (1990). "MT3D: A modular three-dimensional transport model". S.S. Papadopulos and Associates, Inc., Bethesda, MD.

Zheng, C., and P.P. Wang (1999). MT3DMS, a modular three dimensional multi-species transport model for simulation of advection, dispersion and chemical reactions of contaminants in groundwater systems; documentation and user's guide. U.S.Army Engineer Research and Development Center Contract Report SERDP-99-1, Vicksburg, MS.

Zhou, P., and B.H. Gu (2005). Extraction of oxidized and reduced forms of uranium from contaminated soils: Effects of carbonate and pH. Environ. Sci. Technol., 39, 4435-4440.

Zhu, C., and D.S. Burden (2001). Mineralogical compositions of aquifer matrix as necessary initial conditions in reactive contaminant transport models. J. Contam. Hydrol., 51, 145-161.

Zimmerman, R.W., G. Chen, T. Hadgu, and G.S. Bodvarsson (1993). A numerical dual-porosity model with semianalytical treatment of fracture/matrix flow. Water Resour. Res., 29, 2127–2137.

Zinn, B., and C. Harvey (2003). When good statistical models of aquifer heterogeneity go bad: a comparison of flow, dispersion, and mass transfer in connected and multivariate gaussian hydraulic conductivity fields. Water Resour. Res., 39:1051. doi:10.1029/2001WR001146.

Zinn, B., L.C. Meigs, C.F. Harvey, R. Haggerty, W.J. Peplinski, and C.F. von Schwerin (2004). Experimental visualisation of solute transport and mass transfer processes in two-dimensional conductivity fields with connected regions of high conductivity. Environ. Sci. Technol., 38, 3916–26.

Zoetemeyer, R.J., J.C. van den Heuval, and A. Cohen (1982a). pH influence on acidogenic dissimilation of glucose in an anaerobic digester. Water Research, 16, 303-311.

Zoetemeyer, R.J., P. Arnoldy, A. Cohen, and C. Boelhouwer (1982b). Influence of temperature on the anaerobic acidification of glucose in a mixed culture forming part of two stage digestion process. Water Research, 16, 313-321.

13. Published papers

Rotter, B.E., D.A. Barry, J.I. Gerhard, and J.S. Small (2007a). Modelling U(VI) Biomineralization in Single and Dual Porosity Porous Media. Water Resources Research, In submission (submitted June 2007).

Rotter, B.E., D.A. Barry, and J.I. Gerhard (2007b). Modelling the Effectiveness of U(VI) Biomineralization in Dual Porosity Porous Media. Journal of Contaminant Hydrology, In submission (submitted July 2007).

Rotter, B.E., D.A. Barry, J.I. Gerhard, and J.S. Small (2006). Parameter and process significance in mechanistic modelling of cellulose hydrolysis. Bioresource Technology, accepted October 2007.

Appendix A – CHAMP model formulations

A.1. Probability of contact

The aim of this appendix is to develop a simple model describing the probability of diffusion-driven contact of two different sized groups of particles in a liquid. The system is idealized as consisting of two representative sheets of particles. That is, the interaction between free biomass cells and cellulose particles is modeled by considering the interaction between two planar "particle sheets". The sheets are oriented in the *y*-*z* plane, orthogonal to the *x* axis. One sheet lies at $x = 0$ and diffuses with coefficient d_1; the other lies at $x = s$ and diffuses with coefficient d_2. The probability distribution function for the position of each sheet is given by

$$p_1 = \frac{\exp\left(-\frac{x^2}{4d_1t}\right)}{\sqrt{4\pi d_1 t}} \tag{A.1}$$

and

$$p_2 = \frac{\exp\left(-\frac{(x - s)^2}{4d_2t}\right)}{\sqrt{4\pi d_2 t}} \tag{A.2}$$

Here, the parameter t is the model time step. The probability of particles meeting by diffusion in the solution is approximated by the overlap of the two curves in equations A.1 and A.2. The intersection of the two curves, obtained by $p_1 = p_2$ occurs at x_s which is given by

$$x_s = \frac{s - \sqrt{\frac{d_2}{d_1}s^2 + 2t(d_2 - d_1)\ln\left(\frac{d_2}{d_1}\right)}}{1 - \frac{d_2}{d_1}} \tag{A.3}$$

where is has been assumed that $d_2 < d_1$. The probability of the sheets diffusing into each other is given by the intersection of p_1 and p_2,

$$P = \int_{xs}^{\infty} p_1 \, dx + \int_{-\infty}^{xs} p_2 \, dx \tag{A.4}$$

Integration of equation A.4 yields

$$P = \text{erfc}\left(\frac{x_s}{\sqrt{4\pi d_1 t}}\right) + 1 - \text{erfc}\left(\frac{x_s - s}{\sqrt{4\pi d_2 t}}\right) \tag{A.5}$$

A.2. Erf function

PHREEQC uses the BASIC programming language for the coding of kinetic reactions. BASIC does not, however, have the erfc function built-in. Thus, an approximation for the function erfc is used,

$$\text{erfc}(x) \approx \exp(-x^2)\frac{1}{1 + \frac{z_0 x}{1+\frac{z_1 x}{1+z_2 x}}} \tag{A.6}$$

where

$$z_0 = \frac{2}{\sqrt{\pi}}, \tag{A.7}$$

$$z_1 = \frac{-2}{\sqrt{\pi}} + \frac{\sqrt{\pi}}{2} \tag{A.8}$$

and

$$z_2 = \frac{\sqrt{\pi}}{6}\left(\frac{3\pi - 8}{4 - \pi}\right) + \left[\frac{\sqrt{\pi}}{2}\left(\frac{4 - \pi}{\pi - 2}\right) - \frac{\sqrt{\pi}}{6}\left(\frac{3\pi - 8}{4 - \pi}\right)\right]\frac{x^{z_3}}{\frac{341}{144} + x^{z_3}} \tag{A.9}$$

where

$$z_3 = \frac{37}{35} \tag{A.10}$$

The maximum relative error of this approximation is 0.02%.

A.3. Step function

To achieve numerical stability, it is necessary to change the step function *H* such that it varies smoothly. This is achieved by making use of a "shape factor", *S*, which changes its value throughout the model run. It is used by *W*, the new smoothly varying step function. Parameters are first defined to implement this:

$$X_{diff} = X_b - X_{max} \tag{A.11}$$

$$S_{max} = \frac{10}{\delta} \tag{A.12}$$

where X_{diff} is the indicator for the switch between states, S_{max} is the chosen maximum value S can take. S_{min} is the chosen minimum value which can be taken by the shape factor, S, valid for X_{max} - $X_b \geq 0$. δ is an arbitrary parameter value chosen such that the largest value of $X_b = X_{max} + \delta$ (where $0 < \delta << X_{max}$). The argument for the shape factor, G_{arg}, is calculated as

$$G_{arg} = \frac{10X_{diff}}{\delta} \tag{A.13}$$

The shape factor, S, is then calculated

$$S = S_{min} + \frac{S_{max} - S_{min}}{2}[1 - \tanh(-G_{arg})] \qquad \text{for } G_{arg} > 0 \tag{A.14}$$

$$S = S_{min} + \frac{S_{max} - S_{min}}{2}[1 - \tanh(G_{arg})] \qquad \text{for } G_{arg} \leq 0 \tag{A.15}$$

The new step function, W, is then defined as

$$W = 1 - \frac{1 - \tanh(X_{diff}S)}{2} \qquad \text{for } X_{diff} > 0 \tag{A.16}$$

$$W = \frac{1 - \tanh(-X_{diff}S)}{2} \qquad \text{for } X_{diff} \leq 0 \tag{A.17}$$

In this work, δ takes the value 10^{-8} and S_{min} takes the value 1000.

Appendix B – Modelling code files

This appendix lists the PHREEQC input files used to obtain the results reported in this work. The files may be found on the CD attached to the thesis hardcopy. This appendix lists the directory structures; the directory names used as titles within this appendix. Each section title corresponds to a directory name and lists the files associated with each respective modelling exercise.

B.1. Surface complexation model

This directory contains files for the simulations conducted in Chapter 3 regarding surface complexation modelling.

Table B.1. List of files for surface complexation model.

Filename	Application
validate-Barnett	Validation run for Barnett et al. (2002) data
validate-Missana-data-withBarnett	Validation run for Missana et al. (2002) data using model parameters of Barnett et al. (2002)
validate-Missana-data-notbyBarnett	Validation run for Missana et al. (2002) data using modified model parameters
validate-Barnett-link	Validation run for Barnett et al. (2002) data with modeled surface linked to ferrihydrite mineral

B.2. Model validation

This directory contains files for the simulations conducted in Chapter 4. They are simulation files for the validation of the biogeochemical reactive transport model.

Table B.2. List of files for model validation to experimental data.

Filename	Application[a]
transp-schoepite-diss3-dp	Schoepite dissolution model (result not shown in validation chapter text)
new	Case A
new2	Case B
new3	Case C
new3col3only3a	Case D

[a]see validation chapter text

For the model run used for validation to the existing model of Wang et al. (2003), the file is in the *DPvSP model* directory, and is named *newmultibc-Wang-sp-biomob*.

B.3. DPvSP model (Single/Dual Porosity comparison simulations)

This directory contains files for the simulations conducted in Chapter 5.

The filenames, and the systems they relate to, are as follows:

newmultibc-Wang-sp-biomob: single porosity system

newmultibc-Wang-sp-biomob: single porosity system, without surface complexation

newmultibc-Wang-dp-biomob-poros[x][transferrate]trans-m: single porosity system

where x = 2 for θ_m=0.1, θ_i=0.25; x = 3 for θ_m=0.25, θ_i=0.1

and *transferrate* may be *low*, *mean* or *high* with values as specified in the text.

These runs consider systems in which carbonate is present. This may be removed from the run by removal of the "*C 1000*" lines for SOLUTION's 0 through 401 (inclusive).

B.4. DPG analysis

This directory contains files for the simulations conducted in Chapter 6. The simulation run files for the DPG analysis study are given in Table B.3. Each row represents a set of filenames. Each of the filenames in each set will end with a number. These numbers (x) run from 1 up to some value. The sequence of x numbers and the DPG values associated with each x run are given by the following sequences:

A - the sequence of values used in run numbers x = 1 to 10 is from 0.0001 to 100000, in increments of 10, respectively.

B - the sequence of values used in run numbers x = 1 to 6 is from 0.1 to 100000, in increments of 10, respectively.

C - the sequence of values used in run numbers x = 1 to 21 is 0.10101, 0.12, 0.16, 0.2, 0.3, 0.4, 0.5, 0.6, 0.7, 0.8, 1.2, 1.6, 2, 2.4, 2.8, 3.2, 3.6, 5, 10, 100, and 33.33333, respectively.

Table B.4 lists the simulation runs for varied mineralogical conditions. The run numbers follow the same pattern, with the sequence of DPG values given in the "x range" column (start value…end value, increment; for all run numbers).

Table B.5 lists the simulation files for the model application example given in Chapter 6.

Table B.3. List of files for DPG simulations.

Filenames	***Pe***	ω	***Dk***	θ_p	**x sequence**
basDk[x]	1	range	1	1	A
DkdDm[x]	1	range	0.16	1	A
DkuDm[x]	1	range	1000	1	A
basDm[x]	1	1	range	1	A
DmuDk[x]	1	6.3	range	1	A
DmdDk[x]	1	0.32	range	1	A
newbas2Pe[x]	range	1	1	1	B
newDmu3Pe[x]	range	1000	1	1	B
newDmu2Pe[x]	range	10	1	1	B
newDmd4Pe[x]	range	0.5	1	1	B
newDmd2Pe[x]	range	0.1	1	1	B
newDku3Pe[x]	range	1	100	1	B
newDku2Pe[x]	range	1	10	1	B
newDkd4Pe[x]	range	1	0.5	1	B
newDkd2Pe[x]	range	1	0.1	1	B
new9basth[x]	1	1	1	range	C
new9Dmuth[x]	1	6	1	range	C
new9Dmdth[x]	1	0.3	1	range	C
new9Dkuth[x]	1	1	1000	range	C
new9Dkdth[x]	1	1	0.3	range	C
new9Peuth[x]	100	1	1	range	C

Table B.4. List of files for adjusted mineral content.

Filenames	*Pe*	ω[a]	*Dk* [a]	θ_p [a]	Mineral[b]	Range of x[c]
ms24Dm[x]	1	R	1	1	L	A
ms23Dm[x]	1	R	1	1	I	A
basDm[x]	1	R	1	1	H	B
ms24Dk[x]	1	1	R	1	L	A
ms23Dk[x]	1	1	R	1	I	A
basDk[x]	1	1	R	1	H	B

[a]R = range

[b]see text for mineral concentrations; L=low, I=Intermediate; H=High.

[c]A means values of range for parameter follow sequence: 0.001, 0.01…10000; B means sequence: 0.0001, 0.001… 100000

Table B.5. List of files for the model application, Section 6.4.

Filename	*Pe*	ω	*Dk*	θ_p
newnew6a	4.3	0.32	0.76	0.9
newnew6b	4.3	0.32	45.8	0.9
newnew6aopt	0.43	3.2	7.55	0.9
newnew6bopt	0.43	3.2	458	0.9

B.5. Bioresidency

This directory contains files for the simulations conducted in Chapter 7.

In all cases the filename format follows these conventions:

newmultibc-bio[region][run]-[transfer]trans-[outregion]

[region] is the region(s) in which bioactivity is taking place (mob,imm,both = mobile,immobile,both)

[run] is the run number, each run is associated with a different porosity ratio

[transfer] indicates the mass transfer rate used in the run

[outregion] indicates the region for which output is made - may be mobile (m) or immobile (i)

Runs at different **spatial discretisations** can be found in the files:

newmultibc-biomob2-avtrans-mx[1 through 4]

newmultibc-biomob-avtrans-mx[1 and 2]

The *biospeed* directory contains files for adjusted **bioactivity rates**.

The *mineralogy* directory contains files for adjusted **mineralogies**. The file format is:

newmultibc-bio[region]-avtrans-min[run]-m

[region] is the region(s) in which bioactivity is taking place (mob,imm,both = mobile,immobile,both)

[run] is the run number, each run is associated with a mineral change in a different region: 9 for lower mineral presence in the mobile region, 10 for lower mineral presence in both regions, and 11 for lower mineral presence in the immobile region

B.6. Reoxidation

This directory contains files for the simulations conducted in Chapter 8.

In all cases the filename format follows these conventions:

newmultibc-bio[region]-[transfer]trans-[outregion]-[mack]-[dx]-[tol]

[region] is the region(s) in which bioactivity is taking place (mob,imm,both = mobile,immobile,both)

[transfer] indicates the mass transfer rate used in the run

[outregion] indicates the region for which output is made - may be mobile (m) or immobile (i)

[mack] indictes whether the run includes the presence of mackinawite (no identifier) or the absence of mackinawite (nomack)

[dx] indicates a discretisation change (no identifier means Δx = 0.25 m and Δt = 0.025 yr; dx2 means Δx = 0.5 m and Δt = 0.05 yr, dx4 means Δx = 0.3 m and Δt = 0.03 yr)

[tol] indicates a run conducted with increased convergance tolerance for the element mole-balance equations

B.7. CHAMP model

This directory contains files for the simulations conducted in Chapter 9.

B.7.1 Basecase

This directory contains two files: one for the fast base case and one for the slow basecase model simulations.

B.7.2 ProcessSignificance

This directory contains the files for the process significance section of analysis.

The runs for the "Influence of diffusive biomass transfer" section may be found in the *Alpha* directory, those for the "Influence of biomass transfer: free population" in the *Transfer and Xf* directory, those for the "Influence of initial cellulose particle size" in the *Particle Size* directory, and those for the "Influence of cellulose particle shape" in the *Transfers* directory. Table B.6 lists the individual filename within each directory and states which parameter adjustment is made.

Table B.6. List of files for process significance study.

Directory	Based on base case	Parameter change	File
Alpha	Fast	$\alpha = 0$	ParticHydrolProbab10bc-fast-new3a0
	Fast	$\alpha = 0.8$	ParticHydrolProbab10bc-fast-new3a08
	Slow	$\alpha = 0$	ParticHydrolProbab10bc-slow-new3a0
	Slow	$\alpha = 0.8$	ParticHydrolProbab10bc-slow-new3a08
Particle size	Fast	ϕ_i = 42 μm	ParticHydrolProbab10bc-fast-new3-bc
	Fast	ϕ_i = 64 μm	ParticHydrolProbab10bc-fast-new3-big
	Fast	ϕ_i = 20 μm	ParticHydrolProbab10bc-fast-new3-small
	Slow	ϕ_i = 42 μm	ParticHydrolProbab10bc-slow-new3-bc
	Slow	ϕ_i = 64 μm	ParticHydrolProbab10bc-slow-new3-big
	Slow	ϕ_i = 20 μm	ParticHydrolProbab10bc-slow-new3-small
Transfer and Xf	Fast	$X_{fi} = 10^{-2}$ mol/l	ParticHydrolProbab10bc-fast-new3-1e-2
	Fast	$X_{fi} = 10^{-3}$ mol/l	ParticHydrolProbab10bc-fast-new3-1e-3
	Fast	$X_{fi} = 10^{-5}$ mol/l	ParticHydrolProbab10bc-fast-new3-1e-5
	Slow	$X_{fi} = 10^{-2}$ mol/l	ParticHydrolProbab10bc-slow-new3-1e-2
	Slow	$X_{fi} = 10^{-3}$ mol/l	ParticHydrolProbab10bc-slow-new3-1e-3
	Slow	$X_{fi} = 10^{-5}$ mol/l	ParticHydrolProbab10bc-slow-new3-1e-5
CylvsSphere[a]	ParticHydrolProbab 10bc-slow-new3		

[a]Modified formulation for cylindrical cellulose particle

B.7.3 Sensitivity

This directory contains the files for the sensitivity study. All parameters were varied (increased) by both 1 and 10%, and this was done for both the slow and fast base cases. This directory therefore contains four more directories, each for (i) either a fast or slow case and (ii) either a 1% or 10% parameter value change. Each of these four directories contains the files listed in Table B.7, each of which varies the value of a single parameter.

Table B.7. List of files for sensitivity study.

Filename	Parameter varied
Varyalpha	α
VaryCelluDiam	ϕ_i
VaryDb	D_b
VaryDf	D_f
Varyh	h
VaryKb	K_b
VaryVb	V_b
VaryXb	X_{bi}
VaryXf	X_{fi}
VaryYb	Y_b

B.7.4 AlphaV

This directory contains the files for the dimensionless parameter analysis results presented in Section 9.6. Table x lists the files and corresponding adjustments made to the parameter values in each run (file).

Table B.8. List of files for sensitivity to variables α and V.

Filename	D_b (s^{-1})	α/V	V (s^{-1})	α (s^{-1})	D_b (s^{-1})	D_f (s^{-1})
a1	1.70E-10	0.00E+00	3.08E-09	0.00E+00	1.70E-10	1.88E-10
2	1.70E-10	1.00E-01	3.08E-09	3.08E-10	1.70E-10	1.88E-10
3	1.70E-10	2.00E-01	3.08E-09	6.16E-10	1.70E-10	1.88E-10
4	1.70E-10	3.00E-01	3.08E-09	9.24E-10	1.70E-10	1.88E-10
5	1.70E-10	4.00E-01	3.08E-09	1.23E-09	1.70E-10	1.88E-10
6	1.70E-10	5.00E-01	3.08E-09	1.54E-09	1.70E-10	1.88E-10
7	1.70E-10	6.00E-01	3.08E-09	1.85E-09	1.70E-10	1.88E-10
8	1.70E-10	7.00E-01	3.08E-09	2.16E-09	1.70E-10	1.88E-10
9	1.70E-10	8.00E-01	3.08E-09	2.46E-09	1.70E-10	1.88E-10
10	1.70E-10	9.00E-01	3.08E-09	2.77E-09	1.70E-10	1.88E-10
11	1.70E-10	1.00E+00	3.08E-09	3.08E-09	1.70E-10	1.88E-10
12	1.70E-11	0.00E+00	3.08E-09	0.00E+00	1.70E-11	1.88E-11
13	1.70E-11	1.00E-01	3.08E-09	3.08E-10	1.70E-11	1.88E-11
14	1.70E-11	2.00E-01	3.08E-09	6.16E-10	1.70E-11	1.88E-11
15	1.70E-11	3.00E-01	3.08E-09	9.24E-10	1.70E-11	1.88E-11
16	1.70E-11	4.00E-01	3.08E-09	1.23E-09	1.70E-11	1.88E-11
17	1.70E-11	5.00E-01	3.08E-09	1.54E-09	1.70E-11	1.88E-11
18	1.70E-11	6.00E-01	3.08E-09	1.85E-09	1.70E-11	1.88E-11
19	1.70E-11	7.00E-01	3.08E-09	2.16E-09	1.70E-11	1.88E-11
20	1.70E-11	8.00E-01	3.08E-09	2.46E-09	1.70E-11	1.88E-11
21	1.70E-11	9.00E-01	3.08E-09	2.77E-09	1.70E-11	1.88E-11
22	1.70E-11	1.00E+00	3.08E-09	3.08E-09	1.70E-11	1.88E-11
b1	1.70E-10	0.00E+00	3.08E-08	0.00E+00	1.70E-09	1.88E-10
2	1.70E-10	1.00E-01	3.08E-08	3.08E-09	1.70E-09	1.88E-10
3	1.70E-10	2.00E-01	3.08E-08	6.16E-09	1.70E-09	1.88E-10
4	1.70E-10	3.00E-01	3.08E-08	9.24E-09	1.70E-09	1.88E-10
5	1.70E-10	4.00E-01	3.08E-08	1.23E-08	1.70E-09	1.88E-10
6	1.70E-10	5.00E-01	3.08E-08	1.54E-08	1.70E-09	1.88E-10
7	1.70E-10	6.00E-01	3.08E-08	1.85E-08	1.70E-09	1.88E-10
8	1.70E-10	7.00E-01	3.08E-08	2.16E-08	1.70E-09	1.88E-10
9	1.70E-10	8.00E-01	3.08E-08	2.46E-08	1.70E-09	1.88E-10
10	1.70E-10	9.00E-01	3.08E-08	2.77E-08	1.70E-09	1.88E-10
11	1.70E-10	1.00E+00	3.08E-08	3.08E-08	1.70E-09	1.88E-10
12	1.70E-11	0.00E+00	3.08E-08	0.00E+00	1.70E-10	1.88E-11
13	1.70E-11	1.00E-01	3.08E-08	3.08E-09	1.70E-10	1.88E-11
14	1.70E-11	2.00E-01	3.08E-08	6.16E-09	1.70E-10	1.88E-11
15	1.70E-11	3.00E-01	3.08E-08	9.24E-09	1.70E-10	1.88E-11
16	1.70E-11	4.00E-01	3.08E-08	1.23E-08	1.70E-10	1.88E-11
17	1.70E-11	5.00E-01	3.08E-08	1.54E-08	1.70E-10	1.88E-11
18	1.70E-11	6.00E-01	3.08E-08	1.85E-08	1.70E-10	1.88E-11
19	1.70E-11	7.00E-01	3.08E-08	2.16E-08	1.70E-10	1.88E-11
20	1.70E-11	8.00E-01	3.08E-08	2.46E-08	1.70E-10	1.88E-11
21	1.70E-11	9.00E-01	3.08E-08	2.77E-08	1.70E-10	1.88E-11
22	1.70E-11	1.00E+00	3.08E-08	3.08E-08	1.70E-10	1.88E-11
c1	1.70E-10	1.00E-07	3.08E-09	3.08E-16	1.70E-10	1.88E-10
2	1.70E-10	1.00E-06	3.08E-09	3.08E-15	1.70E-10	1.88E-10

Filename	D_b (s^{-1})	α/V	V (s^{-1})	α (s^{-1})	D_b (s^{-1})	D_f (s^{-1})
3	1.70E-10	1.00E-05	3.08E-09	3.08E-14	1.70E-10	1.88E-10
4	1.70E-10	1.00E-04	3.08E-09	3.08E-13	1.70E-10	1.88E-10
5	1.70E-10	1.00E-03	3.08E-09	3.08E-12	1.70E-10	1.88E-10
6	1.70E-10	1.00E-02	3.08E-09	3.08E-11	1.70E-10	1.88E-10
7	1.70E-10	1.00E-01	3.08E-09	3.08E-10	1.70E-10	1.88E-10
8	1.70E-10	1.00E+00	3.08E-09	3.08E-09	1.70E-10	1.88E-10
9	1.70E-11	1.00E-07	3.08E-09	3.08E-16	1.70E-11	1.88E-11
10	1.70E-11	1.00E-06	3.08E-09	3.08E-15	1.70E-11	1.88E-11
11	1.70E-11	1.00E-05	3.08E-09	3.08E-14	1.70E-11	1.88E-11
12	1.70E-11	1.00E-04	3.08E-09	3.08E-13	1.70E-11	1.88E-11
13	1.70E-11	1.00E-03	3.08E-09	3.08E-12	1.70E-11	1.88E-11
14	1.70E-11	1.00E-02	3.08E-09	3.08E-11	1.70E-11	1.88E-11
15	1.70E-11	1.00E-01	3.08E-09	3.08E-10	1.70E-11	1.88E-11
16	1.70E-11	1.00E+00	3.08E-09	3.08E-09	1.70E-11	1.88E-11
d1	1.70E-10	1.00E-07	3.08E-08	3.08E-15	1.70E-09	1.88E-09
2	1.70E-10	1.00E-06	3.08E-08	3.08E-14	1.70E-09	1.88E-09
3	1.70E-10	1.00E-05	3.08E-08	3.08E-13	1.70E-09	1.88E-09
4	1.70E-10	1.00E-04	3.08E-08	3.08E-12	1.70E-09	1.88E-09
5	1.70E-10	1.00E-03	3.08E-08	3.08E-11	1.70E-09	1.88E-09
6	1.70E-10	1.00E-02	3.08E-08	3.08E-10	1.70E-09	1.88E-09
7	1.70E-10	1.00E-01	3.08E-08	3.08E-09	1.70E-09	1.88E-09
8	1.70E-10	1.00E+00	3.08E-08	3.08E-08	1.70E-09	1.88E-09
9	1.70E-11	1.00E-07	3.08E-08	3.08E-15	1.70E-10	1.88E-10
10	1.70E-11	1.00E-06	3.08E-08	3.08E-14	1.70E-10	1.88E-10
11	1.70E-11	1.00E-05	3.08E-08	3.08E-13	1.70E-10	1.88E-10
12	1.70E-11	1.00E-04	3.08E-08	3.08E-12	1.70E-10	1.88E-10
13	1.70E-11	1.00E-03	3.08E-08	3.08E-11	1.70E-10	1.88E-10
14	1.70E-11	1.00E-02	3.08E-08	3.08E-10	1.70E-10	1.88E-10
15	1.70E-11	1.00E-01	3.08E-08	3.08E-09	1.70E-10	1.88E-10
16	1.70E-11	1.00E+00	3.08E-08	3.08E-08	1.70E-10	1.88E-10